Observational and theoretical aspects of tsunami sedimentation

Shi, Shaozhong

Award date:
1995

Awarding institution:
Coventry University

OBSERVATIONAL AND THEORETICAL ASPECTS OF TSUNAMI SEDIMENTATION

by

SHAOZHONG SHI

Dissertation submitted in partial fulfilment of the University's requirements for the degree of Doctor of Philosophy

Coventry University

July 1995

STATEMENT OF COPYRIGHT

DECLARATION

This dissertation is the result of the author's own work. Data or information from other authors which are referred to or quoted in the text are acknowledged at the appropriate point in the text.

Observational and Theoretical Aspects of Tsunami Sedimentation

Shaozhong Shi

ABSTRACT

This dissertation presents the detailed results of investigations into the coastal geomorphological effects and sedimentation processes associated with a recent large tsunami event which took place on the 12th December 1992 in Flores, Indonesia, and the stratigraphical and sedimentological study of a widespread sand layer preserved in coastal sedimentary sequences along the eastern coast of Scotland representing a low-frequency, high-energy marine event, which took place at *circa* 7,000 radiocarbon years B.P.. With modern analogues, established in this dissertation, of both tsunami and storm surge sedimentary characteristics and sedimentation processes as the key, together with high-resolution sedimentological evidence obtained from the *circa* 7,000 radiocarbon years B.P. event, competing hypotheses of the likely causes of the marine flooding by either a tsunami or storm surge event are tested. It is concluded that the *circa* 7,000 B.P. marine flooding event was a tsunami, believed to have been generated by one of the world's largest submarine landslides in the Norwegian Sea - the Second Storegga Slide.

The particle size composition of tsunami sediments is found to vary from well sorted to poorly sorted and is controlled by both the characteristics of the source sediment (local coastal sediments) and sedimentation processes associated with tsunami inundation. Tsunami sediments deposited on land are believed to form continuous and discontinous sedimentary sheets ascending up to levels distinctively higher than contemporary sea levels and to contain a general landward-fining trend and multiple sets of grading (fining-upward) sequences, reflecting spatial changes in particle size composition. A conceptual model of coastal tsunami sedimentation is established including processes of seaward and landward sediment movements, episodic rapid deposition, sediment accumulation and erosion.

ACKNOWLEDGEMENTS

I wish to express my sincere thanks to my Director of Studies Prof. D. E. Smith, and Dr. A. G. Dawson and Dr. I. D. L. Foster, my second supervisors, for their support and advice provided in all aspects of this work, and especially for their patience during the preparation of this dissertation. Thanks are also given to many other members of the Geography Division for their encouragement and valuable discussions. I am also grateful to Mrs. S. Addleton for her assistance in preparing maps and diagrams.

I would also like to acknowledge and express my sincere thanks to Dr. C. R. Firth for his advice and assistance in the field, Dr. R. A. Cullingford for advice and helpful discussion, Mr. D. Long for X-ray photography and helpful discussion, Dr. B. A. Haggart for providing some samples and results of diatom analysis, Dr. J. A. Dearing for his advice and discussion on mineral magnetic analysis, Dr. D. D. Harkness for providing advice on the calibration of radiocarbon dates, Mrs. Christine Dawson for the analysis of samples using a Scanning Electron Microscope, and landowners in the Dornoch Firth, especially at Dounie, for permission to undertake coring on their land.

Finally, I would like to thank my family and close friends for their continued support and encouragement.

Contents

List of Figures

List of Plates

List of Tables

List of Appendices

Chapter 1
General Introduction

1. INTRODUCTION

Though rare in occurrence in comparison to other geomorphological agents, and somehow neglected in geosciences, tsunamis have long been recognized to be one of the most powerful natural phenomena occurring on the Earth. There have been numerous literature accounts of their powerful impacts on low-lying coastal areas dating back to as early as 479 BC, especially in regions around the Pacific, Indonesia, the Caribbean and the Mediterranean.

Scientific study of tsunamis, however, is relatively recent, largely as a result of inadequate direct observations of such extreme phenomena. The most extensive studies, so far, have concerned descriptive accounts and physical and mathematical modelling of the events. Descriptive accounts have been primarily made for their destructive effects, flood level measurements and physical characteristics of recorded waves along coasts. In parallel, physical and mathematical modelling has focused on the mechanisms of tsunami generation, propagation and coastal dynamic effects. With recent technological advances in computing, mathematical modelling has entered an era of numerical reconstructions and predictions of

tsunami wave hydrodynamics. However, little is known of the geomorphological and sedimentary processes associated with tsunamis, a problem identified following recent developments in studies of palaeo-tsunamis. Recent studies of layers of sediment produced by high energy/low frequency marine flooding events in coastal sedimentary sequences concentrated upon stratigraphical and microbiological investigations (eg. Moore and Moore, 1984 and 1988; Atwater, 1986; Reinhardt and Bourgeois, 1989; Atwater and Yamaguchi, 1991; Minoura and Nakaya, 1991 and Foster, Albon, Bardell, Fletcher, Jardine, Mothers, Pritchard and Turner, 1991).

2. TSUNAMIS

The term tsunami is derived from the Japanese word "harbour wave" and is a rarely known phenomenon compared to other forms of sea waves. A tsunami can be described as a radially spreading, transoceanic, long-period and long-wave length gravity-wave system caused by any large-scale impulsive displacement of massive sea water. Tsunamis generally have wavelengths in the order of tens of kilometres, which are much greater than the depths of the oceans (typically several kilometres) and thus their propagation is governed by shallow-water wave hydrodynamics (Van Dorn, 1987). Tsunami wave periods are typically in the order of tens of minutes. Such waves are sometimes called 'tidal waves', which is a misnomer since tsunamis have nothing to do with tides in terms of either causal mechanisms or hydrodynamics.

Tsunamis are known to be caused by sudden displacements of a large volume of water over a wide area, associated with crustal deformation of the sea-floor, volcanic eruptions or/and submarine slides on large scales. Once a tsunami is generated, a train of waves disperse radially and propagate outwards from their source area across the ocean. In the deep ocean, the amplitudes of the tsunami waves are small and scarcely raise the sea surface (typically no more than 1-2 m). Tsunami waves are weakly energy-dissipative and thus the total energy of a tsunami wave is more or less conserved after travelling over a long distance whilst its

intensity (energy per unit along the ridge of the wave) decreases with distance from the source. The travelling velocity of a tsunami wave is controlled by the depth of the water which it travels through and can be approximately defined by the following equation:

where V is the velocity of the wave, g the gravitational acceleration, and D the depth of the water. A tsunami wave travels at a high speed in deep water and slows down in shallow water (cf. Wiegel, 1964).

When a tsunami wave reaches the coast, it encounters a shallowing seafloor and thus its velocity is reduced whilst its amplitude increases because the velocity is inversely proportional to the fourth root of the water depth. In areas close to the coast, the shallowing effect significantly reduces the speed of the front of the wave while the back swells into a wall of water and finally the waterbody grows unstable and surges upon the coastal lowlands as massive torrential currents of water.

Such a process is often complicated due to the effects caused by the offshore bathymetry, where wave reflection, refraction, diffraction and resonance take place as a result of the interaction of waves with irregular confining boundaries. Sometimes such effects can be so significant that resultant waves form complex patterns and their energy is unevenly distributed. In estuaries, the confining underwater valley sides and ever-narrowing channels can converge and trap wave energy. Consequently the waves can increase in size and cause great damage and loss of life.

3. OBJECTIVES AND STRUCTURE

The differentiation of sedimentary forms produced by various extreme coastal flooding processes have remained as a long-standing myth in geology. Tackling the detailed sedimentation issues is fundamentally necessary and is also an immensely huge task. Observational evidence has been found to be rather scarce and fragmentary, although

theoretical studies have attempted to be explanatory and coherent. This dissertation is primarily concerned with the geomorphological and sedimentological aspects of tsunamis. It is intended to put together the previous fragmentary scientific accounts and the author's detailed studies to further understanding of particular aspects of tsunami sedimentation. The aspects studied are not intended to provide a comprehensive analysis of tsunami characteristics, but it is hoped that the results here will add to current knowledge and further understanding of these fascinating phenomena. Sedimentary characteristics are the main factors studied here. As the sediments, lain down upon land by tsunamis, are often of limited thickness and do not possess distinctive structures, new sedimentological approaches are developed here for high-resolution studies designed to assist in the identification of the sedimentary processes involved. The objectives of this dissertation are to:

1) evaluate and apply high resolution sedimentological methods;
2) investigate and understand geomorphological changes and sedimentation processes associated with modern tsunamis; and describe particle size characteristics of modern tsunami sediments;
3) investigate a particular Holocene sediment layer interpreted as having been deposited by a palaeo-tsunami and infer the sedimentation processes involved;
4) evaluate competing hypotheses of storm surge and tsunami origin for the Holocene sediment layer in the coastal sediment sequences along the coast of eastern Scotland.

This account has three main foci and the structure of the dissertation is as follows:
Following a general introduction to tsunami phenomena in Chapter 1, Chapter 2 contains information on methods employed in this research, particularly with respect to techniques of particle size analysis including appraisal of the application of a newly available instrument (the Malvern Laser Granulometer) in high-resolution sedimentological studies. It also contains information on detailed experiments conducted in the evaluation and comparison of different analytical techniques of particle size study, including the Malvern Laser

Granulometer, which has been employed in the research, a sedimentation method (Sedigraph), dry sieving and the image analyser (Optomax). In search of high-resolution techniques, other analytical studies of sediments including mineral magnetic and geochemical analyses have also been employed. The descriptions and procedures of these are contained in this chapter.

Following a review of previous scientific investigations of coastal geomorphological processes associated with tsunami inundation in Chapter 3, Chapter 4, entitled "The 1992 Flores Tsunami", contains the first up-to-date detailed and comprehensive investigation, undertaken by the author, of coastal geomorphological and sedimentary changes and processes associated with a modern tsunami: the 1992 Flores tsunami, in Indonesia. Based upon field evidence and analytical results of high-resolution particle size analysis, downcore and lateral variations in particle size are described and deductions are made of tsunami sedimentation processes. Thereafter, inferences are also made with regard to a conceptual model of coastal geomorphological processes associated with tsunami flooding.

Chapter 5, entitled "The Second Storegga Slide Tsunami", examines evidence for an inferred *circa* 7,000 yrs B.P. tsunami along the eastern Scottish coast, thought to have been associated with one of the world's largest submarine landslides (the Second Storegga Slide). It examines the alternative hypotheses that the widespread flooding was caused either by a storm surge or by a tsunami and reviews the current knowledge of coastal sedimentary processes during storm surges as well as presenting the results of particle size analysis of the sediments deposited during the January 1978 North Sea storm surge event. Set in the context of glaciation history, land movement and relative sea level change since the last glacial maximum, it examines the sediments of the *circa* 7,000 yrs B.P. event with high-resolution sedimentological techniques at a number of sites along the Scottish coast and identifies the processes by which the sediment was laid down in an attempt to evaluate the

proposed origins of the event. The wider significance of the flood layer as a chrono-stratigraphic marker is also examined.

Finally, Chapter 6 presents a summary of the findings and conclusions made and existing problems indentified during this research.

The significance and implications of the findings are considered to be manifold, not only in aspects of geomorphology and sedimentology, but also in studies of coastal evolution as well as in development and application of high-resolution sedimentological methodology. It is hoped that this dissertation will provide useful information to many geo-scientists and further our understanding of aspects of tsunami sedimentation.

4. DEFINITION OF TERMS

The definition of technical terms of particle size, mineral magnetic and geochemical parameters is given together with the description of the methods in Chapter 2. As scientific study of tsunamis is relatively recent, there has not been a clarified and explicit system of terminology and some of terms have been used inconsistently. The following text attempts to clarify these terms used in the study.

Runup

A tsunami event often consists of a train of waves, frequently with different amplitudes, which propagate into coastal regions and subsequently inundate coastal lands. As a result, subsequent episodes of inundation often surge up to different elevations upon coastal land. Excursion of erosive saline water is manifested by various types of evidence, including debris and water marks on trees and buildings. As the highest flood level can be readily recognised without much doubt when immediate post-tsunami observation is made, it is often the most common one to be determined and referred to as **runup** in relation to the sea

level at the time when the tsunami struck. The determination of **runup** is often undertaken by measuring the highest flood level against the sea level contemporaneous with the observation, which is then corrected to the calculated sea level contemporaneous with the tsunami inundation. This descriptive concept is mostly in current use and the definition of **runup** is the maximum inundation level reached by a tsunami event in relation to the contemporaneous local sea level.

The term **runup** has also been used in various senses in other fields of the study. In mathematical/numerical modelling, it is often referred to as the highest predicted value of tsunami amplitude at any given point along the coast. In geological studies, since it is often difficult to determine the contemporaneous sea level, it has been referred to as the flood level indicated by geological evidence in relation to reference levels, such as a geologically inferred high water mark (Dawson *et al.*, 1989).

Moreover, the term **runup** has also been used to denote the up-surging process of one episode of tsunami wave. An alternative term to denote the process has been **upsurge**. **Runup** is adopted here, since the term is widespread in current usage.

Inundation distance

Inundation distance is used here to denote the maximum distance which a tsunami event reachs upon land perpendicular to and from the coastline at any given point.

Backwash

This term is used here to denote the drainage back of an elevated waterbody into the sea during an episode of tsunami inundation.

Sedimentation process

In this study, **sedimentation process** is defined as including processes of sediment **erosion/reworking, transportation** and **deposition** as well as associated **sorting** processes. In order to maintain a consistent conception in sedimentology, the term **sorting** is used here to denote the **processes** by which the particles are selectively or differentially transported or deposited, and also to indicate the **degree of uniformity** of particle size distribution of sediment. The sediment is described as 'well sorted' when the degree of uniformity is high, as indicated by the **kurtosis** and **standard deviation** of a particle size distribution (defined with the description of laboratory methods in Chapter 2). It is important to note that sorting is expressed on a relative term and is not specifically defined, since no classification scale has been ever designed specifically for the method employed.

In the establishment of a preliminary conceptual model of tsunami inundation, the **average velocity** or **energy** of a current is defined as the magnitude of a flow regime at any given time. The current possesses a specific **capacity** to transport a certain amount of sediment, related to the energy of that current. Sediment **load** denotes the actual amount of sediment the current carries at the time, which is less or equal to the capacity.

Chapter 2
Methodology

1. INTRODUCTION

Methods employed in this study include both field investigations and laboratory-based analytical techniques. Field investigations have primarily involved lithostratigraphical studies which have provided information on both sedimentary structures and relationships between sedimentary units. High-resolution analytical techniques have been used to study physical properties of sediments of particular interest and their vertical and lateral variations. Such information has provided information on the processes by which the sediments studied have been deposited. Applications of conventional methods are briefly described below, while newly applied techniques are assessed in detail and their values of application evaluated. In particular, a comparative study of particle size techniques has been undertaken and the suitability and accuracy of the instrument employed (Malvern Laser Granulometer 2600) are critically assessed.

2. FIELD STRATIGRAPHICAL SURVEY

The study of geomorphological changes associated with the 1992 Flores tsunami, Indonesia, was undertaken through a field survey two weeks after the event. The geomorphological

investigation and participation in flood level identification and measurement lasted for a period of nearly two weeks. Geomorphological changes were identified through visual inspection of coastal areas and interpreter-assisted interviews of local residents and eyewitnesses. During the field survey, tsunami sediments were visually identified with careful observation of partly-buried vegetation and ground surfaces. Visual inspection of stratigraphical and sedimentary structures related to the tsunami sediments, typically thin and loose, was made at sites through excavation. Sediment cores and surface samples for laboratory analysis were obtained with plastic tubes of 5 cm diameter at selected sites. Core tubes were first driven manually into the tsunami sediments and underlying deposits, and then the sediment was kept as undisturbed as possible.

For studies of the sediments deposited by palaeo-floods along the coast of eastern Scotland, geomorphological mapping on Ordnance Survey 1:10000 maps was undertaken and stratigraphical investigations were made using shallow coring equipment. Each borehole was instrumentally levelled relative to Ordnance Datum (Newlyn). Boreholes were made using Hiller pattern or Eijkelkamp Gouge samplers for the construction of cross-section profiles along traverse lines. The former has a cylindrical chamber of 3 cm in diameter and 33 cm in length whilst the latter has a semi-cylindrical chamber of 3 cm in diameter and 100 cm in length. A power-operated Stitz percussion corer (giving cores 5 cm in diameter and 1 to 1.2 m in length) was used for the collection of samples to be analysed. Occasionally samples were collected from exposed sections using monolith tins, and in this case surfaces were cleaned with spades and trowels before sampling. Lithological descriptions were made of cores and exposed sections following visual inspection.

3. LABORATORY TECHNIQUES

3.1 Introduction

Sediment accumulations are composed largely of various types of minerals, such as quartz, feldspar, magnetite and etc, that are present as grains of various sizes. Variations in the

mineralogy and grain size can provide information on processes of sedimentation. However, a combined classification of the content of both mineral grains and their sizes is difficult and immensely tedious to achieve, and consequently various methods have been developed to classify or study either the mineralogical or grain size composition of sediment.

Traditionally, studies of mineralogical composition is undertaken in elaborate and tedious ways: partition and identification of specific mineral grains or gravimetric separation of light and heavy minerals using liquids with intermediate specific gravities (e.g. bromoform), to yield statistics for the assessment of the heavy-mineral content of sands. Recent studies (de Meijer, Put , Schuiling, de Reus and Wiersma, 1988 and de Meijer, Lesscher, Schuiling and Elburg, 1990) have suggested that heavy-mineral composition is related to specific radioactivity and that variations in heavy-mineral content can be determined and estimated with radiometric methods.

In this research, sedimentological investigations have been undertaken using mineral magnetic, geochemical and particle size analyses (see below). Although the mineral magnetic and geochemical analyses employed do not provide information on the composition of specific mineral groups within the sediment, they offer valuable information on patterns of changes in the bulk properties of sediment which result from variations in magnetic mineral concentration. Detailed mineral magnetic analyses were undertaken on several cores from two sites (Dounie and Creich) at 1 cm intervals. Geochemical analysis was conducted on one core only (Core 56) from the site at Dounie. A more extensive sedimentological study was conducted with a laser granulometer (Malvern 2600), with which fine-interval classification of particle sizes of sediment can be made and their spatial variations can be studied at detailed resolutions. Descriptions of the methods employed and parameters are as follows:

3.2 Mineral magnetism

The analysis is employed here to study possible variations in the bulk mineral magnetic properties of sediment samples, which are related both to the mineralogical and particle size changes of sediments due to the interaction of magnetism-bearing particles. Since the sediment studied is composed largely of quartz grains which do not bear magnetism (diamagnetic), the presence of magnetic mineral grains will result in distinct signals in magnetic parameters. Thus, the variations in magnetic mineral parameters are thought to provide information on the changes in magnetic mineral concentration, which is believed to be associated with sedimentation processes since the magnetic minerals have heavier specific densities (Dearing, 1994). Natural minerals can be classified as ferromagnetic, ferrimagnetic, antiferromagnetic, paramagnetic and diamagnetic. Ferromagnetic and ferrimagnetic minerals retain some of their magnetism after being subject to a magnetic field, whereas paramagnetic minerals are susceptible to magnetization but tend to be weakly magnetised and do not retain their magnetism after removal from a field, whilst diamagnetic minerals resist magnetization. Antiferromagnetics have a property in which the atomic magnetic moments form an ordered array which alternates so as to produce no net total magnetic moment in zero applied magnetic field. All types of magnetic substance, except diamagnetic materials, behave as if they were paramagnetic above the Curie temperature. Here all experiments were undertaken at room temperature.

Visual inspection of the samples studied here revealed that the samples were predominantly composed of quartz grains, which are diamagnetic. Diamagnetism is extremely weak compared with other magnetic effects and so it tends to be swamped by all other types of magnetic behaviour. Diamagnetism arises from the interaction of an applied magnetic field with the orbital motion of electrons and it results in a very weak negative magnetisation. The magnetisation is lost as soon as the magnetic field is removed. Strong magnetic fields tend to repel diamagnetic materials. Diamagnetism is, for all practical purposes, independent of temperature. Many common natural minerals, such as quartz, feldspar and calcite exhibit

diamagnetic behaviour (Thompson and Oldfield, 1986). The measurement of various magnetic parameters of the samples were undertaken mainly following the methodology described by Thompson *et al.* (1986), and the description of the parameters measured in this study is as follows:

1. Magnetic Susceptibility (χ_{lf}, χ_{hf})

Magnetic susceptibility is the magnetization of a material per unit applied field, namely the ratio of magnetization induced to the intensity of the applied magnetic field. It describes the magnetic response of a substance to an applied magnetic field. In this study, the magnetic susceptibility of a sediment sample is measured with a dual magnetic susceptibility sensor for 10 ml volume sample holders and expressed as a mass specific susceptibility in a unit of $\mu m^3 kg^{-1}$. As only a small magnetic field is applied with the method (0.1 mT), such magnetizations are generally reversible so that no remanence is retained. In natural surface environments, magnetic susceptibility is often proportional to the concentration of ferrimagnetic minerals within a sample, e.g. magnetite, titanomagnetite and maghemite in the sample although in reality it is a complex parameter highly dependent upon the intrinsic susceptibility of individual 'magnetic' minerals in the sample, their grain size and shape. χ_{lf} and χ_{hf} are low frequency and high frequency susceptibility. The values of these are expressed in a mass specific unit of $\mu m^3 kg^{-1}$.

The following remnant magnetic measurements were undertaken using the Molspin magnetometer at room temperature (Dearing, 1994).

2. SIRM - Saturation Isothermal Remnant Magnetization

The samples are magnetised in an 0.8 T pulse magnetiser (Molspin Ltd). When the sample is removed from the pulse magnetiser it is returned to zero field and magnetization declines

from 'Saturation Isothermal Magnetization' (M_s) to SIRM. It measures the highest remnant level of the magnetism which is induced in the sample in an applied field. It is an indicator of the volume concentration of minerals retaining some of their magnetism after removal from the magnetization within a sample, and thus generally indicates the concentration of ferrimagnetic minerals since ferromagnetic minerals are either prone to weathering processes or rarely present in natural surface environments. The values of SIRM are expressed in a mass specific unit of mAm^2kg^{-1}.

3. SIRM/X - Saturation Remnance to Susceptibility Ratio (k Am^{-1})

4. S - Remnance Ratio

IRM (Isothermal Remnant Magnetization) is measured after the sample was remagnetized in a reverse -0.1 Tesla field. The remanence ratio 'S' is defined as -1*IRM/SIRM. The loss of magnetisation at back field of 0.1 Tesla will be due to the imperfect antiferrimagnets such as haematite and goethite. The values of S are dimensionless.

5. HIRM

It is the 'S' value expressed on an absolute basis, e.g. HIRM = SIRM*(1-S)/2. The values of SIRM are expressed in a unit of k Am^{-1}.

3.3 Geochemical analysis

The analytical procedures of sequential chemical extractions designed by Tessier, Campbell and Bisson (1979) were modified and used for analysing Core 56 at 1 cm intervals. The sequential extraction procedures can extract particular trace metal elements selectively by using appropriate chemical agents. These offer the advantage that the procedures simulate to a certain extent various environmental conditions to which the sediment may be subjected. Therefore, deductions can then be made about the trace metal levels likely to be observed under these conditions in the environment. The measured particulate trace ions of Na, Ca,

Mg and Mn were partitioned into the following four fractions:

1.Exchangeable - absorbed and water soluble ions;

2.Bonded to carbonates - Ca as $CaCO_3$ and Mg as $MgCO_3$;

3.Bonded to organic matter such as detritus of a living organism;

4.Residual - containing ions bonded to primary and secondary minerals.

Since the sediment studied had most likely been subject to underground water activities over a considerable period of time, the analysis is employed here to characterise the sediment and investigate the possibility of mineralogical changes within.

3.4 Particle size analysis

Particle size distributions of samples were determined using the Malvern laser granulometer. About 5 grams of each sample was used because in the particular sediment studied such a quantity was sufficient to enable a representative distribution to be obtained from the same sample and the difference between different samples to be determined (see Section 4.6.2, Chapter 2).

Since analysis of particle size composition was adopted as a scientific means of describing and studying physical properties of sediment, various types of statistical methods have been designed to describe particle size composition in a quantified manner. Most such devices are based upon normal distribution theory. As particle size distributions of natural sediment are found to be often close to normal distributions when expressed against a log-scale, a log-normal theory of particle size distribution has long been widely used and accepted as a conventional rule by geo-scientists. There are also a variety of graphical presentation methods which have been developed and widely used, including histograms, relative frequency curves and cumulative percentage curves.

Derived statistical parameters, based upon log-normal theory, provide a general characterisation of a particle size composition as a whole, and make it convenient to

undertake further statistical analysis of a large group of sediment samples. There are also a variety of statistical methods designed for this purpose, the level of sophistication of which is often high.

Although such statistical methods are certainly useful, it is important to note here that the parameters produced with these methods are the results of statistical generalization, which summarises and compresses information on particle size distributions. As a result, information on the composition of particle sizes is often obscured or lost. With the introduction of high-resolution particle size analysis, it is intended in this research to observe particle size composition and its variation, which are thought to provide important and valuable information upon sedimentary processes. Pronounced variations occur in certain sections of particle size distributions and these reflect changing compositions of particle sizes. Combined with the complicating factor of clearly non-normal distributions of a large number of samples, conventional statistical methods and their parameters are found not to be able to describe such variations satisfactorily. There are no available statistical methods yet developed for describing such variations in a satisfactory manner. Therefore, histograms or frequency curves are used here to illustrate compositions of particle sizes and their variations within sediments, including stacked histograms of consecutive samples.

There are methodological difficulties in designing a meaningful and practical calculation method for deriving statistical parameters. Many authors have worked with the problem in different ways (eg. Van Orstrand, 1925; Hatch and Choate, 1929; Krumbein, 1936; Friedman, 1962a and b; and Kane and Hubert, 1963). The method employed in this study adopts the formulae of moment statistics based on the log-normal theory, which have been widely used (McBride, 1971). The Malvern instrument provides analytical results in the form of percentages of different size classes and the lower and upper limits of the classes are in dimensions of micrometers (μm). The calculation used involves conversion of values in micrometers into phi values. The conversion is calculated from:

$$\text{phi } (\phi) = -1 \times \log_2 X \qquad 2.1$$

where X = the size in mm.

Mean is the mean diameter of particles in a sample and is calculated with the following equation.

$$\text{Mean (d)} = \frac{\Sigma X_i d_i}{\Sigma d_i} \qquad 2.2$$

where d_i is the midpoint of class i, namely the arithmetic mean of the higher and lower limits of the class (in phi). X_i is the percentage of particles in the size band i.

2. Standard deviation is a measure of the spread from the mean diameter and is calculated from:

$$\delta = \left[\frac{\Sigma(d_i - d)^2 X_i}{\Sigma X_i}\right]^{1/2} \qquad 2.3$$

3. Median the second quartile or 'middle size' of the particle size distribution. It is the size point that divides the distribution into two equal parts. The values used are provided by the instrument and are determined with a cubic spline program.

4. Skewness is a measure of the degree and direction which a frequency distribution leans to, i.e. the deviation from normality. It is calculated from:

$$s = \frac{\Sigma(d_i - d)^3 X_i}{\Sigma \delta^3 X_i} \qquad 2.4$$

5. **Kurtosis** is a measure of uniformity of a particle size distribution and is calculated from:

$$k = \frac{\Sigma X_i (d_i - d)^4}{100\,\delta^4} \qquad 2.5$$

Finally, it is important to note that the above moment statistical procedures are used in this dissertation to provide information for general reference only and are used for comparison with other work, since other scientists have used these. In fact, the particle size parameters given by such kinds of statistical methods are often inappropriate, and can be misleading when particle size distributions deviate from normal distributions. In this dissertation, interpretation the dynamics of sedimentation from the results of particle size analysis is made with particular attention to the modes and corresponding subpopulations and variations reflected by them rather than from the parameters derived with the moment statistics. Limited application of such parameters are made where distributions are predominantly unimodal and very close to normal distributions and that variations between samples are significantly large. The rationale of this interpretation is also highlighted by the following justification.

In this study, sediments are frequently found to be composed of particles that cluster into several subpopulations. Some of these particles are clay and fine silt, the hydrodynamic behaviour of which has been difficult to interpret. It has been generally regarded that fine sediments such as clay and fine silt are hydrodynamically cohesive. However, the size threshold between cohesive and non-cohesive particles is unknown. McCave *et al.* (1995) recently attempted to solve this problem by examining the dynamics of sediment erosion, depositon and aggregate breakup taking place on ocean floors. They suggested that this boundary lies at *circa.* 10 μm in grain size (determined with Sedigraph results) and that fine sediment behaviour is dominantly cohesive below 10 μm in grain size and non-cohesive

above this size. By inference, fine silt below 10 μm behaves cohesively in the same way as clay (< 2 μm), whereas non-cohesive grains with sizes greater than 10 μm can be subject to size sorting in response to hydrodynamic processes. Therefore, inferences regarding the dynamics of sediment transport and deposition can be made from variations in particle size composition in the size range greater than 10 μm, which reflect the associated sorting processes. In addition, the compositional characteristics can, in turn, be used to interpret provenances of sediment as a result of comparison in the size range below 10 μm. Furthermore, the study of modern tsunami sediment shows that modal peaks of populations in the size range finer than the coarsest subpopulation (much greater than 10 μm) reflect the characteristics of source sediment as a result of poor sorting. Since many particle size distributions are distinctively multi-modal and modal positions along the size scales remain relatively constant, the characteristics of the fine tails of particle size distributions are considered to reflect sediment provenances. This understanding has been applied in this study and can be found as a basis for interpretation throughout. It is noted that laser granulometers yield results clearly different than those of Sedigraphs, as indicated in the comparative study of laser granulometers and Sedigraphs (McCave *et al.*, 1995; also see Section 4.7, Chapter 4). However, although determined with Sedigraph results, the 10 μm boundary between cohesive and non-cohesive hydrodynamic behaviours of particles determined by McCave *et al.* still offers a general guide for interpreting results obtained with laser granulometers (refer to the diagramatic comparisons of results in McCave *et al.*, 1995 and Section 4.7, Chapter 2 in this dissertation).

4. EXAMINATION AND EVALUATION OF THE MALVERN GRANULOMETER 2600

4.1 Introduction

The particle size of fine sediment cannot be determined by direct measurement, and a variety of techniques have been developed in order to determine particle size. However, definition of particle size becomes problematic for particles which have a complex and non-spherical shape.

Only a sphere can be uniquely defined by one single linear dimension, i.e. its diameter. The size of a cube can be defined by the length of one of its edges. If the length is considered to be one unit, then the equivalent spherical diameter can be obtained by the following equation

$$d = \sqrt[3]{\frac{6V}{\pi}} \qquad 2.6$$

where V is the volume, giving 1.24 units. Thus, a particle passing through a square sieve with an aperture size of 1 unit theoretically has its diameter defined as 1.24 units by another instrument which determines spherical diameter of a particle. Moreover,when a cube rests on the most stable surface, the diameter of the projected area is 1.13 units, derived from the formula

$$d_a = 2\sqrt{\frac{A}{\pi}} \qquad 2.7$$

where A is the projected area.

The averaged diameter of the projected area of random orientations will be greater than 1.13 units. For an irregular particle, the relationship becomes much more complicated.

Particles in nature are rarely spherical and when one attempts to measure the size of a particle with an irregular shape by a single dimension, an assigned diameter has to be derived from a certain particle size-dependent property (see below).

Sieving is the most conventional and well-known technique for determining the particle size characteristics of the sediment, while many others have been developed. Different instruments use a variety of methods to measure particle size so that many different method-dependent or instrument-dependent diameters are produced. The diversity of the instruments available has led to a confusion about the nature of the different particle sizes referred to. The technique, or combination of techniques chosen to conduct the analysis, depends first on the purpose of the analysis. What is measured initially by any instrument is a property of the particle that is not only size-dependent but also depends largely on the nature and quantity of the sediments under investigation. The availability of a particular instrument, cost , ease of use, speed and accuracy need be also considered in choosing the most appropriate technique of measurement.

An objective of this study is to understand the differences in comparability, accuracy and coverage between several instruments and the analytical particle size distributions obtained with them. This is important to a correct interpretation of the analytical results since, to the least extent, any interpretation involves applying or referring to the established knowledge which has been somehow gained with various methods. In particular, emphasis is put on an evaluation of the suitability of the Malvern Laser Granulometer, Model 2600. The instruments compared include the Sedigraph 5000D, Malvern 2600, Square aperture sieves, and the Optomax V. The comparison of different instruments is inherently a huge task requiring detailed studies. It is not intended here to be exhaustive but to sum up the information obtained during the search for a suitable technique and to add to our knowledge on some specific aspects. Thus, the information given here focuses on some specific issues thought to be important in sedimentological investigation and interpretation, rather than

providing a comprehensive account.

Previous comparative studies of different instruments have been conducted on their respective capabilities and relative accuracy, and comparisons between them have been made (McCave, Bryant, Cook and Coughanowr, 1986; Singer and Anderson, 1988 and Allen, 1990). As particle sizes cover several hundreds or thousands of micrometres down to below one micrometre, as well as different forms from powder to paint pigment, the instruments have been designed for different size ranges, different materials and different applications (cf. Miller and Lines, 1988 and Allen, 1990). Comparative studies have been undertaken within particular size ranges since different instruments are capable of analysing samples in different size ranges. For example, McCave *et al.* (1995) compared various instruments for particle size analysis within a size range below 100 μm. Similarly, in this study, comparisons of the Malvern laser granulometer with the Sedigraph, Optomax and dry sieving methods can only be made in accordance with the size ranges which the instruments can sufficiently cover. The Sedigraph can only be suitably applied to grain sizes smaller than 100 μm, whereas the Optomax and dry sieving techniques can only be used to provide meaningful analytical results for grains coarser than silt (> 63 μm). Therefore, the comparisons of the Malvern laser granulometer with the other instruments are made in two separate size ranges: the Malvern with the Sedigraph in the silt and clay range and the Malvern with the Optomax and dry sieving methods in the sand range.

4.2 Derived parameters and distribution statistics

Since particle size is dependent on the instrument from which it is obtained, the definition of size is given in conjunction with the principle of the instrument in the respective section. A particle size distribution can be characterised in a simple and concise manner by a measure of the central tendency of the size distribution of individual particles (i.e. mean or median diameters), the spread about the central tendency (i.e. standard deviation or span) and the skewness. For the purpose of comparability, calculations follow the definitions of the parameters and their mode of calculation, as described by Malvern Instruments (1989) and

solely used in the study of these instruments. The calculation method employed by Malvern Instruments follows a different log-normal statistical model. Thus the results yielded from the calculation are different from those produced with the method used conventionally in geo-sciences. For the definitions of the parameters used in the sedimentological studies, see Section 3.4, Chapter 2.

1. Mean - mean diameter of particles in a sample. This is calculated using Equation 2.8.

$$\textbf{Mean (d)} = \frac{\Sigma X_i d_i}{\Sigma d_i} \qquad 2.8$$

where d_i = square root of the higher limit times the lower limit of size band i, namely the geometric mean of the higher and lower limit of size band i; X_i is the percentage in the size band i.

2. Standard deviation is a measure of the spread from the mean diameter and is calculated using equation 2.9.

$$\delta = \left[\frac{\Sigma(d_i - d)^2 X_i}{\Sigma X_i}\right]^{1/2} \qquad 2.9$$

3. Median the second quartile or 'middle size' of the particle size distribution. It is the size point that divides the distribution into two equal parts and is calculated with cubic spline programs (Malvern Instruments, personal communication).

4. Skewness is a measure of the degree and direction which a frequency distribution leans to, i.e. the deviation from normality, and is calculated using equation 2.10.

$$s = \frac{\Sigma(d_i - d)^3 X_i}{\Sigma \delta^3 X_i} \qquad 2.10$$

5. Span gives a measure of the width of the distribution relative to the median and is calculated according to equation 2.11.

$$\text{Span} = \frac{P(90)-P(10)}{P(50)} \qquad 2.11$$

P(90), P(10) and P(50) are the diameters in micrometers (μm) at percentage points 90, 10 and 50 on the undersize cumulative curve.

6. Uniformity is a measure of the absolute deviation from the median diameter and is defined in equation 2.12.

$$\text{Uniformity} = \frac{\Sigma V_i |P(50) - d_i|}{P(50)\ \Sigma V_i} \qquad 2.12$$

where Vi is the volume of grains in size band i.

It is important to note that the values obtained for each of the above parameters have different meanings between methods. For the Malvern and the Optomax, the results are presented as volume distribution. For dry sieving, results are presented as weight distribution and V_i represents the weight in the size band i. Detailed descriptions of these are given in the following respective sections.

4.3 Dry sieving

"Sieving is an obvious means of powder classification and it has been used since early Egyptian times for the preparation of foodstuffs" (Allen, 1990). The sieves in the Coventry laboratory are made of woven wire and have square apertures. Such sieve analysis is one of the simplest, traditional and most widely used methods of particle size analysis in environmental studies and covers the size ranges between 45 μm - 2,000 μm in most laboratories. Particles are sorted into categories depending on whether a particle can pass through a sieve with a pre-defined aperture size. The sieving operation may be undertaken

with assistance of water or not, namely wet or dry sieving, and the sediments are agitated manually or mechanically.

Two sand dune samples were analysed for the purpose of comparing results of particle size distributions in the sand range obtained using different instruments. To limit factors involved in the results of particle size analyses, such as the obvious influence of organic detrius on the results obtained with the laser and image analysers, these two standard samples were pretreated in the ways described below.

Sand A. A yellowish sand dune sample from the Scilly Isles provided by Dr. I. D. L. Foster. It has a low organic content and its main mineral component is irregularly shaped quartz grains. No treatment was given prior to analysis.

Sand B. A yellowish sand dune sample from the Dornoch Firth, Scotland with a relatively high organic content. It has similar mineral content to sand A. The treatment of this sample was as follows:

1. HCl was added to the sample to destroy carbonate cements.
2. H_2O_2 was added to remove organic material. The sand sample was left overnight to react and was heated for 3 hours on a hot plate on the following day. Additional H_2O_2 was added in to avoid desiccation.
3. The sample was ultrasonically treated several times and washed clean. A 63 μm sieve was used and anything that did not pass through was retained for further analysis.

Steps 2 and 3 were repeated 3 times so that a sample was produced which was free of any organic matter and with a minimum quantity of particles smaller than 63 μm in terms of the sieving diameter.

Dry sieving was employed and the sieves were shaken on a mechanical vibrator for twenty minutes. The sieves were chosen at 0.25 phi interval of aperture from 4.5 phi to 0 phi, i.e. 45 μm to 1,000 μm. Each analysis had to be divided into three sieving stages due to the loading limitation of sieves on the shaker. The results are given in Table 1 in Appendix A. Figure 2.1 is a graphical presentation of the results.

Figure 2.1 Frequency and cumulative curves of sand A and sand B obtained with dry sieving.

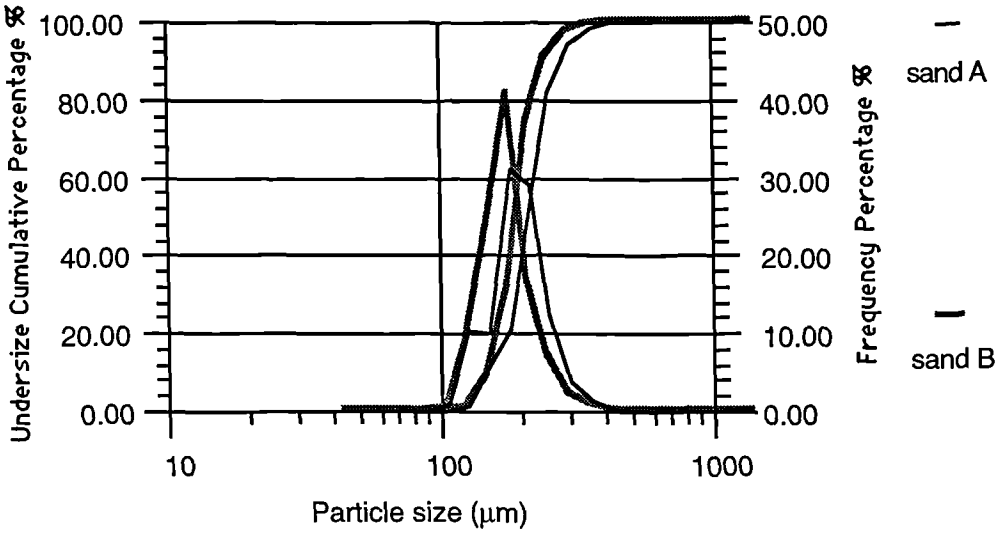

Table 2.1 Parameters of sand A and sand B obtained with dry sieving

	Mean μm	Median μm	Standard Deviation	Skewness	Span	Uniformity
Sand A	213	210	52.67	1.53	0.60	0.21
Sand B	198	193	43.80	1.58	0.52	0.15

Allen (1990) summarised the factors that influence the results of a sieving operation, such as the shape of the openings, sieve loading, presence of fine particles, method of agitation, time of sieving, particle shape, cohesiveness of the powder and friability. It is important to note that the diameter of the particle measured by sieving is the width of the minimum square aperture through which the particle will pass.

4.4 Sedimentation (Sedigraph)

The Sedigraph 5000D Particle Size Analyser is one of the devices using a sedimentation method to determine the size distribution of fine particles. It measures the sedimentation rates of particles in suspension. The instrument determines, by means of a finely collimated beam of X-rays, the concentration of particles remaining at decreasing sedimentation depths as a function of time. It can produce the size distribution within a maximum range of 100 to 0.1 μm, as a cumulative mass percent distribution in terms of the Stokes's diameter on a three-cycle, semi-log graph. Stokes's diameter is the free-falling diameter of a particle in the laminar flow region (Re < 0.2)* (Allen, 1990).

The typical size range yielded by the instrument is 50 to 0.18 μm. The time required for analysis is inversely proportional to the particle-liquid density differences and to the minimum size of sediment being analysed.

Subsamples of an estuarine deposit (carse) from Dounie, Dornoch Firth and of a suspended sediment from the Yellow River, China have been analysed with several replicate samples using the Sedigraph 5000D in the Geography Department of Exeter University. The samples were dispersed ultrasonically in a Calgon solution (defined in 3.4.2.6.1) for 5 minutes prior to the analysis. The results are shown in the Figures 2.2 and 2.3. Lines with different styles represent different results of measurements.

* Re stands for Reynolds number. The experimental relationship between the Reynolds number and drag coefficient shows a laminar flow or Stokes's region is restricted by Re < 0.2. It is assumed that in this region, the drag on a spherical particle falling in a viscous fluid of infinite extent is due entirely to viscous forces within the fluid when the terminal velocity is reached. Here, the drag force is equal to the motive force on the particle, that is, the difference between the gravitational attraction and the Archimedes upthrust. Hence, the size of the particle can be calculated. Beyond this critical region, the Stokes's Law becomes invalid. See Allen, 1990 (p252).

Figure 2.2 3 repeated measurements of the carse sample using the Sedigraph

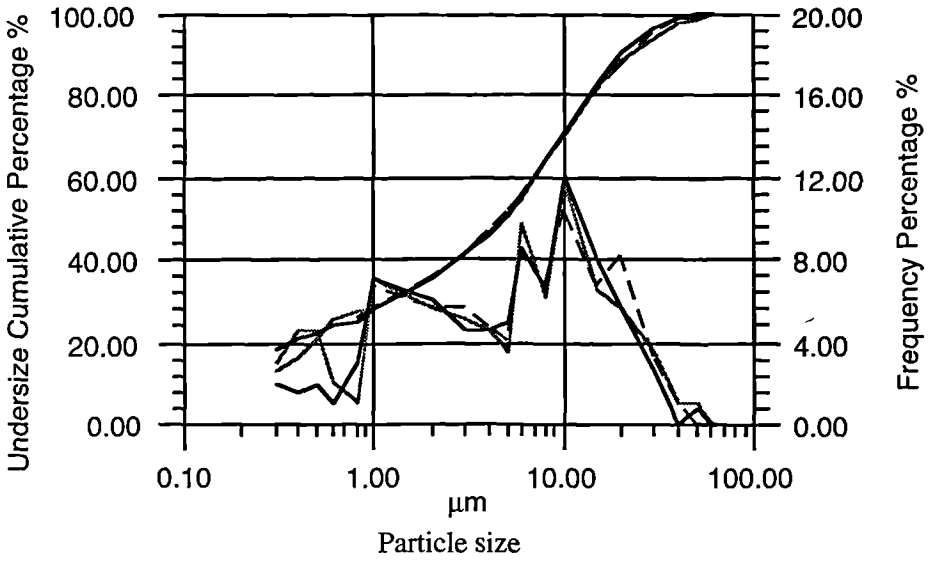

Figure 2.3 4 repeated measurements of Yellow River sediments in suspension using the Sedigraph

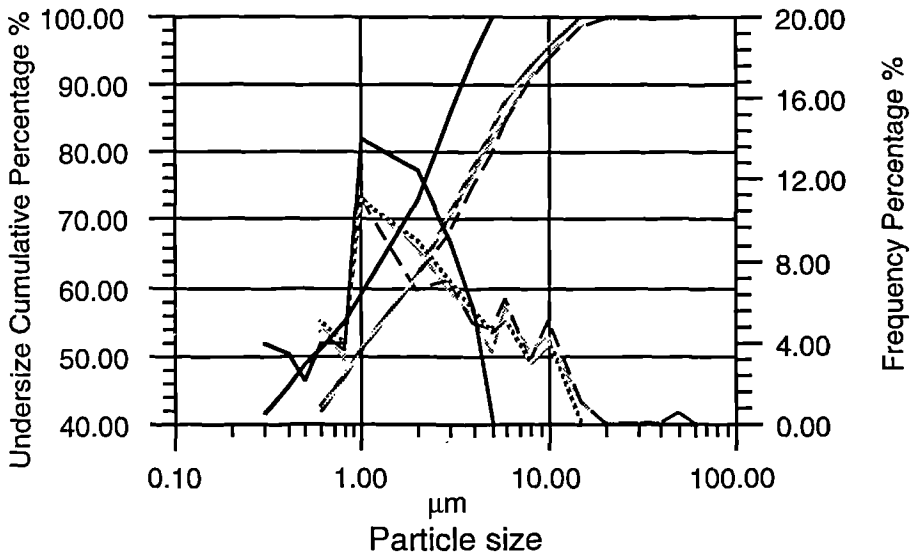

A Bentonite sample, which is believed to have a very fine and narrow size distribution, was also tested but no distribution result was obtained due to poor dispersion of the sample and severe flocculation.

Potential errors involved with the instrument can include the influence of the wall of the container; particle acceleration; heat input by the measuring system; particle-to-particle interaction; discontinuity of the fluid; Brownian Motion; diffusion; electronic and mechanical

factors (Allen, 1990, Sedigraph Manual). It is generally regarded that Brownian Motion becomes active when particles are as small as 1 μm.

4.5 Microscopy (Optomax)

Optomax V is an automatic image analysis device, which comprises an optical microscope, a TV camera and display, and an image-analyzing IBM computer. Together with other microscopic methods, optical microscopy is regarded as an absolute means of particle size classification in which the individual particles are examined and measured. Microscopy is also the only method that allows particle shape to be determined in a single system. Determination of particle shape is the commonly used function where particle size analysis can not be undertaken using other apparatus.

With Optomax, particles can be examined by the naked eye using binocular eyepieces, so that particles can be viewed in a three dimensional form using refractive lighting. Transmission light or back lighting is also available. However, the image of a particle that is taken by the camera to be counted is two-dimensional. This image is bit-mapped which is understood by the automatic image-analyzer as a gathering of many pixels. From this cluster of pixels the primary geometric properties of a particle can be measured, such as intercepts, Feret's diameter* (which depends on the direction of the measurement and orientation of a particle), perimeter, longest dimension, area and so on. From them some other parameters can be derived, such as sphere diameter and Form Factor. The last two were used in this study as they are more relevant to the matter being investigated. The definition of these are as follows.

Sphere diameter (actually projected area diameter), Da, is the diameter of a circle having the same area as a particle viewed normal to a plane surface on which the particle is at rest in a stable position (Allen,1990).

* Feret's diameter is the distance between two tangents on opposite sides of the particle, parallel to some fixed direction.

$$d_a = 2\sqrt{\frac{\overline{Area}}{\pi}} \qquad 2.13$$

Form factor is an estimation of roundness of a particle, i.e. shape of a particle, and is defined as equation 1.7.

$$\text{Form Factor} = \frac{4\pi x \text{Area}}{\text{Perimeter}^2} \qquad 2.14$$

A graticule was used to calibrate the image analyzer, i.e. build a relationship between a distance and pixels. The magnification x5 was chosen for the sand samples and the calibration scale is 6.02 microns per pixel. Sand A and sand B (described in Section 4.3 above) were used for the analysis and several slides for each sample were carefully produced to gain a good dispersion of sand grains on the slides. The data from the analysis are contained in Table 2, Appendix A. The size distributions are shown as Figures 2.4 and 2.5, and the variations of the descriptive parameters can be seen in Table 2.2.

Allen (1990) summarised particle size measurement using optical microscopy and suggested that a severe limitation of the method is the depth of focus. The level of focus and resolution of the detector or image analyzer play critical roles. At the x5 magnification, the calibration factor is about 6.02 μm/pixel. This would result in a potential error of 12% at 50 microns, 6% at 100 microns and 2% at 300 microns and shows that the effect of the calibration resolution (6.02 microns per pixel) is more serious for small particles. Different magnifications will need different calibrations and these give different resolutions. Therefore measurement of grain size does not maintain a constant linear resolution.

Figure 2.4 6 repeated measurements of Sand A with the Optomax

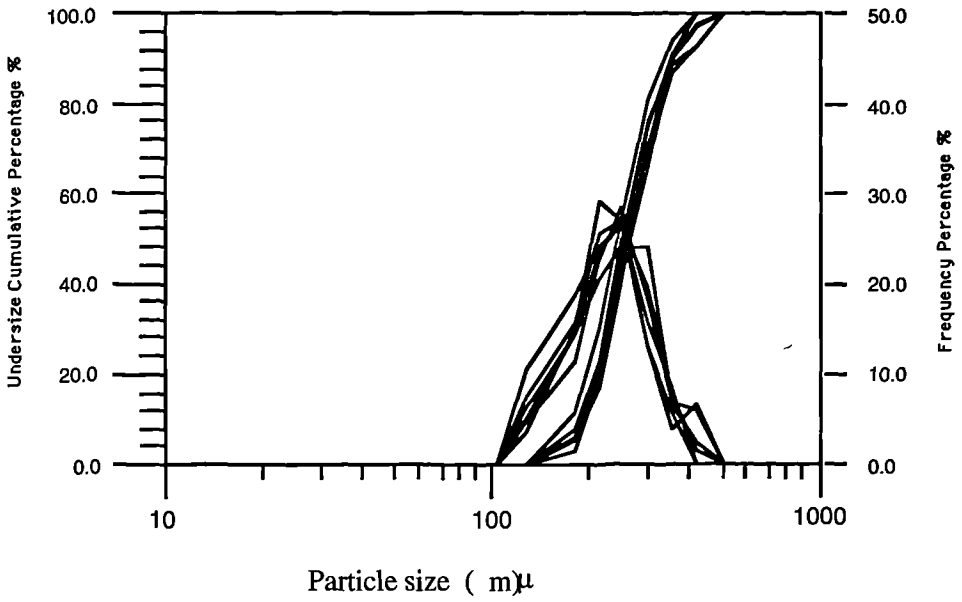

Figure 2.5 4 measurements of sand B with the Optomax

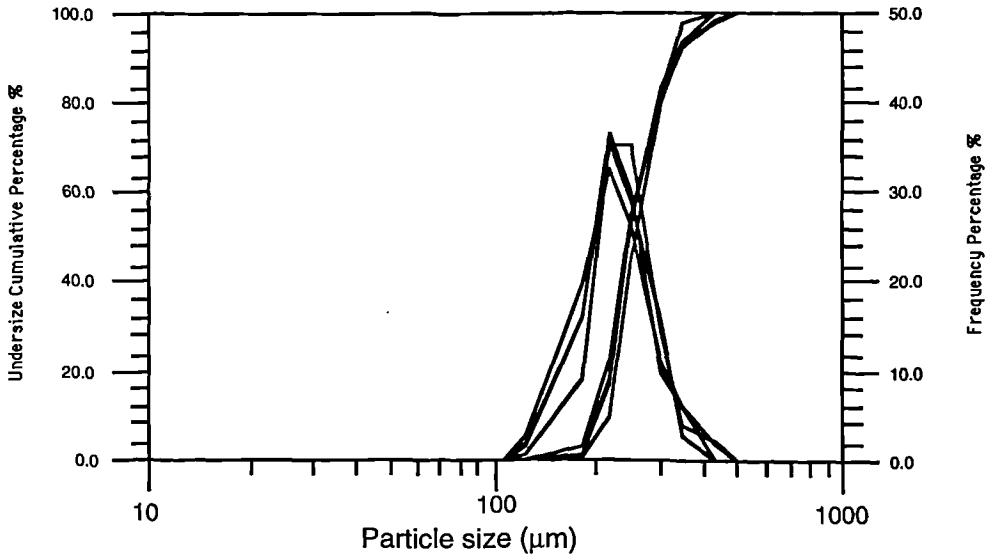

Table 2.2 Descriptive statistics on the parameters of particle size distribution obtained with the Optomax

Sand A	N	MEAN	STDEV	MIN	MAX	95.0 PERCENT C.I.		99.0 PERCENT C.I.	
Mean (μm)	6	264.81	9.98	247.16	276.76	254.33	275.29	248.38	281.24
Median (μm)	6	257	9.96	242	268	246.54	267.46	240.6	273.4
Standard deviation	6	68.58	6.85	59.56	76.76	61.39	75.78	57.31	79.86
Skewness	6	0.5317	0.2352	0.3	0.94	0.2847	0.7786	0.1444	0.9189
Span	6	0.6483	0.0412	0.61	0.71	0.6051	0.6916	0.5805	0.7161
Uniformity	6	0.21	0.01265	0.19	0.23	0.19672	0.22328	0.18918	0.23082

Sand B	N	MEAN	STDEV	MIN	MAX	95.0 PERCENT C.I.		99.0 PERCENT C.I.	
Mean (μm)	4	258.53	5.62	254.76	266.86	249.58	267.48	242.1	274.95
Median (μm)	4	248.25	5.32	244	256	239.79	256.71	232.73	263.77
Standard deviation	4	53.72	5.28	48.19	60.56	45.33	62.12	38.31	69.13
Skewness	4	0.925	0.306	0.53	1.24	0.438	1.412	0.032	1.818
Span	4	0.5175	0.0492	0.48	0.59	0.4391	0.5959	0.3737	0.6613
Uniformity	4	0.1675	0.015	0.16	0.19	0.14363	0.19137	0.12369	0.21131

Sampling techniques and sample preparation also play a critical part in the representativeness of a sample due to the minute quantities of particles under examination. It is very hard to produce such a slide that can be representative of the entire size distribution. The repeatability of sizing the sand samples is shown in Figures 2.4 and 2.5, and statistically in Table 2.2. These factors also imply that measurement obtained with this system varies between operators. The method covers a limited range and can not be used for analysing very fine particles in the fine silt and clay range.

4.6 Laser diffraction (Malvern 2600)

The success of the industrial application of the Fraunhofer diffraction (also known as far-field, or low angle diffraction) principle of laser light has resulted in a rapid growth in the use of such instruments recently (Miller *et al.*, 1988). The Malvern 2600 is a laser particle size analyzer that comprises an optical measurement unit that senses the scattered monochromatic light pattern and a computer that converts the light energy distribution on the detector rings into a size distribution of particles producing results in graphical and tabular form.

The system employs conventional Fourier optics so that the scattering of a laser beam by a particle depends on its size regardless of its motion and position in the laser path (Malvern Instruments, 1989). Small particles scatter light at high angles and larger particles at low angles. The diameter produced is the volume diameter - the diameter of a sphere having the same volume as the particle.

Since Helium-Neon laser light has a wavelength of approximately 0.6 μm, and there are different focal lenses available with the Model 2600, the size range that can be detected by the Malvern is very wide (Figure 2.6). Because available instruments cover different size

Figure 2.6 Particle size ranges with different focal lengths

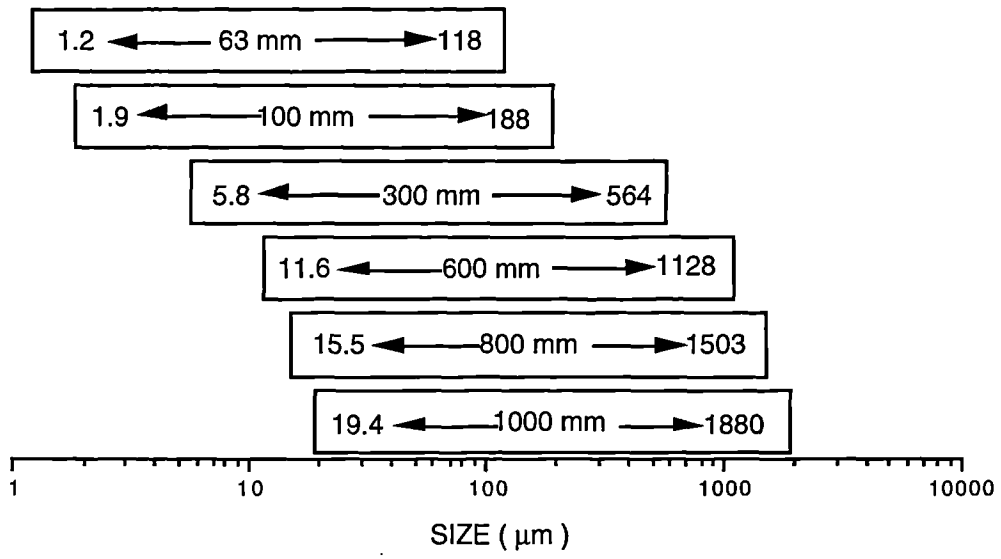

ranges and the intercomparison of particle size distribution obtained with different instruments becomes complex due to the effect of other properties of particles, the following section explores the capability and suitability of application of the Malvern Laser Granulometer in sediment studies in the silt and clay range and in the sand range, and makes comparisons with other methods.

4.6.1 Requirements of Sample Preparation

The necessity of pre-treatment depends on the properties of the sample and purpose of the study. For coarse particles (eg. sand), good dispersion and measurement can be achieved

solely by mechanical dispersion, such as by mechanical and ultrasonic stirring. This can only be achieved if foreign material such as organic matter has been excluded and binding of the particles has been broken down. It was found that sand samples can be well dispersed in a very short time with mechanical and ultrasonic dispersion and that the effect of the Calgon solution is not significant.

For samples comprising fine particles, a combination of chemical and physical methods are needed to achieve a good dispersion of particles. Several samples, such as carse clay and suspended sediments from the the Yellow River, were used to find out whether a chemical dispersion was required. They were left in the Malvern system and agitated mechanically using the ultrasonic bath of the system. The results were taken automatically at regular intervals. As the process was repeated, the particle size distribution became finer. It took approximately 15 to 20 minutes for it to reach a stable position. It is generally regarded that the maximum presence of fine particles indicates a good dispersion so that a sample comprising fine particles needs a suitable dispersant to aid this process.

Two surfactant solutions were used as the dispersant agents. One is Nonidet and the other is Calgon. It was found that Nonidet caused bubbles in the solution and flocculation. This may have been caused by a wrong concentration of the solution. The Calgon solution (0.4 % sodium hexametaphosphate) currently used with the Sedigraph in Exeter University is made of 6.7 gm sodium hexametaphosphate and 1.3 gm sodium carbonate dissolved in 2 litres of distilled water. The same dispersant appeared to work efficiently with the Malvern.

There are many different dispersing solutions which may be used for different types of materials. the majority of them are surface active agents. Bernhardt (1988) discussed comprehensively different dispersing processes in terms of binding mechanisms and gave recommendations for different dispersing agents for different materials.

4.6.2 Repeatability of Measurements

In order to test whether the same particle size distribution can be reproduced by analysing the same sample, the factors by which a sample may affect the results should be minimised. These factors can be the effect of certain properties of a sample, such as friability, and attachment of particles to each other, which may be broken apart by the ultrasonic sound of the system while measurements are made. The sample used was a subsample of about 5 to 6 gms from sand B, which was placed in the ultrasonic bath for a further 40 minutes. It was then analysed with 800 mm lens and left circulating within the system while 30 measurements were obtained automatically at an interval of about 52 seconds. There is no guarantee, however, within the 52 second count period, that the same particles are always measured.

Table 2.3 The descriptive statistics and confidence intervals (95% and 99%) of mean, median and span etc.

Parameters	MEAN	MEDIAN	STDEV	MIN	MAX	95.0 PERCENT C.I.	99.0 PERCENT C.I.
mean(μm)	240.75	241.47	1.75	237.41	244.32	(240.097, 241.404)	(239.870, 241.631)
median(μm)	228.95	228.47	1.49	226.15	231.93	(228.394, 229.506)	(228.201, 229.700)
SD	78.823	78.725	3.858	70.88	90	(77.382,80.264)	(76.882,80.765)
skew	2.578	2.2	0.906	1.46	4.99	(2.239,2.916)	(2.122,3.034)
span	0.64733	0.65	0.0286	0.59	0.69	(0.63664, 0.65803)	(0.63292, 0.66175)
unif	0.22767	0.23	0.0077	0.21	0.24	(0.22478, 0.23056)	(0.22377, 0.23156)

The statistical table shows that the Malvern 2600 adequately reproduces the size distribution. The small variations could be due to the differences between particle subpopulations that were present in the laser path during the short measurement period. This can be improved by prolonging measurement duration if desired.

Do different lenses produce different results? It was reported that different particle size distributions were produced by different lenses of the Model 3000D of Malvern granulometer (McCave *et al.*, 1986). Wanogho (1985), however, found that the Malvern 3000D's different lenses produce the same results. In order to examine this problem, analysis was undertaken on sand B. Ten subsamples of about 5 to 6 grammes were

analysed with 600, 800 and 1,000 mm lenses respectively. The variations of the parameters, such as median, mean, standard deviation, skewness, span and uniformity, obtained from the subsamples with each of the three lenses are shown in the Table 2.4.

Table 2.4 Descriptive statistics on the parameters of particle size distribution of Sand B obtained with three different lenses of the Malvern granulometer. (Codes 08, 10 and 06 indicate for the 800, 1000 and 600 mm lens respectively and median and mean values are in μm)

	N	MEAN	MEDIAN	STDEV	MIN	MAX	95.0 PERCENT C.I.		99.0 PERCENT C.I.	
median08	10	240.58	240.32	3.99	235.63	249.15	237.73	243.43	236.48	244.68
median10	10	239.27	238.85	1.97	236.39	243.39	237.86	240.682	237.243	241.299
median06	10	242.71	241.51	2.81	239.68	247.38	240.697	244.725	239.818	245.604
mean08	10	253.65	252.84	5.72	247.01	267.7	249.56	257.74	247.78	259.53
mean10	10	251.96	252.23	4.16	246.38	260.49	248.98	254.93	247.67	256.24
mean06	10	252.46	251.55	3.84	247.56	257.64	249.72	255.21	248.52	256.41
SD08	10	85.95	84.18	5.84	80.38	100.31	81.77	90.13	79.94	91.95
SD10	10	102.29	99.04	16.05	81.18	136.8	90.8	113.77	85.78	118.79
SD06	10	90.61	91.51	5.2	80.34	95.97	86.89	94.33	85.26	95.95
skew08	10	2.702	2.22	1.059	1.74	4.95	1.944	3.46	1.614	3.79
skew10	10	6.035	6.09	0.827	4.81	7.28	5.443	6.627	5.185	6.885
skew06	10	4.006	4	0.2981	3.43	4.55	3.7927	4.2193	3.6995	4.3125
span08	10	0.674	0.66	0.0453	0.64	0.79	0.6416	0.7064	0.6275	0.7205
span10	10	0.64	0.64	0.0210	0.61	0.68	0.62491	0.65509	0.61833	0.66167
span06	10	0.649	0.65	0.0172	0.63	0.69	0.63663	0.66137	0.63123	0.66677
unif08	10	0.231	0.23	0.0152	0.22	0.27	0.2201	0.2419	0.21534	0.24666
unif10	10	0.234	0.23	0.0150	0.22	0.27	0.22323	0.24477	0.21852	0.24948
unif06	10	0.226	0.23	0.0084	0.21	0.24	0.21997	0.23203	0.21733	0.23467

Median, mean, span and uniformity show small deviations around their averaged values whereas standard deviation and skewness are significantly variable, within measurements with particular lenses and between lenses.

One way analysis of variance was used to test the similarity (agreement) of each parameter from the three sets. The result of the statistical test shows there is good agreement for the parameters, such as median, mean, span and uniformity at the 95% confidence level. Although there is a possibility that averaged diameters, especially median, are different from each other, the difference is only in the order of 1 to 2 microns.

The standard deviation and skewness varied significantly. The discrepancies between different measurements of standard deviation and skewness could be due to the way in

which they are calculated, which is very sensitive to small variations and to different lenses covering different ranges. It could also be due to a strong sensitivity to the minute quantity of particles measured. There is no guarantee that the same particles were in the laser path when a measurement was taken. Smaller variations can be achieved by prolonging the duration of the experiment. The "Sweeps"function available on the Malvern is used to reset the number of sweeps of the detector to be made for sample or background measurements etc. The data obtained by the sweeps of the detector is an averaged value.

4.7 Comparison of Malvern Laser Granulometer with other instruments designed to measure silt and clay

In earlier studies emphasis was placed on the silt and clay size range since some of the instruments can only cover this range (eg. McCave, 1986; Singer *et al.*, 1988). The comparison study relies highly on the way in which a standard is prepared. The original results produced with the Sedigraph, in the form of an undersize percentage cumulative curve, commences measurement at 63 μm. The results obtained with the Malvern are truncated to show a cumulative curve under 63 μm in order to enable direct comparisons to be made. Graphical comparison of results obtained with the Sedigraph and Malvern in Figures 2.7 and 2.8 shows that the differences are very significant. The Sedigraph yielded much finer size distributions than the Malvern although there appears to be some correspondence of modal peaks between the results. Similar findings were obtained by McCave *et al.* (1995), who appeared to doubt the validity of the Sedigraph result.

Why are the results with the Malvern much coarser than the ones with Sedigraph ? Singer *et al.* (1988) made two sets of standards with 0.5 phi interval by repeatedly decanting unsorted glacial silt and milled Ottawa sand using Stokes's Law. They employed four instruments, namely The Malvern Laser Sizer, Electrozone Particle Counter, Sedigraph, and hydrophotometer operated by different individuals who were not told of the real intention. They suggested that the effect of densities of different particles played their parts in the differences of particle size classifications as determined by the four techniques. Singer *et al.*

concluded that the Malvern Laser Sizer, Electrozone Particle Counter, Sedigraph, and hydrophotometer performed well in the analysis of sorted silt standards. Sedigraph and hydrophotometer results show high proportions in the glacial silt standards finer than 6.0 phi. These differences are attributed according to the sediment property measured.

Figure 2.7 Particle size distributions of an estuarine clay sample obtained with the Malvern and Sedigraph

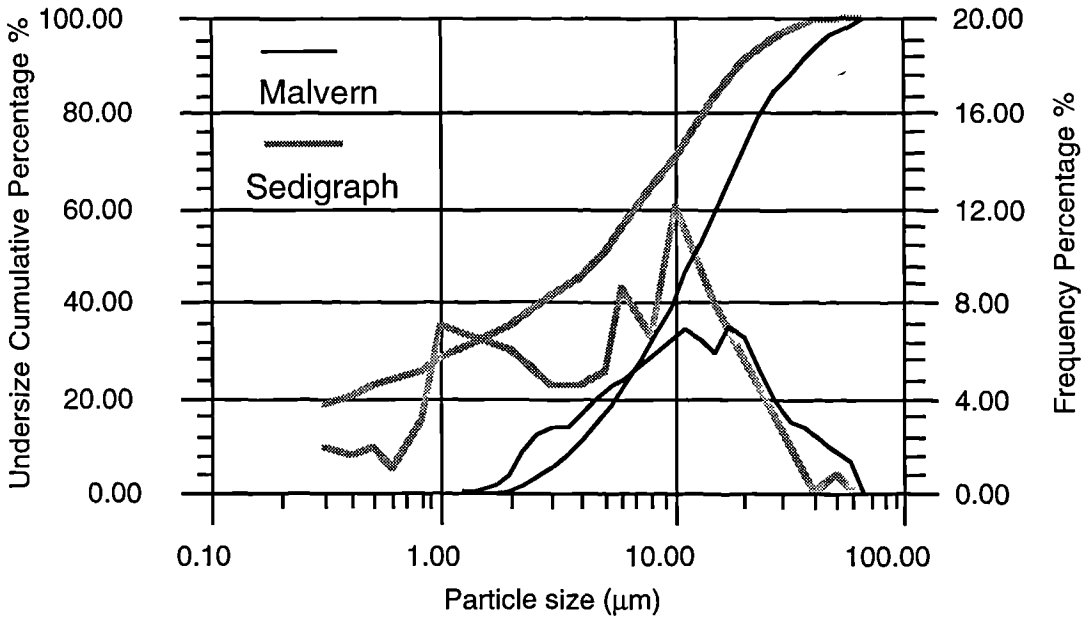

Figure 2.8 Particle size distributions of a Yellow River sediment in suspension obtained with the Malvern and Sedigraph

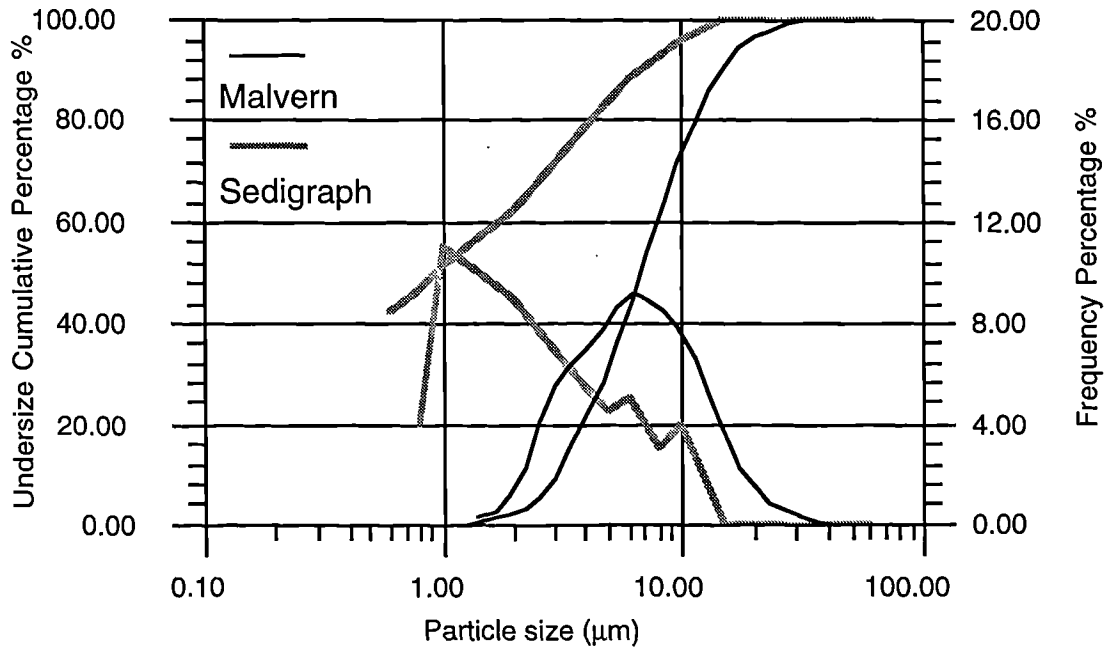

The lower limit that should be sized using gravitational sedimentation is 1 μm because Brownian Motion becomes significant below this limit; therefore, absolute size data in the submicron range from the Sedigraph is of questionable reliability. Singer *et al.* (1988) suggested that "no specific concentration is required for the analysis, providing the dispersed sample reduces the radiation beam by 60 percent to 40 percent." They also suggested that "an improper shift toward finer grain sizes occurs for concentrations greater than 2-3 Vol. %(about 50-75 g/L), and a 1.0 g sample with concentration 20 g/l is recommended(i.e., <1 Vol. %)." Therefore, it seems very difficult to establish practical conversions of the results obtained with different instruments through comparative studies. However, Wanogho (1985) suggested that there is a good agreement between sieving and the Malvern results.

4.8 Comparison of the Malvern with other instruments in the sand range

Before a comparison is made between the dry sieving and the Malvern, it has to be assumed that since sand A and sand B mainly comprise quartz grains, the averaged density of each size band has to be assumed to remain the same. Furthermore, the averaged particle shape of each band is assumed to be unchanged.

Figure 2.9 Graphical comparison of the particle size distributions of Sand A obtained with dry sieving, the Malvern and Optomax.

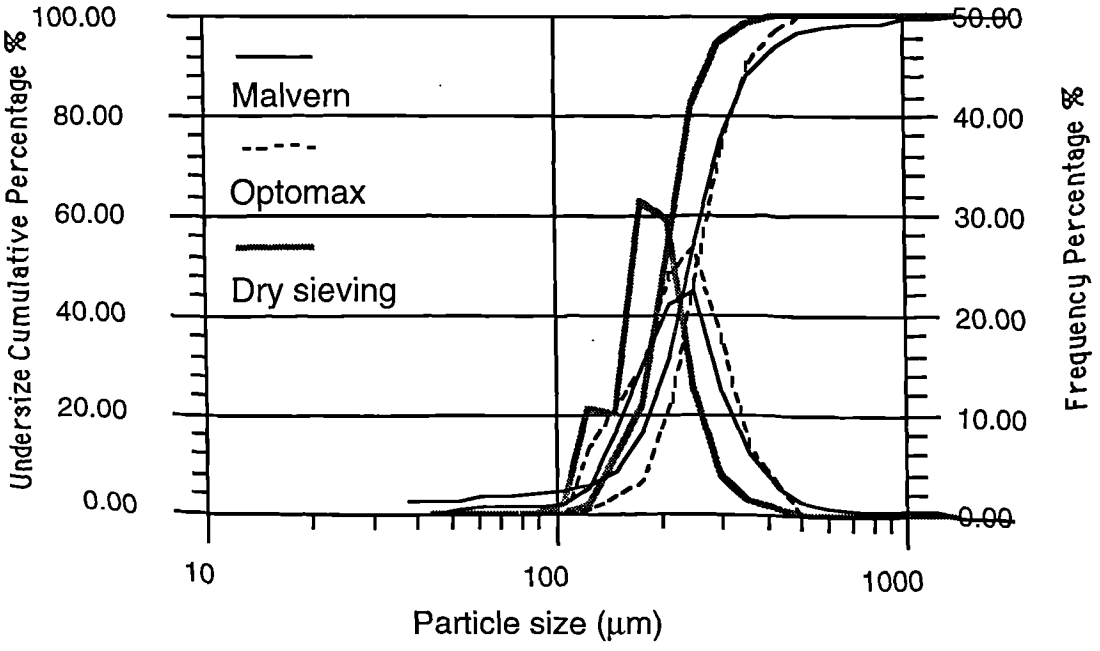

The particle size distributions obtained with the Malven, Optomax and Dry Sieving are compared graphically in Figures 2.9 and 2.10. Both figures show that the Malvern and Optomax have a good agreement considering that they measure different properties of particles. The difference is that the Optomax produces a peaked distribution whereas the Malvern produces a broad one. Figure 2.11 shows the wide distribution of form factors (defined in section 4.5, Chapter 2) of particles, reflecting significant differences in the shapes of particles.

Figure 2.10 Graphical comparison of the particle size distributions of sand B obtained with dry sieving, the Malvern and Optomax.

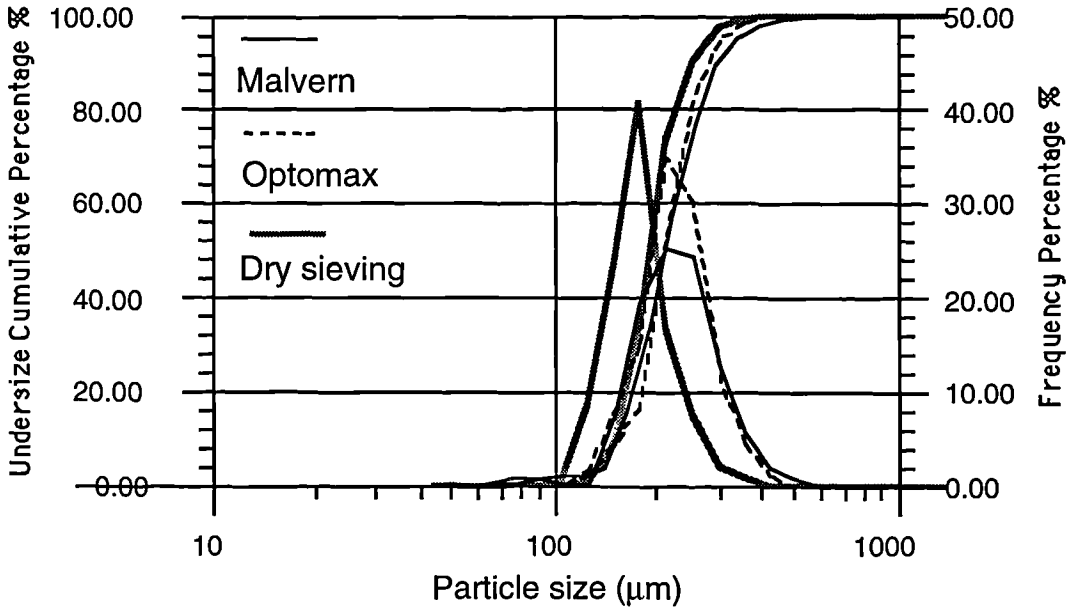

Figure 2.11 The scatterplot of form factor versus particle size for sand B

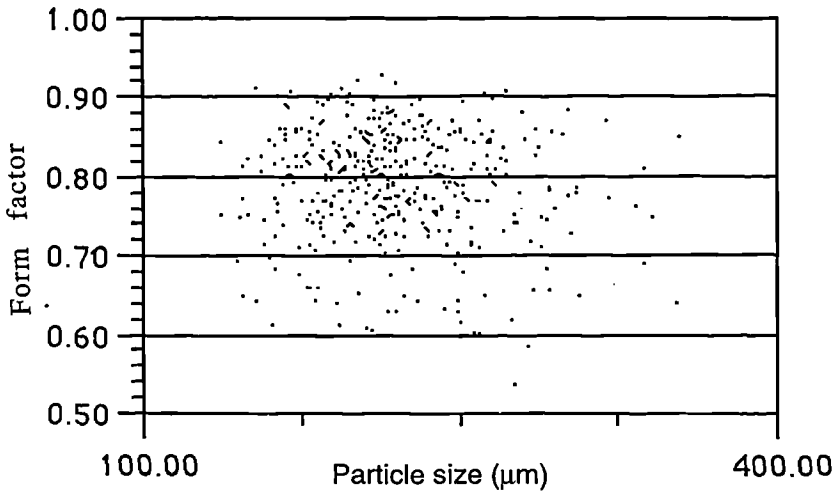

The dry sieving results are generally finer compared with the last two methods. This may well be due to the fact that a sieve measures the intermediate diameter of a particle. The Malvern produces a significant long tail towards the fine end for Sand A. This may be due to the much enhanced performance of dispersion by the Malvern compared to the other two methods (sieving and Optomax). It can be seen that many fine particles were separated from the surfaces of big particles by ultrasonic and mechanical stirring prior to measurement by the Malvern. It was found by examination under a microscope that quartz particles became much clearer after being dispersed ultrasonically in the Malvern system. This is confirmed by comparison of the histograms of the original sample of Sand B and pre-treated Sand B. The former indicates the presence of fine particles, whilst the latter does not possess any significant tail as a result of removal of fine particles during the pre-treatment (see Section 4.3, Chapter 2).

4.9 Conclusion

The following conclusions can be made:

1. Different properties of particles are measured by different instruments so that comparison of results obtained from them reveals significant differences.

2. The method of dry sieving is generally used with large intervals in sieve apertures. When a detailed size distribution is desired, and many sieves are employed, the analysis takes a long time and a large quantity of sample is required to produce a representative result. It is very often the case that fractionation is undertaken and the sub 63 μm fraction is analysed by another instrument.

3. As it is often unknown what types and proportion of minerals are contained in a natural clay sample to be sized, there is an uncertainty with the Sedigraph regarding the influence of interaction and settling behaviour of particles with significantly higher or lower specific gravities. For example, mica has a low density and flaky shape and settles slowly. A good knowledge of the average density of the sample is crucially important as the size distribution is derived from it. The uncertainty with the Sedigraph is related to a few critical factors. It is generally used in conjunction with the sieving method as it covers the sub 100

μm range.

4. The Optomax is a very useful instrument when particle shape is to be considered and produces similar results to the Malvern. However, it is very time consuming to analyse a representative particle size distribution from a sample.

5. The Malvern 2600 is a very versatile, high speed, highly reproducible and suitable particle size analyzer for sediment study. It can cover a wide range of particle sizes and types of material so that a sediment can often be analysed without fractionation. Only small quantities of a sample are required and this can be of great practical value.

Some limitations with the Malvern may be overcome by fine-tuning the configuration of the system or upgrading the software with better solutions in terms of interpreting or converting the light energy into a size distribution of particle size. For example, duration of measurement of a very coarse sample can be prolonged to achieve an average distribution that could be more representative of its parent distribution. In view of the high reproducibility demonstrated by the instrument and the requirement for only a small quantity of sample, the Malvern Laser Granulometer was employed in the work described in the following text. It permits the granulometric variations within sediments composed of a wide range of particles including sand grains to be investigated on a far finer resolution in a clarified manner than has previously been possible. It is only through such detailed investigations that realistic interpretations of sedimentary processes can be achieved, especially given that sediment cores are of limited thickness.

Chapter 3

Previous Scientific Investigations of Coastal Geomorphological Processes Associated with Tsunami Inundation

1. INTRODUCTION

In recent years, detailed stratigraphical and sedimentological studies have disclosed evidence for palaeo-tsunamis in coastal sedimentary sequences (eg. Atwater, 1986 and Dawson, Long and Smith, 1988). Such studies have examined a variety of geological evidence including, in particular, the intercalation of sediment layers reflecting high-magnitude low-frequency events within deposits accumulated in low-energy environments. The sediments reflective of high energy regime have been correlated with tsunami-genic events, such as offshore earthquakes, offshore volcanic activity or submarine landslides thought to be of similar age. Mathematical/numerical models have been used to model water displacement, the likely form of the tsunami waves and the extent of tsunami runup at the coast. However, at present, little is known of the coastal sedimentary processes and the characteristics of the sediments associated with tsunami flooding.

In the following pages a review is presented of previous accounts of the characteristics of tsunami sediments as well as the geomorphological and sedimentological effects associated with tsunami flooding. The following review describes geological aspects of tsunami events as well as of interpretations of particular deposits considered to have been deposited by palaeotsunamis.

2. RECENT TSUNAMI EVENTS

There have been some general accounts of historical and modern tsunamis (e.g. Myles, 1985), which, in the main, provide information upon the destructive effects but do not provide detailed information upon sedimentation processes associated with tsunamis. It is clear from such accounts that tsunamis are one of the most powerful geomorphological agents and can be immensely destructive (eg. Myles, 1985). Few studies, however, noted detailed specific coastal effects of tsunami (Jaggar, 1946; Miller, 1960 and Lemke, 1967). These effects include the breaching of coastal barriers (beaches and dunes), and the transportation and deposition of sediments. In recent years, there has been an increase in the detailed description and study of the detailed geomorphological effects of tsunamis, e.g. the 1992 Nicaraguan tsunami (Bourgeios, 1993), the 1983 and 1993 tsunamis in the Japan Sea (Sato *et al.*, 1995) and the 1994 Java tsunami (Dawson, Shuto and Takahashi, 1995) (Figure 3.1).

Among the limited number of geomorphological accounts of recent tsunamis, one of the most important is an investigation of the 1960 seismic disturbance and tsunami along part of the Chilean coast (Wright and Mella, 1963). A severe earthquake took place at 10:02 GMT on the 21st of May, 1960, with its epicentre in the Pacific Ocean west of the Arauco peninsula (Figure 3.2). Further shocks on the following day were accompanied by tsunamis, which caused severe effects along the coastline between the Arauco Peninsula and the southern tip of Chiloe Island. A survey was undertaken two weeks after the event.

Figure 3.1. World map of the location of areas mentioned in the text.

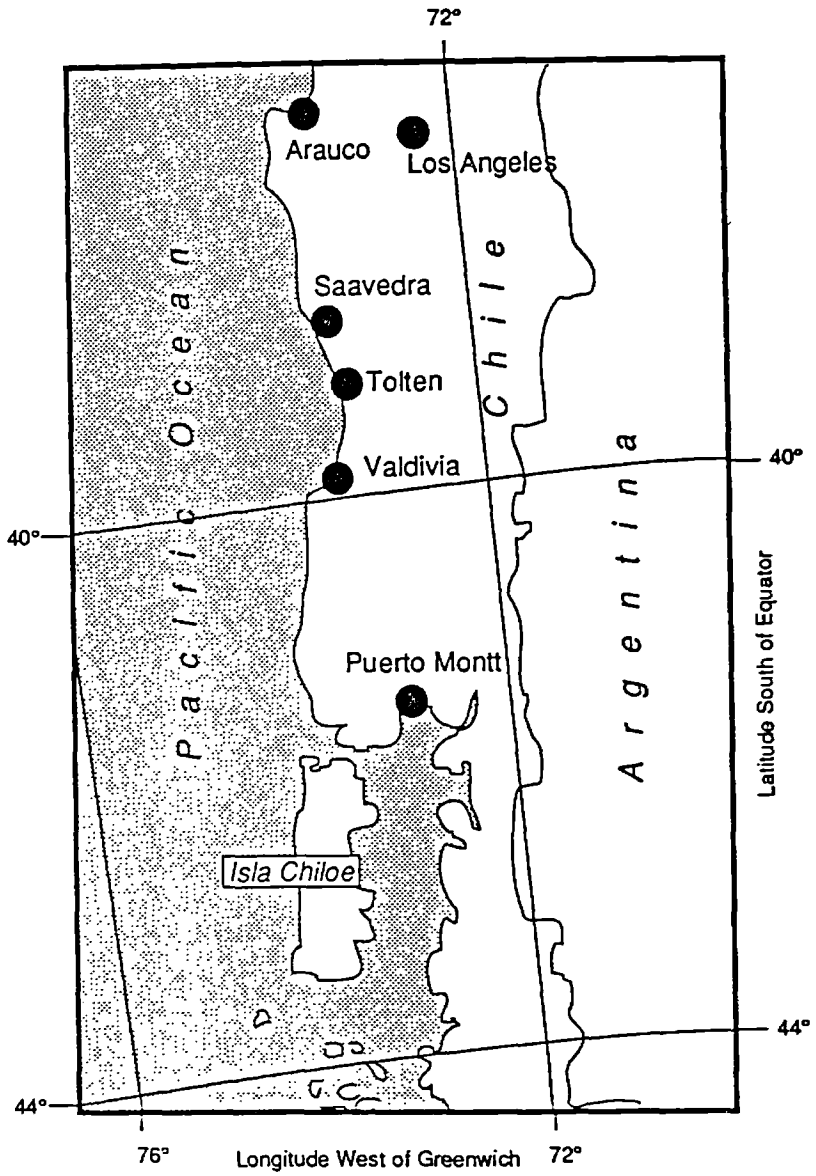

Figure 3.2. Location map of the Arauco peninsula, Saavedra, Tolten and Chiloe Island, Chile.

The observed geomorphological effects associated with the tsunami included the re-deposition of dune sand upon alluvial deposits on land. Detailed accounts of two sites (Puerto Saavedra and Tolten) in the paper are of particular importance in the understanding of the coastal hydrodynamics associated with tsunami inundation.

Puerto Saavedra was almost completely destroyed, largely by the third or fourth tsunami waves (Figure 3.3). The details of the tsunami were provided by eyewitness accounts, who noted that the onset of inundation was comparatively gentle; larger waves were not more than a few metres high and that the town was flooded to an estimated maximum depth of 3.75 m. When the tsunami waves from the open ocean approached the shore, they engulfed all but the highest parts of the sand spit (Figure 3.3) and moved across a channel behind towards the coastal lowlands and the town. At one place, part of the sand spit was eroded away and enabled water to drain into the sea without following the 1.5 km wide channel behind the spit. In addition, it was noted that the coastal lowlands were subject to differential erosion of surface soil of up to a few cm while a 1 - 2 cm veneer of marine sand was deposited over pre-existing alluvial deposits.

The town of Tolten is located near the mouth of the Rio Tolten and rests upon an alluvial plain nearly 2 km inland from the bank of the river (Wright *et al.*, 1963) (Figure 3.4). From the river channel seawards lies a 1.25 km wide sand spit. Ten minutes after the first episode of flooding, which reached a depth of about 1.5 m, the second wave engulfed the town to a maximum water depth of 3 m. Here, apart from localised coseismic subsidence, the coastal effects included erosion of surface soil in those areas poorly protected by vegetation cover as well as the deposition of sand.

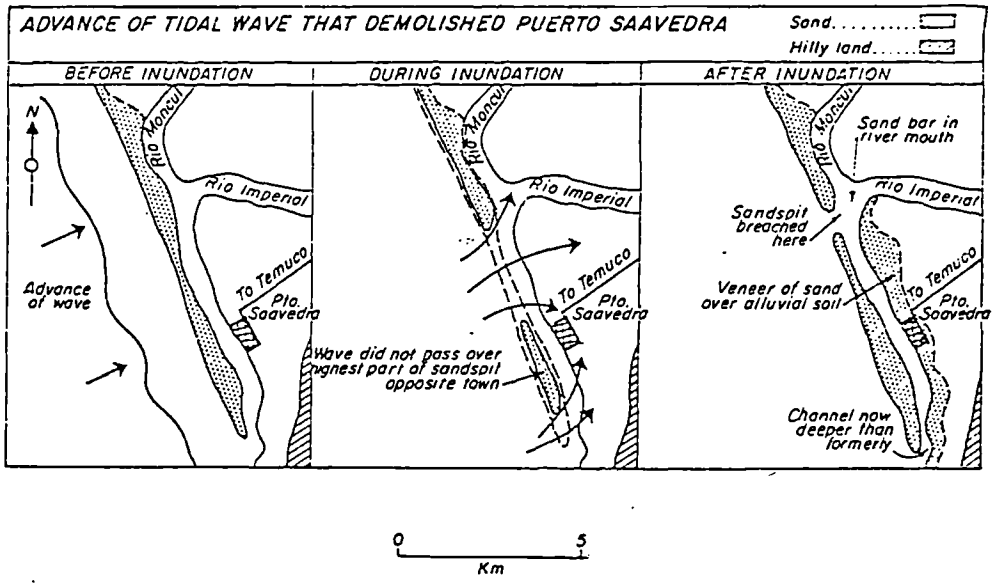

Figure 3.3 The inundation process of the 1960 Arauco tsunami and consequent geomorphological changes along the coast at Puerto Saavedra, Chile (after Wright and Mella, 1963).

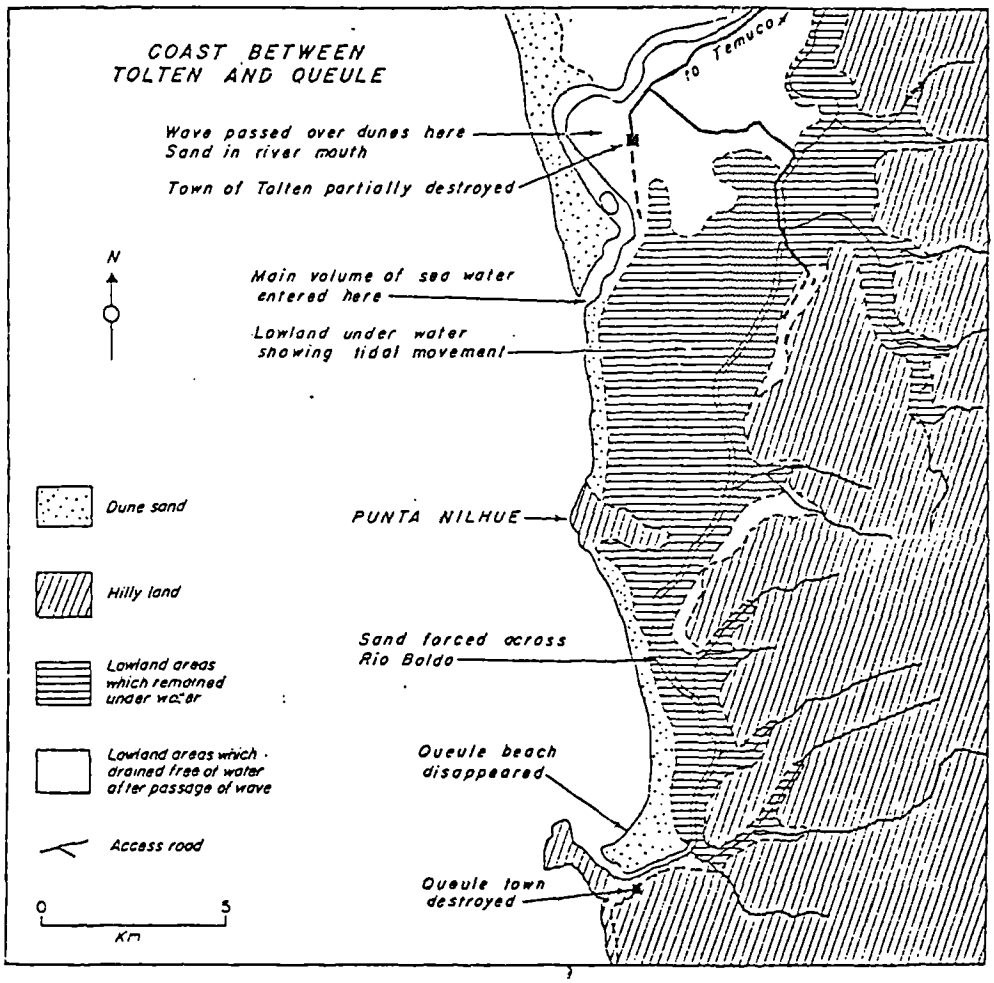

Figure 3.4 The geomorphological effects of the 1960 Arauco earthquake and tsunami along the coast between Tolten and Queule, Chile. Lowland areas which remained under water after the event subsided due to earthquake-induced compaction of unconsolidated mottled peaty clays and peat loams (after Wright and Mella, 1963).

Similar studies of coastal geomorphological processes associated with recent tsunamis have been undertaken in Japan. Sato *et al.* (1995) investigated geomorphological and sedimentological effects caused by the 26th May 1983 Japan Sea and 12th July 1993 Hokkaido tsunamis at various sites along the coasts of northwestern Japan and Okushiri Island (Figure 3.1). The geomorphological effects of the 1983 Japan Sea tsunami were previously studied by Minoura and Nakaya (1991) along part of the coast of the Tsugaru and Sendai Plains. This tsunami was generated by an earthquake of magnitude 7.7 in the Japan Sea on the 26th of May, 1983. The effects were described as including the surge of tsunami waves across rivers, the breaching of beach ridges and coastal dunes and the flooding of coastal lowlands. As a result of the tsunami, various materials and sediments were transported both landwards and seawards, and deposition of sediment occurred both offshore and upon coastal lowlands and in coastal lakes. In particular, waves with heights exceeding 14 m above the contemporary sea level were observed at the coast to one side of a peninsula (Minoura *et al.*, 1991). Here, numerous man-made structures along the beach were destroyed by tsunami runup, and a large number of blocks, each weighing 10 tons or more, were transported over a few hundred metres inland from the foreshore as a result of the first runup (Minoura *et al.*, 1991).

Sato *et al.* (1995) investigated the 1983 tsunami at sites along the coast of southern Aomori and northern Akita prefectures. They found that coastal erosion occurred both on beaches and coastal lowlands and also that the spatial extent of flooding was considerably larger than the area of the deposited sediment. In general, the deposits were described as consisting of sand or gravel that formed discontinuous sheets of less than 20 cm thick, whilst materials capable of floating were much more widespread. Of particular interest is a detailed study at three sites of rice paddies and surrounding areas at the village of Minehama. Here, uneven or non-uniform erosion occurred in areas of beaches, dunes, coastal land and rice paddies, whereas tsunami deposits up to a maximum thickness of 22 cm were observed at least 650 m inland from the shoreline. The thickness of deposits

exhibits a gradual decrease inland, except for one site where the maximum thickness occurred 400 m inland from the shoreline. Deposits at these three sites consist of a sand layer and an overlying thin layer of mud also deposited by the tsunami. Sato *et al.* (1995) suggested that the tsunami sand was transported from adjacent beaches and dunes whilst the mud was derived from the rice paddies and the surrounding land surfaces. Intraclasts of local soil ripped up by the tsunami were also noted within the sand layer.

The coastal effects of the 1993 Hokkaido tsunami were investigated along the southern coast of Okushiri Island off the coast of SW Hokkaido (Figure 3.1), where flooding took place up to between 15 and 30 metres above sea level (m.a.s.l.) (Sato *et al.*, 1995). The deposition of sediments by the tsunami took place in most of the area flooded by the tsunami. Tsunami deposits were identified in the tidal zone, roads, farm fields, rice paddies, grasslands and in the floors of houses. Deposited materials include debris capable of floating such as wood, plants, artefacts and light bioclasts (sea urchins); bioclasts of an intermediate density such as shells, coral and foraminifera; and dense siliclastic fragments such as gravel, sand and mud. The spatial distribution of these deposits was found to be very variable. Materials capable of floating were distributed widely over most of the flooded area whereas siliclastic sediments formed either isolated patches of deposits or widespread sediment sheets (Sato *et al.*, 1995).

Locally derived sand or gravel sheets were observed as having been deposited by the tsunami along the shoreline of Okushiri Island and at several places along the western coast of Hokkaido in areas below 10 m above sea level. Visual inspection of the characteristics of a thin (2-3 cm) poorly sorted sandy mud with primary current lineations and the surficial soil of an adjacent farm field suggested that the siliclastic deposits were transported over a distance of a few tens of metres by tsunami backwash. They also noted other incidences of deposition of locally derived siliclastic sediments, which were typically less than a few centimetres in thickness and extended over several metres. The

sediments ranged in size from mud to gravel and reflected the characteristics of the source sediments.

According to Sato *et al.* (1995), at sites where tsunami runup was higher than 10 m, widespread siliclastic deposits were typically only a few centimetres in thickness; the composition varying from place to place according to the type of sediment available on shores and coastal lowlands. In particular, Sato *et al.* described various depositional and erosional features including patches of gravel several tens of centimetres thick and up to 2 m wide lying at the seaward base of a shore protection wall and on a road surface, together with grooves several metres in width that trended parallel to shoreline. These were used to reconstruct flow patterns. Instrumental surveying of erosional and depositional features was undertaken to estimate the volumes of materials removed and subsequently deposited at several locations. Of particular importance were several types of sedimentary structures, observed to have formed within the tsunami deposits. In the northern part of Aonae, Okushiri, planar, low angle cross stratification with a 5 degree dip toward the seaward, was observed within deposits which were composed of well-sorted medium to fine sand. Sato *et al.* (1995) stated that this type of sedimentary structure is very similar to that of upper flow regime planar beds produced on the foreshore. In the southern part of Aonae, current ripples and primary current lineations were frequently found on the surface of tsunami deposits. The current directions reconstructed from these sedimentary structures are in agreement with directions determined from bent grass and were argued to represent tsunami backwash. In general, the flooded area was described as having been greater than the spatial extent of the tsunami sediment. Moreover, they concluded that the thickness and distribution of tsunami deposits are controlled by factors including the magnitude of tsunami (represented by runup height) and the availability of sediment supply. The sedimentary structures associated with tsunami deposits were interpreted to have formed under both low and high flow regimes. The composition and grain size of the

sediments are found to be controlled by the nature of sedimentary materials in the source areas.

3. PALAEOTSUNAMI SEDIMENTATION

3.1 Deposition of fine-grained sediments

In the Masuda Plain (Figure 3.1), Japan, layers of dark grey muddy sand (typically 10 cm thick) were identified and interpreted as having been deposited by a tsunami event (Minoura and Nakata, 1994). Radiocarbon dating of wood from the top of a mud layer beneath the muddy sand gave an age of 930 ± 80 years B.P., which was correlated with a destructive tsunami that took place on the 16th June 1026 A.D.. This tsunami has been documented in Japanese historical accounts. Interesting features associated with the inferred tsunami layer are flame structures at the interface between the sandy layer and underlying organic mud. The latter projects upwards into the overlying sand layer. This flame structure was interpreted as the result of rapid deposition of sand upon a hydroplastic mud accumulation in a coastal marshy pond.

The grain size composition of the tsunami deposit was shown to contain predominantly well-sorted medium to fine sand, small amounts of coarse sand and gravel, and a significant amount of clay or mud (up to 40 %). The occurrence of brackish benthic diatoms was noted within the tsunami sediments. It was suggested, by correlating particle sizes with likely provenances, that the individual size fractions of grains were derived from separate sources, namely mud from an estuarine environment; well-sorted medium to fine sand from beach or dune systems; and coarse sands and gravels from fluvial deposits. Minoura *et al.* (1994) stated that no grading or structures occur within the tsunami sediment.

In a recent geological investigation of sedimentary sequences in low-lying areas along the eastern coast of Kamchatka (Figure 3.1), Bondevik *et al.* (1994) described three separate layers of sand in coastal sedimentary sequences and attributed these to the three most destructive historical tsunamis which occurred in the region, at 1737, 1923 and 1952 A.D.. The ages of the depositional events were established through the stratigraphical correlation of volcanic ash layers within sedimentary sequences with a well-established and detailed tephrachronology of the region. The tsunami sand layers were described as characteristically only a few centimetres in thickness. The particle sizes of the tsunami sediments are typically of well-sorted medium to fine sands. In particular, the sediment of the 1737 A.D. tsunami is composed of a mixture of well-sorted medium sand and numerous pieces of wood, whereas the deposits attributed to the 1923 tsunami are composed of well-sorted sand of a mafic airborne tephra which possesses a bimodal size distribution (Figure 3.5). The frequency curves of particle size distribution were divided into three separate curve sections. Curves I and II (Figure 3.5) in the coarser range represent a modal distribution of medium to coarse particles which were interpreted as constituting bedload, whereas a separate modal distribution (Curve III in Figure 3.5) was interpreted as having been transported as suspension load. Comparing these results with the unimodal distribution characteristic of sediments thought to have been deposited by tsunamis and preserved in coastal sedimentary sequences in Japan (Minoura and Nakata, 1994), it was suggested that the presence of snow during the 1923 Kamchatka tsunami inundation had allowed bedload to be transported inland together with suspension load without the loss which would otherwise have been caused by ground friction due to vegetation. This interpretation of bimodal particle size distributions is of particular interest, since multi-modal particle size distributions have been observed as being characteristic of the sediments deposited by a recent tsunami in Flores, Indonesia, which were obtained from well-vegetated areas. It is suggested that the observed multi-modality reflects the characteristics of the available sediments (Chapter 4).

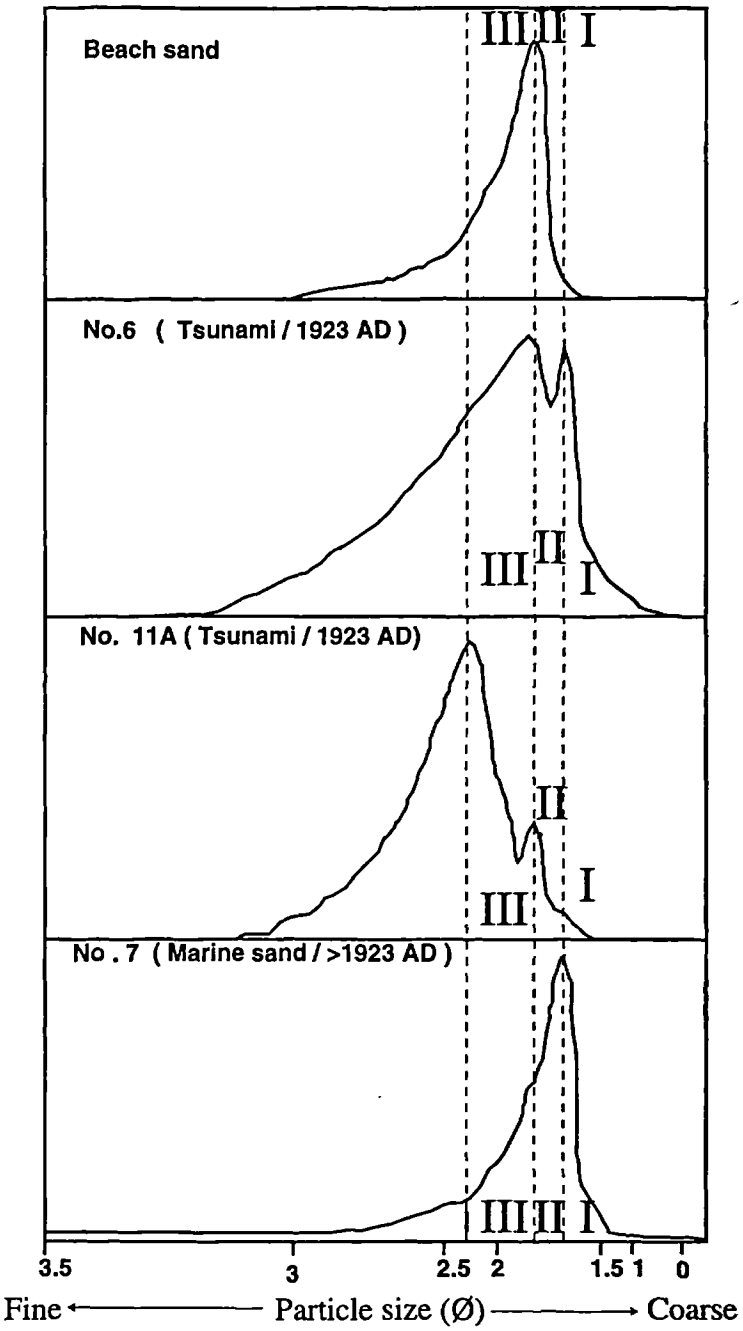

Figure 3.5 Representative particle size distributions of marine sand and tsunami sediments in Kamchatka (Bondevik *et al.*, 1994). The frequency curves of particle size distribution are divided into three separate sections, thought to correspond with grain groups transported as different types of load. Note that the vertical scale was not given in the report by Bondevik *et al.* (1994).

In the Scilly Isles, Southwest England (Figure 3.1), Foster *et al.* (1991) undertook a detailed investigation into coastal sedimentary sequences and argued that a layer of marine sand might have been deposited by the 1755 A.D. Lisbon tsunami. The sand layer occurs within an infilled lagoon, rests unconformly upon a peat accumulation and contains numerous small clasts of reworked peat within. The sand layer was described as being composed of marine sands of up to 1 m in thickness, tapering landward and consisting of a series of fining-upwards sequences.

In Australia, sedimentary sequences have been studied and are thought to contain evidence of former tsunamis at a number of locations along the coast of New South Wales (Bryant *et al.*, 1994) (Figure 3.1). In an accumulation of estuarine clay, a shell was dated at 6,600 ± 800 radiocarbon years B.P., is overlain by a layer of beach sand with a TL age of 7,400 ± 800 years. The beach sand is overlain by a layer of humate sand dated between 22,000 to 25,600 ± 3,400 TL years, which is in turn covered by a layer of pumice 20 to 30 cm in thickness with a TL age of 25,200 ± 6,200 years. The humate sand is 1.0 to 1.2m in thickness and contains isolated boulders. Bryant *et al.* (1994) interpreted this sequence as representing the impact of a tsunami that took place after 6,600 radiocarbon years B.P.. They speculated that the tsunami swept over contemporaneous beaches and deposited the sand layers. The transport of sand was so rapid that none of the sand was leached of its TL signal. During tsunami inundation, sand and pumice were separated. The sand was deposited upon estuarine clays. The humate sand is believed to be the result of sediment being coated with organic material and recemented into humates later. The pumice is believed to have been drifted into a lagoon and subsequently sealed by sand accumulation as a result of post-tsunami beach development.

The sources of the tsunamis responsible for the features described above have not been defined and located with certainty. Bryant *et al.* (1994) suggested that earthquakes and/or

submarine slides on the Macquarie Ridge at the edge of the Australian plate southwest of New Zealand could have been one of sources.

3.2 Tsunami boulder and gravel deposition

On the islands of Lanai and Molokai, Hawaii (Figure 3.1), an 8 m thick bed of gravel and boulder deposits rests as high as 326 m above present sea level. It is named as the Hulopoe Gravel and is believed to have been laid down during the last interglacial (Stearns, 1940; Moore and Moore, 1984, 1988). The gravel and boulder bed is composed of variously sized clasts, predominantly of basalt and partly of limestone including coral fragments. The bed was observed at exposures 200 m inland from the Lanai coastline where it consisted of three distinctive layers of 2, 4 and 2 m in thickness respectively. Each of these layers can be divided into an upper sub-layer of large basalt boulders in a sandy matrix, and a lower sub-layer of basalt and limestone gravels with sand and cobbles, as well as boulders up to 0.5 m in diameter which are distributed over areas almost 50 m above present sea level (Moore and Moore, 1988). These boulders appear to display a progressive decrease in size from seaward to landward.

The deposition of the gravel bed was first interpreted as having being accumulated during a high stand of relative sea level and as having subsequently emerged during the Quaternary (Stearns, 1940). This interpretation was recently contradicted and it has been proposed that the gravel bed was deposited by three successive waves of a large tsunami generated by a large submarine slide or debris avalanche. The avalanche is believed to have taken place *circa* 105,000 years ago on the western flank of the Manua Loa volcano (Moore *et al.*, 1989, 1992). Moore *et al.* (1984, 1989 and 1992) argued that the lower sub-layers can be attributed to deposition associated with tsunami run-up while the upper sub-layers can be assigned to episodes of tsunami backwash.

At the coast of Chile, Paskoff (1991) noted the presence of scattered large boulders up to 2 m in diameter embedded in shelly beach deposits upon an elevated marine abrasion platform near Coquimbo (Figure 3.1). The rock platform is considered to be older than the last interglacial period (isotopic stage 5e) and probably *circa* 300,000 years in age (isotopic stage 9), as suggested by the results of amino acid epimerization studies, U-series and Electron Spin Resonance dating.

The petrographic information on the boulders (medium to fine grained monzonite or tonalite and andesite or diabase) and rocks of the platform (Upper Miocene soft sandstones) presents a distinct contrast and indicates that the boulders are not locally derived but were probably transported over a distance of about 2 km from a rocky peninsula located farther seawards. Thus, Paskoff (1991) postulated that the boulder deposits may represent a high-magnitude tsunami event.

In Japan, Kawana and Nakata (1994) described a study of radiocarbon dating of coralline boulders, believed to have been deposited by tsunamis originating from the surrounding seas during the late Holocene, on land and on the fringing reef-flats of the Southern Ryukyu Islands. The dating is based on samples of aragonite from the uppermost parts of the boulders and indicates that the area could have been struck by tsunamis at *circa.* 500, 600, 1,100, 2,000, 2,400, 3,750 and 4,450 radiocarbon years B.P. (Kawana *et al.*, 1994). The lack of stratigraphical information and also data on the relative sea level history leaves their conclusions unsupported. Of particular concern is their assumption that there is a direct linkage between possible tsunami events and radiocarbon dates obtained with samples of aragonite. The authors assume that these had been broken off reefs at the time of tsunami and not to have been overturned during transportation.

Boulder deposits have been found to be difficult to interpret, particularly due to lack of detailed stratigraphical evidence. For example, Bourrouilh-Le Jan and Talandier (1985)

studied several areas of coral reef at Rangiroa, Tuamotu archipelago, Southeast Pacific (Figure 3.1) where large-scale geomorphological changes were represented by a large number of giant blocks up to 75 m^3, which had been transported from the foreshore inland. In particular, they noted that the pattern of boulder distribution often exhibits a progressive decrease in block size landward with some individual blocks transported across the atoll rim and into lagoonal areas. They considered both tsunamis and hurricane-induced storm surges as alternative causes and were in favour of palaeo-tsunamis as probable transportational and depositional agents. In contrast, Tessier (1969) believed that corraline reef blocks of several tonnes in weight had been transported by high-energy wave action at Rangiroa, Tahiti during the 15 January 1903 hurricane event. In accordance with the interpretation of Tessier (1969), Pirazzoli *et al.* (1988) disagreed with the conclusions made by Bourrouilh-Le Jan and Talandier (1985) and argued on several grounds that most reef boulders had been deposited by cyclone-induced storm surges.

3.3 Tsunami deposits associated with coseismic subsidence

Stratigraphical investigations of sedimentary accumulations at a number of sites in low-lying coastal areas in Washington, Oregon, northern California and British Columbia (Figure 3.1), have revealed evidence for distinct variations in environments of sediment accumulation including several sets of terrestrial to marine successions. By correlating these sedimentary sequences over this wide area, large earthquakes (Mw of 8 or 9) have been inferred as having occurred at the boundary between the Juan de Fuca and North America plates in the Cascadia Subduction zone off the North American continent during the late Holocene (Atwater, 1987, 1992; Adams, 1990; Darienzo and Peterson, 1990; McInelly and Kelsey, 1990; Atwater and Yamaguchi, 1991; Clarke and Carver, 1992; Nelson, 1992; Clague and Bobrowsky, 1994). At most of these sites, the stratigraphy was observed as containing a number of buried soil horizons, each of which is abruptly overlain by intertidal muds predominantly composed of clay and silt. The soil-mud couplets are laterally continuous over large areas while extensive sheets of sand are

intercalated between the soils and muds. In general, the sand layers taper out landwards and are interpreted as having been deposited by tsunamis that accompanied the inferred earthquakes. It is believed that this stratigraphy represents a series of short-lived events involving coseismic subsidence, sometimes coupled with widespread deposition of sand along this long stretch of the North American coast.

The evidence for coseismic subsidence and tsunami deposition has been studied in detail at various sites along the western coastline of North America. However, there appear to be a variable number of such events preserved in the coastal sedimentary sequences. For instance, at sites along the coast of Oregon, coseismic subsidence evidence include events dated at *circa.* 300 calendar years ago and between 1400 and 1900 years ago (Atwater, 1992). Among these, the earliest and latest were thought to have been associated with tsunamis (e.g. Atwater, 1992). In some areas, three separate events are believed to have occurred at 300, 1700 and 3100 calendar years ago. The stratigraphical and palaeontological evidence is believed to correlate for the most recent sudden submergence and tsunami at *circa* 300 calendar years ago over a wide area along the Pacific coast of North America. The event was dated by conventional or accelerator mass spectrometry radiocarbon dating of organic matter and by dendrochronological analysis of trees rooted in the uppermost horizon of soil beneath the tsunami sediment (Atwater and Yamaguchi, 1991; Atwater *et al.*, 1991; Nelson and Atwater, 1993 and Clague *et al.*, 1994, Clague *et al.*, 1994). Of particular interest is the work of Atwater (1992) and Atwater and Yamaguchi (1991), who described sedimentary sequences along the Copalis River, Southern Coastal Washington that contain three buried soil horizons. The upper soil has been interpreted as having developed in a forested lowland, and having been subsequently overlain by a layer of very fine to fine sand as a result of a tsunami. The sand tapers out inland and is in turn overlain by deposits of an intertidal salt marsh. This soil contains in situ roots of Sitka spruce (*Picea sitchensis*) and western red cedar (*Thujaplicata*). The trunks of the latter project through the sand and mud as standing snags. In contrast, the

overlying accumulation of mud contains rhizomes of *Triglochina maritima*, reflecting an environment of saltwater tideflat. The change from terrestrial to tidal flat depositional environments was interpreted as reflecting the occurrence of coseismic subsidence, whereas the intercalated sand layer was considered to have been deposited by a tsunami. Atwater and Yamaguchi (1991) noted that the outermost tree-rings of bark-bearing deceased Sitka spruce stumps are incompletely developed in contrast to the inner rings of continuous and vigorous growth. They inferred that this indicates that the trees were subject to sudden death due to marine flooding.

Darienzo *et al.* (1994) investigated Holocene coastal sediments in the estuaries of Necanicum, Nestucca, Siletz and Yaquina Rivers, Oregon. The stratigraphy at various sites typically exhibits a sequence of six repetitive successions within the top 3m of peaty horizons, each being overlain by estuarine muds. These were interpreted as representing six events of coseismic subsidence due to earthquakes in the Cascadia Subduction zone within approximately the last 2,800 radiocarbon years. Occasionally, layers of sand derived from the shore zone occur between peat and underlie estuarine mud. The sand layers are interpreted as having been deposited by tsunamis, which may have accompanied the earthquakes attributed to the respective coseismic subsidences. This paper is primarily concerned with stratigraphical evidence at the sites studied whereas the ages of the events and correlations with similar sequences along the northern Oregon coast are not discussed in detail. The study by Darienzo *et al.* includes particle size analysis, mineralogical analysis, organic content determination with loss-on-ignition, qualitative analysis of diatoms and plant macrofossil studies.

In view of the number of events with close temporal intervals and the tectonically-active nature of this long stretch of the coastline, it is unclear whether coseismic subsidences were localised or widespread as suggested. Attempts were made to improve the determination of the time of the transition from soil to tidal mud accumulations by

applying accelerator mass spectrometer (AMS) radiocarbon dating, using very small samples (Nelson *et al.*, 1992). A test of the AMS method undertaken by Nelson *et al.* (1992) shows that standard deviations on mean AMS ages of samples, believed to be contemporaneous, can be confined within ±25 to ±40 radiocarbon years. However, in attempting to correlate and distinguish sedimentary layers buried at close time intervals, possibly within a period of 440 years, Nelson *et al.* (1992) could not distinguish them apart and could not provide definite correlation of individual layers between sites, based upon the AMS dates obtained.

3.4 Geomorphological changes caused by tsunamis

Tsunamis are also found to cause profound reorganisation of coastal barrier systems. The findings of a study on the effects of the 1755 A.D. Lisbon tsunami in the Algarve region of Portugal (Figure 3.1) show that the Ria Formosa barrier island system was significantly modified and re-organised as a result of the tsunami (Andrade, 1992). This is associated with other geomorphological changes including widespread submergence, barrier breaching, the deposition of large washover fans and the complete reorganisation of backbarrier drainage systems.

At various coastal sites in the Tasman Sea region, Australia (Figure 3.1), Bryant *et al.* (1994) studied coastal depositional and erosional features. They presented evidence for repetitive catastrophic tsunamis, citing them as factors in both coastal erosion and accretion in the relatively tectonically stable area. The various features attributed to tsunami activity in the area include splayed sand layers, chaotic mixtures of variously sized clasts deposited in the form of mounds and ridges, sculptured bedrock, aligned and imbricated boulders and slabs.

The authors suggested that tsunamis may also have been responsible for the creation or modification of large rock platforms. Tsunami waves are believed to have ripped

enormous slabs of bedrock from promontories and cliff faces up to heights of 40-50m above contemporary sea levels. Beaches have been overwashed with boulders up to 49 m^3 in size and as much as 90 tonnes in weight re-deposited in aligned and imbricated or stacked piles, up to altitudes as high as 33 m.a.s.l. In addition, ramps are proposed to have been formed or extensively modified along cliffs, while headland cliffs rising over 40 m.a.s.l. are considered to have been truncated and marine barriers eroded (Young and Bryant, 1993; Bryant *et al.*, 1994).

Identification of remnant Pleistocene and Holocene marine deposits shows that these features were once extensively developed along this coastline and subsequently either stranded or highly dissected. The destruction is attributed to the impact of repetitive tsunamis. Using thermoluminescence (TL) dating supplemented by conventional radiocarbon methods, Bryant *et al.* (1994) identified a number of Pleistocene barriers dated younger than 80 Ka and considered patterns of erosion and barrier preservation in these regions. They postulated that the mechanism accounting for the patterns of erosion and barrier accretion and preservation is most likely to have been repetitive catastrophic tsunamis.

4. SUMMARY

It can be clearly seen that the current understanding of tsunami-induced geomorphological effects and characteristics of tsunami deposits is incomplete, since there have been few detailed studies, particularly of contemporary events. It is not surprising that interpretation of some past coastal floodings as having been the results of tsunami are contradicted by alternative explanations such as storm surges. Knowledge on the geomorphological effects of tsunamis and on the study of palaeo-tsunami deposits have been made in parallel. At present, evidence for large-scale geomorphological changes and sedimentological effects has been described but, in some cases, definitive explanations remain difficult to make in view of the uncertainty as to whether tsunamis or storm surges

are involved, especially in the absence of detailed stratigraphical and sedimentological evidence. It seems evident that detailed geomorphological, stratigraphical and sedimentological studies, together with the extensive accumulation of detailed descriptions of known and inferred tsunami deposits, can help differentiate tsunami and storm surge sediment in coastal sedimentary sequences.

Chapter 4
The 1992 Flores Tsunami

1. INTRODUCTION AND OBJECTIVES

As reviewed in the previous chapther, at present, there have been relatively few studies of coastal sedimentary processes and the characteristics of resultant sediments associated with tsunamis. In this research, a detailed investigation was undertaken on the coastal geomorphological changes and sedimentation processes associated with a recent tsunami event - the 12th December 1992 tsunami in Flores, Indonesia. Set in the context of the region's geography and geology, the following text presents a detailed geomorphological account and the results of particle size analysis as well as inferred sedimentation processes. The aims of the investigation undertaken here are to:

1) describe the evidence produced by a modern tsunami, in particular, its coastal geomorphological and sedimentary effects;

2) describe the particle size characteristics of sediment deposited by the tsunami, using laser granulometric investigations;

3) identify sedimentary processes associated with the tsunami and hence establish a sedimentation model;

4) determine the implications for the interpretation of palaeo-tsunamis.

2. GEOGRAPHY AND GEOLOGY OF THE FLORES REGION

Stretching across the equator between the Pacific and Indian Oceans in southeast Asia, lies the long belt of the Indonesian archipelago (Figure 4.1). The archipelago is located at the tectonically active intersection of three lithospheric megaplates (Figure 4.2), namely Indian-Australian, the Pacific and the Asian plates, and is characterised by a rugged interior with both dormant and active volcanoes. Historically, major earthquakes, volcanic eruptions and tsunamis have been frequent. Among them is the most well known and immensely destructive eruption of the Krakatau volcano in 1883, which created enormous and disastrous tsunamis.

The island of Flores is one of larger islands of the archipelago, and is located at 90°S, 121°E, approximately 1800 km east of the capital Jakarta in eastern Indonesia. Tectonically, the island lies at the transition between the Sunda and Banda island arcs. The former arc system is where the Indian Ocean lithospherical plate is being subducted, and the latter where the oceanic arc collides with the continental plate of Australia (Yeh, Imamura, Synolakis, Tsuji, Liu and Shi, 1993). Seisimty is active in and around the region, and 13 significant tsunamis including dramatic and destructive ones are recorded for the period 1815 to 1979 (Gusiakov, 1993). The coastal region, in contrast to the mountainous interior, is characterised by relatively flat coastal lowlands that are densely covered by tropical vegetation and locally disected by fluvial activity. In the nearshore zone coral reefs are frequently well developed and thriving, and form a narrow belt fringing the coast. The

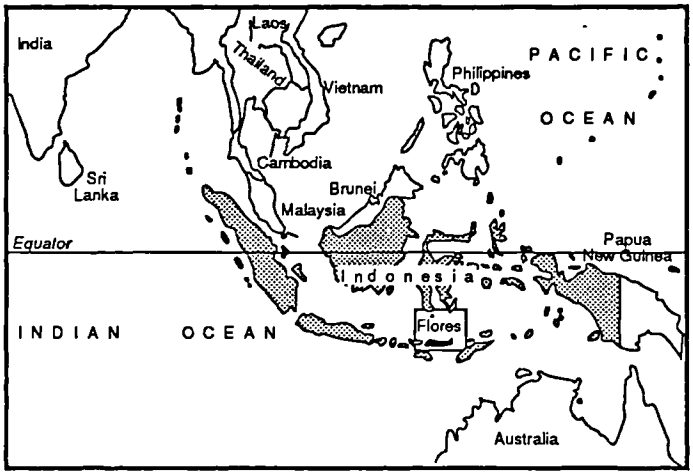

Figure 4.1. Location map of Flores, Indonesia

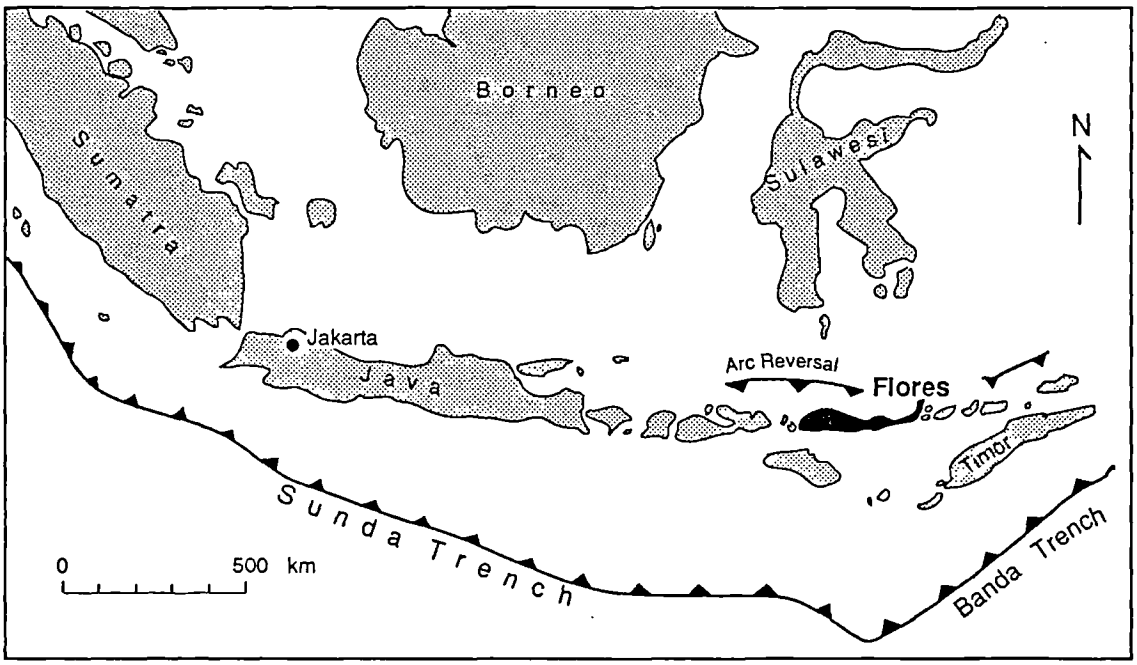

Figure 4.2. Map of the Indonesian region and Flores Island. Only the Sunda Trench and Banda Trenches are shown (after Hamilton, 1988).

surface of the reefs commonly lies at a water depth of less than 10 metres and the topography of the sea floor descends sharply from the edges to the deep water. The coastal zone of the islands is locally characterised by the growth of mangrove trees and the development of narrow beaches.

3. EARTHQUAKE AND TSUNAMI CATASTROPHE

On 12th December, 1992, at 1:30 pm (05:30 GMT), a major back-arc thrust earthquake of magnitude Ms 7.5 took place offshore approximately 50km north of Maumere, the capital of Flores Island (Figure 4.3). Several minutes later a large tsunami struck the northern coastline

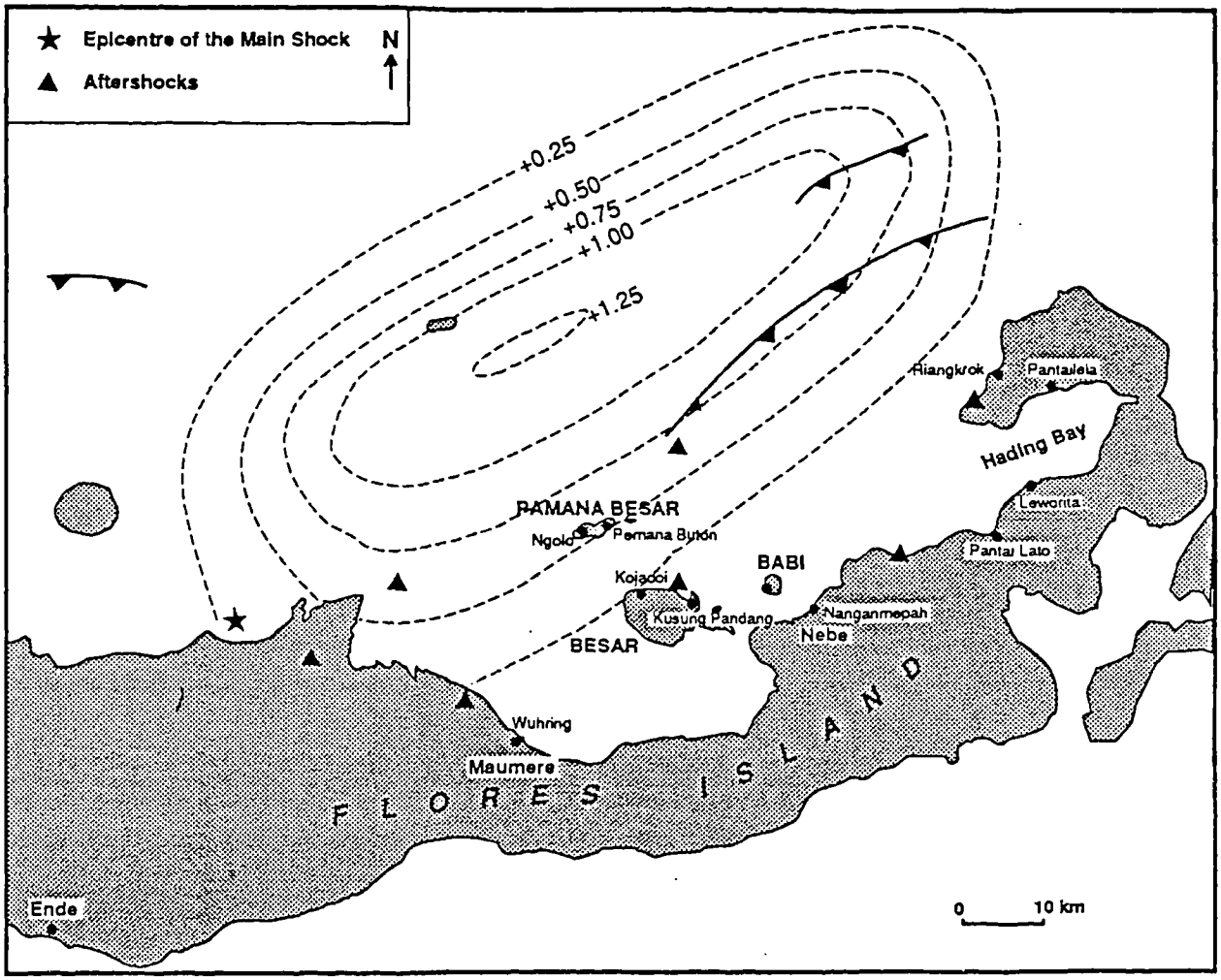

Figure 4.3. Map of eastern Flores, Indonesia showing the epicentre of the 12th December 1992 Flores Sea Earthquake and the possible source area of the associated tsunami. The contours denote the isobases of estimated vertical displacement of the crust (modified after Yeh, *et al.*, 1993).

of Flores. It is estimated that 2,080 people were killed with about half of the deaths attributable to the tsunami.

The geomorphological field investigations were undertaken approximately 2 weeks after the disaster and took place under the auspices of an International Tsunami Survey Team consisting of scientists from Japan, Indonesia, UK, USA and Korea. The results presented in this dissertation are believed to be the first detailed descriptions of geomorphological and sedimentological processes and resulting deposits associated with the inundation of a coastline by a tsunami.

4. EARTHQUAKE RELATED DAMAGE AND COASTAL GEOMORPHOLOGICAL EFFECTS

Preceding the arrival of the tsunami waves, catastrophic damage and destruction were caused by the major earthquake to man-made structures including buildings, bridges and roads, and a heavy loss of life occurred in association with the failure of structures. The heaviest destruction occurred in the areas of Maumere and Ende (Figure 4.3). The geomorphological impact was significant both in the interior and along the coast. The geomorphological processes associated with the earthquake included landslides/slope failure, failure of rock on high ground, ground cracking and liquefaction.

The coastal impact of the earthquake imposed direct geomorphological change as well as effects on the tsunami magnitude and erosion. In the coastal zone near Leworahang (Figure 4.4), the most striking scene observed was widespread landsliding (*circa* 2 km along the coast) and the formation of well-defined soil scarp slopes with submerged coconut trees. Some of the trees were still standing and the treetops were exposed out of the water. An earthquake-damaged road terminates seaward at the western end of the coastal cliff. In this area the tsunami runup is estimated to have been *circa* 5m while the waves reached as far as 150m inland. The run-up height was apparently higher than in the surrounding area (Figure

4.4). Moreover, the earthquake-related cracking and liquefaction weakened the coastal deposits prior to the arrival of the tsunami waves. There is clear evidence of severe cracking and liquefaction on the coastal lowlands in many areas.

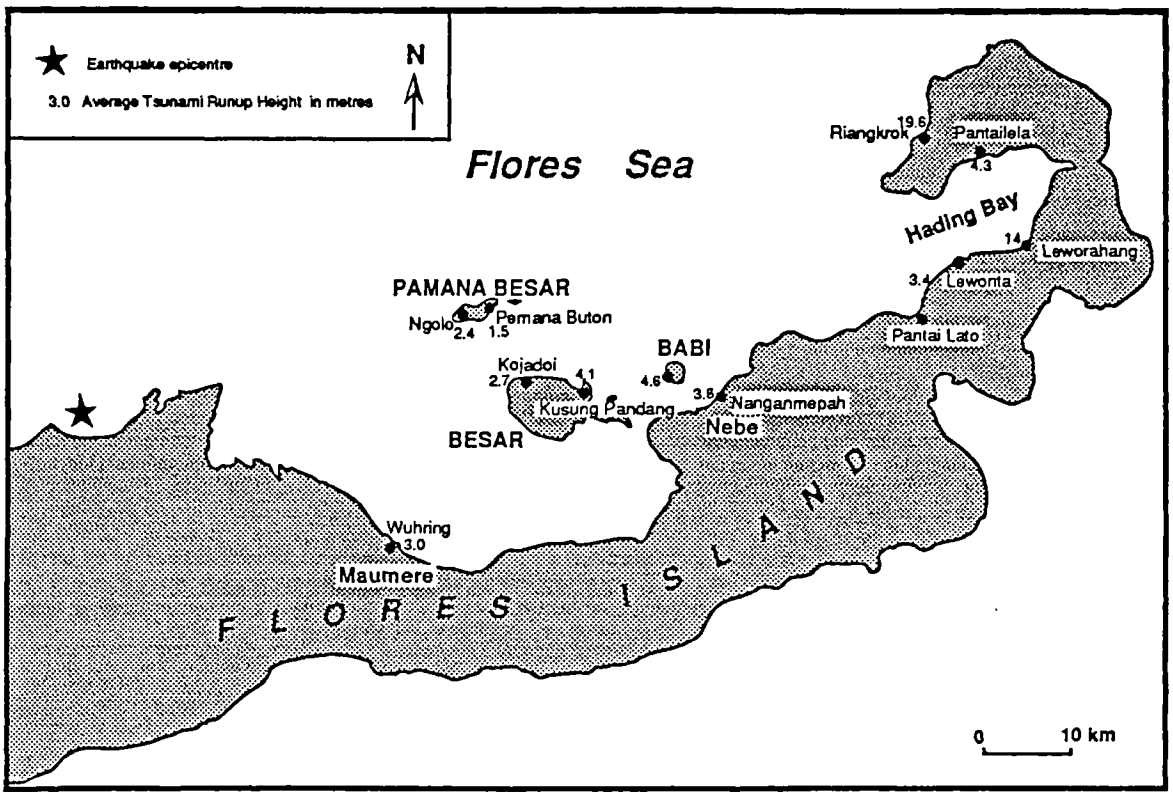

Figure 4.4. Map of eastern Flores, Indonesia showing locations mentioned in text. The numerical values denote the altitudes of mean tsunami runup (in metres) at the time of inundation as measured by the International Survey Team (Yeh, *et al.*, 1993).

5. TSUNAMI RUN-UP

The field measurement of maximum tsunami run-up heights and inundation distances was carried out collectively by separate groups of the team. The methods applied were tape measuring of distance and instrumental levelling for elevations of upper limits of inundation marks against the sea level of the time when a measurement was taken. The tide level at the time when the tsunami waves first struck was estimated by the International Survey Team from reconstruction of tidal cycles in the area. The reconstruction was made through calculating tide tables with harmonic equations, which were corrected by comparison with a half-cycle of tide measured at Permata Sari Hotel, Maumere on the 1st January, 1993 (Choi,

B. H. and Tsuji, Y., personal communication). The run-up height is defined as the maximum elevation that the flood reached, relative to the initial contemporary tide level. When measurements of run-up were more than one at a location, the mean was taken of several run-up heights. In general the mean runup was about 3 or 4 m although several local areas experienced considerably higher runup levels (Figure 4.4). For example, at Babi Island and along the adjacent Flores coastline runup was approximately 4.6m while farther east at Raingkrok and at Leworahang runup levels reached some 20m and 14 m respectively. In the latter areas, the exceptionally high values of runup are believed to be related to extensive submarine landsliding (Yeh *et al.*, 1993).

6. INUNDATION PATTERN

According to eye-witness accounts the first wave struck the Flores coastline approximately 5 minutes after the earthquake. Several eye-witness accounts provide information on the sequence and relative magnitude of the successive waves that struck the coast. For example, at Ngolo, Pemana Besar Island, accounts observed that the first tsunami wave was the largest (*circa* 3m high) and that this was followed by 5 smaller waves, each *circa* 0.5m high. At nearby Pemana Buton and at Kusang Padang (Figure 4.4), 3 major waves struck the coast, each with a similar magnitude.

The flow patterns of tsunami inundation were more complicated than bi-directional swashes. The densely populated and low-lying Wuring peninsula projects northeastwards into the sea, and it was reported by eyewitnesses that the tsunami inundation had behaved uni-directionally. The tsunami waves struck the area from the northwest, swept over and returned southeastwards into the sea (Plate 1). At Nebe, the bend of a sheet metal roof and the transportation of heavy objects including concrete slabs indicates that the tsunami waves struck perpendicularly to the coast, but broken-off trees and flattened tall grass and shrubs form a complex pattern. Some of these are aligned in accordance with the morphological

Plate 1. Destruction on Wuring Peninsula, Maumere by tsunami inundation. The sea struck the area from the northwest with a maximum runup up to 3 m, and receded towards the southeast.

relief and the orientation of these were probably largely controlled by the backwash of the final inundation. At Riangkrok, an eyewitness maintained that the tsunami travelled northeastwards and hit the village to the northern side of the valley (1, Figure 4.5); then the flood rushed eastwards into the inland end of the valley (2), and finally the sea withdrew westwards (3). The greatest loss of life occurred on the island of Babi where approximately 750 people lost their lives and 100 are still missing. Most tsunami damage was inflicted along the southern shore of Babi despite the fact that the tsunami waves were propagated from the north. This phenomenon may partly be explained as the result of wave diffraction and refraction around Babi island and also by the presence of narrow coral reefs that enabled the waves to break relatively close inshore. A recent numerical simulation (Imamura, 1994) suggests that there are significant differences in hydraulic force between northerly incident

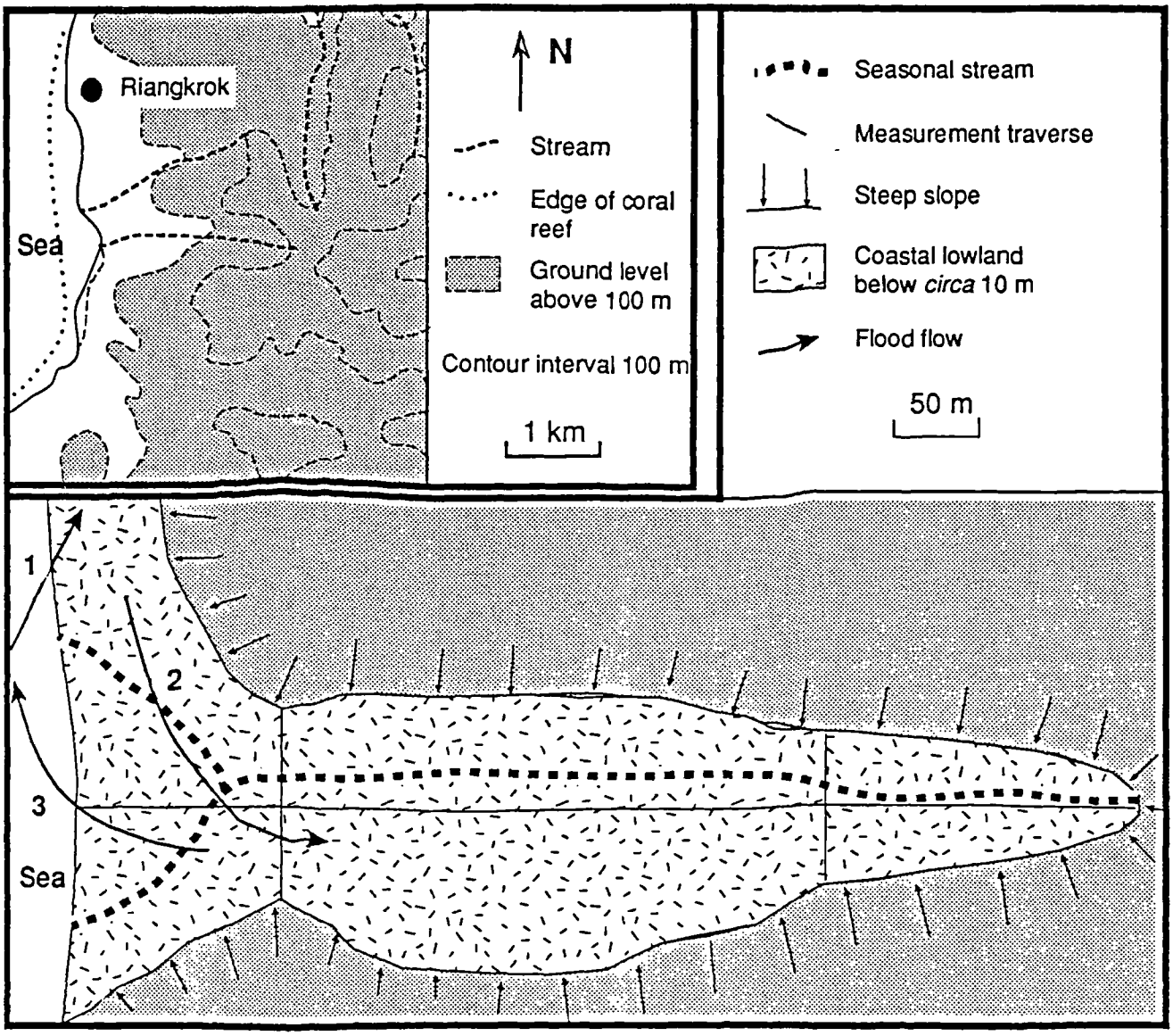

Figure 4.5. Morphology of the coastal valley and flow pattern of the tsunami flood at Riangkrok. The flood flow pattern is reconstructed according to an eyewitness account.

waves and reflected waves from the adjacent coast of Flores Island. The northerly propagating tsunami waves struck the island with low hydraulic pressures, whilst the reflected waves exerted high pressures upon the southern coast of Babi Island.

7. ASSOCIATED GEOMORPHOLOGICAL CHANGES

During the survey, detailed field investigations were undertaken at several sites where there was clear evidence for specific geomorphological and sedimentological processes associated with tsunami flooding. In some areas, the tsunami was associated with widespread erosion

while in other areas, extensive sediment deposition was evident. Many geomorphological processes associated with the tsunami were influenced by pre-tsunami earthquake damage. For example, earthquake-related cracking and liquefaction of coastal sediment accumulations resulted in an increased susceptibility to marine erosion while in several areas, extensive landslide activity took place. At several locations it proved possible to determine the position of the coastline prior to the arrival of the tsunami. For example, identification of the boundary between areas of coconut trees and mangroves frequently provided a reliable indicator of the former coastline. In other coastal areas, the profile of the ground surface prior to the tsunami was determined by measuring the elevation of tree bases where the roots had become exposed as a result of tsunami erosion. Elsewhere, the direction of trees (and also grasses) knocked over by the tsunami provided information regarding water current movements associated with coastal flooding.

7.1 Coral Reef Erosion and Lag Deposits

At some locations, large numbers of rock fragments eroded from coral reefs were deposited onshore. In general, coral reef erosion appears to have been restricted to the Riangkrok area where tsunami runup was exceptionally high (up to 26m). In this area, hundreds of coral boulders (typically 1m in diameter) were deposited as far as 200 m inland (Yeh *et al.*, 1993). At nearby Pemana Besar Island (at Ngolo and Pemana Buton) where the maximum tsunami runup was *circa* 4m eroded coral boulders are also present although here the boulders rest upon a medium to coarse coralline sand also considered to have been deposited by the tsunami. In contrast, some large coral boulders (up to 2 m in diameter) were found to have been left behind after the removal of surrounding soil by the backwash flow and appeared segregated. Some of these large lag deposits were observed to be partially in situ (Plate 2).

7.2 Coastal Erosion and Deposition

The tsunami resulted in very extensive coastal erosion and deposition at the small mountainous island of Babi (Figure 4.4). Both of the two villages on the island, located on

Plate 2. Scene of severe erosion and lag-deposits of local boulders at Riangkrok. The lag-deposit is just below the trimline in the middle distance.

two small strips of low-lying land, were destroyed (Plate 3 and 4). Almost the whole area was subject to severe erosion with multiple sets of erosional cliffs and gullies developed along a 100-200 m wide strip of coastline (Plate 5). The presence of many tree stumps with roots exposed demonstrates that the coastal land surface was lowered by *circa* 0.5-1m while eyewitness accounts point to considerable coastal retreat as a result of the tsunami. Superimposed upon the modified coastal land surface is an extensive sheet of medium to fine sand that is succeeded farther inland by a discontinuous sand cover.

At Nanganmepah, Nebe, detailed measurements of profiles across the beach and adjacent coastal lowland showed that at least $10m^3$ of sediment per metre of coastline had been removed by the tsunami. The area subject to erosion is continued by an area of tsunami sediment deposition represented by a discontinuous sheet of medium to fine sand (Figure 4.6). The latter area is also characterised by large numbers of concrete slabs each up to

Plate 3. Total demolition by the tsunami of the village in the west of Babi Island. The sea is to the left of and behind the scene, which presents a veneer of medium to fine sand up to a few centimetres covering the area.

Plate 4. Total demolition by the tsunami of the village in the west of Babi Island. Nothing remains intact but the foundation of a house, which is partly covered by the extensive thin sheet of sand.

Plate 5. The development of gullies and soil cliffs along the coast of Babi Island due to erosion during the tsunami inundation.

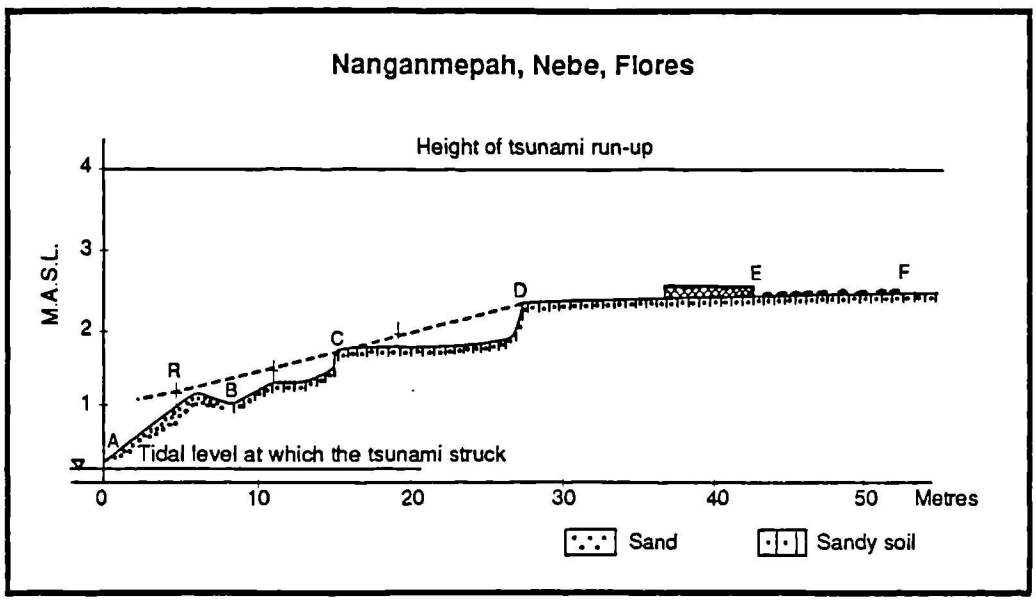

Figure 4.6. Tsunami-induced changes in the coastal profile as measured by instrumental levelling at Nanganmepah, Nebe. Profile B,C,D represents the observed ground surface lowering from the inferred original surface (R-D). Two prominent clifflines were produced at locations C and D. Profile A,R B indicates the position of a beach ridge produced after the period of tsunami activity. The landward movement of large concrete slabs (see text) took place between E and F. Position E also shows the inland edge of the house foundation from which the concrete slabs were transported. MASL (metres above sea level).

$0.14m^3$ in volume that have been transported landward from the foundations of a house by the tsunami waves (Plate 6). The Nanganmepah profile also indicates the presence of a well-developed beach ridge that was produced several days after the tsunami. Along this part of the Flores coastline, evidence for tsunami deposition is indicated by extensive sediment sheets that range in thickness from a few centimetres to as much as 0.5m. Similar sediment sheets deposited by the tsunami are also present at Ngolo, Pemana Besar Island, where there is a transition from continuous sheets of sediment at the coast to discontinuous sheets farther inland. In the inland area, it is difficult to define the thickness of the sediments deposited by the tsunami since the underlying ground surface is highly disturbed as a result of ground cracking and liquefaction.

At Kojadoi, Besar Island, sediment accumulations deposited by the tsunami and consisting of medium coralline sand form a large sheet over the whole area. The thickness of the sediment sheet is between 0.7 and 1.0m near the coast and decreases to several centimetres inland. In this area, the base of the sand sheet is relatively easy to define as the underlying ground surface is represented by a dark soil cover. Moreover, a fisherman excavated his belongings from beneath a 1m thick sand layer, while elsewhere a pair of trousers and a fish net were recovered from beneath the deposit. The landward extent of sediments deposited by the tsunami at Kojadoi also corresponds closely with the upper limit reached by the tsunami as determined by the position of wooden debris deposited by the tsunami waves.

Tsunami sediment sheet deposition also took place at Kusung Pandang (Plate 7). Here, eyewitness accounts show that tsunami flooding was associated with a coastal retreat of *circa* 10m while tsunami erosion has resulted in a lowering of the ground surface by *circa* 0.7m and the removal from this area of as much as $43m^3$ of sediment per metre of coast (Figure 4.7). Here, sediment liquefaction, ground cracking and gullying during the earthquake preceded the period of tsunami erosion and deposition. The former process is represented by the presence of several small scarp slopes while the latter is indicated by a well-developed

Plate 6. Concrete slabs transported from the foundation of a house by the tsunami at Nanganmepah, Nebe.

Plate 7. A sheet of medium to coarse sand on the coastal lowland at Kusung Pandang.

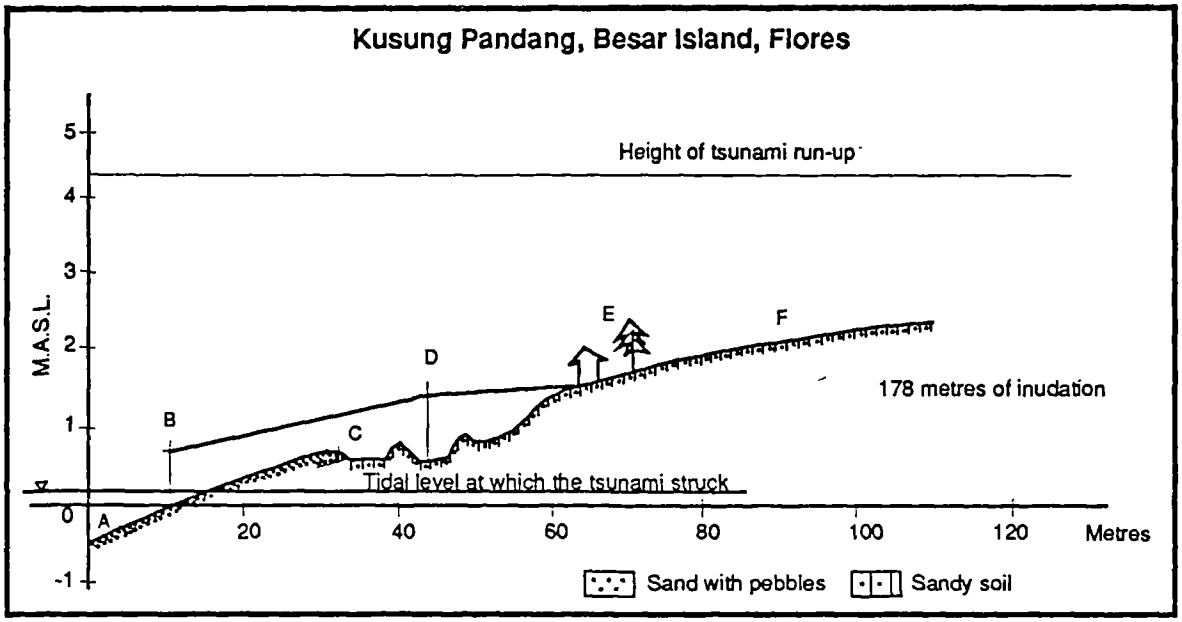

Figure 4.7. Tsunami-induced changes in coastal profile as measured by instrumental levelling at Kusung Pandang, Besar Island, Flores. Measurement of ground surface lowering (from B-E) was assisted here by eye-witness reports referring to the new exposure of sections of the wooden posts (B and D). Areas C and F represent zones of liquefaction visible on the ground surface. Severe erosion took place between A and E while a continuous sediment sheet was deposited between A and C. Discontinuous sediment accumulations, deposited by the tsunami, occur between C and F while very sporadic deposits occur landward of F. M.A.S.L. refers to metres above mean sea level.

sediment sheet that is continued inland by discontinuous and thin sediment accumulations. Similarly, at Lato, where tsunami runup (to +3m) reached as far as 150m inland across a relatively flat coastal surface, a thin continuous sheet of sand covers a 40m-wide belt of land near the coast while farther inland the tsunami sediment cover is discontinuous and only a few centimetre in thickness.

Evidence of remarkable coastal erosion and retreat also occurs at Panteilela where the tsunami had a maximum runup of 4.8m and extended as far as *circa* 150m inland. In this area, coastal retreat ranges locally between 20 and 50m while significant lowering of the land surface, caused by tsunami erosion, has also taken place. In this area, the lowered beach surface is mantled by many isolated tsunami deposits a few centimetre in thickness. This type of

observation is believed to be extremely important because the lowered ground surface produced in this manner can easily be mistaken as evidence to demonstrate the occurrence of coseismic subsidence.

7.3 Vegetation Destruction and Stripping of Bare Ground

Large areas of vegetation including trees, bushes and grasses were destroyed by the tsunami waves. At most locations, the destruction is mostly attributable to the stripping-away of the soil surface as well as to the effects of saline water intrusion. In areas where the tsunami currents were particularly strong (eg. Riangkrok and Babi Island) as well as along certain coastal zones, groups of trees were knocked over by the tsunami and only tree stumps remain visible. At Riangkrok where the maximum runup height (up to 26 m) was measured, the most striking scene is between the vegetated hill-top and the bare lower slopes. In such areas, the tsunami has resulted in the development of a "trim-line" that defines the upper limit of erosion (Plate 8), which is observed to be exceeded by the maximum levels of run-ups.

Plate 8. A conspicuous trimline defines the upper limit of erosion, which is exceeded by the maximum elevation of the tsunami runup, at Riangkrok.

In this area, large amounts of vegetation, including numerous coconut trees, were observed to have been eroded during tsunami runup and subsequently transported seaward by an exceptionally strong tsunami backwash that probably also removed any sediment previously deposited by the tsunami. In areas where groups of trees lie on their sides, the orientation of the trees provides important information on the direction of approach of the most destructive tsunami waves. However, it is possible that the orientation of some trees may have been determined by strong backwashes.

8. PARTICLE SIZE ANALYSIS OF THE FLORES TSUNAMI SEDIMENT

Cores and surface samples of the tsunami sediments as well as local sediments were obtained at selected sites and studied with particle size analysis in the laboratory. The sites include Nebe and Pantai Lato on Flores island and Kojadoi on an adjacent small island - Besar island. The following provides information on the compositional characteristics of both tsunami and local sediments and vertical and lateral variations in particle size composition of the tsunami sediment. In conjunction with these, information relevant to sedimentological processes is provided including site-specific morphology and its changes associated with the tsunami inundation.

8.1 Nebe

At Nebe, where an extensive area of coastal lowland extends along the coast, the observed tsunami run-up of *circa* 4 m was associated with the transport of large volumes of sediment and debris including concrete blocks and artifacts. Eyewitnesses observed that there was a very limited amount of sediment on the coral reef and a narrow beach was flanked by mangrove trees prior to the inundation. As mentioned above, tsunami flooding resulted here in coastline retreat of *circa* 10 to 20 metres with at least 10 m^3 of sediment per metre of coastline removed by the tsunami (Figure 4.6). The newly-formed coastline was typically crenulate in plan profile with distinctive soil cliffs of almost 1 m in height. Sediment exposures along this cliffline indicate the presence of a coral platform overlain by dark sandy

soil. These sediments are, in turn, mantled by an extensive and discontinuous sheet of sand sediment, apparently having been deposited by the tsunami. This sediment is composed of grey medium sand near the coast to grey fine sand farther inland forming extensive sediment sheets ranging in thickness from as much as 0.5 m down to a few centimetre.

Three sediment cores analysed and discussed below were obtained in a morphological depression by a stream near the coast (Figure 4.8). This hollow is separated from the sea by a slightly eroded ground surface with soil cliffs seawards. In addition, 9 surface samples from the thin sediment sheet were obtained along a line from the coast inland at intervals of *circa* 15 metres west of the hollow (Figure 4.8). Examination of the cores revealed that a sharp unconformity exists between the tsunami sediment and the underlying deposit. There is clear indication that erosion took place prior to the deposition, as indicated by an absence of the upper part of topsoil and vegetation cover. The tsunami sand sediment is very coarse

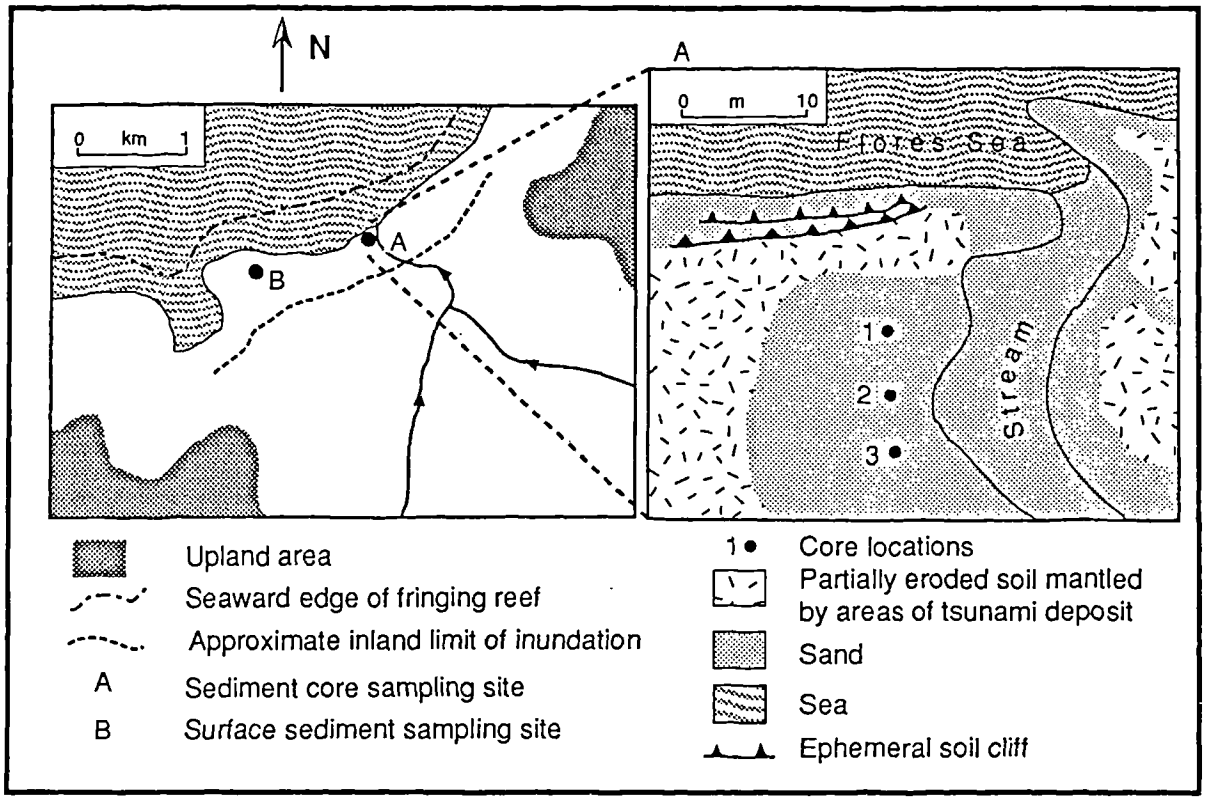

Figure 4.8. Map of the site at Nebe.

and contains grit and pebbles at the base but does not display distinctive grading. Coarse clasts including sandy intraclasts or grits occur intermittently at several levels. The intraclasts are composed of friable dark sandy soil that closely resembles the local soil in appearance.

8.1.1 Particle Size Analysis: Downcore Variations

The core was visually examined and sliced into contiguous samples at 0.3 cm intervals and representative particle size distributions of the tsunami sediment are given in Figures 4.9, 4.10 and 4.11. Particles of the tsunami sediment contained in the core largely fall into a size range of 100 to 1,000 μm with occasional fractions coarser than 2mm. Large variations in particle composition are illustrated by the percentage frequency curves that vary from well-sorted to poorly-sorted distributions. The particle size distributions occur as three broad groups:

1) size distributions with a dominant primary modal sub-population of near log-normal distribution (indicative of well-sorted sediments) in the sand range and a much less prominent tail in the finer range (silt and clay); The fine fraction generally amounts about 5 % and the primary modal position varies in a size range of *circa* 200 to 500 μm; About half of the samples are of this type.

2) multi-modal distributions with an additional coarse sand sub-population, sometimes with small amounts of grit (>2mm). The coarse sand sub-population occurs in a size range of 600 μm to 2 mm (2,000 μm) but sometimes it is composed of a broad size range of particles with no distinct mode. Although much less significant, a third sub-population can be identified with a modal peak in the range of 100 to 150 μm.

3) rarely, poorly sorted broad distributions without distinct modal peaks.

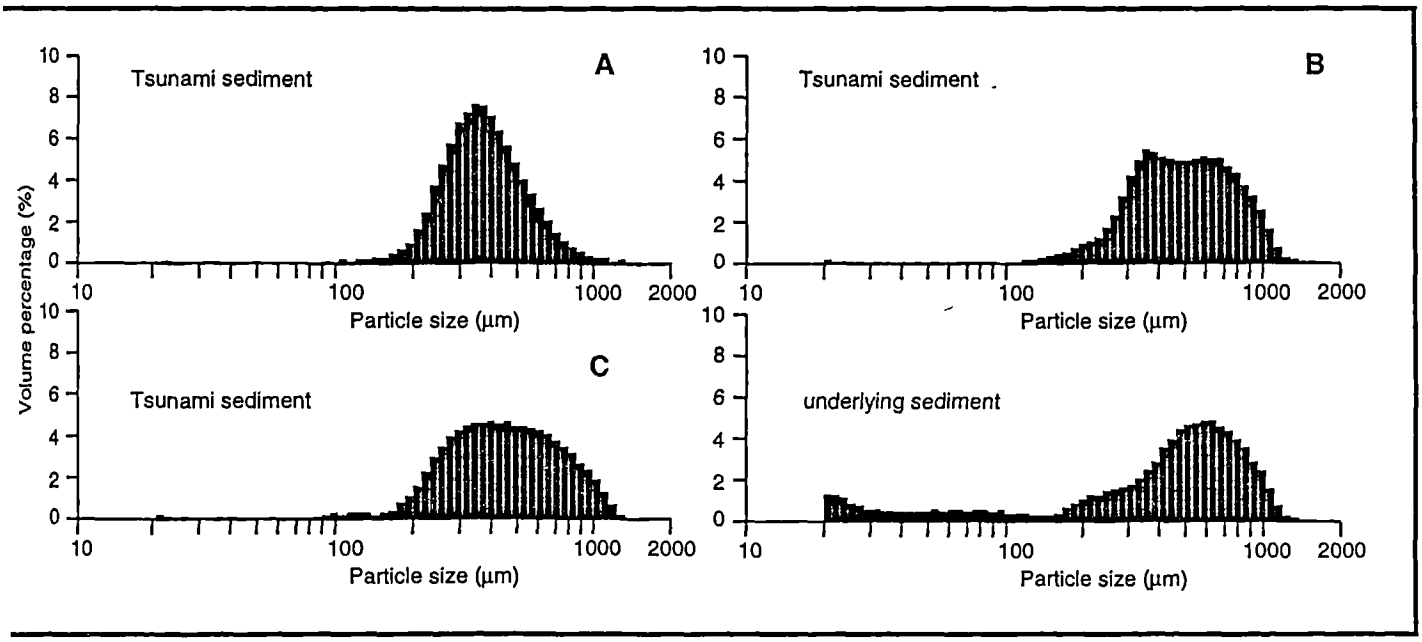

Figure 4.9. Particle size characteristics of tsunami sediment and underlying sediment at Core 1, Nebe. The positions of the samples are shown in Figure 4.12.

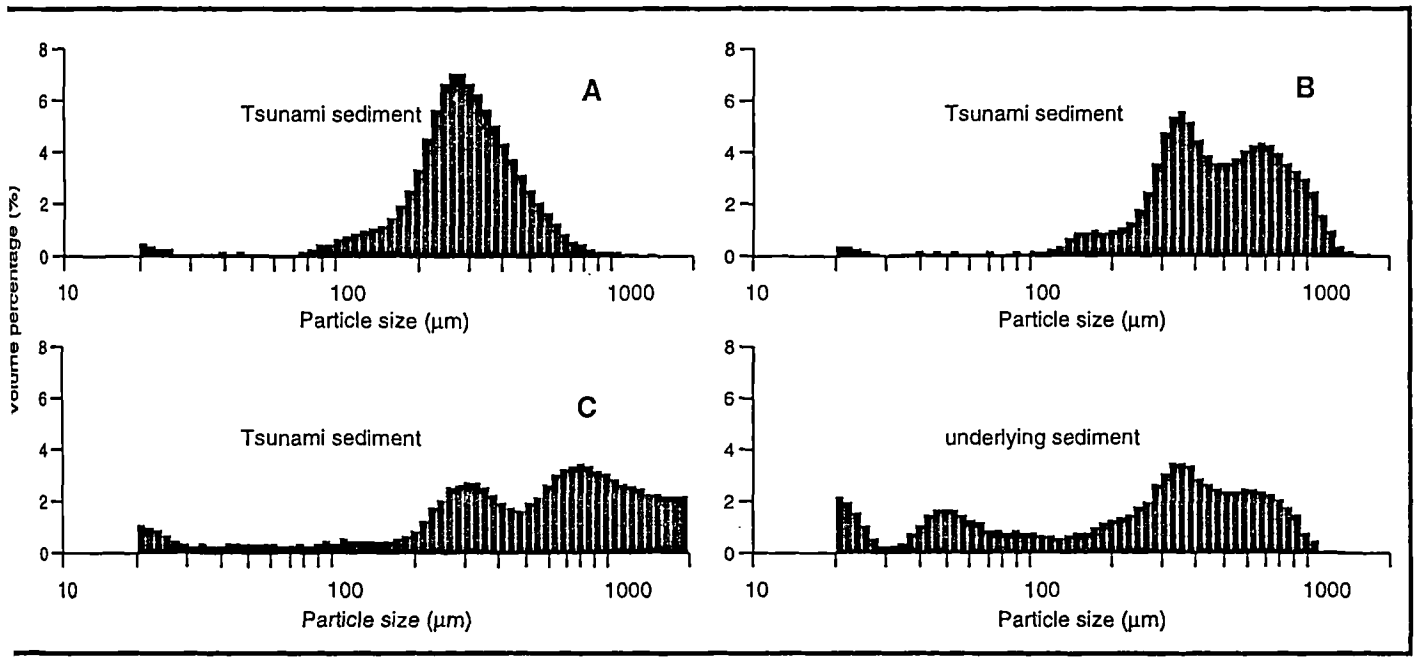

Figure 4.10. Particle size characteristics of tsunami sediment and underlying sediment at Core 2, Nebe. The postions of the samples are shown in Figure 4.13.

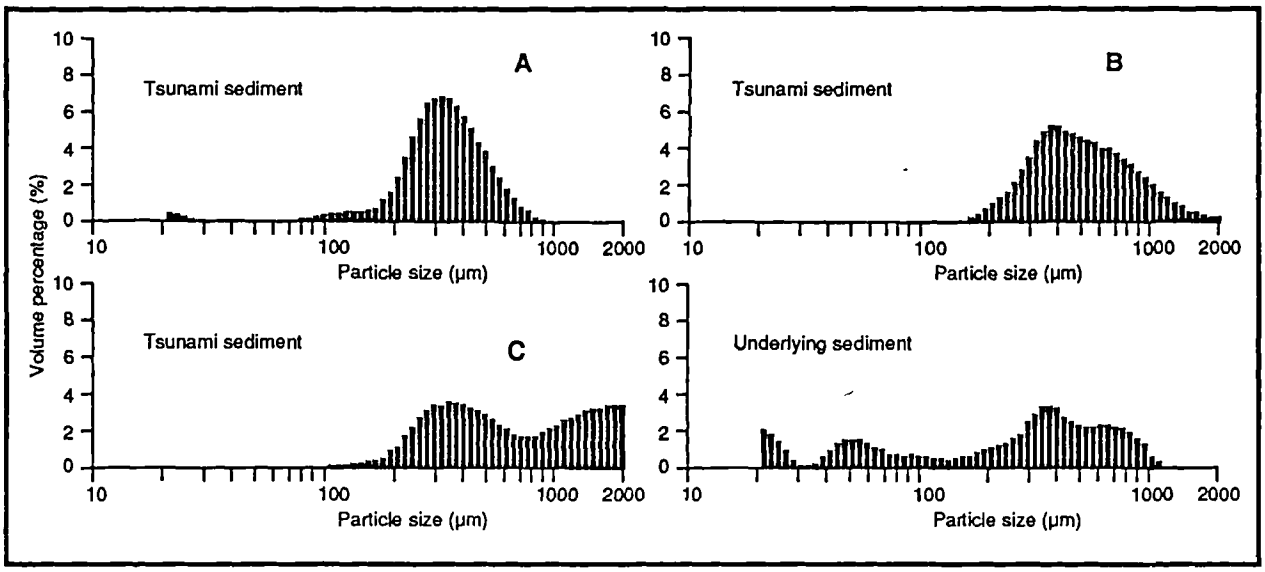

Figure 4.11. Particle size characteristics of tsunami sediment and underlying sediment at Core 3, Nebe. The positions of the samples are shown in Figure 4.14.

Size distributions of types 2 and 3 sometimes coincide with occurrence of intraclasts or gravel. In summary, the tsunami sediment can be generalized as composed of three principal subpopulations, i.e. a major subpopulation at *circa* 300 to 350 μm, a smaller component population in the range of 100 to 150 μm, and a coarse sand population at *circa* 600 μm.

Vertical variations in textural properties are featured by episodic changes in particle size composition. This is clearly illustrated by the saw-toothed curves of variations in values of mean particle size, kurtosis and standard deviation with depth (Figures 4.12, 4.13 and 4.14). It can be seen that there appears to be a general fining-upward trend that corresponds with a general upward increase in sorting. The episodic variations actually consist of multiple fining upward sequences, which can be more or less seen in the variations in mean particle size. Some fining-upward sequences are represented by better sorted, near uni-modal particle size distributions, within which secondary subpopulations are much less distinctive but often recognisable. Together with the fining-upward sequences of distinct multi-modal populations, they form a multiple set of fining-upwards sequences through the whole of the sediment. Within each fining upward sequence, conspicuous variations are found to occur at the coarse end of the composite particle size distributions. This is well

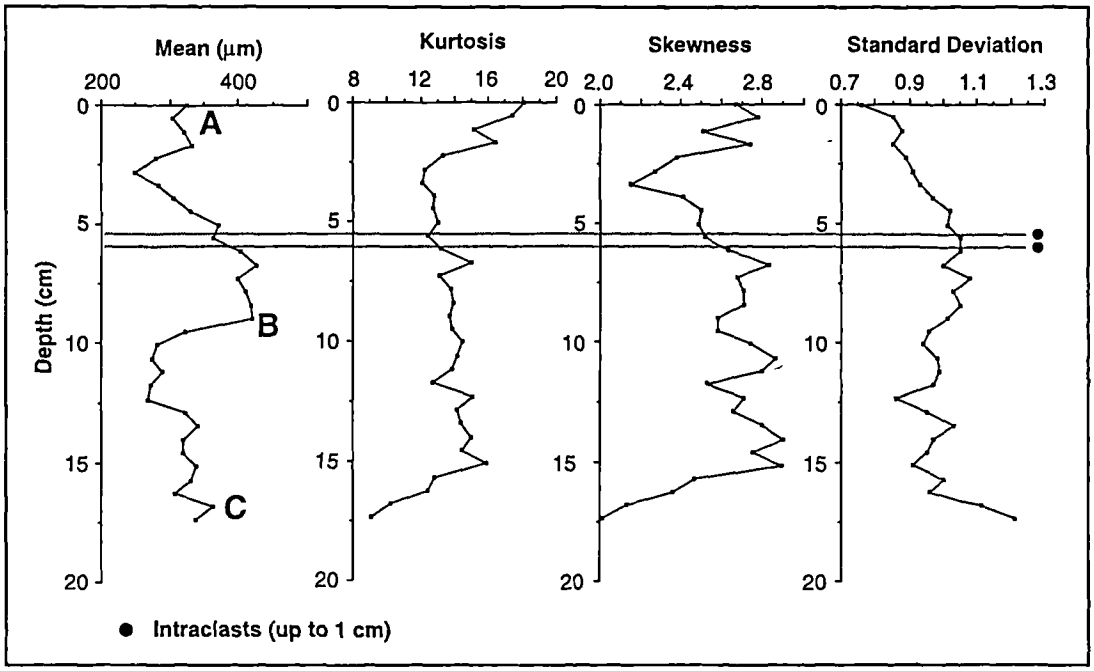

Figure 4.12. Vertical variations in the parameters of tsunami sediment particle size distribution, Core 1, Nebe. Letters A, B and C denote particle size distribution histograms shown in Figure 4.9.

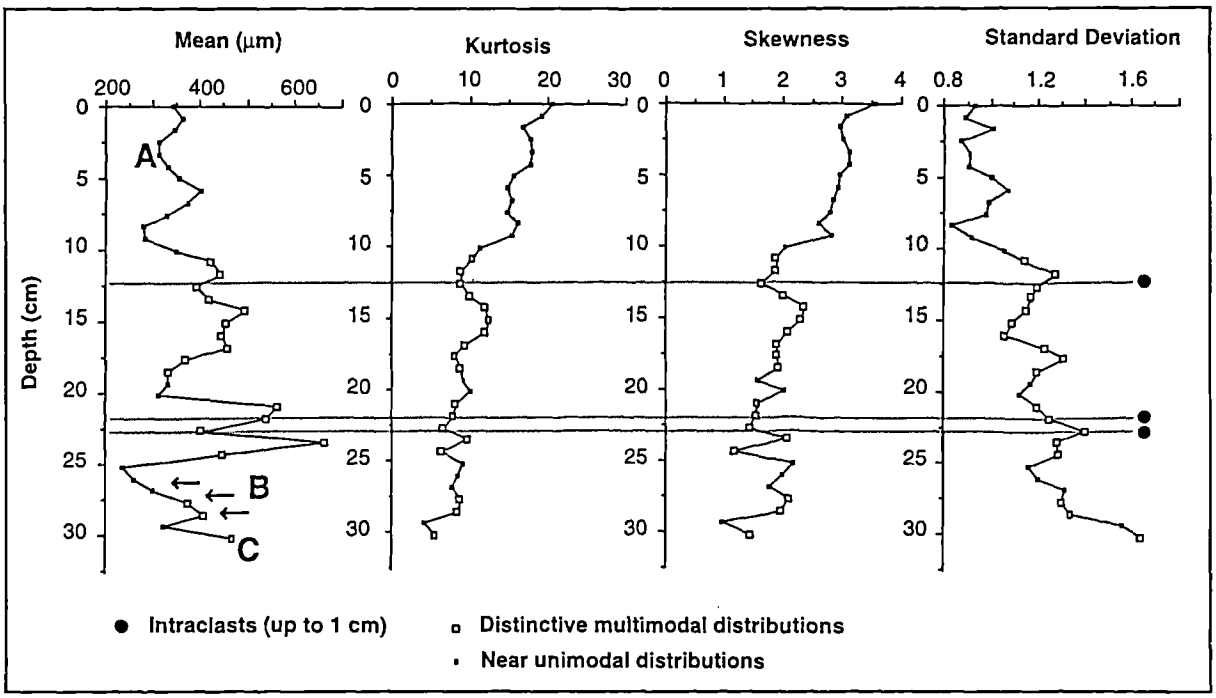

Figure 4.13. Vertical variations in the parameters of tsunami sediment particle size distribution, Core 2, Nebe. Letters A, B and C and arrows denote particle size distribution histograms shown in Figure 4.10 and Figure 4.15 respectively.

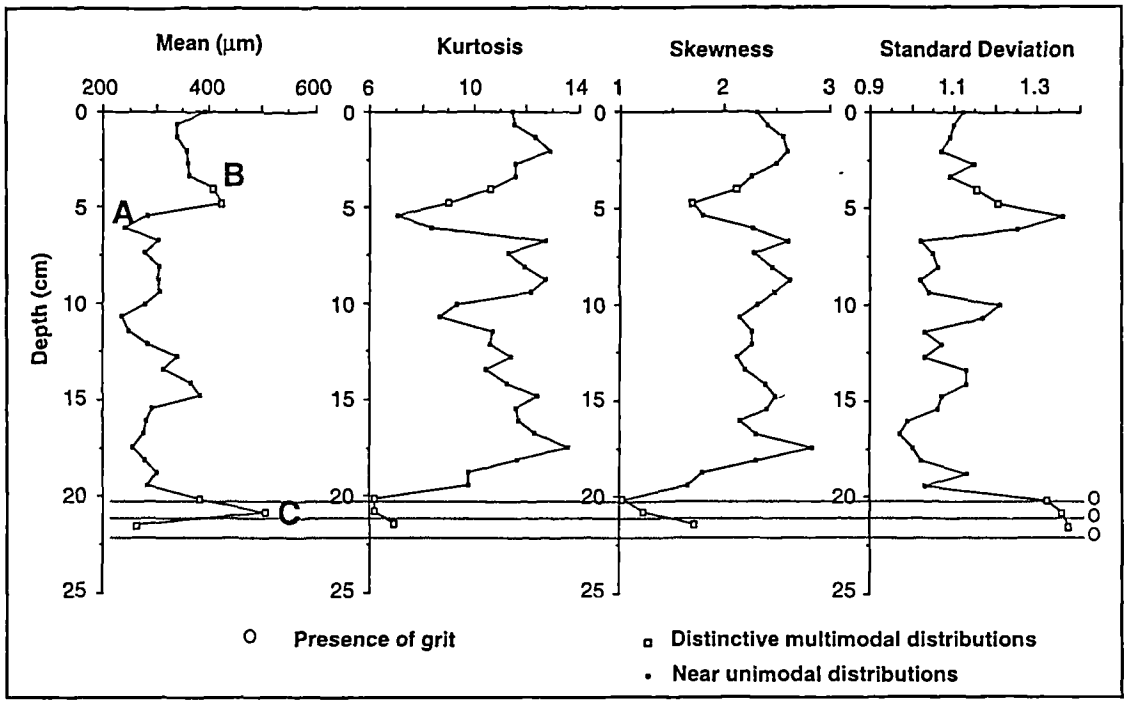

Figure 4.14. Vertical variations in the parameters of tsunami sediment particle size distribution, Core 3, Nebe. Letters A, B and C denote particle size distribution histograms shown in Figure 4.11.

illustrated by upcore progressive compositional changes of multi-modal distributions (Figure 4.15). The modal positions of the subpopulations occur within consistent size ranges but the coarsest subpopulation fines and decreases in proportion upwards.

8.1.2 Particle Size Analysis: Spatial Variations

Surface samples were obtained along a line perpendicular to the coast in order to investigate landwards variations in the particle size of the tsunami sediment (Figure 4.8). The result shows a general trend of particle size fining landwards and upon this trend are superimposed fluctuations in mean particle size (Figure 4.16). The fluctuations in the general trend correspond to an area near the coast, where an undulating topographic depression occurs.

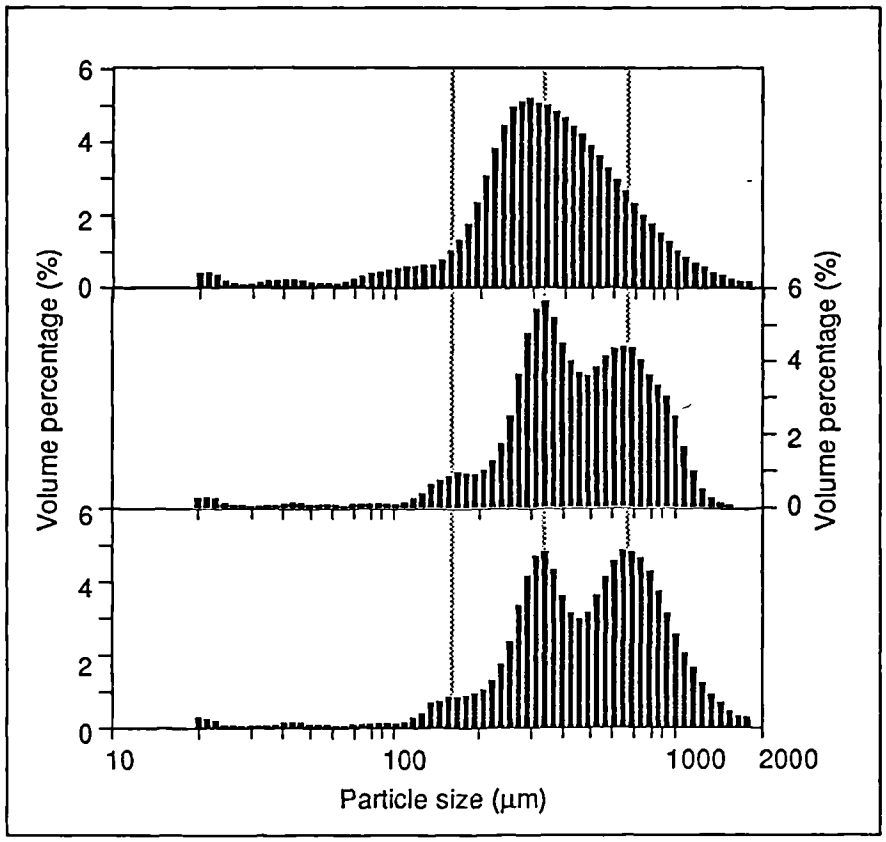

Figure 4.15. An example of the upward progression of variations in multi-modal distribution within some of multiple fining-upward sequences preserved in the tsunami sediment at Nebe. Note that significant modification occurs at the coarsest end of the composite overall population. The positions of the samples are shown in Figure 4.13.

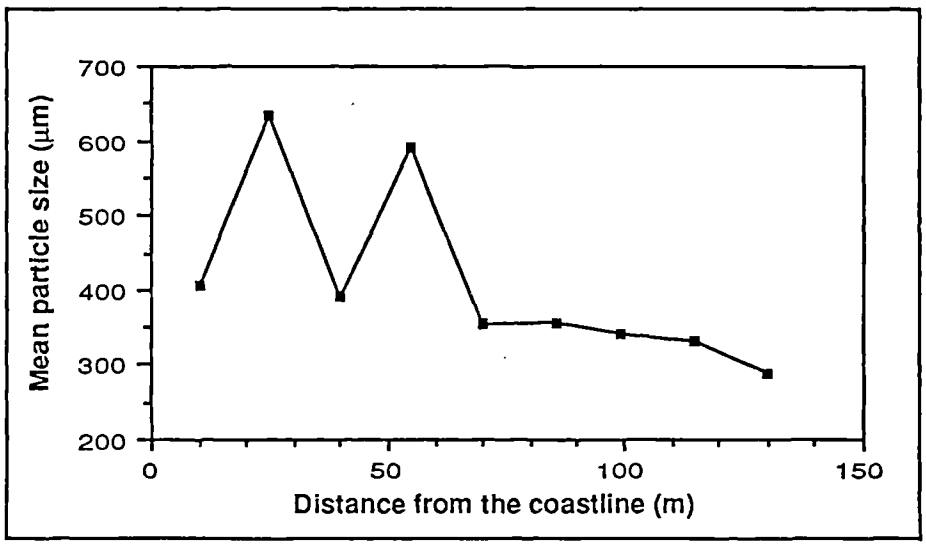

Figure 4.16. Variations in mean particle size along a 130 m traverse perpendicular to the coastline at site B, Nebe (see Figure 4.8).

8.1.3 Characteristics of Local Soil

The local soil is composed of a mixture of sand, silt and clay and is characterised by multi-modal and broad particle size distributions. It contains a large amount of clay and fine silt in contrast to the tsunami sediment (Figures 4.9, 4.10 and 4.11). When observable, subpopulations of particle sizes are consistent in their respective ranges. The modal peaks of identified sand subpopulations occur at *circa* 300 and 600 μm on the size scale, which clearly correspond to respective subpopulations typical of the tsunami sand.

8.2 Kojadoi

Kojadoi is a small area of coastal lowland, lying at the bottom of a valley on the north side of Besar island, which runs into a small bay (Figure 4.17). Along the seaward edges of the bay, rocky cliffs stand and associated deposits are characteristically large clasts, including

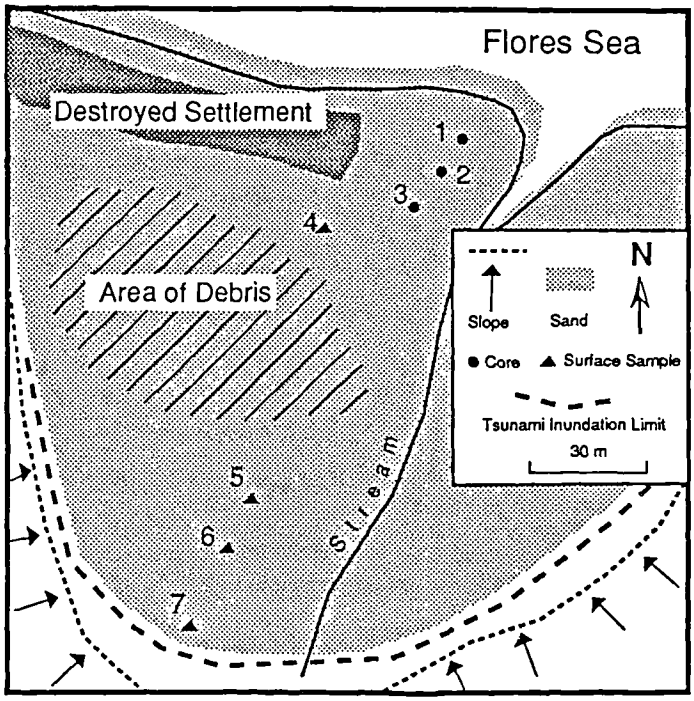

Figure 4.17. Schematic map showing the impact of tsunami inundation at Kojadoi, Besar Island. Here, a continuous sand sheet is present and its inland limit is close to the runup limit of the tsunami flood.

earthquake-induced fallen boulders. Eyewitness accounts indicate that the inner edge of the bay was bounded by a narrow strip of beach and that the tsunami inundation of the coastal lowland consisted of five episodes of horizontal passage of sediment-carrying turbulent water, more or less perpendicular to the coast. The inundation surged further inland from the first episode to the second, and reached its maximum at the third. Subsequently, it reached only where at the first episode and the final upsurge just managed to encroach upon the land. The accounts also claimed a significant retreat of the coastline as a result of the inundation. By the time field observation was made, a narrow beach had been developed at the position of the newly established coastline, the extent of which was marked by sand ripples produced by ordinary swash waves.

At this site, the measured maximum runup amounts to 2.7m. The sediment deposited by the tsunami is composed largely of medium coralline sand near the coast and fine sand inland and forms a continuous sheet, which rises up to the maximum limit of the inundation. The thickness of the sediment sheet is between 0.7 and 1.0 m near the coast and decreases to several centimetres inland. Near the coast, examination of the stratigraphy revealed that a sharp unconformity exists between the tsunami sediment and the underlying deposit. Sporadic coral pebbles rest upon the erosional surface and form part of the tsunami deposit, which also contained a noticeable amount of various materials, including blue paint chips, wooden debris and broken vegetation. The tsunami sediment was observed not to display any structure but only a vague grading. Three cores were obtained on land near the coast and four surface samples farther inland for particle size study in the laboratory (Figure 4.17). The sampling locations were carefully chosen to avoid possible influence by the sea, or the small stream and the settlement. The likely sediment sources are former beach sand and local ground deposits at Kojadoi.

8.2.1 Particle Size Analysis: Downcore Variations

As far as the conditions of the cores allowed, particle size analysis of Cores 1, 2 and 3 was carried out at 0.5, 0.6 and 0.8 cm contiguous intervals respectively and representative particle size distributions are given in Figures 4.18, 4.19 and 4.20. In the all three cores, the grain size composition is mainly confined in the size range of 100 to 2,000 μm, and occasionally consists of very coarse material which is relatively abundant at the base of the cores. The particle size distribution exhibits a variety of forms, including log-normal or near log-normal and multi-modal. Similar to that at Nebe, well-sorted sediments, characteristically of log-normal or near log-normal, have a dominant primary subpopulation with a modal position ranging around 300 μm with recognisable inclusions of a subpopulation at *circa* 150μm and fractions of another subpopulation at the coarse end. When the distribution is clearly multimodal, sediments are found to consist of three component subpopulations with their modal positions at *circa* 150, 350 and 700 μm. Each modal position remains relatively constant in the size ranges when distinguishable. Occasionally, the sediment is very poorly sorted and has a broad distribution of particle sizes. Unlike that at Nebe, there is a general lack of particles smaller than 100 μm and the sediment is better sorted.

Similar to that at Nebe, vertical variations in textural property are shown by episodic changes in particle size composition, as clearly illustrated by the saw-toothed curves of variations in values of mean particle size, kurtosis and standard deviation with depth (Figures 4.21, 4.22 and 4.23). It can be clearly seen that there is a general fining upward trend that corresponds with a general upward increase in sorting. In general, there are more multimodal distributions within the lower parts of the cores and especially, the sediment has more broad particle size distributions at the lower levels than above (Figure 4.24). The episodic variations actually consist of multiple fining upward sequences. Some fining-upward sequences are represented by better sorted, near uni-modal particle size distributions with

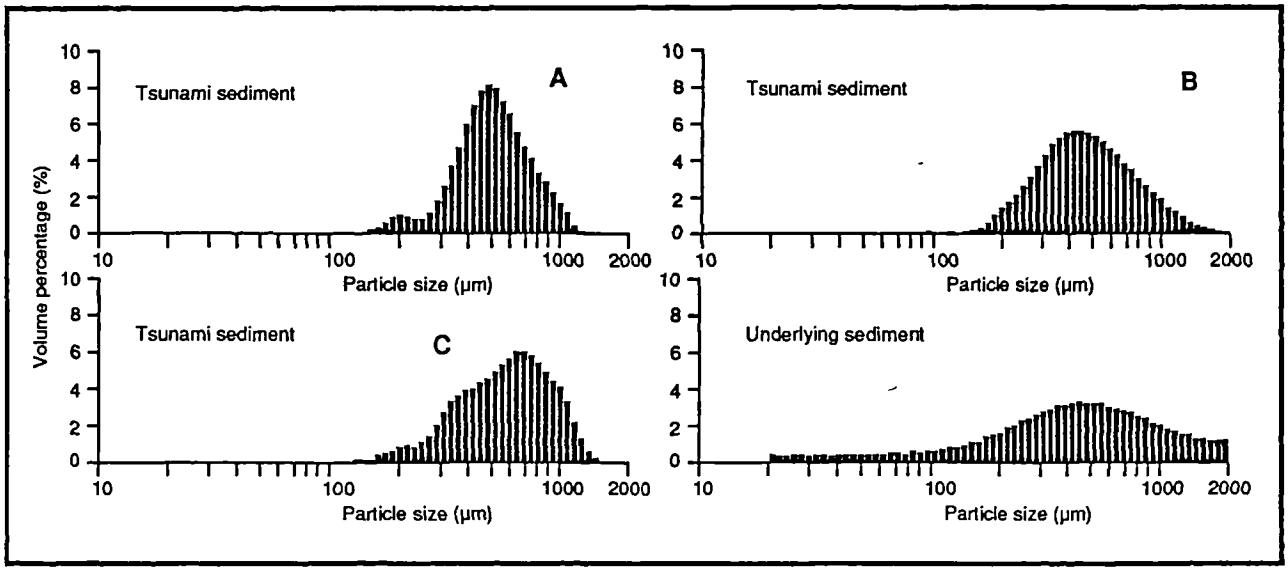

Figure 4.18. Particle size characteristics of tsunami sediment and underlying sediment at Core 1, Kojadoi. The positions of the samples are shown in Figure 4.21.

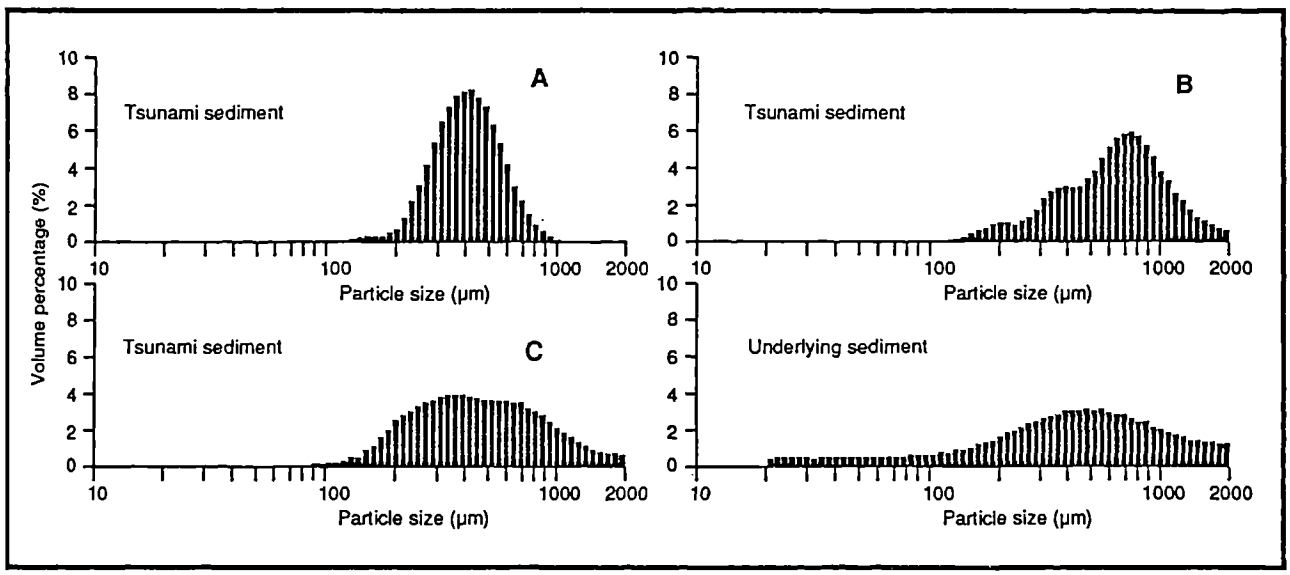

Figure 4.19. Particle size characteristics of tsunami sediment and underlying sediment at Core 2, Kojadoi. The positions of the samples are shown in Figure 4.22.

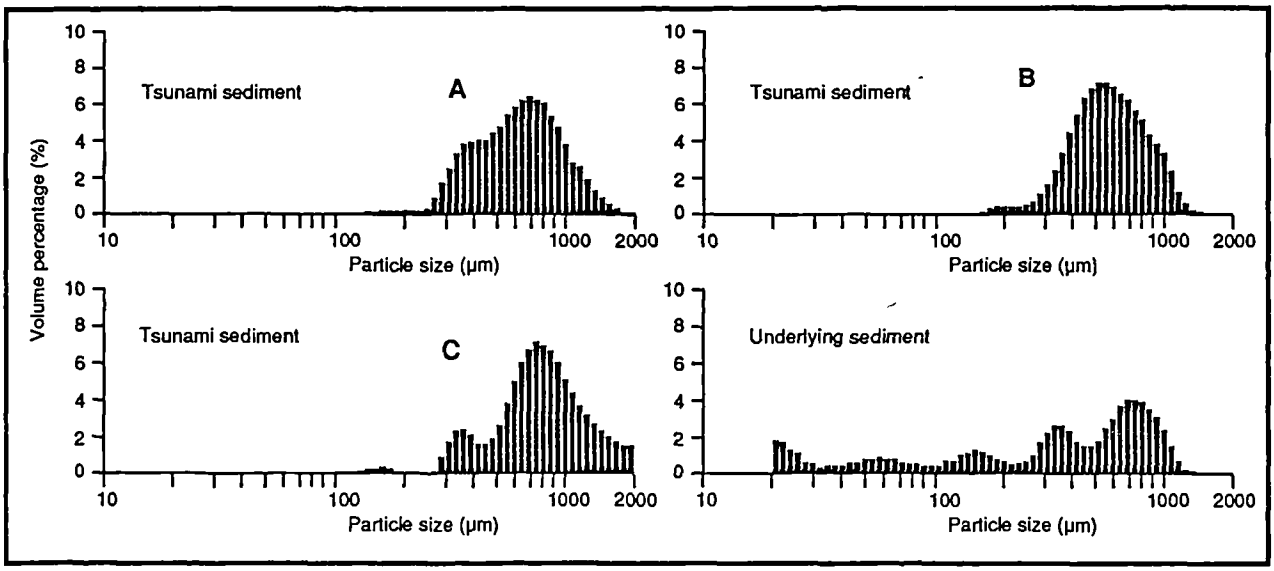

Figure 4.20. Particle size characteristics of tsunami sediment and underlying sediment at Core 3, Kojadoi. The positions of the samples are shown in Figure 4.23.

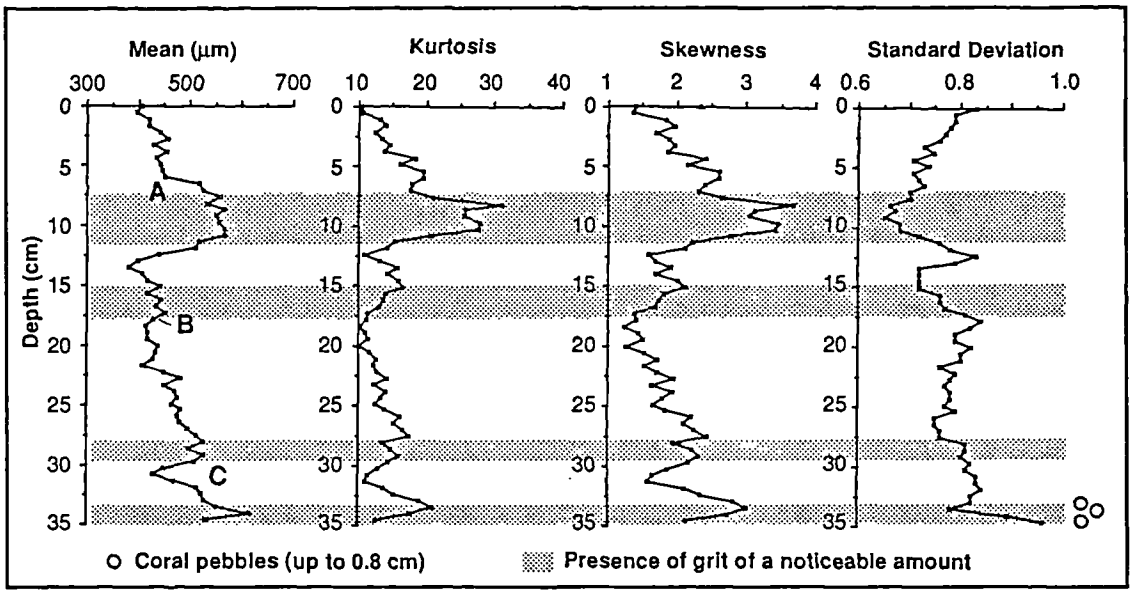

Figure 4.21. Vertical variations in the parameters of tsunami sediment particle size distribution, Core 1, Kojadoi. Letters A, B and C denote particle size distribution histograms shown in Figure 4.18.

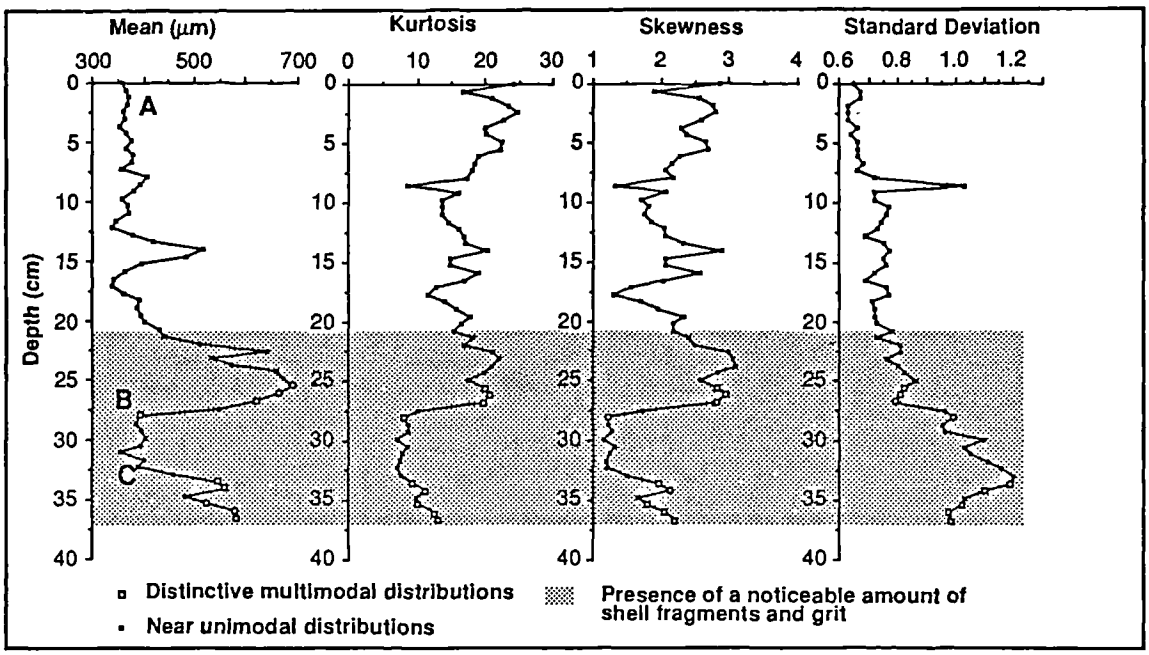

Figure 4.22. Vertical variations in the parameters of tsunami sediment particle size distribution, Core 2, Kojadoi. Letters A, B and C denote particle size distribution histograms shown in Figure 4.19.

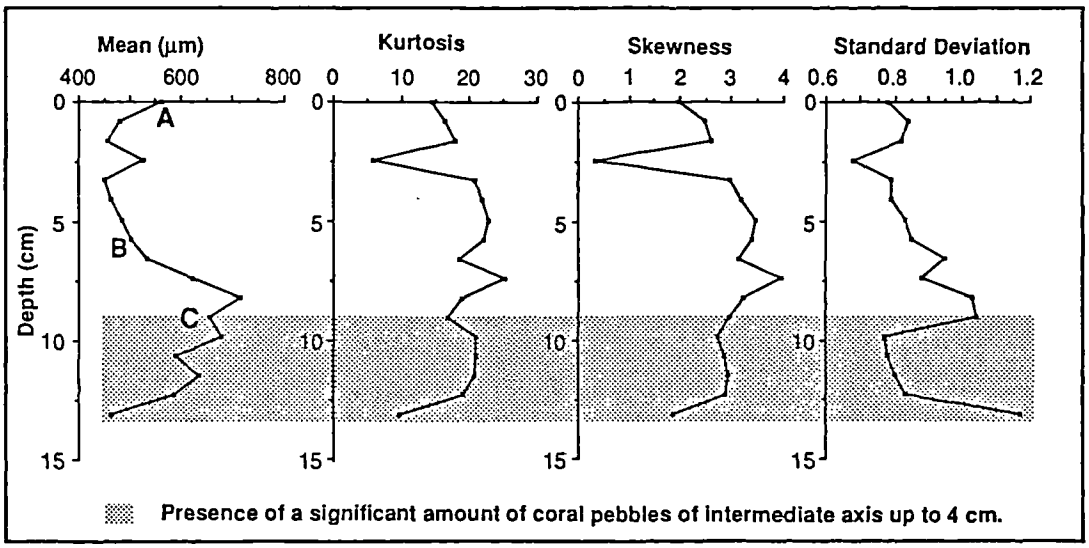

Figure 4.23. Vertical variations in the parameters of tsunami sediment particle size distribution, Core 3, Kojadoi. Letters A, B and C denote particle size distribution histograms shown in Figure 4.20.

modal positions ranging about *circa* 300 μm, within which secondary subpopulations of finer and coarser sands are much less distinctive but often recognisable. Together with the fining-upward sequences of distinct multi-modal populations, they form a multiple set of fining-upwards sequences through the whole of the sediment. Within each fining upward sequence, conspicuous variations are found to occur at the coarse end of the composite particle size distributions. This is well illustrated by upwardly progressive compositional changes of multi-modal distributions (Figure 4.24). The modal positions of the subpopulations occur within consistent size ranges but the coarsest subpopulation fines and decreases in proportion upwards.

8.2.2 Particle Size Analysis: Spatial Variations

Four surface samples were obtained further inland from where the cores were obtained and were analysed. Together with the samples from the top of each core, they provide information on lateral variations in particle size composition of surficial sediment (Figure 4.25). It can be seen that there are apparent fluctuations in mean particle size but a general fining-landward trend is present.

8.2.3 Characteristics Of The Local Sediments

The ground sediment in the area consists of a mixture of dark brown sand, shell fragments and coral pebbles, and are not as uniform as those at Nebe. The particle size distributions are characteristically very broad or multimodal, indicative of poor sorting or composition of a wide range of particle sizes (Figures 4.18, 4.19 and 4.20).

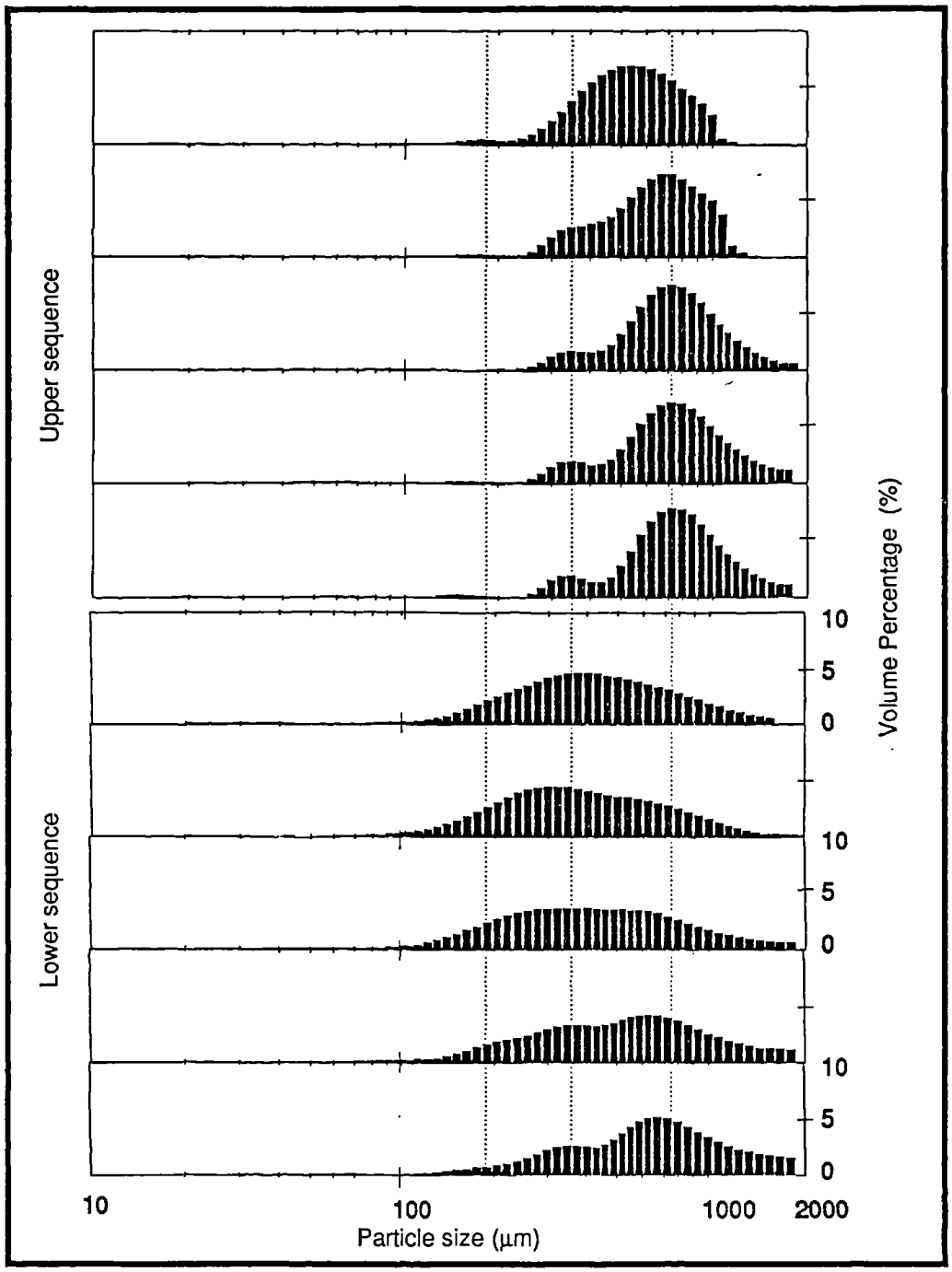

Figure 4.24. Two examples of upward progressions of sediment fining of multimodal distributions within the tsunami deposit from Core 2 at Kojadoi, Flores. The lower and upper sequences consist of selected histograms from the fining-upward sequences at depths of 34 and 20 cm respectively (see Figure 4.22). Three modal classes can be readily identified within the tsunami deposit and are located at *circa* 150, 250 and 700 µm respectively. The progressions display an upward fining of the coarsest subpopulation accompanied by a decrease in its proportion. Such variation patterns are believed to be a product of complex interplay of source material characteristics and the hydrodynamics of the tsunami.

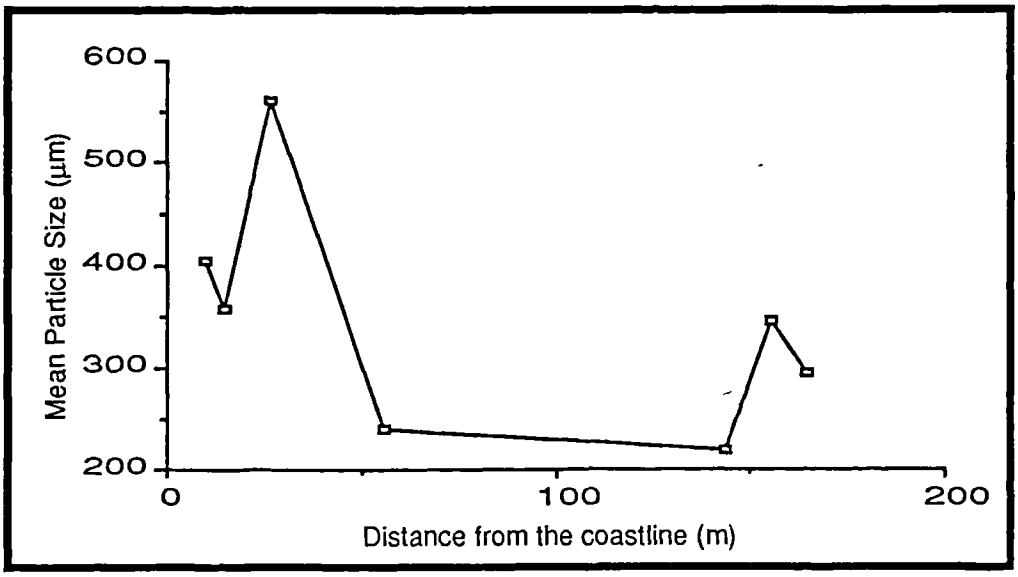

Figure 4.25. Lateral variations in mean particle size of the surficial tsunami sediment at Kojadoi, Besar Island. The sampling points are marked in Figure 4.17.

8.3 Pantai Lato

8.3.1 Particle Size Analysis: Lateral Variations

At Pantai Lato, there is an area of coastal lowland, lying at the inner edge of the Wai Prung Bay (Figure 4.26). Along the outer edges of the bay, rocky coasts flank the hilly coastal lands, upon which earthquake-induced damage, fallen rocks and ground cracking occur. Here, only erosional features produced by the tsunami were observable along the coastline whilst the effects of the coastal flooding include discoloured vegetation and its debris, which marks the maximum inundation level upon the slopes of the hilly ground.

On the coastal lowland at Lato, the maximum run-up was measured as *circa* 3 m with inundation reaching as far as *circa* 140m inland. Tsunami sediments were deposited here as a continuous sheet of thickness up to a few cm and restricted to an area 80m inland from the coast (Figure 4.27). Four surface samples were obtained along a line perpendicular to the coast, and the result of particle size analysis is illustrated in Figure 4.28. The particle size

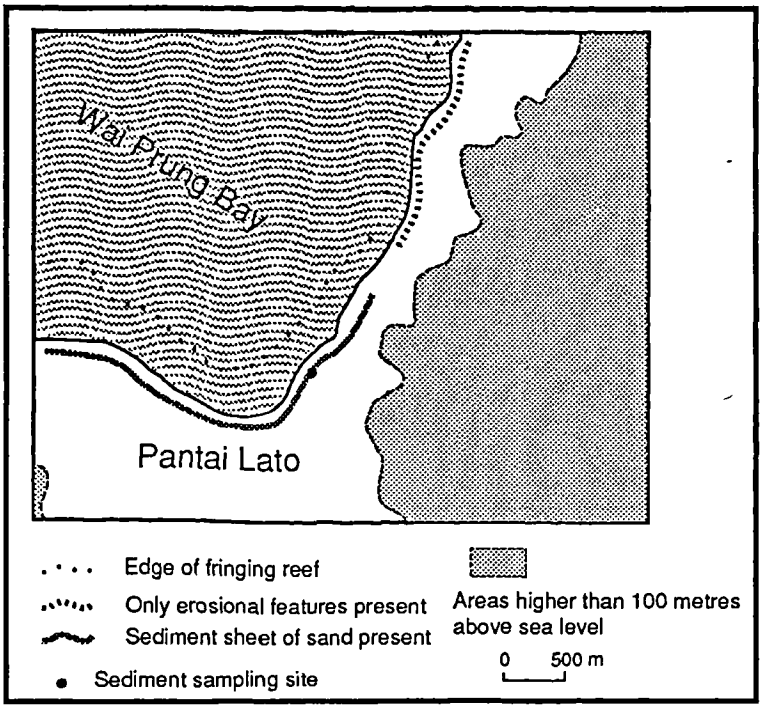

Figure 4.26. Location map of the site at Lato.

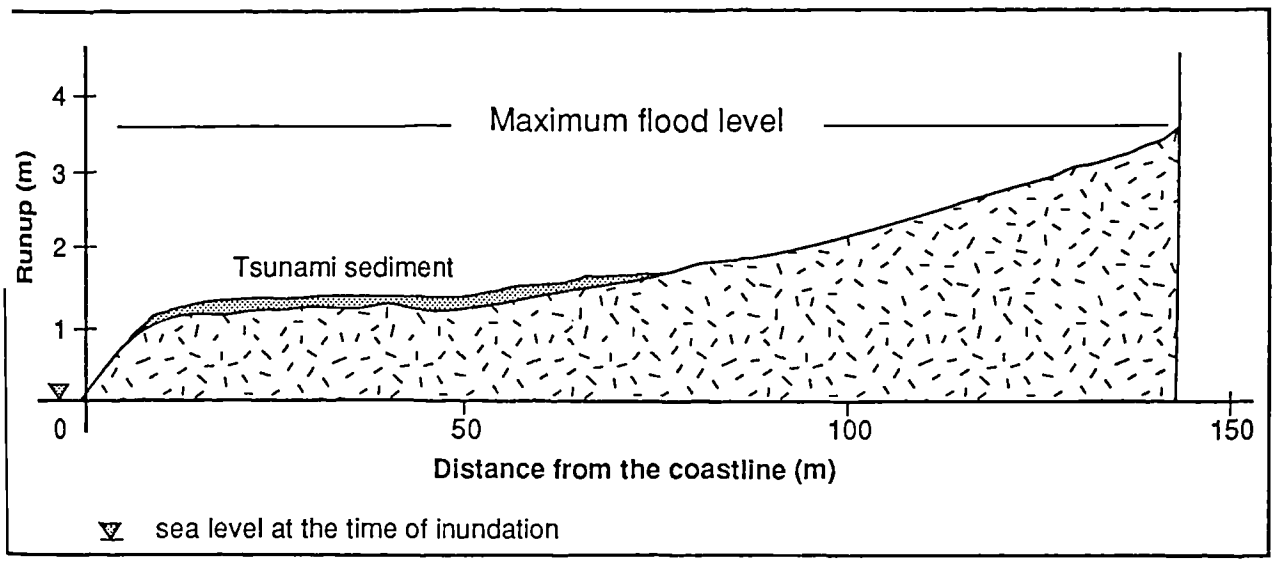

Figure 4.27. Schematic diagram showing the measured maximum inundation distance (*circa* 140 m), the altitudinal limit of run-up (3.5 m) and the extent of a continuous sand sheet at Lato. Note that the thickness of the sand sheet is only a few centimetres and is exaggerated here. Farther inland from the sheet, only isolated patches of fine sand occur and their thicknesses are in the order of a few millimetres.

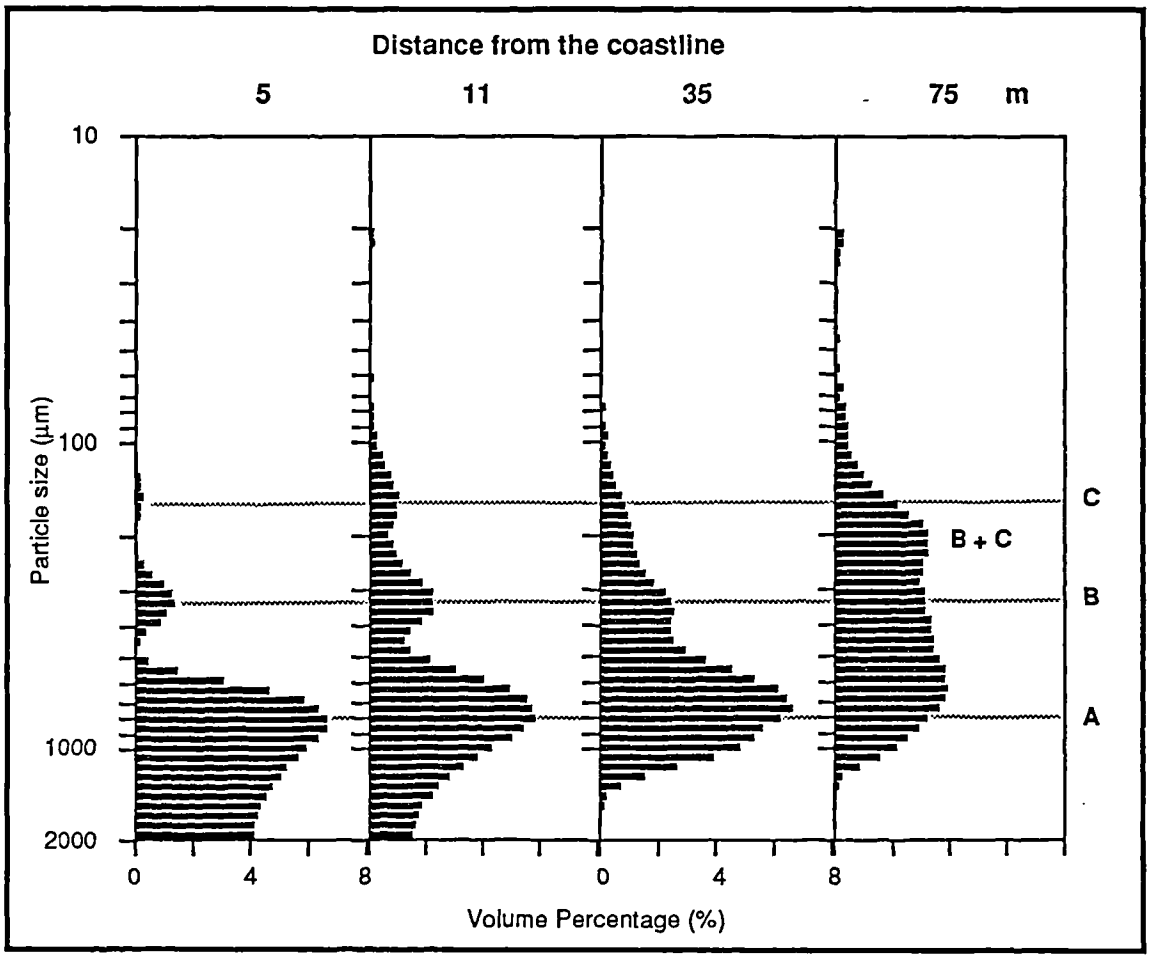

Figure 4.28. Lateral variations in the characteristics of particle size distribution of surface sediment at Lato. For convenience, the three subpopulations of particles are named population A, B and C respectively from the coarsest to the finest. From the coast inland, the proportion of the coarsest population A decreases and its modal position shifts towards finer size range, while populations B and C increase and both their modal positions remain relatively constant at *circa* 300 and 150 μm on the size scale respectively for the first three samples. The most landward sample appears to exhibit a bimodal distribution with its finer modal postion (*circa* 200 μm) resting between the modal positions of populations B and C. Clearly, it is very likely that an enhancement in the proportion of population C has led to a seemingly new population as a result of the merging of populations B and C. Unequivocally, the sediment fines landwards.

distributions are all multi-modal and show clear lateral variations in their frequency curves, which reflect changes in the relative abundance of respective subpopulations. It can be clearly seen that a landwards fining trend is associated with a decreasing abundance of the coarsest subpopulation.

8.4 Interpretation and Discussion

8.4.1 The Role of the Source Sediment

Although there is difficulty in quantifying and interpreting the relative contributions of specific sediment sources, there are ample indications that the source of sediment for tsunami deposition was largely drawn from local coastal soil at Nebe. Such indications include appearance (especially light-grey colour) of the tsunami sediment, local morphological changes and scarcity in sediment on the coral reef. The particle size distributional characteristics of the sediment are found to be dependent on the characteristics of its source material and the processes of transportation and deposition. The source material (local soil) is composed of particles, which cluster into several size ranges forming subpopulations. The subpopulations in the sand range are readily identifiable in the tsunami sediment and this compositional characteristic imposes significant controls upon the resulting characteristics of the tsunami sediment. Modification of the transported sediment has also conceivably occurred as a result of differential transportation and sedimentation of different sized grains. It is considered here that dynamic processes involved can be inferred from variations in particle size composition since sandy deposits concerned are not cohesive in nature, as discussed in Chapter 2 - Methodology (Pages 18 and 19). The significant difference in composition between the local soil and tsunami sediment indicates that a large amount of clay and silt has been removed and transported into the sea. In addition to this, other modification or sorting processes of particle size composition associated with transportation and deposition are conceptually derived from the granulometric evidence and are given in the following respective sections.

Although it is not as clear as at Nebe, source sediments are believed to have been derived from both the beach and the coastal lowland at Kojadoi. Nevertheless, it is clear that similar variations in the composition of the particle sizes within the tsunami sediment are replicated here, and that the multimodal characteristics of the tsunami sediment should reflect that of the mixture of particle size subpopulations transported by the inundating currents.

8.4.2 Deposition and Sorting Processes

At both Kojadoi and Nebe, the inherited multi-modal characteristics (in the sand range) borne by the tsunami sediment clearly reflect that sedimentation took place at fast rates and that particles settled out simultaneously although at different rates. This is well illustrated by some of the individual fining-upward sequences of typical multi-modal distributions which consist of consistent sand subpopulations. Progressive compositional variation of the sediment within such fining upwards sequences indicates that the modal positions of subpopulations occur within consistent size ranges and the coarsest fraction fines and decreases in proportion upwards. Such a variation trend registered in the sediment indicates that the coarsest particles were progressively decreasing in concentrations in the transporting waterbody when sedimentation took place. This clearly indicates a unique settling process, in that rates of tsunami sedimentation are so high that both fine and coarse particles settle together, although the coarser particles have higher sedimentation rates than the finer ones.

8.4.3 Tsunami Runup and Backwash

Tsunami inundations consist of both run-up and backwash processes and both types of these contribute to processes of reworking, transporting and depositing sediment. The occurrence of a multiple set of fining-upwards sediment sequences clearly indicates that there are net accumulations of sediment resulting from different episodes of run-up and backwash. Separate suites of sediment with different granulometric characteristics are identifiable.

8.4.4 Lateral Sorting

The general trend of fining landwards is undoubtedly a result of differential transport, which has winnowed more fine particles farther inland than coarser ones. At Nebe, such a trend has been obscured due to the effects of complex topography and possibly also different episodes of inundation.

Landwards dispersion of sediment associated with a tsunami inundation is best recorded at Lato. The sediment sheet at Lato is interpreted as having been produced by the final inundation of the coastal lowland, because it is very thin and is restricted near the coast although the maximum tsunami inundation distance is much greater. Undoubtedly, the sediment was winnowed landwards and was subject to the influence of backwash. Nevertheless, the lateral variations in particle size composition provide important information on sediment dispersal processes associated with tsunami inundation. The characteristics of the sediment composition and its lateral variation not only reinforce the finding that the particle size characteristics of tsunami sediment are controlled by the characteristics of transported sediment, but also support the view that the sediment exhibits a landwards fining trend which is reflected in the sorting of the coarsest population. As a tsunami inundation is adequately powerful to carry material (eg. concrete slabs) much coarser than the sediment described above, it is very likely that all sized particles of the sediment were transported and dispersed at the same time, with finer particles travelling faster in the transporting water body than the coarser ones. Moreover, it seems to be suggested by the results that lateral sorting was predominantly imposed upon the coarsest fraction of particles by the transporting waterbody.

In summary, the sorting process of the source material by the Flores tsunami can be conceptually understood as having occurred in two different ways. Primary sorting is represented by the removal of a large amount of clay and silt by tsunami backwash.

Secondary sorting resulted in further modification of the transported material during the tsunami transportation and sedimentation. Variability is most pronounced at the coarsest end of particle size distribution within the tsunami sediment. At present, distinction between the sediments deposited by run-ups and backwashes is not fully understood. Nevertheless, the particle size distributions of the sediment and their variations probably reflect a unique process in coastal geomorphology.

9. CONCLUSION AND IMPLICATIONS

9.1 Conceptual Model of Tsunami Inundation

The Flores study indicates that tsunami inundation was an ephemeral process and consisted of several episodes of runup and backwash. The hydrodynamics of runup and backwash were characterised by turbulent flood currents rather than waves. During the runup phase of one episode of inundation, a large amount of energy transferred from the incident offshore wave was dissipated over the coastal topography through destroying, eroding and transporting solid materials as well as was reserved as a result of part of the waterbody being elevated. Examining the hydrodynamics of the runup processes further, there appears to be ample evidence, indicated by eyewitness accounts of the impact upon coastal areas, that tsunami waves broke far away from the coast (near the edge of fringing coral reef), and turned into horizontal passages of turbulent water with great impetus, running across the near-shore zone to strike upon the coastal lowland. Theoretically, once a tsunami wave breaks, its impact can exert a tremendous force on objects and obstacles, and scour up and carry a large amount of material in its path. In the case of the Flores tsunami event, there was a general lack of loose sediment available on the coral reefs and most erosion occurred on the coastline and coastal lowlands.

Immediately following the wave ebbing offshore, backwash taking place due to the gravity of the elevated waterbody (or a pressure gradient), was also erosive and transported materials offshore. As indicated by the evidence presented above, undoubtedly both processes of runup and backwash were turbulent in a strict hydrodynamic sense. Since the backwash only possessed the reserved energy, and might have lasted for a longer duration, it was weaker than the runup. This explains the presence of accumulations of deposits transported landward. However, in some cases, the energy of the backwash flow was so high that there was little trace of deposition and instead extensive erosion. This was undoubtedly due to backwash flow being capable not only of transporting the amount of materials carried landward by unsaturated runups, but also of further eroding, as a result of the lack of sediment supply.

The reason for a limited amount of sediment being supplied to the transporting waterbody is believed to have been strongly linked to the process of erosion, apart from the lack of loose sediment on the reefs. Field evidence indicates that further erosion of sediment making up the coastal lowlands could have taken place. However, this did not occur probably because of the compaction of sediment and dense coverage of vegetation. It is speculated here that the energy required for setting well compacted and vegetation-protected sediment in motion is much greater than that for transporting it.

The scales of geomorphological changes have been found to be related to runup heights over a wide area. In particular, the zone and extent of erosion are found to be conspicuously related to runup height, although no detailed measurements were undertaken. Where runup values ranged between 1 and 4 m, severe erosion was confined to a narrow strip along the coast, whilst erosion was much more extensive upon coastal lands in areas around Riangkrok where the average runup height was 26 m (Yeh *et al.*, 1993).

9.2 Mode of Sediment Transport and Deposition and Diagnostic Features

It seems that the sediment was considerably dispersed and mixed during transport by the currents of runup and backwash. It is probable that the entrained sandy sediment was subject to turbulent suspension during part of the process of transport, as indicated by the scattered presence of concrete slabs or coral gravel, which were transported over significant distances, in the same area where sand was deposited. This is confirmed by the evidence of simultaneous deposition of various sized sand grains observed above, as sand grains are not likely to be cohesive (see discussion in Chapter 2 - Methodology, Pages 18 and 19). Together with the evidence of the dependence of the tsunami sediment characteristics upon its source sediment, this implies that the grain sizes of sediment can not be used to estimate the velocity of currents, since the required velocity for transporting the grains is far less than the maximum velocity of runup and backwash. In general, since the characteristics of the tsunami sediment are controlled by that of the available material, some of which could have been formed in much lower energy regimes, the inferred amount of velocity from grain size information is far less than the likely velocity of actual tsunami currents. This suggestion certainly does not exclude the possible significance of clastic materials in the estimation of current velocity, in the case that there are a large numbers of clasts, covering a wide range up to more than that specific tsunami coastal currents could reach. Summing up the available evidence observed, current energy can be significantly underestimated from particle size information.

The most important feature of the tsunami sediment is perhaps a multiple set of progressive and fining-upward changes in particle size composition, which is believed to reflect simultaneous deposition of particles of different sizes at differential rates during episodes of instantaneous deposition. This episodic instantaneous deposition is believed to be related to the characteristics of hydrodynamics associated with tsunami inundation: a limited number of episodes of turbulent swash action which change swiftly from highly energetic to relatively calm within a short period of time (typically a few minutes, half of the period of tsunami waves). However, the sediment resulting from different simultaneous

accumulations is not necessarily preserved equally in the overall sediment sequence, since reworking of part or whole of the deposited sediment by succeeding waves is very likely.

Sediment movement and accumulation processes associated with tsunami runups and backwashes may therefore be represented by a conceptual model, as shown in Figure 4.29. Here, the average velocity or energy of a tsunami current denotes the magnitude of the flow regime at any given time. The current possesses a specific capacity to transport a certain amount of sediment, related to the energy of that current. Sediment load is the actual amount of sediment the current carries at the time, which is less or equal to the capacity. When the sediment load is equal to the capacity, the current is saturated and its erosive power is at its lowest. When the current capacity becomes less than the sediment load as a result of a decrease in current energy, deposition occurs. In this model, for the purpose of clarity. the change of current energy status is merely depicted as smooth curves and the transition between runup and backwash is drawn as a distinctive status of relative calmness for a very short time span. However, at present, there is no information upon the detailed hydrodynamic processes of tsunami inundation and the model should be regarded as a preliminary one or an ideogram - the visual form of a conceptual model.

Since a runup is more powerful than a backwash and the runup decreases in energy while it travels towards its uppermost limit, a fining-landward trend is present in the particle size of sediment. The presence of this trend suggests that backwashs were not powerful enough to fully rework and redistribute already deposited sediment. This trend was also found to be sometimes disrupted or obscured, as a possibly combined effect of different episodes of inundation with different runups and the irregularity of local topography. However, in such cases, a general trend is still observable and this may represent one of the diagnostic features, which provides information upon the direction of sediment transport.

Alternating phases of erosion and sedimentation during the inundation of a single tsunami wave. On-land deposition is subject to the sufficiency of available sediment relative to the capacity of backwash.

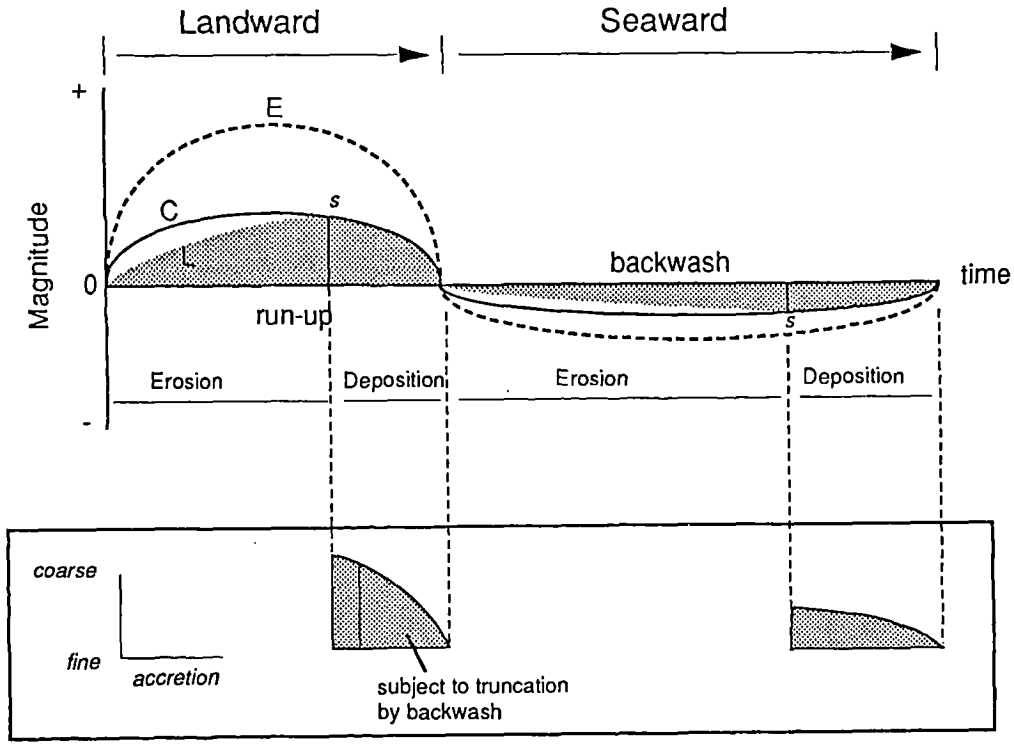

E - average velocity or energy of the current
C - capacity of the current to carry sediment
L - sediment load in the current
s - saturation point of sediment load

A

Example of vertical variations in mean particle size of tsunami sediment at Core 2, Kojadoi.

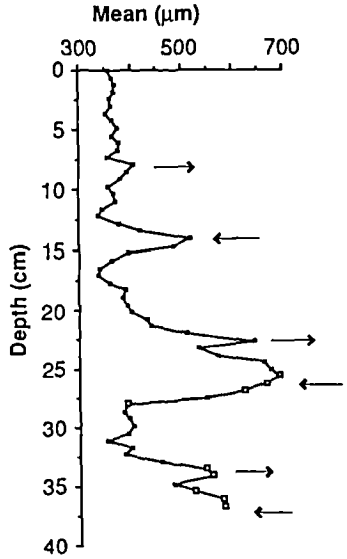

← and → denotes peaks of value of mean particle size, which are inferred to represent the onsets of runup and backwash accretion phases, based upon the assumption that no complete truncation occurred of previous accumulations by succeeding currents.

B

Figure 4.29. Preliminary model of sediment accumulation process associated with tsunami inundation.
NB: Although sediment truncation presents inherent uncertainties in interpreting sediment accretions attributable to processes of runup and backwash, it is clear that the sediment accumulation resulted from a limited number of episodic passages of water.

One of the most important features is extensive sediment sheets extending upon coastal lowlands and ascending from the coast inland. Although the uppermost limit of sediment sheets was found to be lower than the maximum runup height that the tsunami reached, such information is believed to be very important to provide information upon the minimum magnitude of flooding.

The processes described above merely serve as a preliminary model of the bi-directional flow of tsunami flood. However, patterns of runup current can be very complex, largely due to the low degree of refraction of tsunami waves and the complexity of offshore and coastal topography. Similarly, the flow pattern of backwash is also complex, and is probably controlled largely by the local topographic relief. The interplay of turbulence and rapid sedimentation together with the characteristics of the transported material determine the resultant characteristics of the tsunami sediment. The analysis of the Flores tsunami sediments at Nebe, Kojadoi and Lato therefore presents a first attempt to understand the very complex and probably unique processes of sediment transport and deposition associated with tsunami flooding.

Chapter 5
The Second Storegga Slide Tsunami

1. INTRODUCTION

The coastline of eastern Scotland is marked by suites of terraces reflecting former levels of the sea (eg. Sissons, 1976). There are broadly two groups of these terraces: those formed during the retreat of the last ice sheets, and those formed after glacier ice had largely, if not completely, disappeared. The latter group was formed during the last 10,000 years, the Holocene or Flandrian, and generally lie at altitudes below *circa* 14m O.D.. They include large tracts of former estuarine mudflats known locally as carselands.

In recent years, research has disclosed that the sediments of the carselands, though locally variable in composition, contain a particularly widespread and continuous layer of sand, rarely over 30 cm thick (Figure 5.1). Studies of the stratigraphy, microfossil content and age of this layer have shown that it was deposited during a high energy event *circa* 7,000 radiocarbon years before present (Smith, Morrison, Jones and Cullingford, 1980; Smith, Cullingford and Brooks, 1983). It has been suggested that the event may have been a major storm surge taking place during a period of rapid relative sea level rise (Smith, Cullingford

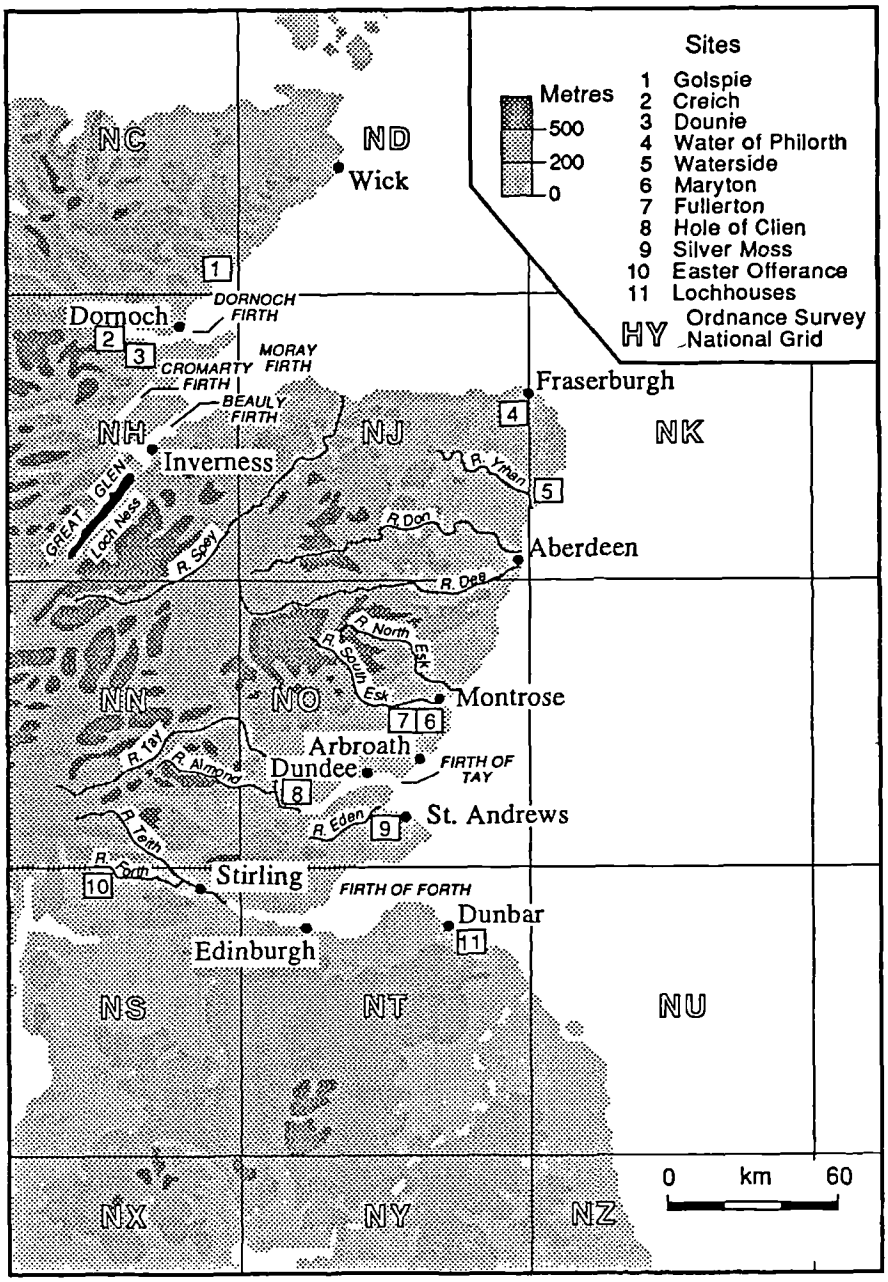

Figure 5.1. Location map of the sites where a continuous sand layer has been found to be intercalated in coastal sediment sequences, marking a high-energy low-frequency flooding event.

and Haggart, 1985) or, more probably, a tsunami (Dawson, Long and Smith, 1988) caused by movement of the second Storegga submarine slide on the continental slope west of Norway (Bugge, Befring, Belderson, Eidvin, Jansen, Kenyon, Holtedahl and Sejrup, 1987).

2. HYPOTHESES AND OBJECTIVES

The identification and differentiation of storm surge and tsunami deposits have been a long-standing problem in geological investigation. This is a challenging geological issue which remains to be solved. In contrast to wave phenomena under normal coastal hydrodynamic conditions, storm surges and tsunamis are both high-energy events and can cause significant coastal geomorphological changes with the movement of a large amount of sediment. As mentioned above, the widespread sand layer has been generally accepted as having been deposited by one of these high-energy events, although it is unclear whether it was deposited by storm surges of extremely high magnitude or by a large tsunami. The aims of the work described here were therefore to:

1) examine the nature and distribution of the sand layer laid down during the Holocene in eastern Scotland;

2) identify the processes by which the sediments were deposited;

3) examine the wider significance of the sand layer as a possible chronostratigraphic marker.

3. STORM SURGE DYNAMICS AND SEDIMENTATION

Storm surges are both high-energy and, in contrast to tsunamis, relatively high-frequency phenomena along coasts. They can cause extensive inundation and impose dramatic geomorphological impacts on coastal areas. It is crucially important here to gain a good understanding of coastal sedimentation processes and sediment characteristics associated

with storm surges before any attempt is made to differentiate storm surge and tsunami sediments from each other.

Extensive research into storm surges has so far concentrated upon empirical and hydrodynamic numerical modelling, while efforts have also been made to predict extreme sea level elevations associated with storm events (cf. Heaps, 1967 and 1983). Among the publications on storm surges are a few works related to the effects of storm surges on coastal sediments and associated sedimentation (eg. Steers, 1953; Heath, 1979; Aigner and Reineck, 1982), and inferences of ancient storm surge events from sedimentary sequences (eg. Brenchley, Newall and Stanistreet, 1979).

3.1 Coastal dynamics

A storm surge event consists of dynamically linked processes of sea water conditions, including greatly increased wave action, currents and extreme elevations of the sea surface. The generation of storms is associated with deep atmospheric low pressure systems, giving stormy weather conditions. As a result of the significant decrease in barometric pressure involved, the sea level is elevated and thus two distinct effects may be expected, a) a drift of water in the same direction as the wind and b) a windwise tilting of the sea surface in order to balance wind shear by means of a pressure gradient. When a low pressure system approaches a coast, and winds are onshore, especially at a time of high tide, the elevated sea surface may significantly increase in level and inundate the coastal lowlands. In order to balance out the onshore flow of the wind-stress induced surface currents, offshore bottom currents are formed and travel offshore across the floor of the shallow coastal sea disturbed by the oscillatory wave motion as a result of the deepened base of wave action (Allen, 1985).

Theoretically, storm surge sedimentation can be described as a process of stirring of the sea floor by oscillatory currents, caused by deepening of the wave base, and lateral sediment

transport from coastal to shelf regions created by gradient currents that flow offshore. These offshore flowing water masses compensate for wind-stress and nearshore water buildup and are often enhanced by ebb tidal currents. As a result of this offshore transporting mechanism, the characteristics of sedimentary sequences are largely controlled by two factors, a) distance from land where coastal sediments serve as source material for offshore storm sand sheets, and b) local water depth since storm effects decrease with increasing depth. The work of Aigner and Reineck (1982) demonstrated such effects as distance and water depth on storm sedimentary characteristics, and they classified sedimentary zones as 'shoreface', 'proximal' and 'distal', forming a similar concept to the 'proximality concept' in turbidites.

3.2 Storm sedimentary characteristics and proximal trends

Aigner and Reineck (1982) conducted a detailed study of modern storm sand deposits (tempestites) in the Helgoland Bight, North Sea, and constructed a stratigraphical model of proximality (Figure 5.2). They reported that the percentage of sand and of graded rhythmites, storm layer thickness, grain size as well as the degree of amalgamation show a continuously decreasing trend from shallow to deeper water. The sedimentary characteristics were classified into three different types, namely shoreface, proximal and distal sedimentary sequences (Table 5.1).

Other studies have also reported seaward sediment transport associated with storm surges and that there is a trend of decrease in the thickness, occurring frequency and grain-size of the resultant sand or silt sheets from coast to offshore (Gadow and Reineck, 1969; Reineck and Singh, 1971). Storm sediments possess clear characteristics and associated trends, although the mechanism of material transport is not clearly understood and a number of mechanisms have been proposed (Aigner *et al.*, 1982).

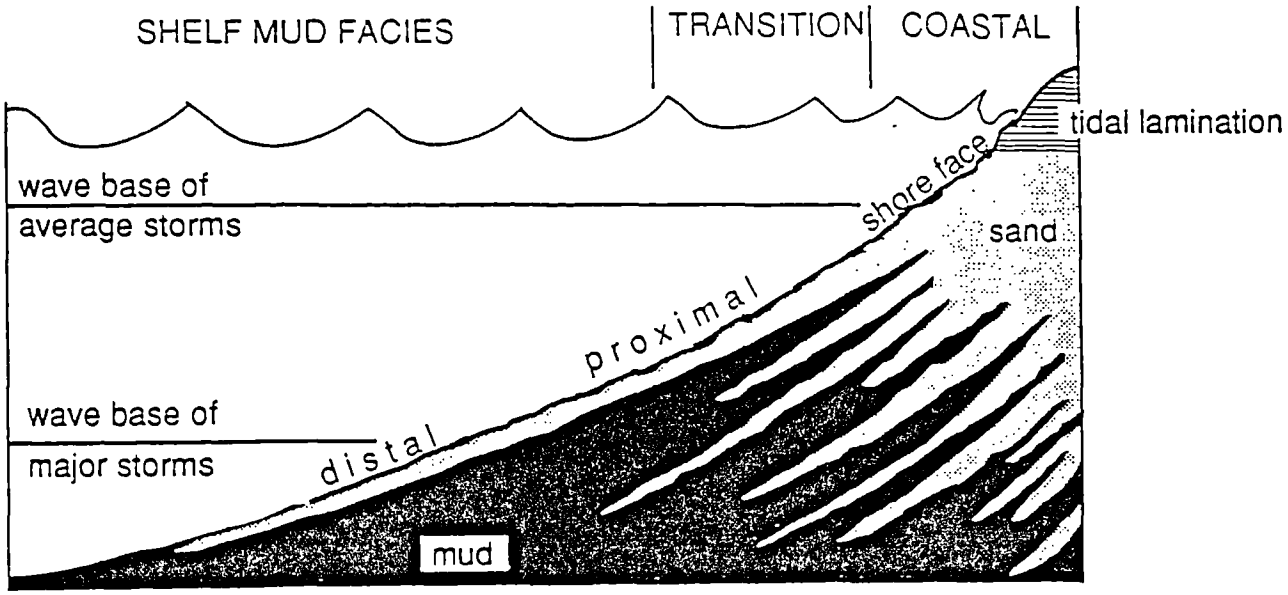

Figure 5.2. Stratigraphical model of storm surge sedimentation (after Aigner and Reineck, 1982).

Table 5.1. Characteristic Storm Stratification and Proximality Classification (after Aigner *et al.*, 1982).

Shoreface Storm Sands
The deposits range in thickness between 5 and 130 cm. The erosive bases are often overlain by shell layers, followed by laminated sand which may be overlain by wave-ripple lamination. Bioturbation of the deposits is mostly minimal, although the upper parts of sequences are often slightly bioturbated. Erosive contacts and amalgamation are conspicuous.
Proximal Storm Sands
The sediments are relatively thick (several cm to tens of cm). The basal surfaces are erosional, often strongly scoured and may sometimes be characterised by gullies. The surfaces are often covered by shell layers (1 mm to several cm thick) of mixed fauna derived from tidal channels or tidal flats. The internal structure of proximal tempestities is mostly characterised of parallel laminated sand which is weakly graded and slightly finer than storm sand at the shoreface. Laminations are often slightly inclined (low-angle laminations) with minor internal discordances. Some of the proximal beds may be entirely composed of wave-ripple lamination, which is most common at the top of many beds. Lying at the top of the sediment is a thin layer of non-bioturbated mud.
Distal Storm Sediments
The distal storm sedimentary layers are thinner (up to just a few mm) and composed of mostly finer-grained sand/silt. The bases are mostly erosional, although sometimes appear non-erosional. Shell layers are composed largely of untransported soft-bottom faunas. Internally, distal sand layers are mostly laminated, seldom as graded rhythmites, and ripple-lamination is conspicuously rare. A blanket of unbioturbated mud rests on the top of the sediment.

3.3 Restricted landward sediment transport by a modern storm surge

Sometimes, storm waves can breach coastal barriers and transport some sediment landwards. The storm surge of 11 January 1978 caused considerable damage on the coasts of Lincolnshire, the Wash, and East Anglia. A previous study revealed the detailed effects of the storm surge, notably including extensive erosion along the coast and localized breaching of coastal barriers and dunes and the consequent transportation of sediments onto adjacent salt marshes (Steers, Stoddart, Bayliss-Smith, Spencer and Durbidge, 1979). Soon after the event, these authors investigated the effects of the storm surge at Scolt Head Island, Norfolk and produced a detailed description of the storm deposits including particle size analysis of the deposits using the sieving method. They observed that mean particle size shows a decrease inland towards the salt marshes and that there is an increase in sorting towards the toes of washover aprons (Steers *et al.*, 1979). In this study, one of the sites previously investigated by Steers *et al.* was chosen for further investigation of the granulometric characteristics of the deposits and their vertical variations within the sediment. Drawing upon these analytical results, the processes by which sand was deposited upon salt marshes is discussed.

3.3.1 Morphology and Stratigraphy

The area on Scolt Head Island studied by Steers *et al.* (1979) is morphologically characterized by coastal dunes and sand ridges at the coast and an extensive salt-marsh area lies between the dunes and the land. The dunes and beaches are curvilinear features exposed to open water, but do not form impenetrable barriers in terms of their lateral configuration. The storm surge of 11 January 1978 caused considerable damage on the coast. Along the North Norfolk coast surge levels varied between 4.6 and 5.9 m O.D., similar to the last severe surge in 1953 (Steers *et al.*, 1979). At the site on the Scolt Head Island dunes were cut back 20 m, and fresh sediment aprons were formed behind the most seaward beach ridge (Figure 5.3). The sediment deposited during the storm surge occurs above salt marsh

deposits and extends less than two hundred metres away from the foot of the dune, whilst its surface declines from the beach towards the salt marsh (Figure 5.4) (Steers *et al.*, 1979).

3.3.2 Grain Size Characteristics of the Sediment

The sediment characteristics of the washover aprons have been previously studied and described along four transects by Steers *et al.* using the sieving method (1979). In their study, it is maintained that the sands of the washover deposits have a median size of 1.59 ø and are very well to moderately well sorted, negatively skewed, and mesokurtic to leptokurtic. In comparison with the sediments of the beaches and dunes at Scolt (Roy, 1967), they most closely resemble in mean characteristics those of the beach environment. However, the former are considerably less variable than the latter. The washover deposits are in general both coarser and better sorted. In mean size the washover sediments resemble dune sands, but the dune sands show a higher degree of sorting. They suggest from the data that both beach and dune sands were incorporated in the washover deposits, but that during the processes of transportation and deposition both grain-size selection and a high degree of sorting of the material took place. They also noted that there is little variation in median grain size along the individual sediment profiles, apart from a fining within 5-10 m of the landward limit. Mean grain size shows a decrease towards the salt marshes. There is an increase in sorting to landward, the toes of the aprons being well sorted (Steers *et al.*, 1979)

In this study, two sediment cores were collected along one of the transects described by Steers *et al.* (1979), Transect 8 (Figure 5.4). Detailed field study showed that it was possible to identify the washover area with some confidence, following the descriptions in Steers *et al.* (1979). The cores were sliced into contiguous 1 cm-thick samples. Representative particle size distributions are shown in Figures 5.5 and 5.6. The particle size distribution of the sediment is generally slightly negatively skewed to log-normal and unimodal, indicative of a high degree of sorting, whilst its modal size rests in the medium

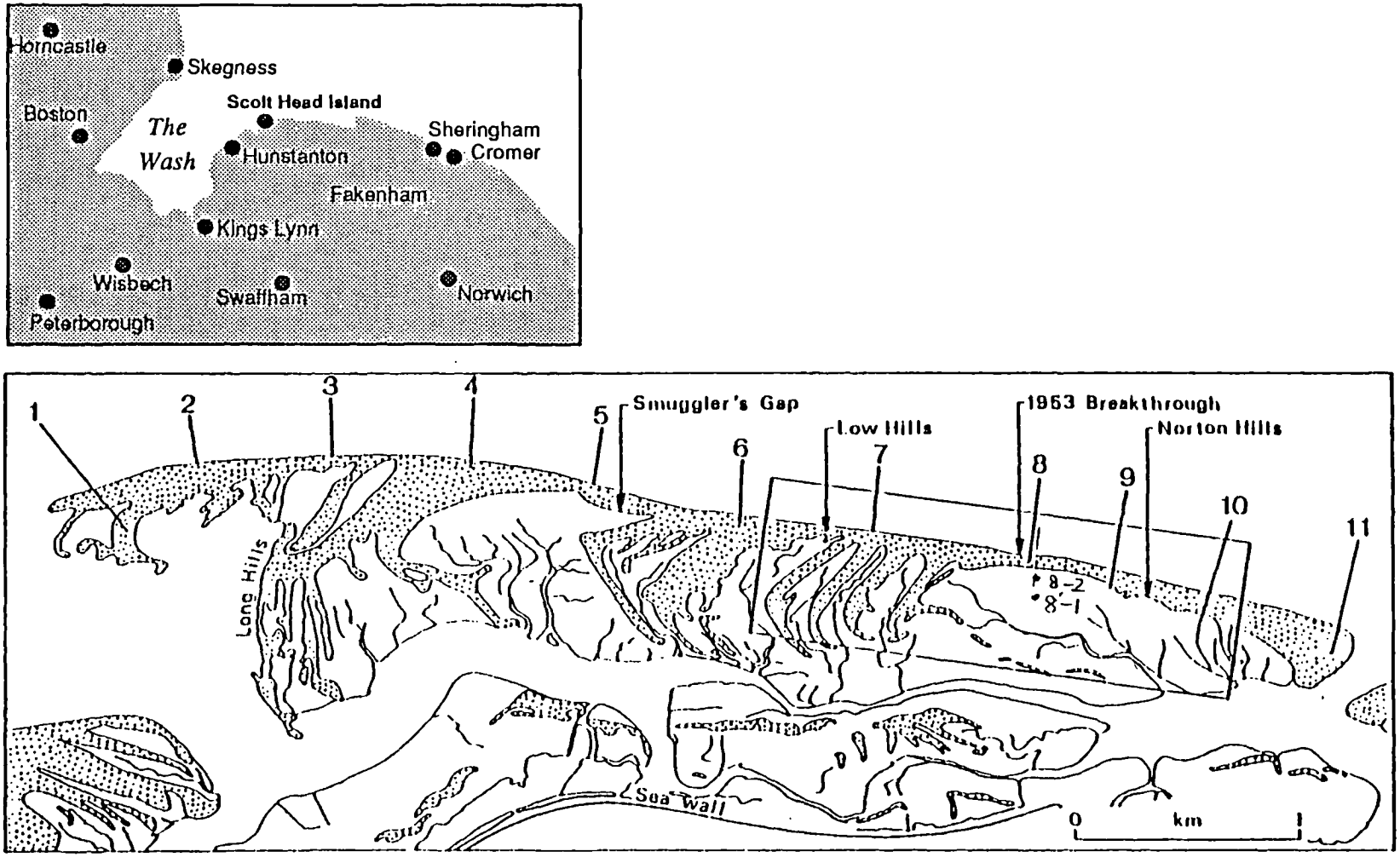

Figure 5.3. Morphology on the Scolt Head Island, Norfolk and the location of investigated profiles of storm surge deposits (Steers *et al.*, 1979). In this study, two sediment cores (8-1 and 8-2) were obtained along Profile 8 for particle size analysis. The dotted pattern indicates areas of sand.

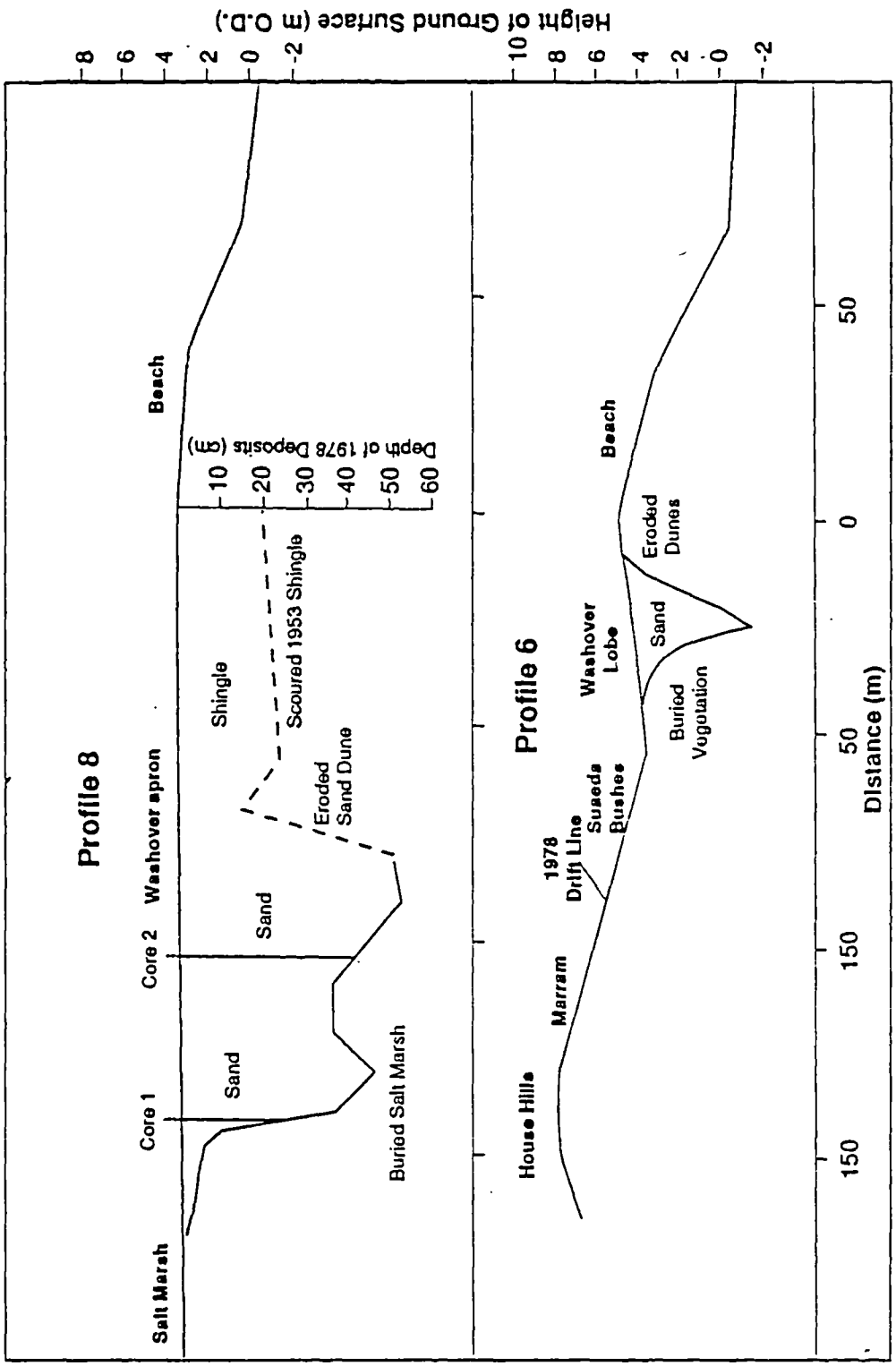

Figure 5.4. Cross-sections of washover sediment aprons deposited during the 11th January 1978 Storm Surge event at Scolt Head, Norfolk (after Steers *et al.*, 1979). The locations of the profiles are indicated in Figure 4.3.

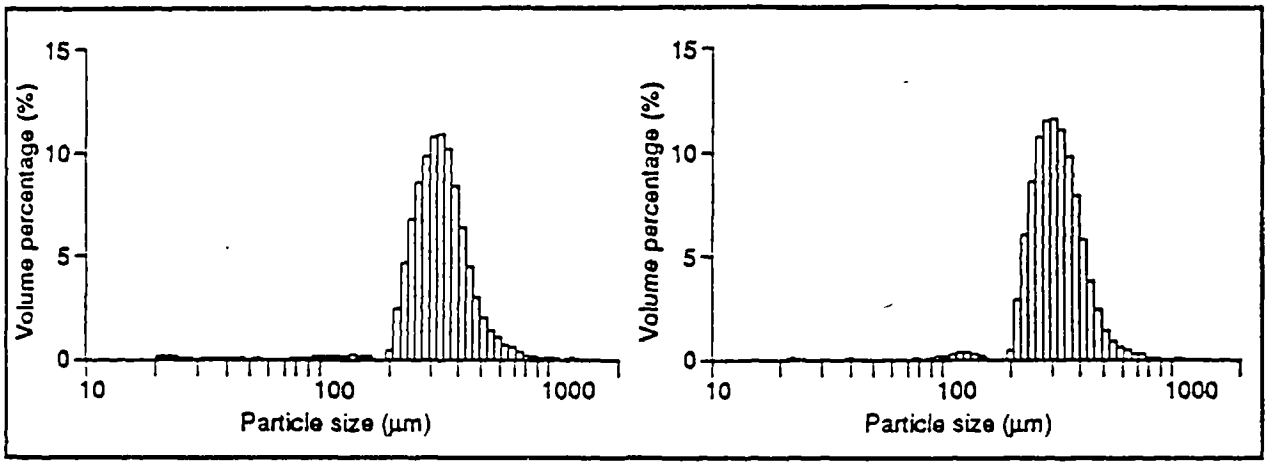

Figure 5.5. Representative particle size distributions of the storm surge sediment at Core 8-1, Scolt Head Island.

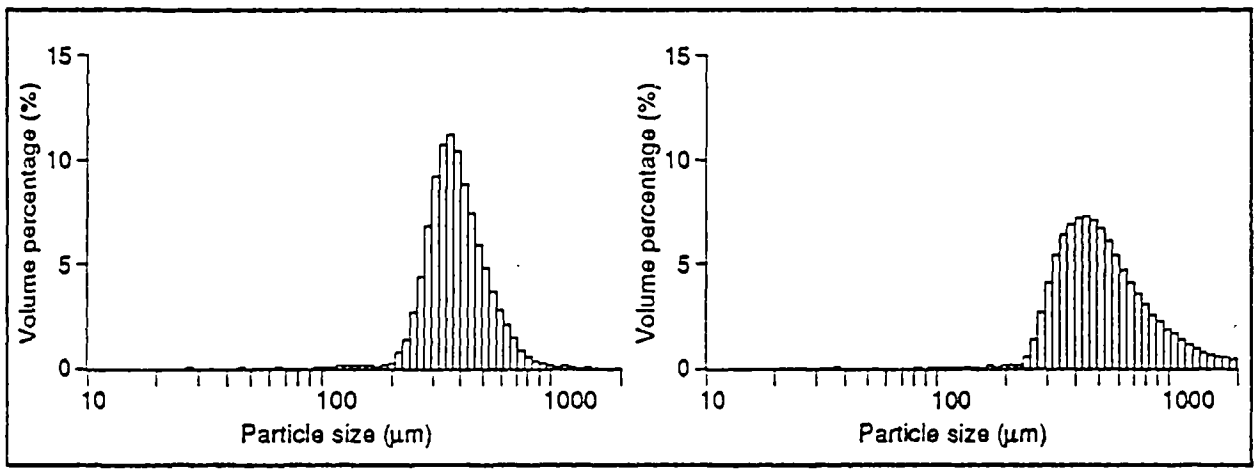

Figure 5.6. Representative particle size distributions of the storm surge sediment at Core 8-2, Scolt Head Island.

sand size range. Most samples of the sediment are characteristically negatively skewed and the rest are very close to log-normal distributions, as exhibited by the histograms of particle size distribution but not reflected by the parameter 'skewness' which is exceedingly sensitive to the minor occurrence of fine particles. The composition of the particle sizes shows a lack of fine particles less than 200 μm.

Downcore variations in the composition of the sediment are very irregular and exhibit neither periodically progressive changes nor distinctive vertical trends, as illustrated by haphazard fluctuations in mean particle size, standard deviation and kurtosis (Figures 5.7 and 5.8).

3.3.3 Interpretation

Breaching of the dunes

It is clear, as pointed out by Steers *et al.* (1979), that the sediment of the deposited sand aprons was derived from the beach and dune sand. It is very likely that derived sediment was re-mixed during its transportation and deposition. Its particle size characteristics (the general lack of particles in the silt and clay range and most of the sediment samples being slightly negatively-skewed) suggest that the salt marsh deposits were not incorporated and that the storm surge sediment was subject to sorting during its deposition. Since the characteristic of being negatively-skewed is so far found to be strongly connected with beach sediments (Visher, 1969 and Malcolm, 1981), the sediments deposited during the storm surge are believed to resemble beach sediments more closely than dune sands.

Processes associated with the breaching of the dunes probably included the rising tide, storm-induced set-up of the sea surface and significantly enhanced swash waves. It is clear that the salt marshes had been flooded to a similar level to that at the foreshore prior to the breaching of the dunes, since these areas were constantly washed by the tides during normal

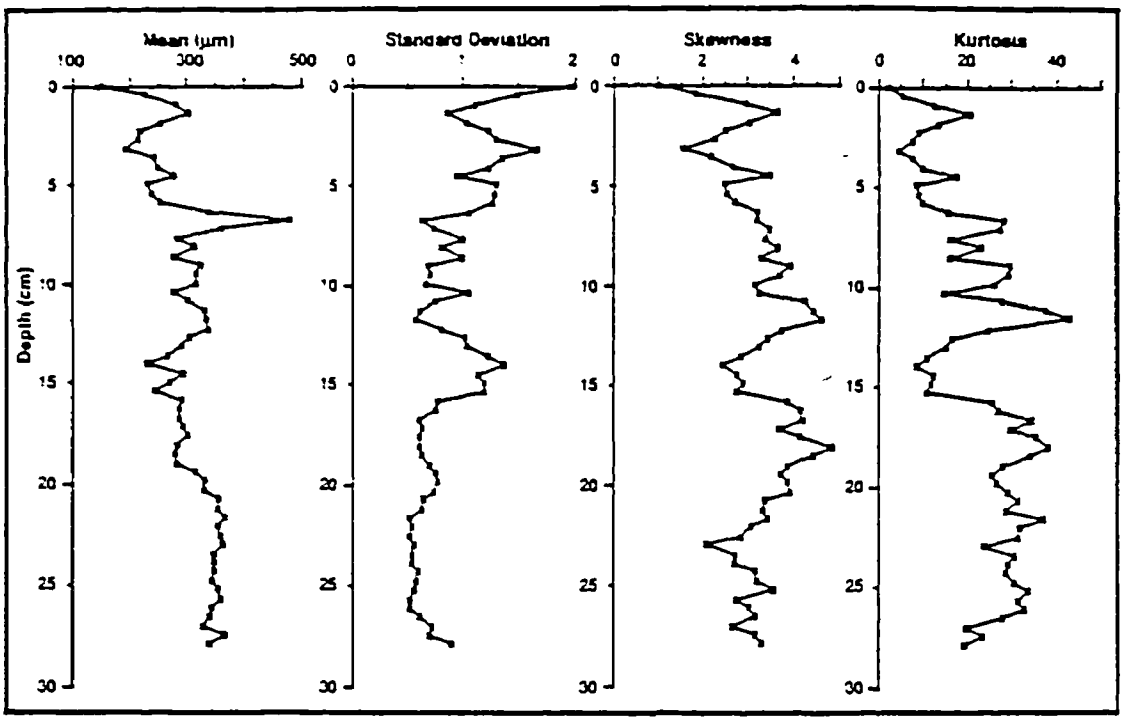

Figure 5.7. Vertical variations in the parameters of particle size distribution of storm surge sediment at Core 1, Scolt Head Island.

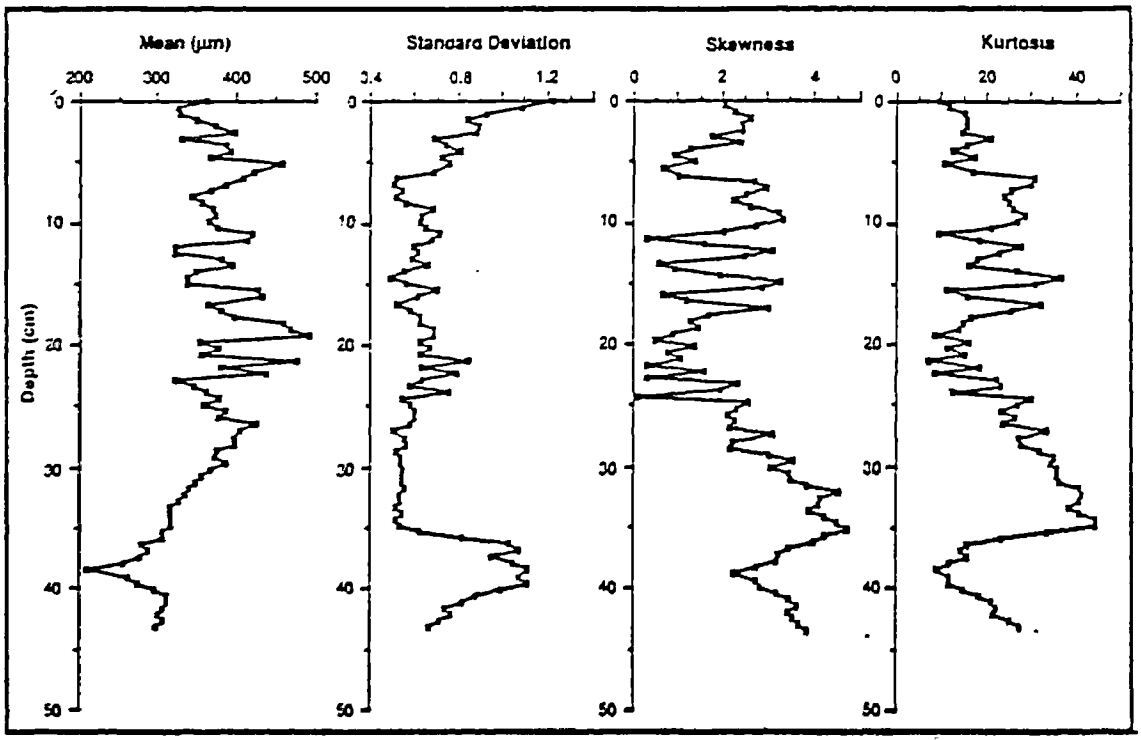

Figure 5.8. Vertical variations in the parameters of particle size distribution of storm surge sediment at Core 2, Scolt Head Island.

weather conditions. It is highly likely that the breaching of the dunes was caused by extraordinarily large breaking waves at the beach, riding upon an abnormally elevated sea surface. Once parts of dunes were breached and cut down, they were much more prone to further breaches of upsurging beach waves.

Although it is difficult to dismiss the possibility that an upper layer of the sea water travelled from the open sea and surged upon and breached the dunes due to its inertia, there is no evidence that it could possess a considerable amount of momentum. This is clearly manifested by the evidence that there was not any significant instantaneous accumulation of sediment behind the dunes, as indicated by the results of the particle size analysis. It is considered that any inertial surge of a waterbody with considerable momentum would have transported a considerable amount of sediment and deposited a graded bed up to a thickness of at least a few centimetres, which is detectable with high-resolution particle size analysis.

Therefore, it can be concluded here that the accumulation of the sand aprons behind the dunes resulted from numerous breaches of the dunes by greatly enhanced wave activity, rather than by a number of episodes of impetus surges of large volumes of water.

3.4 Summary

The sedimentation processes associated with storm surges are the joint product of abnormal high stands of sea level, strong waves and the offshore flow of bottom gradient currents. Effects of storms include coastal erosion caused by significantly enhanced wind-generated waves riding upon abnormally high stands of the sea surface.

Since there have not been many detailed and comprehensive accounts of coastal geomorphological effects associated with storm surges (except studies of flood levels and coastal hydrodynamics), coastal sedimentology can only be speculated upon. The effects of a storm on coastal sediments may result in extensive erosion along the coasts and offshore

transportation and deposition of large amounts of sediment, although there may be localized and restricted net landward transport and deposition of sediment. As such transport is almost exclusively associated with wind-generated waves (the energy of which is partly controlled by nearshore and offshore bathymetry), any possible deposits closely associated with the flood level would be considerably sorted and could be very unlikely to possess any distinctive progressive grading.

Such an abnormal temporary sea level rise takes place over several hours. Although large areas can be inundated and the transportation and deposition of great amounts of sediment can be caused by greatly enhanced wave activity during unusually strong storms, sedimentary dynamics are generally characterised by 1) bottom density flow of fine particles in suspension towards the seabed; and 2) possible net accumulations of deposits in the inundated areas, which form curvilinear features and do not possess sequences exhibiting progressive and fining-upward changes in particle size composition, which are indicative of rapid deposition. However, it is difficult to exclude the possibility that flooding of completely enclosed lowlands or coastal lakes would possess remarkably different sedimentation dynamics, which would be similar to dam-failure mechanisms. This implies that rapid deposition of sediment could be found in such environments, which would possess the kind of sequences indicative of simultaneous settling of particles. In geological studies, this can be differentiated and clarified through reconstructing the environment with stratigraphical and microfossil evidence. Stratigraphical and microfossil evidence can provide information on whether the pre-flooding environment was completely enclosed or linked to the open sea.

4. CONTEXT OF THE HOLOCENE FLOODING EVENT

In examining the distribution of the sediments deposited by the Holocene flooding event along the eastern coast of Scotland, it is important to consider the context in which these sediments were deposited. As indicated in many publications (eg. Sissons, 1983), the recent geological coastal evolution in Scotland has resulted in complex sedimentary sequences across a wide swath of areas and over a significant range of altitudes due to the combined effects of glaciation and relative sea level change. In this context, relative sea level change in Scotland during the Late Devensian and Holocene is examined.

4.1 Relative sea level changes and glacio-isostatic movements during the Late Devensian and Holocene

With the loading and unloading of ice masses on the Scottish landmass, glacio-isostatic deformation of the Earth's crust took place during the Late Devensian and Holocene. The magnitude of land depression at a specific location is a function of the thickness of the loaded ice mass, as is the rate of subsequent land recovery after the removal of the load. It has been demonstrated by many studies of former shorelines (e.g. Sissons, Smith and Cullingford, 1966) that the shorelines reached during and following ice decay have been differentially uplifted and thus tilted towards the centre of glacio-isostatic uplift. The glacio-isostatic movements, combined with the effects of regional eustatic sea level fluctuations, have brought about complex patterns of local relative sea level changes around the coasts of Scotland. Extensive evidence of relative sea level changes has been obtained through laborious and detailed studies as compiled and summarized by Sissons (e.g. 1983). The following text presents a brief summary of relative sea level changes along the Scottish coastline since the last glacial maximum. Set against this background, the unusual sand layer preserved in coastal sedimentary sequences along the eastern Scottish coasts is described and its origin is discussed.

At the maximum of the Late Devensian glaciation, regional sea levels were much lower than present due to glacio-eustatic effects, as manifested by the evidence that a large part of the central North Sea and the outer continental shelf west of Scotland were exposed as dry land (e.g. Sutherland, 1984). In response to isostatic recovery during ice-sheet deglaciation, relative sea level fell and played a major control on the development of complex sedimentary sequences in estuaries and open coasts (Sutherland and Gordon, 1993). It has been inferred, from the presence of raised shoreline sequences, that the rates of isostatic recovery were greater than the contemporaneous eustatic sea-level rise around much of the coasts of mainland Scotland during this period of time (Sissons, 1967). It is only around the coasts of the outer islands that submerged shorelines bear witness to the dominance of the glacio-eustatic rise of sea level (Sutherland *et al.*, 1993).

During the Lateglacial Interstadial, continuing land recovery led to a rapid drop of relative sea level around most of the Scottish mainland coast in the early part of this period. Rates of recovery were higher around the Highland margins, whilst the rapid decrease in relative sea level is demonstrated by the presence of former shorelines below present sea level in areas peripheral to the uplift centre. In the later part of the Interstadial, relative sea level around the Scottish coast was either below its present level or below the level attained following the later Main Postglacial Transgression (Sutherland *et al.*, 1993). This period is marked by a reversal of the trend in relative sea level and a renewed rise in relative sea level took place in South East Scotland forming the Main Lateglacial Shoreline. The shoreline consists largely of erosional features around much of the Scottish coastline (e.g. Sissons 1976, Dawson 1980, 1988, Firth and Haggart, 1989 and Firth , Smith and Cullingford, 1993) and the difficulty in dating it is reflected in recent debate (e.g. Gray, 1974, 1978; Dawson, 1988). It is suggested that it was mainly formed prior to the maximal extent of the Loch Lomond ice mass (eg. Dawson, 1980; Sutherland, 1984). In South East Scotland, a subsequent rise in relative sea level led to the deposition of the High, Main and Low Buried Beaches (Sissons *et al.*, 1966) possibly due to a renewed isostatic depression associated with ice readvance

during the Loch Lomond Stadial (Sutherland, 1984; ; Firth *et al.* , 1993), and although equivalents of the Main and Low Buried Beaches have been described from the Moray Firth (Haggart, 1987) in northern Scotland, they have not so far been identified in western Scotland (Dawson, 1984; Shennan, Innes, Long and Zong, 1993 and Shennan, Innes and Zong, 1994).

The age of the Buried Beaches have been determined in the Forth valley, Beauly Firth and Dornoch Firth. In the Forth valley, Sissons (1966) estimated the age of the High Buried Beach at approximately 10,100 yrs B.P. from the relationship of its deposits to outwash fans as Loch Lomond Readvance ice withdrew from the area, and placed the Main and Low Buried Beaches at *circa* 9,600 and *circa* 8,800 ^{14}C yrs B.P. respectively from radiocarbon and pollen evidence. Robinson (1993) also obtained similar dates for the Main and Low Buried Beaches. In Strathearn, Cullingford, Caseldine and Gotts (1989) obtained dates of *circa* 9,600 ^{14}C yrs B.P. for the Main Buried Beach and *circa* 8,600 for the Low Buried Beach. In the Beauly Firth, Haggart (1982) dated the Main Buried Beach at *circa* 9,600 ^{14}C yrs B.P. whilst in the Dornoch Firth, Smith, Firth, Turbayne and Brooks (1992) dated the Main Buried Beach at *circa* 9,600 ^{14}C yrs B.P.. The regression reached its lowest level between 8500 and 8300 B.P. in the Forth, Tay and Beauly Firth areas (Sissons and Brooks, 1971; Cullingford *et al.*, 1980; Haggart, 1989 and Sutherland *et al.*, 1993).

Thereafter, a rapid regional relative sea level rise overwhelmed the continuing isostatic uplift; the Main Postglacial Transgression took place everywhere around the mainland Scottish coast. This transgression culminated at between *circa* 6000 and 6800 years B.P. in eastern Scotland and the culmination was followed by a general regression spreading outwards from areas close to the centre of uplift (Smith *et al.*, 1983). The Main Postglacial Transgression resulted in extensive deposition of estuarine and marine deposits, which buried pre-existing lower coastal features and associated deposits. The evidence of the Main Postglacial Transgression is widespread and extensive, especially along the east coast of Scotland. The

culmination of the transgression is marked by the Main Postglacial Shoreline, the highest Holocene shoreline over most of Scotland, whose present altitudes are shown in Figure 5.9. Smith *et al.* (1985) suggested that the shoreline culmination of the transgression is measurably diachronous and for example, took place at ages ranging from *circa* 6800 B.P. (Sissons, 1983) at the western end of the Forth lowland to between 6095±75 and 5700 ± 90 B.P. near Fraserburgh. Thus the Main Postglacial Shoreline was believed to have been abandoned progressively later with increasing distance from the centre of uplift. The rapid rise in global sea level terminated around 6,000 B.P. and, as isostatic recovery remained in effect though at a slower rate, a fall in relative sea level ensued over much of Scotland except in areas peripheral to the uplift centre (Sutherland *et al.*, 1993).

4.2 Empirical reconstructions of patterns of glacio-isostasy.

After Jamieson (1865) first put forward the theory of isostasy to account for the presence of raised beaches and tilted shorelines in Scotland, the isostatic effects of loading upon part of the earth's crust was demonstrated in a number of studies, including for example Gilbert's work in the areas around Lake Bonneville (1897). In the latter instance, the previously added load was the weight of water in the basin. It was shown that shorelines of Lake Bonneville are considerably higher on the islands in the centre of the lake than at its margins, and reconstructed isobases exhibit the form of the deformation. Such studies showed that the crustal response to ice loading was determined by the thickness and density of the crust and upper mantle, and the thickness and density of the loading medium. The amount of depression and recovery would vary locally with such variations in the land.

Many studies have been made to reconstruct glacio-isostatic uplift patterns in part or the whole of Scotland using evidence of fragments of former shorelines formed during the Late Devensian and Holocene. In 1967, Sissons reconstructed the generalised patterns of glacio-isostatic recovery since the formation of the Main Postglacial Shoreline, based on a mixture of then available detailed and approximate data. Since Smith, Sissons and Cullingford

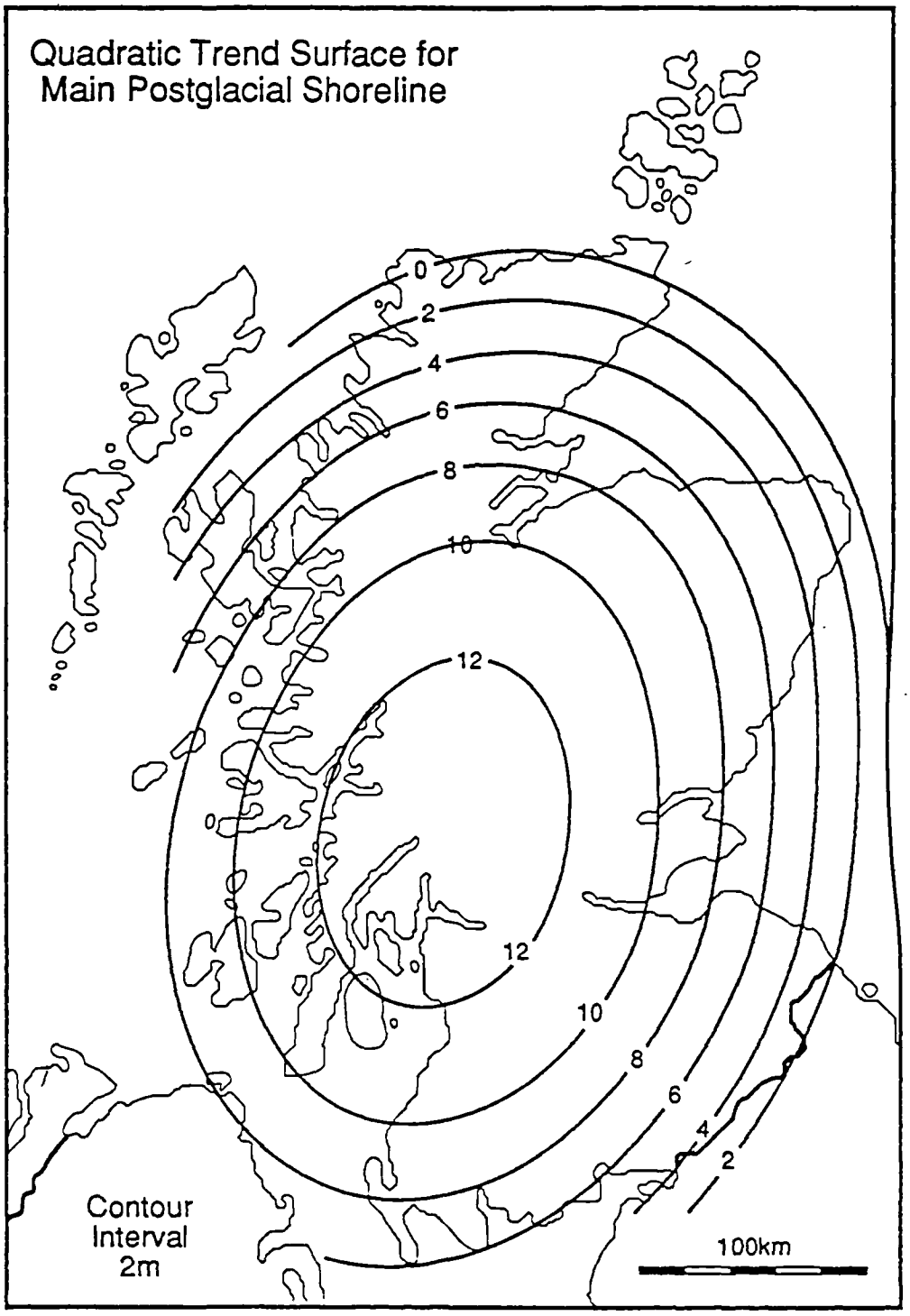

Figure 5.9. Quadratic trend surface for the Main Postglacial Shoreline (after Firth *et al.*, 1993).

(1969) first introduced the application of a three-dimensional surface fitting mathematical technique basing on polynomial equations, known as Trend Surface Analysis, to studies of isostasy, further studies have produced quantified maps of glacio-isostatic uplift patterns in relation to the present sea level, covering the whole of Scotland and many local areas. In particular, maps covering wide areas have been subject to further modifications and improvements in step with an accumulation in shoreline evidence (e.g. Cullingford, Smith and Firth, 1991 and Firth *et al.*, 1993).

Continuing improvements in the reconstruction of patterns of isostatic uplift have been made with three major shorelines, the evidence for which exists over a wide area of Scotland. For example, Jardine (1982) compiled a generalised map of isobases for the Main Perth, the Main Lateglacial and the Main Postglacial Shorelines (Figure 5.10). As discussed in his paper, the reconstruction of the isobases for parts, or the whole, of Scotland was based on a mixture of available detailed and approximate data.

Among these shorelines, much attention has been focused on the Main Postglacial Shoreline since the evidence of this shoreline is very extensive, and has been studied and examined in the greatest detail. Cullingford *et al.* (1991) studied not only the patterns of altitude but also the age variation of the Main Postglacial Shoreline in central and eastern Scotland. In this study, Cullingford *et al.* considered that altitudinal levels indicated by different types of coastal features do not necessarily agree and thus can not be equated. A large amount of data has been obtained through direct measurements of the former shoreline features, including the altitudes of former estuarine mudflats, known as carselands, sand and shingle beaches and shingle ridges. For reasons of equivalence, Cullingford *et al.* (1991) extracted data only from the carselands and suggested that the diachroneity of the abandonment of the shoreline may be detectable from radiocarbon dates. Near the centre of recovery the shoreline was abandoned earlier than in the peripheral regions. The time span is about 1,000 years between the earliest parts in the western Forth valley and the latest parts at Fraserburgh . As

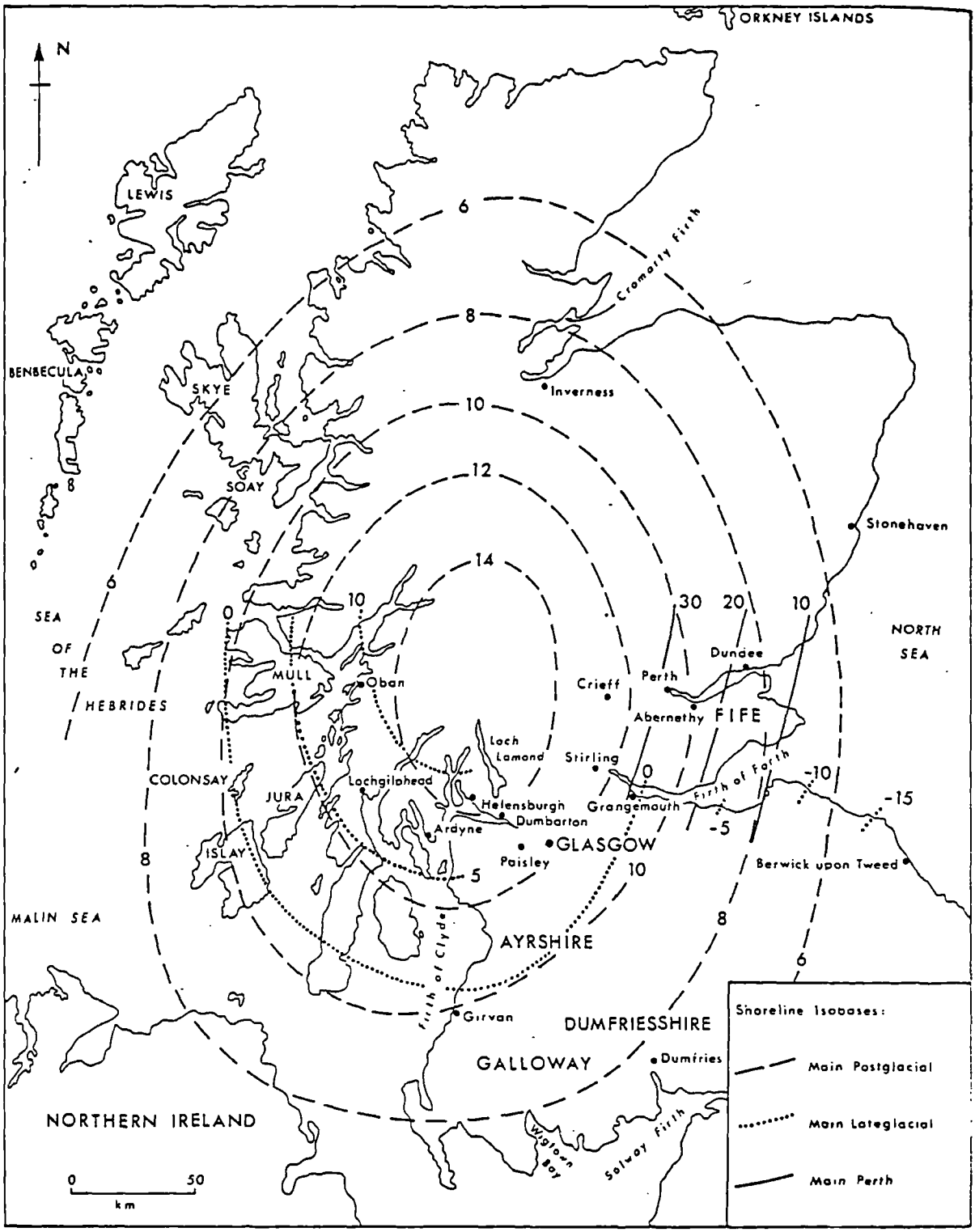

Figure 5.10. Isobases of the elevations of the Main Postglacial, the Main Lateglacial and the Main Perth shorelines. (after Jardine, 1982).

pointed out by Cullingford *et al* (1991), the diachroneity of the shoreline contributes to the altitude variations so that the reconstructed isobases of the isostatic recovery indicated by this shoreline are affected by the lapse of time and thus include the effects of diachroneity.

Firth *et al.* (1993) compiled and correlated the evidence, published in a number of studies, of comparable shorelines formed in Scotland during the Late Devensian and Holocene. Their study provides a series of inferred patterns of glacio-isostatic displacement during this period of time determined with trend surface analysis. The shorelines studied include the Main Lateglacial Shoreline (supposedly formed during the Loch Lomond Stadial according to Sutherland, 1984), the Main Postglacial Shoreline (6,800 - 6,000 ^{14}C yrs. B.P.) and a late Holocene Shoreline. This study provides empirical information on the general history of Scottish glacio-isostatic movements and on the possible effects of Loch Lomond Stadial glaciers, though the isobase maps are of a tentative and generalised nature.

In summary, the reconstruction of patterns and history of Scottish glacio-isostatic movement has gradually improved as more data has become available, although even at present much more data needs to be obtained before detailed isobase maps can be produced with confidence. Furthermore, such studies provide crucially valuable geophysical information. Lambeck (1993a and 1993b) developed high-resolution geophysical models simulating crustal responses to surface loading (glacio- and hydro-isostasy) in and around the British Isles during Late Devensian. The models include the determination and application of a range of geophysical parameters for both earth- and ice-models. The determination of unknown parameters was achieved by applying data sets obtained with empirical observations of ice movements across the British Isles and of relative sea-level changes along the coasts during Late Devensian time. Improving empirical reconstructions of glacio-isostatic movements can further provide valuable information not only for testing geophysical models of glacial rebound, but also for estimating the parameters which define and constrain crustal responses to surface loading.

4.3 A widespread sand layer in coastal sedimentary sequences along the eastern coastline of Scotland

Within the coastal sedimentary sequences of the Main Postglacial Transgression, a layer of sand of marine origin has been discovered at a number of sites along the eastern coast of Scotland, and has been thought to represent a significant flood event. In recent decades, in a number of studies of the stratigraphy of coastal sedimentary sequences associated with the Main Postglacial Transgression, a distinct layer, predominantly of grey micaceous silty fine sand (Figure 5.11), has been identified within the deposits at several locations in eastern Scotland. It was first recorded in the western Forth valley by Sissons and Smith in 1965. At that time, the only available evidence was its stratigraphical relation to the local sedimentary sequence and it was interpreted as a local flood of the river Forth. Subsequently, a similar layer has been identified in accounts of coastal stratigraphical sequences formed as a result of the Main Postglacial Transgression at various sites (Plate 9; Figure 5.1). These sites are located in a number of areas including the Montrose area (Smith *et al.*, 1980 and Smith and Cullingford, 1985), East Fife (Morrison, Smith, Cullingford and Jones, 1981), the Ythan valley (Smith *et al.*, 1983), the Beauly Firth (Haggart, 1982) and the Dornoch Firth (Smith *et al.*, 1992). All the sites studied have remarkably similar lithostratigraphy (Figure 5.11). Raised estuarine deposits of grey silty clay, associated with the Main Postglacial Transgression, wedge landwards into peat accumulations. Within the grey silty clay to seaward a distinctive layer of grey micaceous silty fine sand occurs and within the peat to landward this forms a separate wedge below the wedge of grey silty clay. Smith, Cullingford and Haggart (1985) compiled and discussed information provided by radiocarbon dates obtained on peat samples above and below the layer. By removing the two oldest dates which are associated with possible evidence of erosion, they suggested that the layer was laid down at between 7140±120 and 6870±50 radiocarbon years B.P.. Drawing upon the evidence of marine diatoms in the layer, together with chrono-stratigraphical evidence, they proposed that the layer was laid down by one widespread and short-lived marine invasion, and discussed the causal possibilities of a temporary increase in

the rate of rise of relative sea level or a North Sea storm surge, but found neither possibilities could offer a conclusive answer.

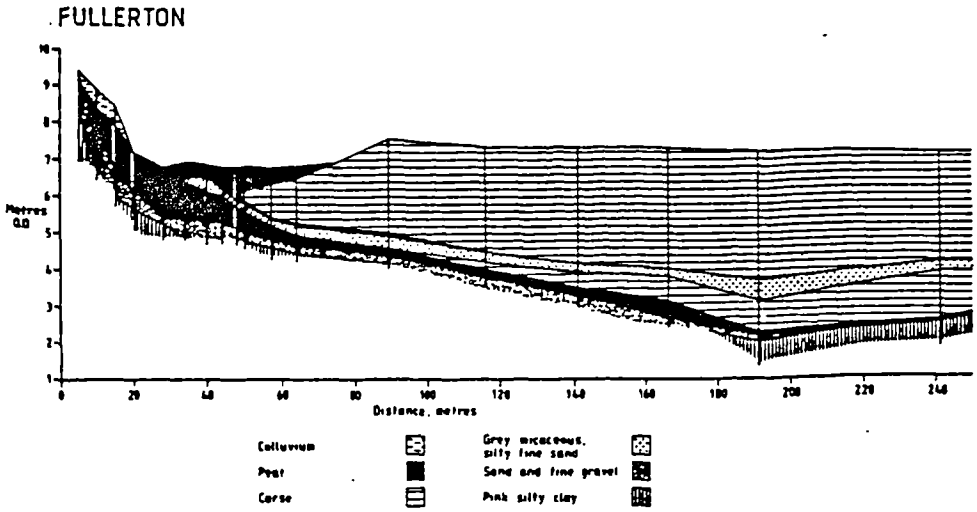

Figure 5.11. Stratigraphical section through the coastal deposits at Fullerton showing the intercalated grey micaceous, silty fine sand layer (after Smith *et al.*, 1980). The location of the site is indicated in Figure 4.1.

4.4 Storegga landslides

In a number of studies of submarine deposits and topographical features off the west Norwegian coast in the North Sea (e.g. Bugge, 1983 and Jansen *et al.*, 1987), the world's largest submarine mass movement events so far identified were described, named as the Storegga submarine landslides, which are dated as having occurred during the last 50,000 years. Among these events, the Second Storegga Slide brought about displacement of around 1700 km^3 of semi-consolidated Quaternary, Neogene and Paleogene deposits over a distance greater than 800 km and through a water depth of 3500 m. The slide has been dated as having been occurred between 8,000 and 5,000 radiocarbon years B.P.. They also suggested that the disturbance of water caused by the slides may have generated large ocean waves (Figure 5.12).

The complex of extensive semi-consolidated deposits on the bottom of the Norwegian Sea is one of the largest submarine landslides deposits in the world (Figure 5.12). Bugge (1983)

Plate 9. Stratigraphical exposure at Maryton, Montrose Basin. A layer of grey micaceous silty fine sand lies just above the blade of the spade, within darker mud and peat accumulations.

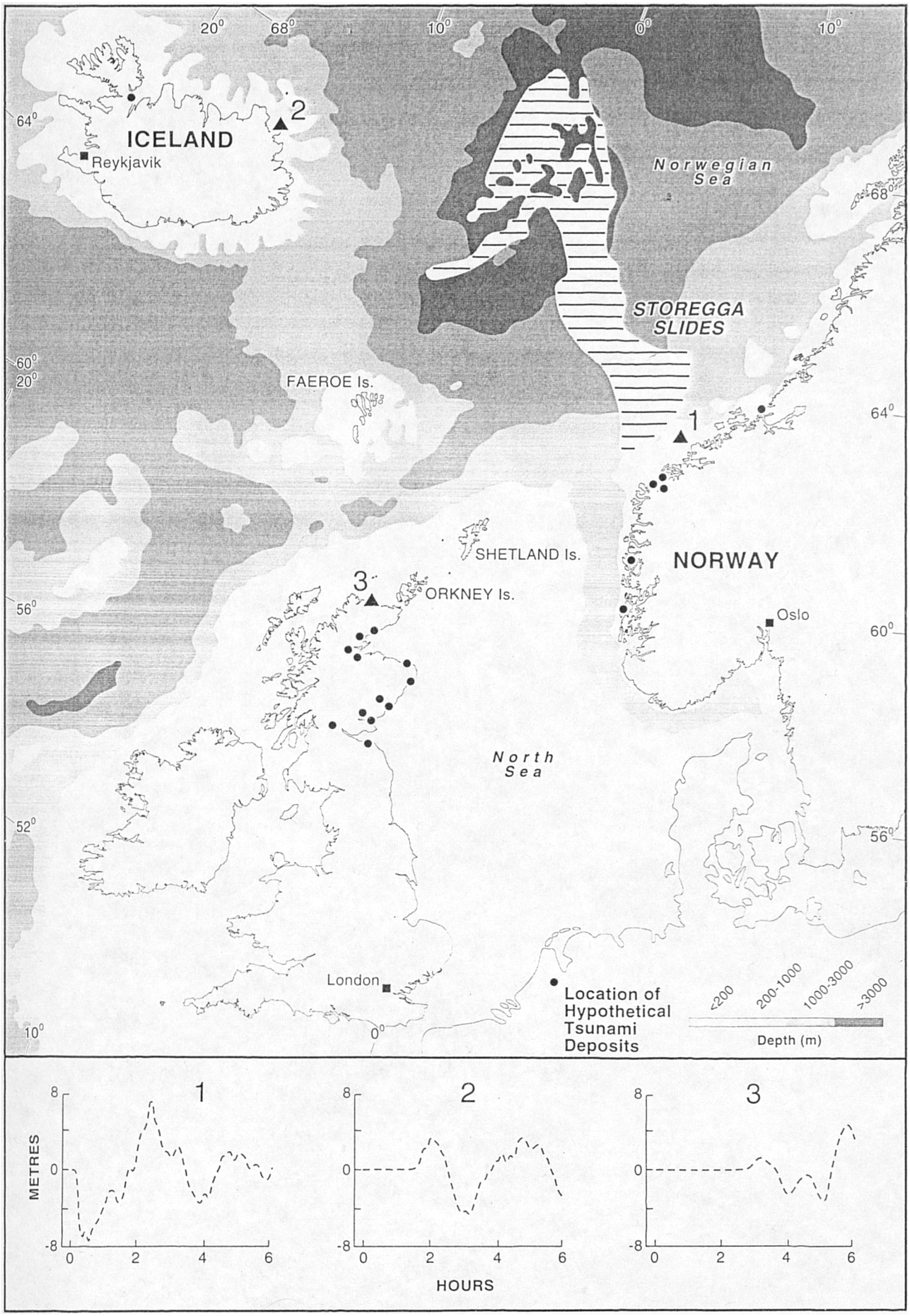

Figure 5.12. Distribution of the Storegga Slides, location of the sand layer sites and numerically simulated wave forms.

distinguished three sets of such deposits and detailed accounts have been subsequently given in several papers (Bugge, Befring, Belderson, Eidvin, Jansen, Kenyon, Holtedahl and Sejrup, 1987; Jansen, Befring, Bugge, Eidvin, Holtedahl and Sejrup, 1987; Bugge, Belderson and Kenyon, 1988). These three sets of the deposits were found to have been transported over considerable distances after slope failures at the edge of the continental shelf off Storegga, Norway at three different stages. They are known as the First, Second and Third Storegga Slides in a relative chronological order. The oldest, the First Storegga Slide, was the largest and involved a movement of approximately 3880 km^3 of sediment. Its age remains unknown although analysis of oxygen isotope stratigraphy suggests an estimate of between *circa* 25,000 -30,000 ^{14}C yrs B.P. (Dawson *et al.*, 1993). The Second and Third Slides were dated to have taken place on separate occasions between 8,000 and 6,000 radiocarbon ^{14}C yrs B.P. (Jensen *et al.*, 1987). The Second Slide, which involved the translation of more consolidated sediments than the First Slide, cut back 6-8 km headwards beyond the First Slide and removed approximately 450 km^2 of the continental shelf edge. This slide involved the movement of some very large quantities of sediment. In particular, two blocks, 150 - 200 m thick and up to 10 - 30 km wide, were transported as far as 200 km downslope over the seabed with average slopes of less than 1° - 20°. The Third Storegga Slide deposits are limited to the upper part of the Second Slide scar area and might have been the product of the movement of the Second Slide in its final stages. The age of this final sliding movement is estimated near 6,000 ^{14}C yrs B.P. (Jansen *et al.*, 1987), but its precise age is uncertain.

4.5 Tsunami origin of the sand layer

Dawson, Long and Smith (1988) related the above mentioned sand layer found along the east coast of Scotland to the Second Storegga Slide and suggested that a high-magnitude tsunami was generated by the slide and caused widespread flooding along the coasts of the North Sea. As a consequence, the widespread sand layer was interpreted to have been deposited by the inundation of the tsunami. Dawson *et al.* (1988) also suggested the height

of the sand layer above the estimated contemporary high water mark would provide a minimum value for tsunami run-up. Based on this, the run-up height was estimated as ranging between about 1 to 4 m. As pointed out by Dawson *et al.* (1988), few studies have so far been made of the particle size characteristics of the sediment, but there seems only limited evidence of any grading. Furthermore, the sand layer has been examined primarily in boreholes and no sedimentary structures have been observed (cf. Long, Smith and Dawson, 1989).

4.6 Archaeological evidence

Long *et al.* (1989) also cited archaeological evidence from published sources and suggested that some coastal archaeological sites were affected by the same tsunami event. The cited sites include Morton within the area of the Tentsmuir sands in Fife (Coles, 1971) and a site on the northern site of the river Tay at Broughty Ferry (Hutcheson, 1886 and Lacaille, 1954)). Subsequently, Dawson, Smith and Long (1990) related the documented lithostratigraphical evidence on a Mesolithic site in Inverness (Wordsworth *et al.*, 1985) and, drawing upon its similarity in appearance and age to that related to the sand layer described above, suggested that the tsunami might have flooded this site.

4.7 Geological investigations into the flooding event in other areas in the vicinity of the North Sea

As tsunamis are transoceanic and the tsunami under investigation is thought to have been generated in the Norwegian Sea, it has been considered that, if it did occur, the Storegga tsunami could have caused widespread impact along the coasts in the North Sea and the East Atlantic region. Following publications made on the Storegga slides and the likely *circa* 7,000 yrs B.P. tsunami event layers along the eastern coast of Scotland, geological investigations into coastal sedimentary sequences have been undertaken in western Norway and Iceland. Svendsen and Mangerud (1990) reported possible evidence for tsunami inundation from three sites in western Norway. As described by these authors, at one site at

Almestadmyra where a lake isolation basin lies at 13.7 m above the mean sea level, a sand layer containing backish diatoms is interbedded in the lower part of a Holocene lacustrine gyttja. The threshold of the basin lies approximately 4 m above the highest altitude reached by relative sea level during the Holocene in this area (the Tapes Transgression). At another isolation basin at Skolemyra the threshold of which is *circa* 5m above the maximum level reached by the Tapes Transgression, these authors described a disturbed layer which include terrestrial turf overlying unconformably upon volcanic ash of Lateglacial age. This disturbed layer lies in the deepest part of the lake and is considered to be due to slumping. Svendsen and Mangerud (1990) argue that because the surrounding area is flat and not conducive to slumping an external cause may be a plausible triggering mechanism. The further work of geological investigation into coastal sedimentary sequences in western Norway is being undertaken. More possible tsunami deposits at various sites are beeing studied in detail (Bondevik and Svendsen, 1993). The results of this work will ultimately shed more light on the present study.

At Bitrufjorour, Hvifahlio, Vestfirdir, Iceland, a possible deposition by the same tsunami has been reported by Hansom and Briggs (1990). The authors described that a raised beach ridge composed of cobbles and sand rests upon accumulations of terrestrial peat which are underlain by marine silts at *circa* 8.5 m above the mean sea level and suggested that the beach ridge could have been deposited by the high energy marine event. The beach ridge has been dated to have been deposited between 8,830 ± 60 and 6,910 ± 100 radiocarbon years B.P. (Hansom and Briggs, 1990) but the significance of the Vestfirdir site is unclear at present.

4.8 Numerical modelling of the Second Storegga Slide

The generation and propagation of the Second Storegga Slide has been numerically simulated by Harbitz (1991 and 1992), based on estimated dimensions of the failed sedimentary masses on the continental slope. The model follows hydrodynamic principles

for shallow water waves and employed a finite difference technique. The simulation revealed that the tsunami run-up values yielded are greatly dependent on the average velocity of the slide as well as other physical conditions such as the shear stress at the interface between the water and the slide body. Given an average velocity of the slide of 35 m per second, average flood run-up values of between +3 and +5 m along the eastern coast of Greenland, Iceland, Scotland and the western coast of Norway are estimated. The initial drawdown of water was possibly in excess of -10 m. These results suggest the slide was associated with two major tsunami waves as well as several minor fluctuations. Based on Harbitz's model, an IBM compatible version of the model was developed, animations of the propagation of the tsunami waves were made and the likely associated water levels along the Dutch coast were calculated by Van Bijl (1993).

In parallel, Henry and Murty (1992) also studied the effects of the Second Storegga tsunami with mathematical models. The models did not simulate the slide and the initial aspects of tsunami generation, but were employed to study the amplitudinal effects of the tsunami accounting for different initial amplitudes in the source region with an one-dimensional analytical model and a two-dimensional numerical model. Values for the initial amplitude of 8, 10 and 12 metres, yielded maximum amplitudes of the tsunami along the east coast of Scotland in the magnitude of several metres (Figure 5.13), in general agreement with observational estimation made by Dawson *et al.* (1988) and Long *et al.* (1989).

All these models were established and applied without consideration of likely concurrent tidal changes, which are difficult to reconstruct but which may have played an important role in the run-up processes of the tsunami. In the present work, the properties of the sand deposits at several sites along the eastern coast of Scotland are examined, especially their granulometric characteristics and spatial variations.

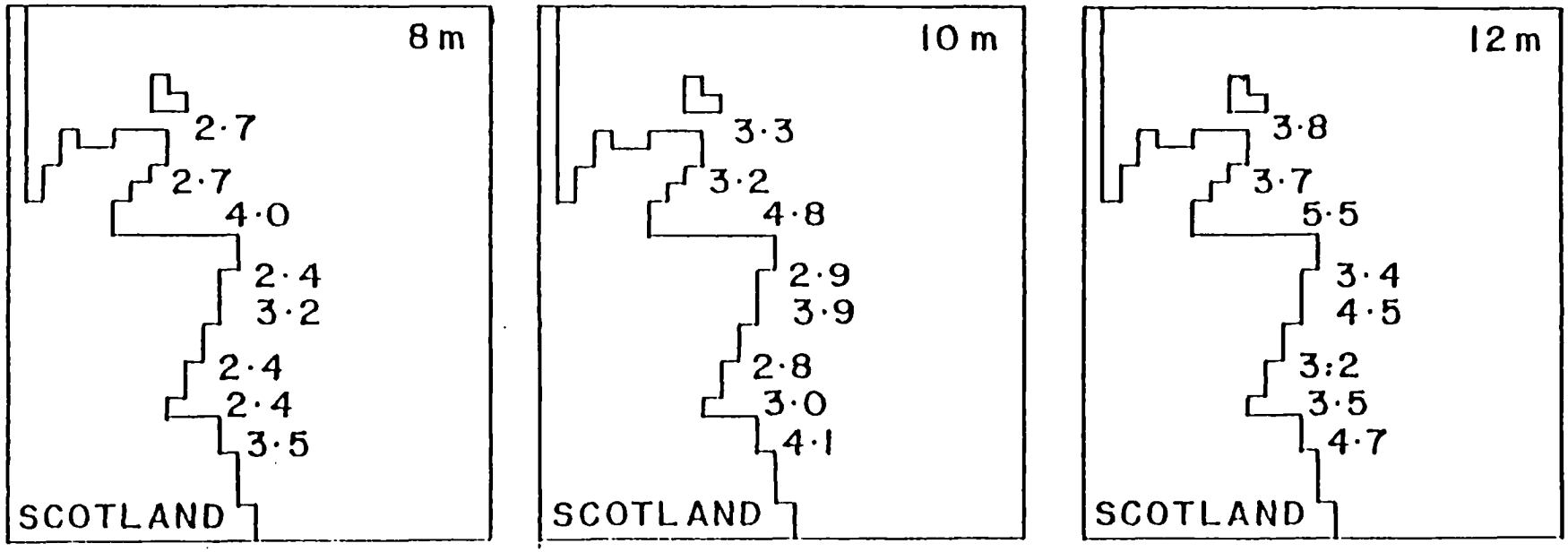

Figure 5.13. Distribution of the maximum amplitudes of the hypothetical *circa* 7,000 radiocarbon yrs B.P. tsunami along the eastern coast of Scotland, which are estimated with numerical models (Henry and Murty, 1992).

5. INVESTIGATION

A total of 6 sites were investigated during this research (Figure 5.14). In the following context the evidence for each site is described and results given, including the results previously obtained by other authors, and site-specific interpretation is also made. The collective account of the field and laboratory evidence is taken into account and correlated at the end of this section for interpretation and discussion.

5.1. Sites in the Dornoch Firth

The Dornoch Firth is an estuarine area stretching virtually east-west from Tarbat Ness to Bonar Bridge, surrounded by rugged and high relief (Figure 5.15). The sides of the Firth are generally steep and rise in places to over 500 m. The general shape of the coastline of the outer Firth appears as a funnel, with its apex pointing to the relatively narrow inner part. Along the coast of the Firth, a number of coastal and fluvial depositional features are present, including sand and pebble beaches, detrital fans and extensive mudflats. In between the fluvial fans and behind the coastal depositional features lie areas of former mudflats, or carselands, at between *circa* 3 to 6 m O.D.. Two sites in the Dornoch Firth were selected and investigated in detail. These were at Creich and Dounie (Figure 5.15).

5.1.1 Dounie

On the south side of the Dornoch Firth, near Edderton, a small embayment is floored with raised estuarine sediments, carselands, reaching up to *circa* 6m O.D. (Plate 10). The embayment is marked at its seaward end by three elevated sand and shingle ridges, and inland by hillslopes and raised alluvial fans descending from higher ground (Figure 4.16). At several places in the embayment, peat outcrops at the inner margin of the estuarine sediments. Survey indicates that the carselands fall into three distinct levels at +5.8 to + 6.7 m, +4.1 m and +3.2 to +3.5 m (Smith *et al.*, 1992). Across the embayment, small streams are incised into the carselands, and in their vicinity the surface of the carselands is discontinuous and fragmented.

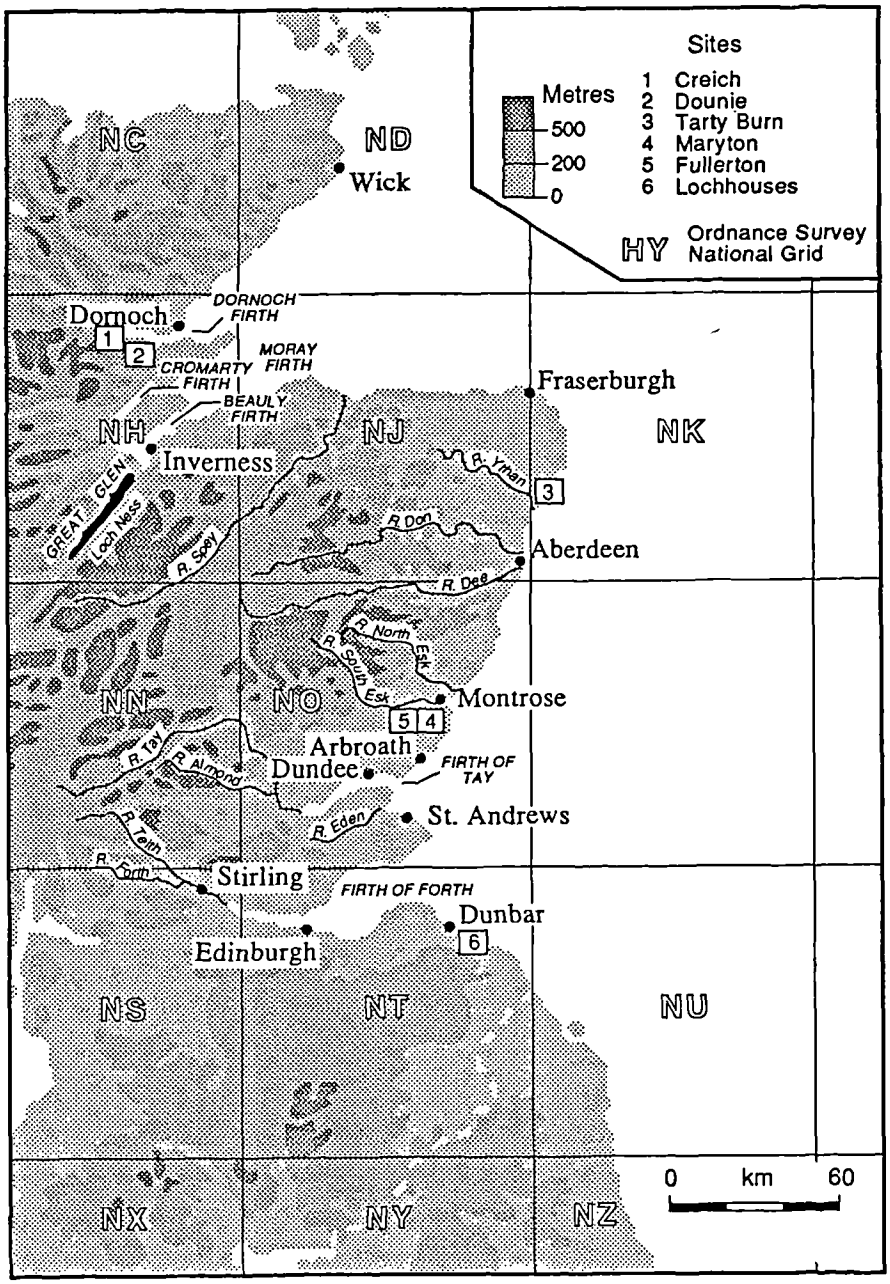

Figure 5.14. Location map of the sites investigated during this study.

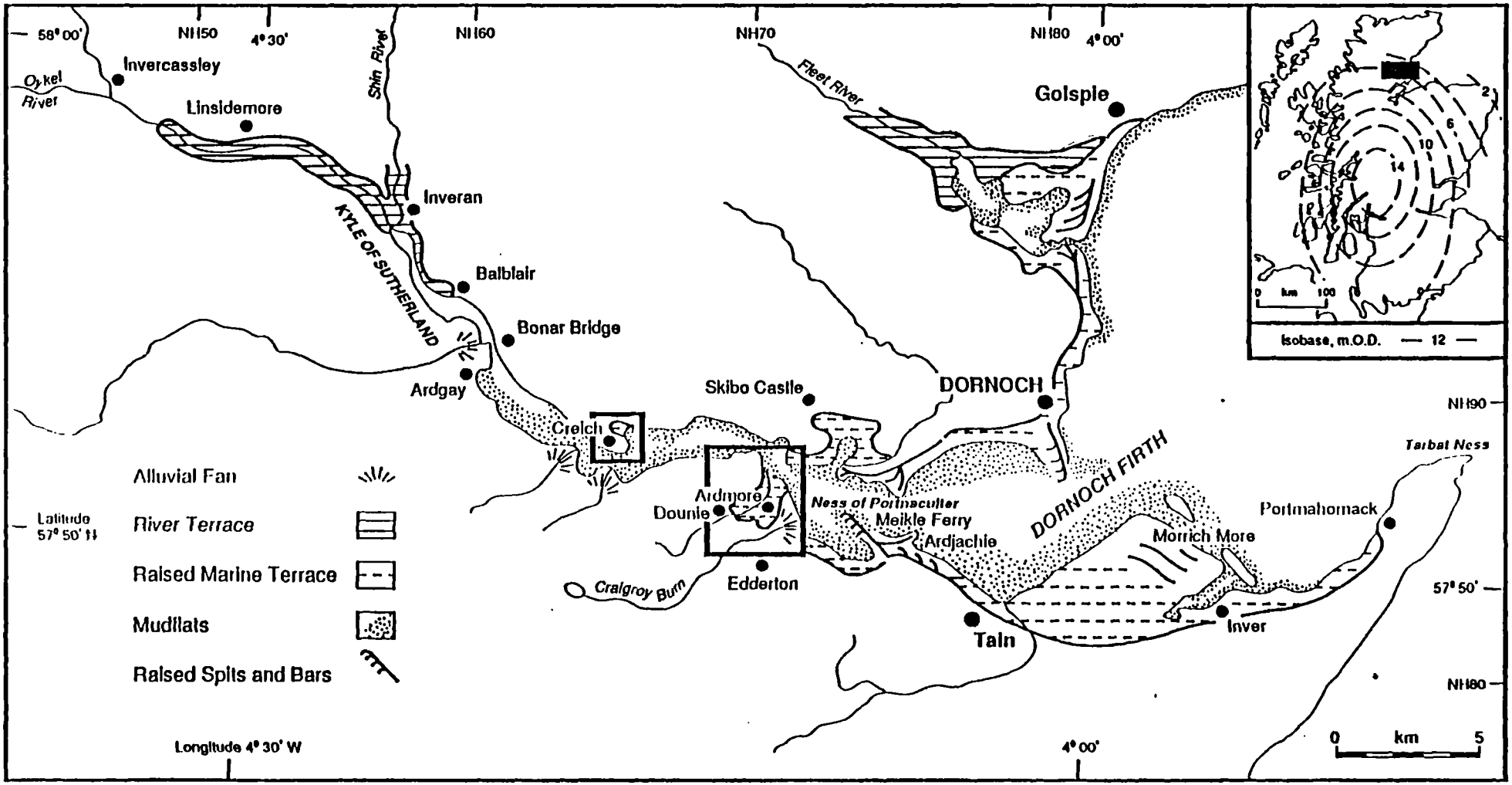

Figure 5.15. Morphological features and the location of the sites at Dounie and Creich in the Dornoch Firth (after Smith *et al.*, 1992).

Plate 10. Site at Dounie, Dornoch Firth. The surface of an area of raised estuarine mudflat (locally known as carseland) lies at *circa* 6 m O.D..

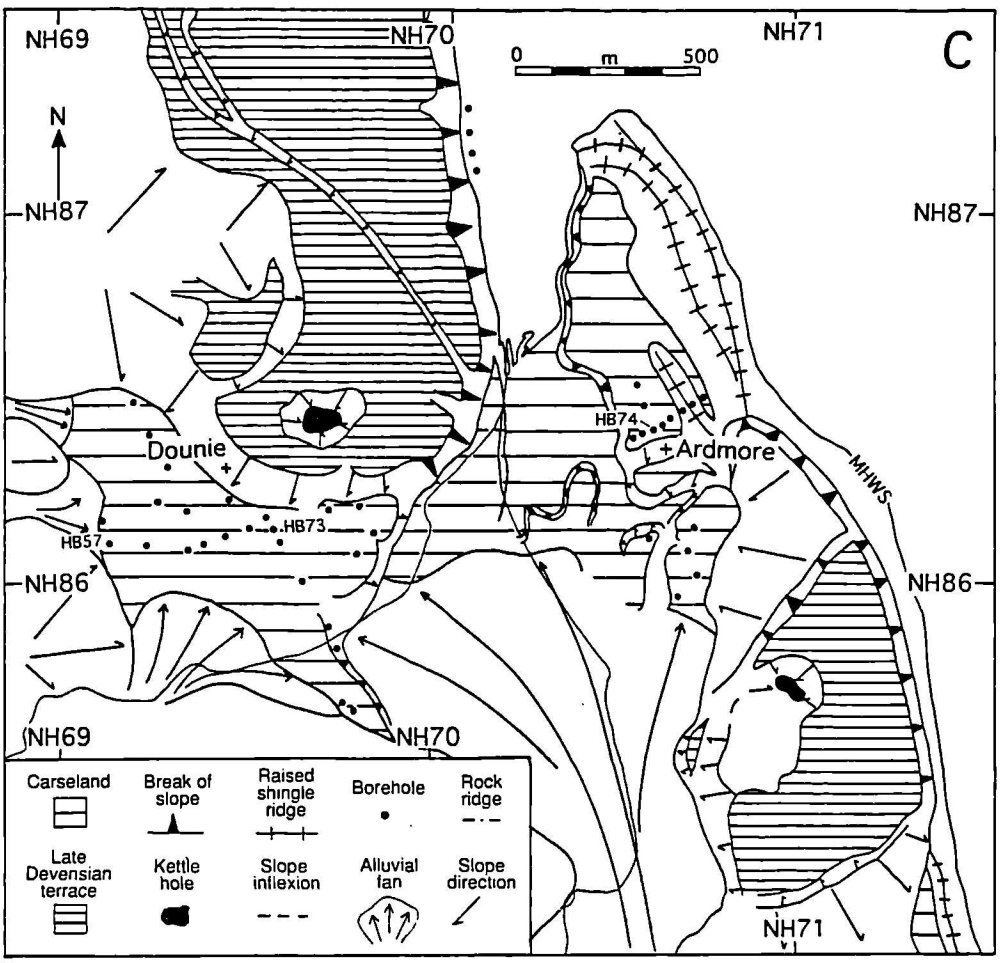

Figure 5.16. Morphology at Dounie, Dornoch Firth (after Firth *et al.*, 1993).

5.1.1.1 lithotratigraphy

The detailed stratigraphical evidence was determined from detailed borehole records (over 100 boreholes) over this area (Figure 5.17). The broad stratigraphy displays, at the base, sand and gravel, and in places till, overlain extensively by peat which in turn is overlain by a grey silty clay. In places, a light grey clay can be seen at the base. The grey silty clay itself is locally overlain by peat, and tapers into peat along the margins of the embayment. To seaward, the grey silty clay rests upon sand and gravel along the flanks of the sand and shingle ridges. Spreading through the grey silty clay and into the peat at the side of the embayment is a layer of sand which itself forms a tapering wedge (Figure 5.18). The sand layer is up to 1 m thick and contains lenses of gravel near and upon the most inland ridge. The level reached by the most inland ridge is determined with borehole information to lie at *circa* 6m O.D. and is covered by an expanse of grey silty clay. The sand layer reaches a maximum altitude of +7.2m O.D., which not only exceed the maximum level of the buried ridge but also is approximately 0.5m higher than the maximum level reached by the grey silty clay at the site. It is important to note here that there is no trace of any similar sandlayer to the seaward of the most landward ridge, although much deeper boreholes were made. Smith *et al.* (1992) found that the sand layer contains peat intraclasts near its base. In places, at the valley side, colluvium covers the surface peat. The sand appears to be predominantly composed of quartz grains.

Cores at boreholes 56, 57, 73 and 84 were chosen for X-ray photography at the British Geological Survey, Edinburgh, but no particular pattern or variation was revealed within the sand layer. At this site, the sand layer has been analysed in detail with particle size, geochemical and mineral magnetic techniques. Cores form boreholes 56, 57, 73 and 84 were initially obtained and sliced into contiguous samples each 1 cm thick. Each complete sample was subject to all three analyses. Four further cores were obtained at boreholes S6,S9, S3 and S44 and were analysed for particle size at contiguous 0.5 cm intervals.

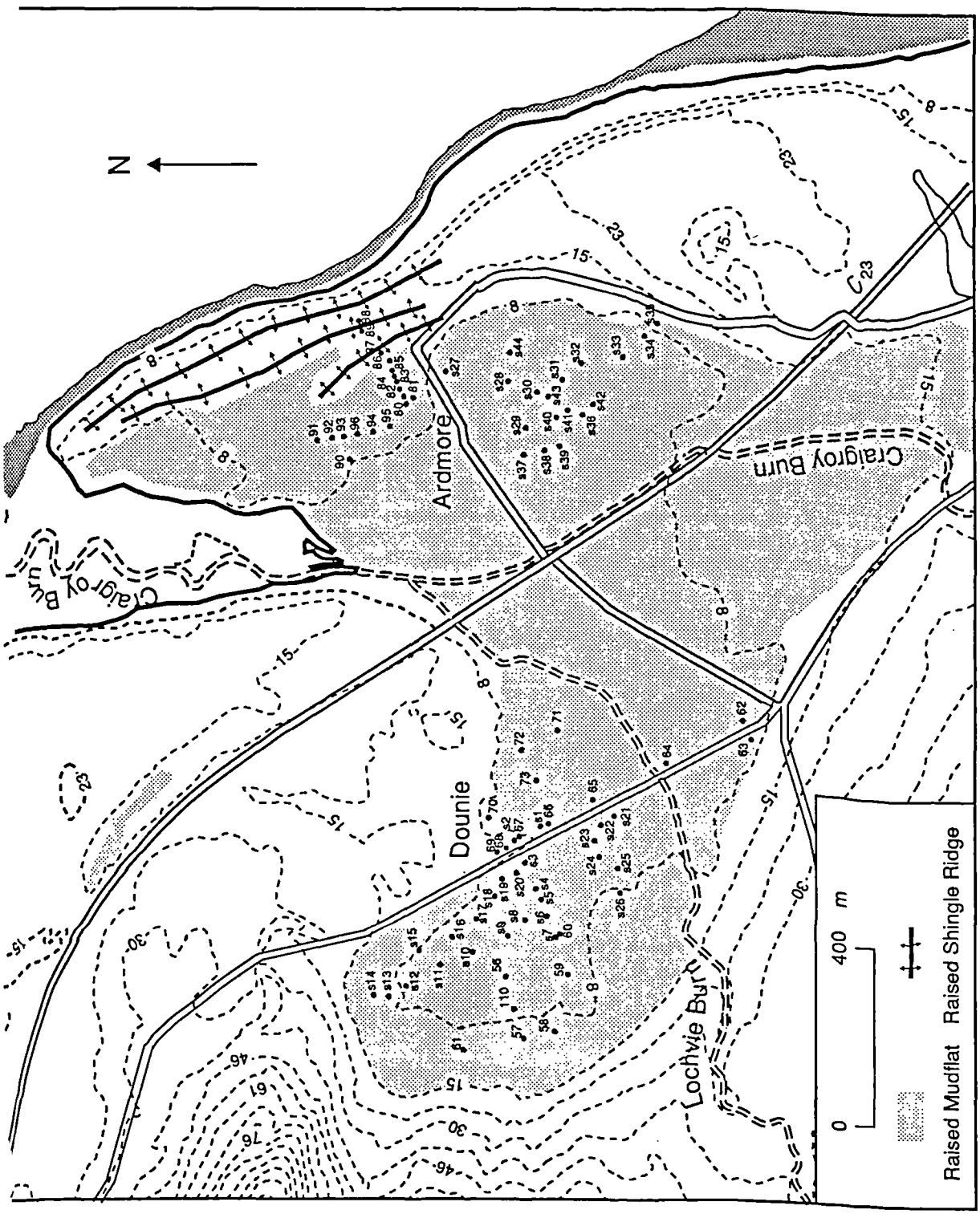

Figure 5.17. Topography and Location of Boreholes at Dounie, Dornoch Firth, Scotland (Not all boreholes are shown).

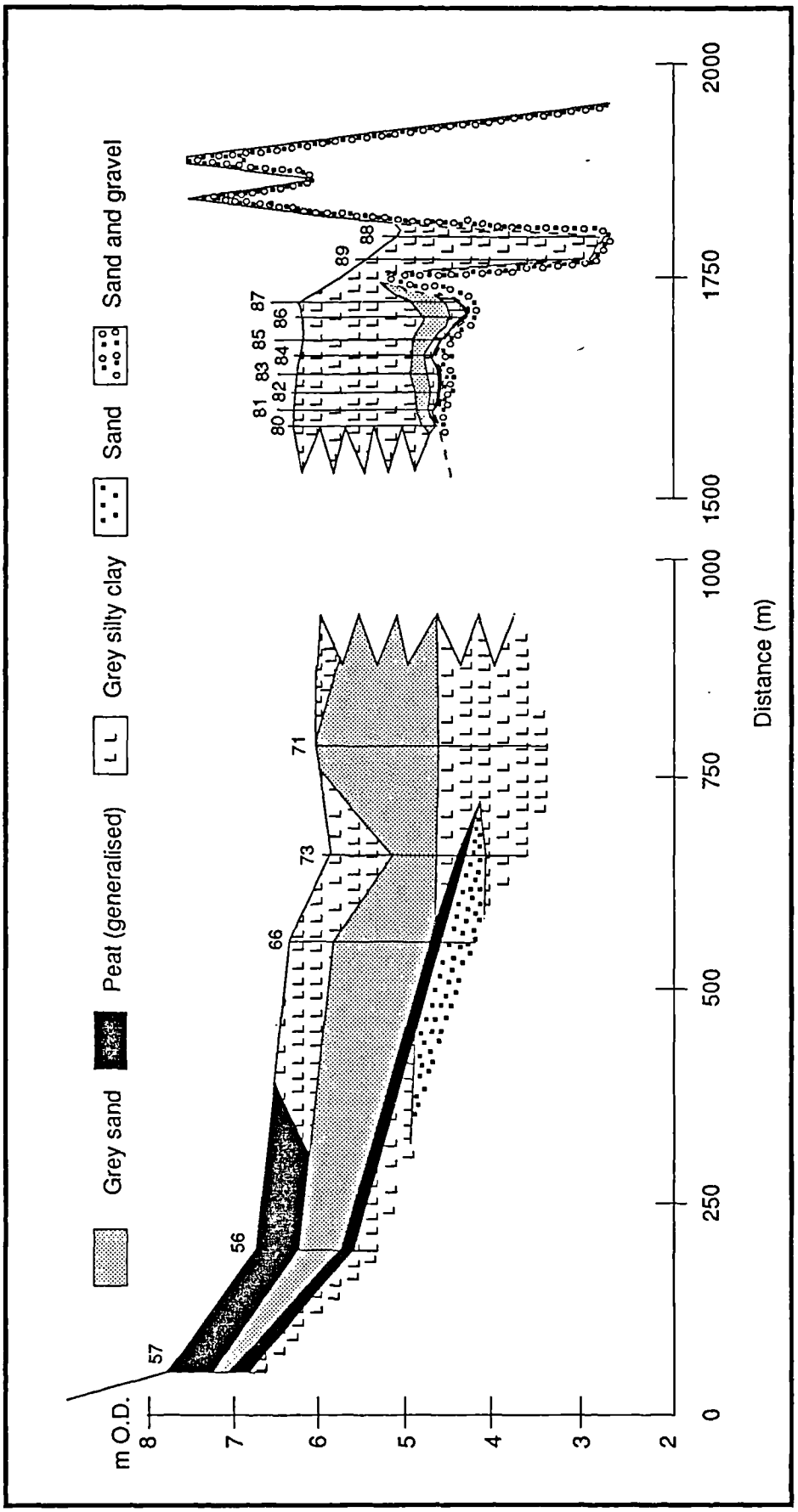

Figure 5.18. Stratigraphy at Dounie.

5.1.1.2 Radiocarbon Dating

Two ^{14}C dates were obtained with 2 cm thick samples of peat directly above and below the sand layer at borehole 56 (Smith *et al.*, 1992).

Sample	Lab. Number	Altitude (m O.D.)	Material	Age(^{14}C Years BP)
D2	SRR-3789	+6.29 to +6.27	Peat directly above sand	5190 ± 65
D1	SRR-3790	+5.73 to +5.71	Peat directly below sand	7120 ± 45

5.1.1.3 Geochemical Analysis

Detailed analysis of the geochemical variations in borehole 57 were undertaken on contiguous 1 cm thick samples through a total sand thickness of 0.52 m, and the results are shown in Figures 5.20 to 5.24.

There is a marked change with depth in the total concentrations of Na, Mn and Mg ions (Figure 5.24). The values of Na and Mn concentrations are particularly high within the upper 0.22 m of the core, whilst the values of Mg concentrations are relatively high within the lowest 0.05 m. The Ca concentrations are generally the highest among the four types of ions, but vary haphazardly and do not exhibit any particular variation trend with depth. The four types of ions extracted from primary and secondary minerals are generally of low concentrations and their values vary in a limited and small range. However, the variations in the ion concentrations suggest that mineralogical changes with depth are present. Ca and Mn concentrations are very low and vary insignificantly while variations in Na and Mg seem to suggest that significant mineralogical changes occur at near the lower part of the sand layer, at a depth of around 20 cm and near the surface of the sand layer. The likely mineralogical change at the depth of about 20 cm also coincides with a change in the organic content as indicated by the ion concentrations bound to organic matters. The values of Na concentration of ions bonded to organic matter marks an enrichment in the upper 0.22 m of the core, which contributes mostly to the total concentrations of Na ions from all fractions.

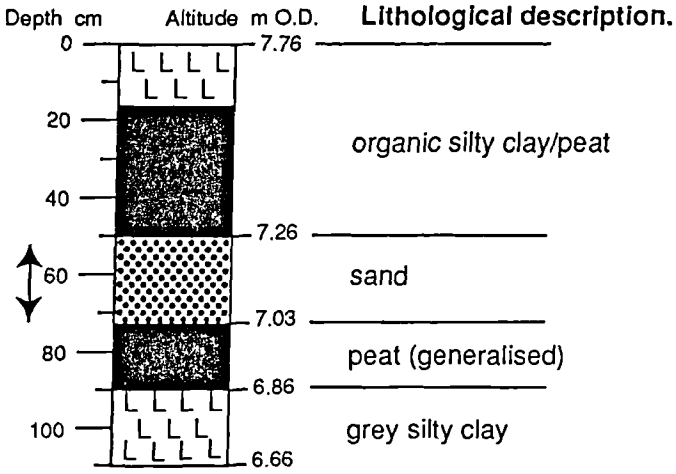

Figure 5.19. Lithostratigraphy of core 57 at Dounie. The arrows mark the core section analysed.

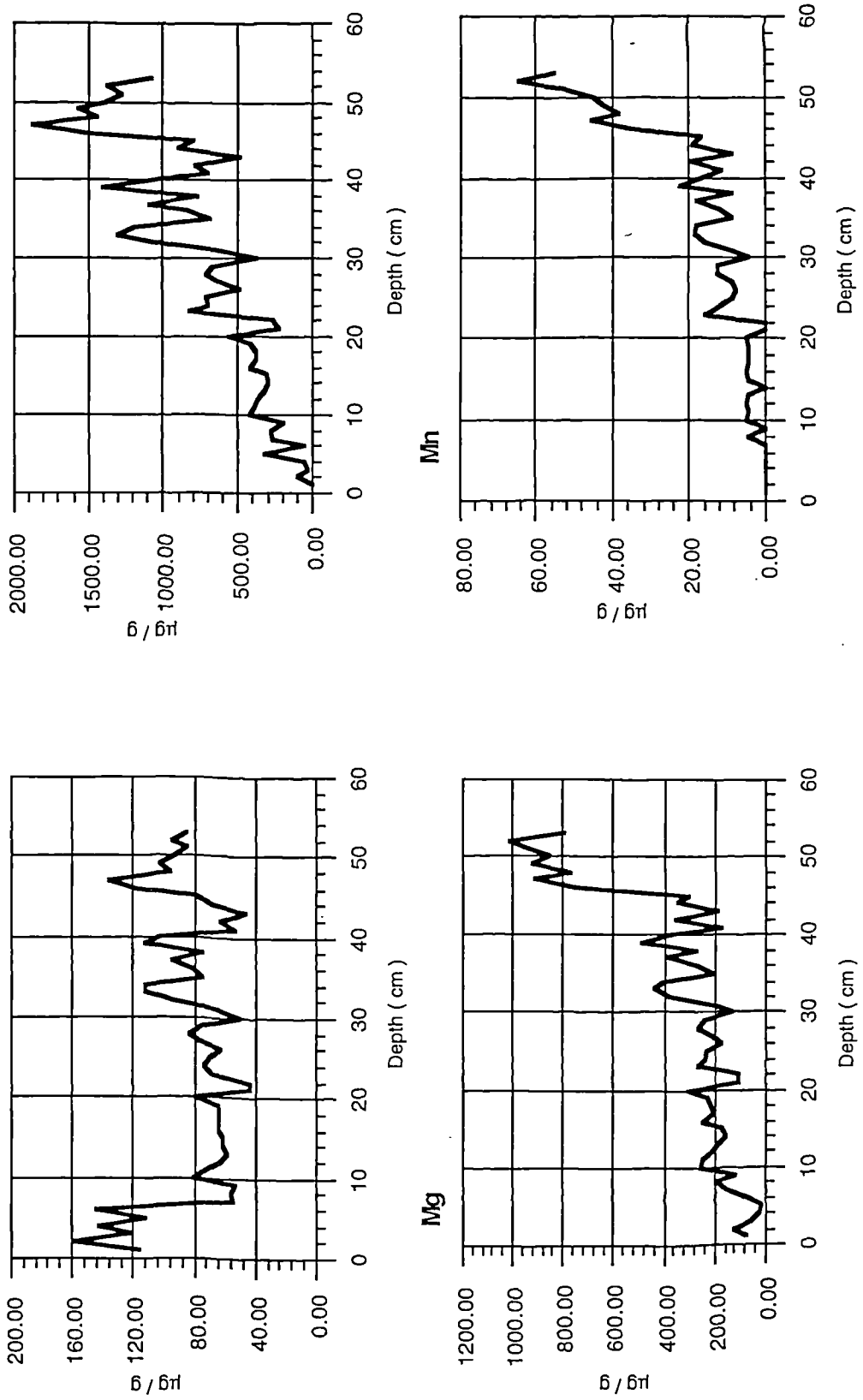

Figure 5.20. Variations in the concentrations of exchangeable ions with depth in the sand layer (Figure 5.19).

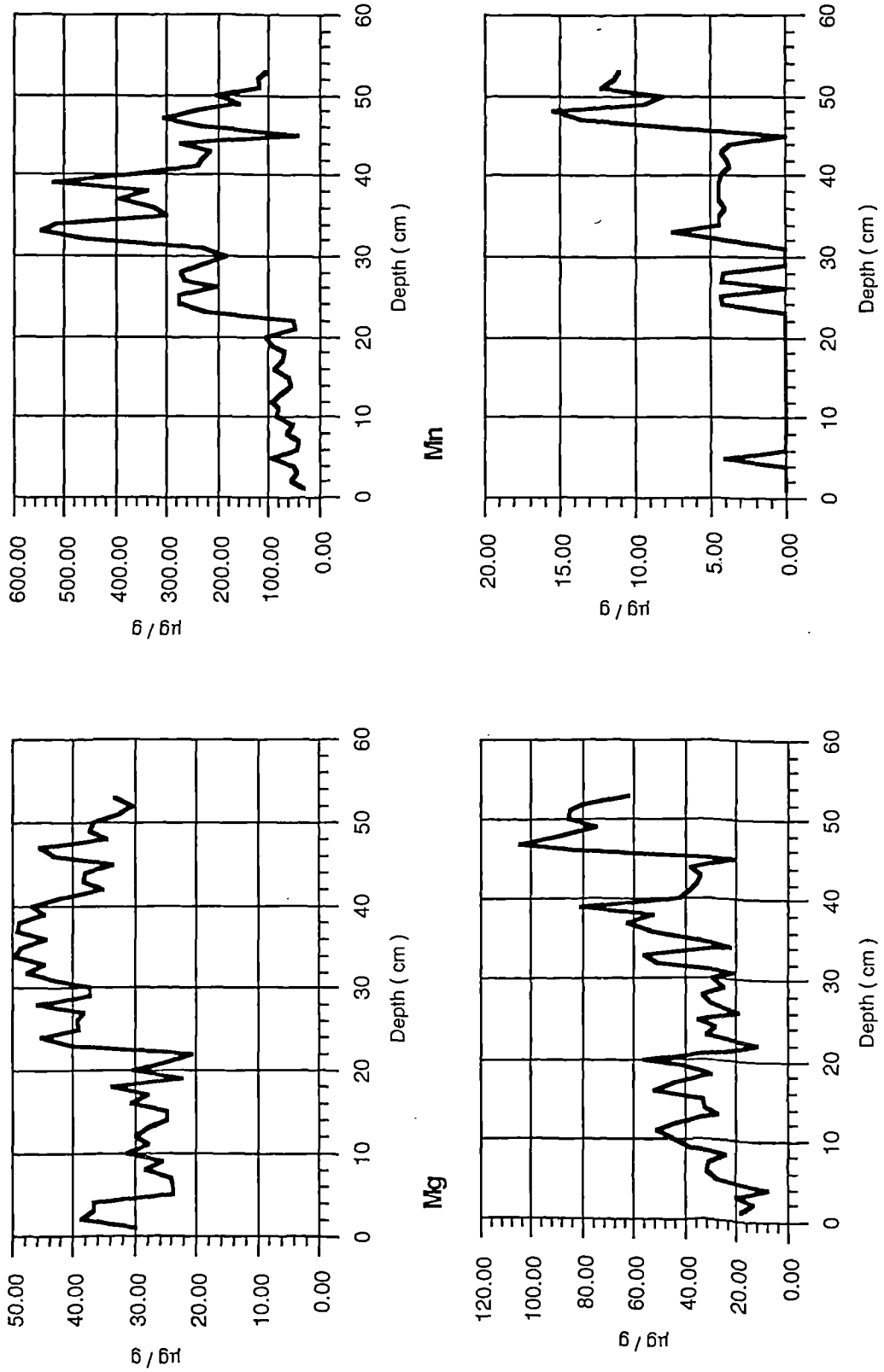

Figure 5.21. Variations in the concentrations of ions bonded to carbonates with depth in the sand layer (Figure 5.19).

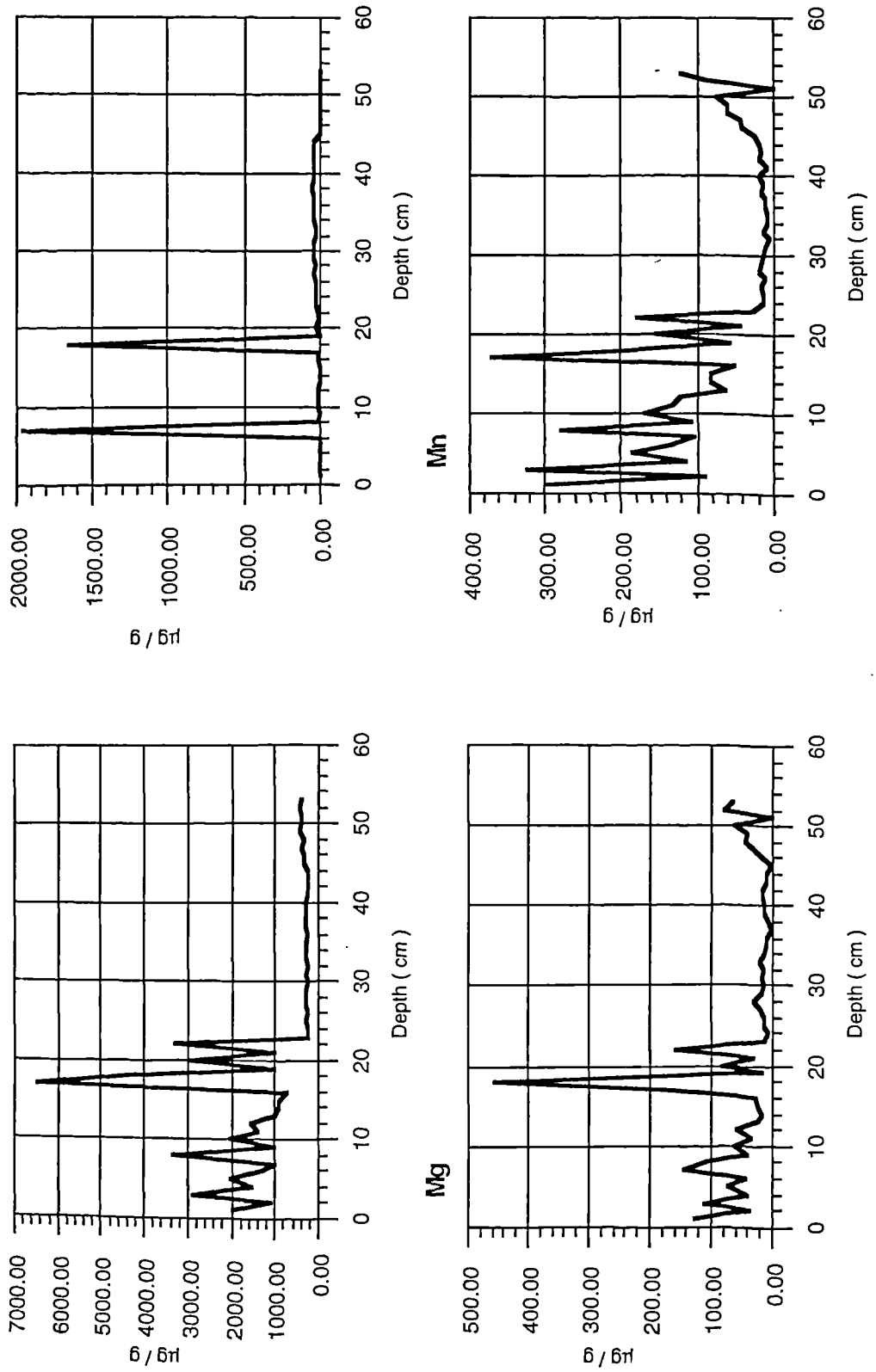

Figure 5.22. Variations in the concentrations of ions bonded to organic matter with depth in the sand layer (Figure 5.19).

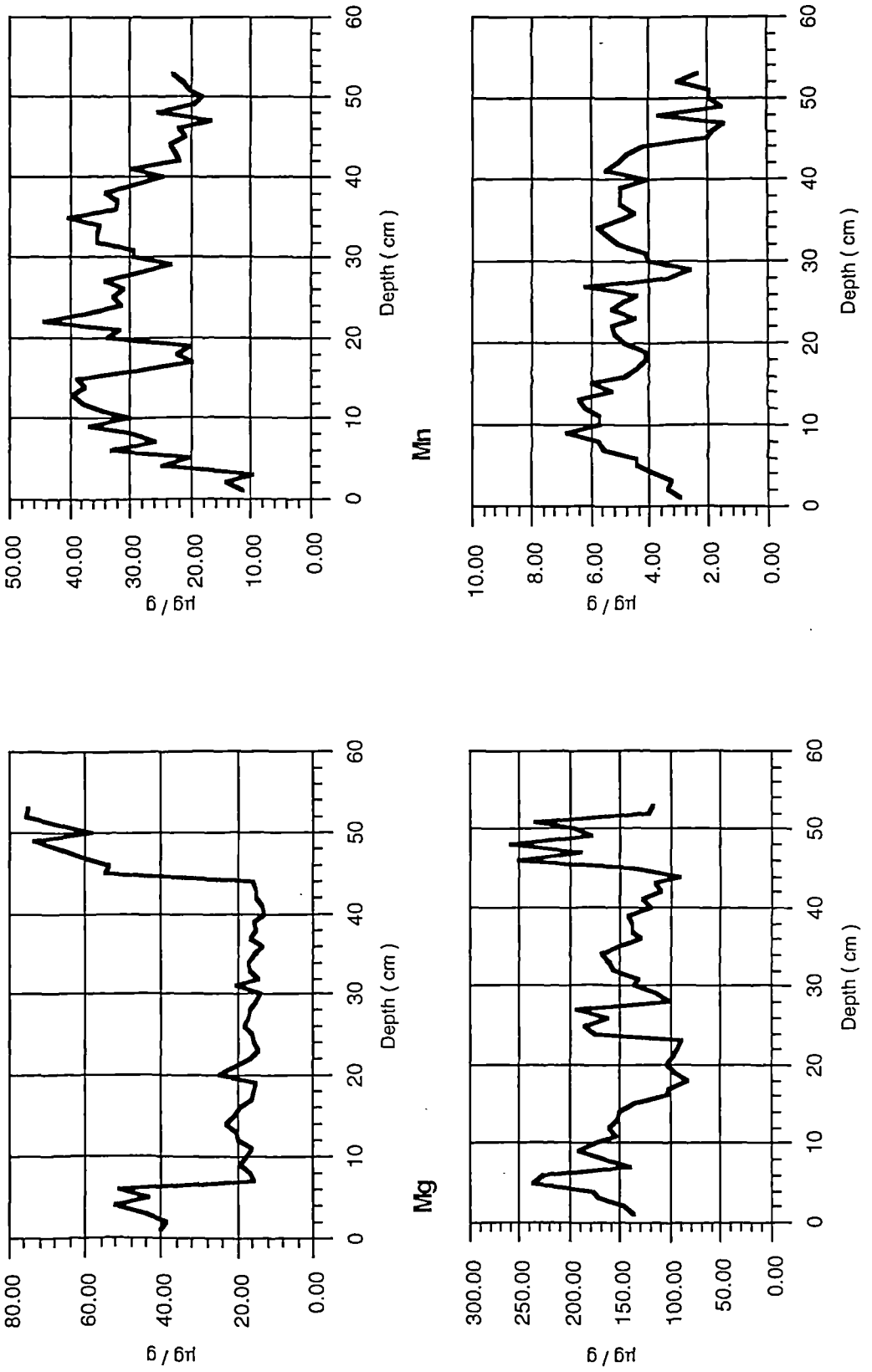

Figure 5.23. Variations in the concentrations of ions residual with depth in the sand layer (Figure 5.19).

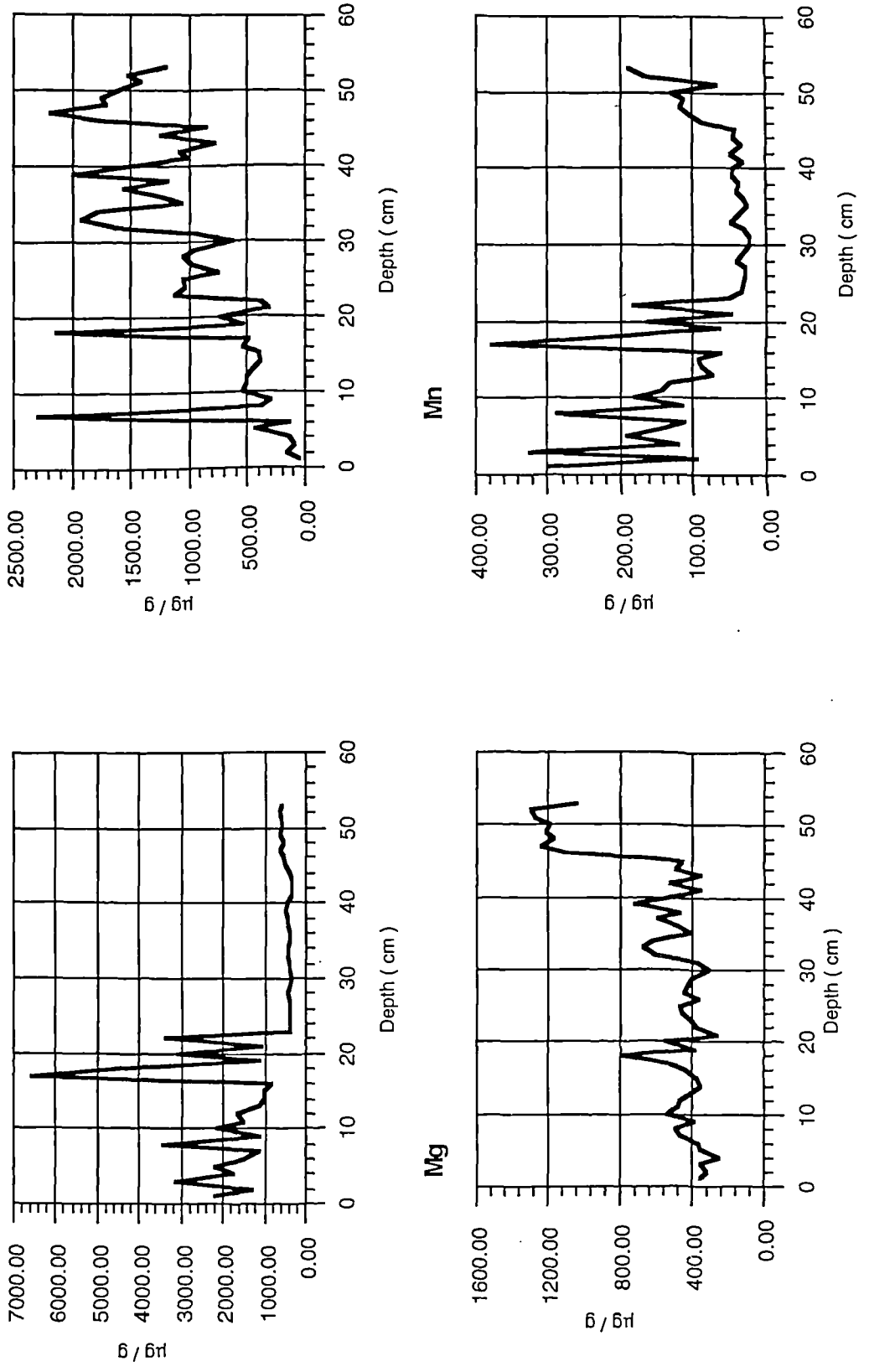

Figure 5.24. Variations in the concentrations of total ions with depth in the sand layer (Figure 5.19).

In contrast to this, concentrations of Ca, Mg and Mn ions bonded to the organic matter are relatively low (Figure 5.22). However, a similar difference through the thickness of the core occurs in values of Mg and Mn ion concentrations, whilst two extraordinarily high values of Ca concentration correspond to prominent peaks of the values for Na, Mg and Mn concentrations.

The concentrations of exchangeable ions and ions bound to carbonates exhibit generally low values in Na and Mn, but relatively high values in Mg and Ca (Figures 5.20 and 5.21). The variations with depth of the Ca, Mg and Mn ion concentrations of the both types illustrates a general trend of increasing concentrations downward through the sediment.

5.1.1.4 Mineral Magnetic Analysis

Mineral magnetic analysis reveals that there are distinct variations within the sand layer at boreholes 57, 73 and 84 though not at borehole 56 which is located farthest inland. The results of the analysis are shown in Figures 5.28 to 5.31 and the definitions of the parameters are given in Chapter 2.

Natural minerals have different magnetic properties and are classified as ferromagnetic, ferrimagnetic, canted antiferromagnetic, paramagnetic and diamagnetic. As already mentioned, the sand is predominantly composed of quartz grains (diamagnetic). χ_{lf} and χ_{hf} both are mass specific measurements of mineral magnetic susceptibility. Ferromagnetic and ferrimagnetic minerals are of high values of mass specific magnetic susceptibility, whilst antiferromagnetic and paramagnetic ones are of low values (Dearing, 1994). χ_{lf} and χ_{hf} at all boreholes vary within a low and narrow value range of 0.1 to 0.6 $\mu m^3 kg^{-1}$. This confirms that the concentration of magnetic minerals is low in the sand layer. SIRM is roughly a measurement of the content of ferromagnetic and ferrimagnetic and canted antiferrimagnetic minerals and HIRM can be understood as a measurement of

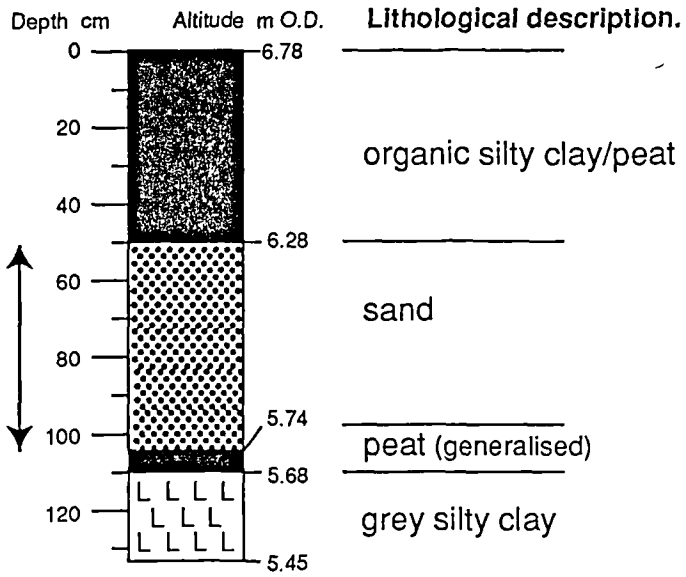

Figure 5.25. Lithostratigraphy of core 56 at Dounie. The arrows mark the core section analysed.

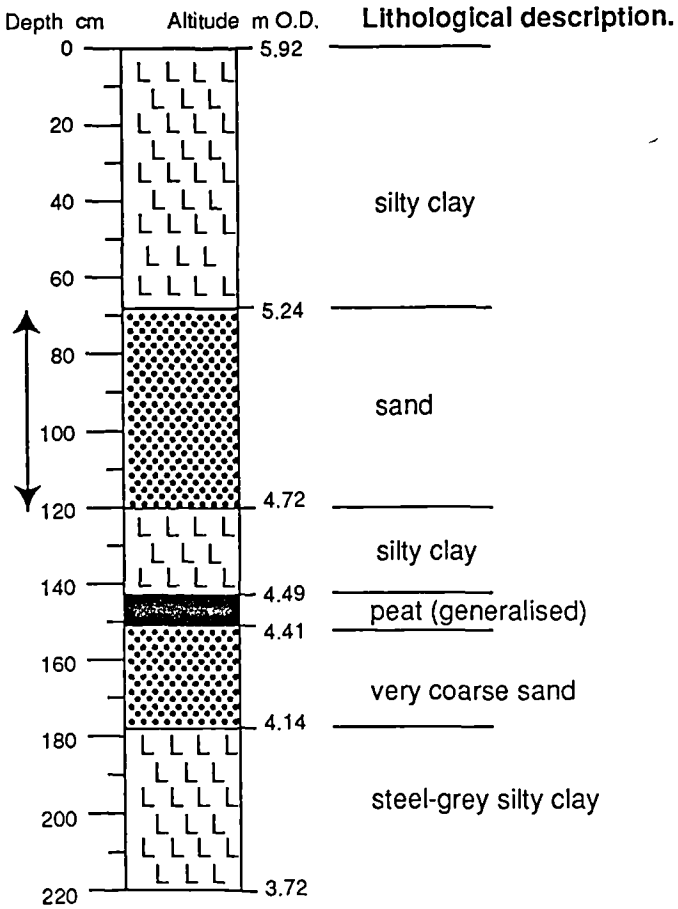

Figure 5.26. Lithostratigraphy of core 73 at Dounie. The arrows mark the core section analysed.

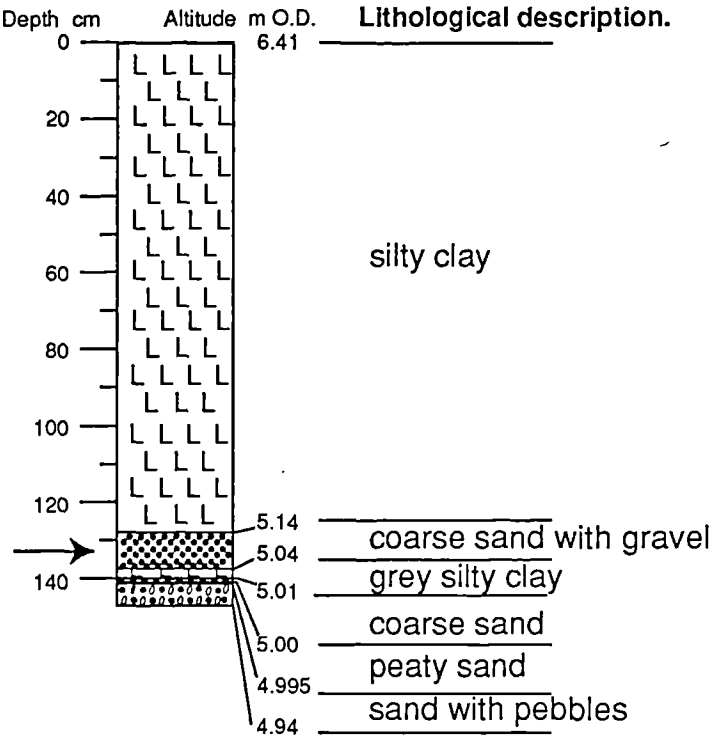

Figure 5.27. Lithostratigraphy of core 84 at Dounie. The arrow marks the core section analysed.

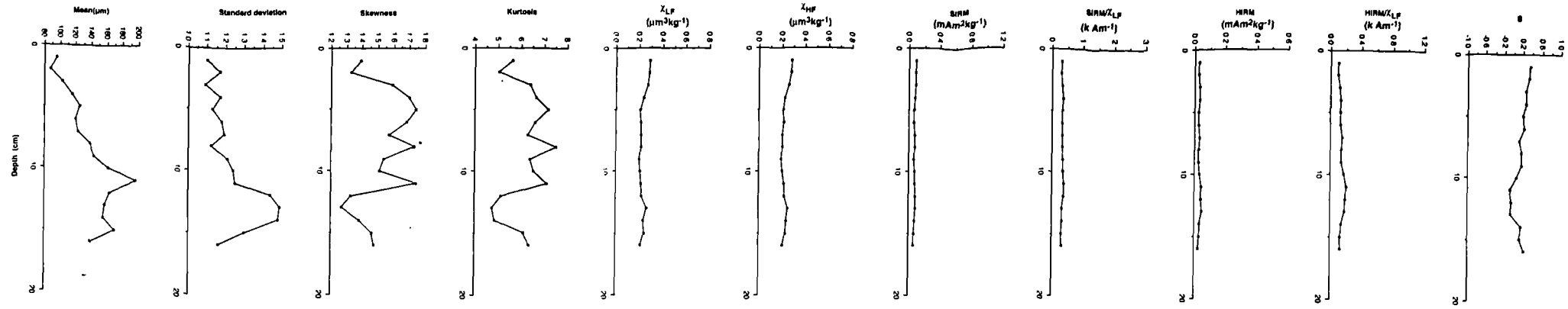

Figure 5.28. Variations in the particle size and mineral magnetic parameters within the sand layer at borehole 56, Dounie **(Figure 5.25).**

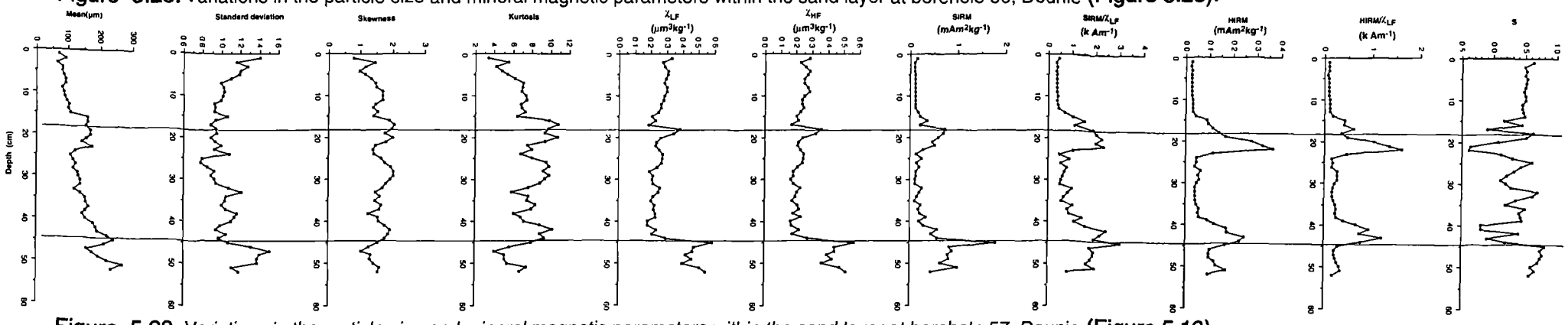

Figure 5.29. Variations in the particle size and mineral magnetic parameters within the sand layer at borehole 57, Dounie **(Figure 5.19).**

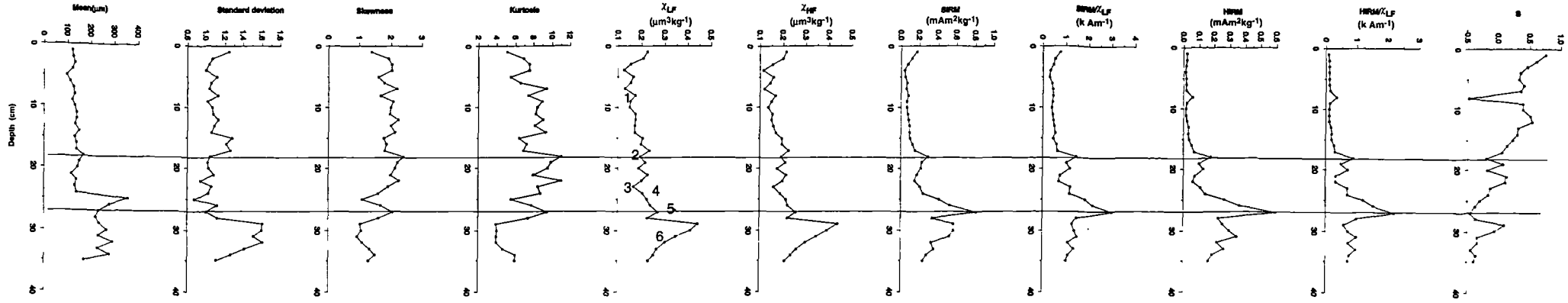

Figure 5.30. Variations in the particle size and mineral magnetic parameters within the sand layer at borehole 73, Dounie **(Figure 5.26).**

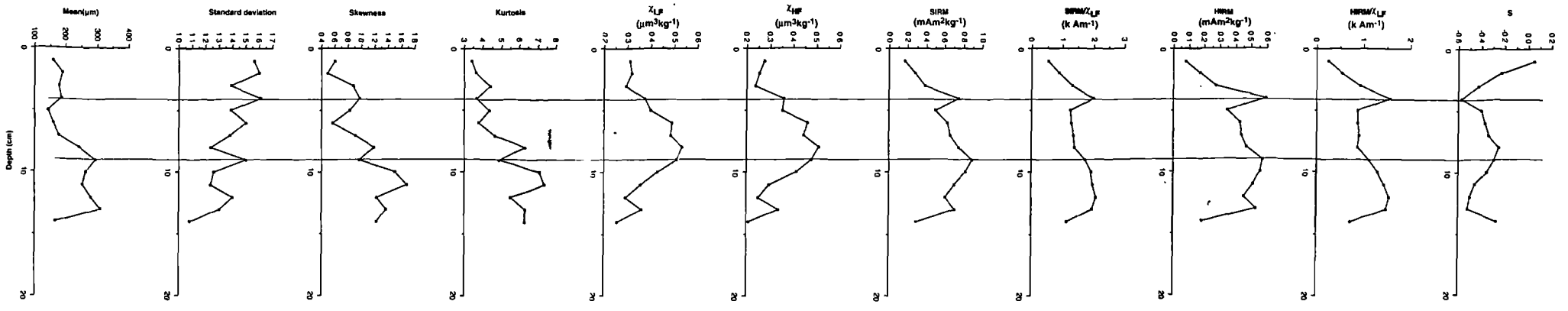

Figure 5.31. Variations in the particle size and mineral magnetic parameters within the sand layer at borehole 84, Dounie (Figure 5.27).
Numerical numbers mark the samples analysed with Scanning Electron Microscopy and the results are given in Table 5.2.

antiferromagnetic and paramagnetic content. Because ferromagnetic minerals are made of pure chemical elements which are rarely present but chemically bound to other elements to form ferromagnetic minerals in natural surface environments, the magnetic mineral assemblage within the sand layer is probably predominantly composed of ferrimagnetic minerals.

As shown in Figures 5.28 to 5.31, high values of mineral magnetic parameters thus mark two bands of enriched concentrations of ferrimagnetic minerals, e.g. titanomagnetite ($FeTiO_3$) (J. A. Dearing, pers. comm.). The changes in magnetic mineral concentration are confirmed by analysis of selected elements with a Scanning Electron Microscope at several levels at borehole 57 (Figure 5.31 and Table 5.2). The Fe concentration (18.9%) corresponding to the enriched concentration band of ferrimagnetic minerals is significantly higher than the rest of tested samples.

Table 5.2 Relative concentrations (in percentage) of selected elements determined with scanning electron microscopy (tested by Mrs. C. Dawson)

Level*	Lab No.	Na	Mg	Al	Si	K	Ti	Fe
1	B110	1.46	1.45	11.91	70.10	7.31	1.42	**6.35**
2	B116	1.19	1.06	8.99	77.52	5.26	1.08	**4.90**
3	B121	0.91	1.20	8.83	77.84	5.87	0.96	**4.39**
4	B123	1.46	0.96	9.95	75.27	6.85	1.03	**4.10**
5	B125	2.18	0.85	9.85	72.79	4.80	1.02	**7.81**
6	B130	1.65	1.83	11.99	57.67	6.13	1.14	**18.19**

*The tested levels are marked in Figure 5.27.

It can be seen that the levels of enriched concentrations of ferrimagnetic minerals correspond to the coarsest calibre of the sand layer. However, close inspection of the variations with depth of the magnetic parameters discloses lags between the peak values of the magnetic and particle size parameters. This suggests that magnetic minerals were subject to settling at differential rates due to their varying geometric dimensions and specific gravities. At borehole 56 at the most inland edge of the sand layer, the magnetic analysis discloses very low values of mineral magnetic parameters, indicating that the concentrations of magnetic minerals are very low throughout the sand layer.

5.1.1.5 Particle Size Analysis

Detailed particle size analysis of the exact samples used for the above mineral magnetic analysis at boreholes 56, 57, 73 and 84 was undertaken initially, followed by four further cores at finer intervals (0.5 cm) at boreholes S6, S9, S3 and S44. This revealed that the sandy sediment is generally composed of a predominant sand grain subpopulation and faintly recognisable but persistent silt and clay subpopulations (Figure 5.32). The silt and clay subpopulations are often present as a prominent curving tail attached to a sand subpopulation in a histogram of log-normal relative frequency.

The results of the analysis at boreholes 56, 57, 73 and 84 are shown in Figures 5.28 to 5.31. There is a general trend of mean particle size fining upward within the sand layer in all four cores, and a general improvement with decreasing depth of sediment sorting in the

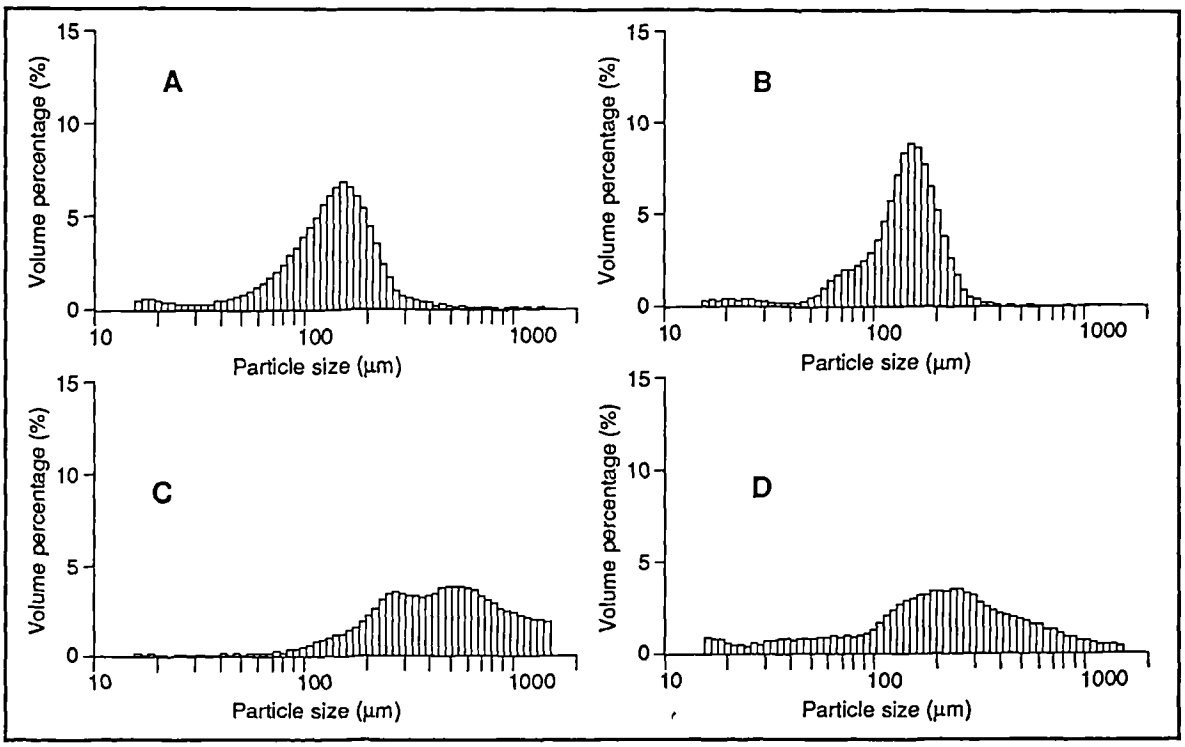

Figure 5.32. Representative particle size distributions of the sediment samples from the sand layer at Dounie. The sediment is characteristically of distributions A and B and is sometimes of multimodal distributions C and D.

cores except for 84, reflected by variations in the standard deviation values. At the most seaward borehole 84, visual inspection revealed that the sand contains grits and pebbles up to 2 cm, which has been sieved out with a 1880 μm mesh after the magnetic analysis and prior to the particle size analysis. Comparing the variation curves of the four cores, a general landward trend of sediment fining can also be observed. Except for core 56, two prominent and progressively fining upward sequences can be identified in the rest and the bases of each such sequences correspond to the above mentioned strong magnetic signals.

Further particle size analysis was undertaken for cores S3, S6, S9 and S44 at *circa* 0.5 cm contiguous intervals. The results confirm the above mentioned two general fining upward sequences within the sand layer, and also disclose further less prominent variations in each fining upward sequence (Figures 5.34, 5.36, 5.38 and 5.40). Six horizons in total are classified with particle size parameters for the cores S6, S9 and S3, and 4 horizons for the core S44. A general landward fining trend is also observed among S3, S6 and S9.

5.1.1.6 Interpretation

The stratigraphy at this site is comparable to the coastal depositional sequence revealed at Creich, where the sand layer and grey silty clay are interpreted as marine deposits based on the lithostratigraphical and microfossil evidence. The estuarine grey silty clay at Dounie bears a close resemblance to the similar deposits found at Creich (see below), but the sand is much coarser and generally contains less silt and clay fractions as revealed by particle size analysis. The sand layer at Dounie is also distinctively thicker and more extensive. This clearly suggests that the sand supply to the marine flood, represented by the sand layer, is much more abundant at this site. As noted above, there is evidence of lenses of gravels and grit within the sand layer landwards of the most inland ridge but no trace of any similar sand layer was found. In addition, since ridges mark areas of high energy environment associated with gathering of abundant coarse materials, it is interpreted here the coincidence

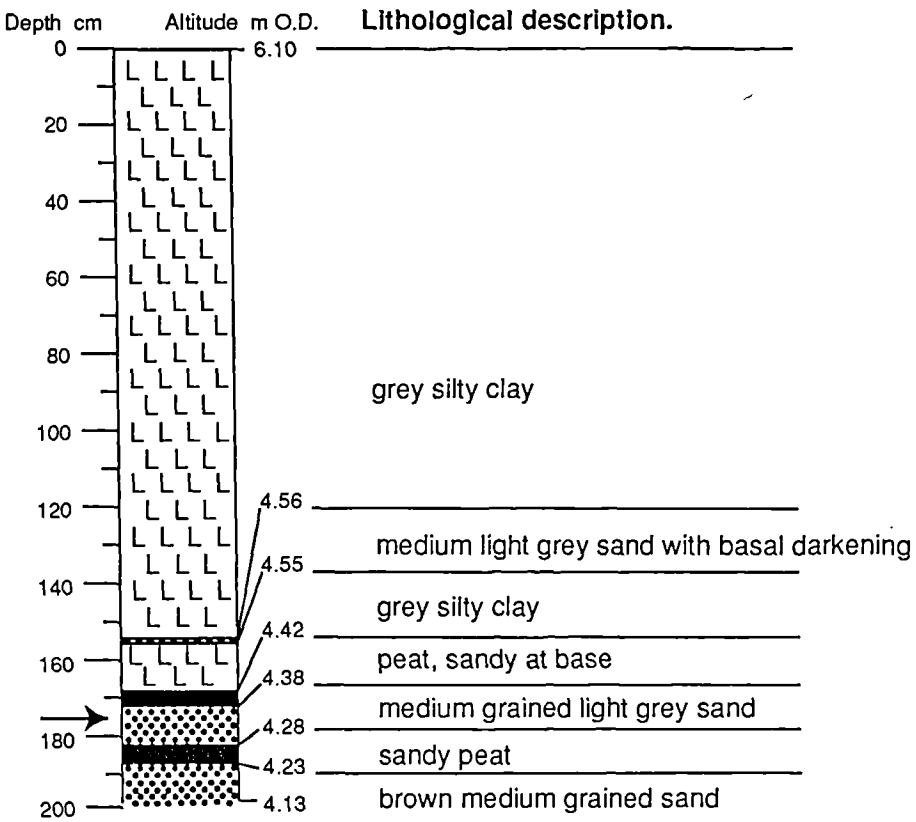

Figure 5.33. Lithostratigraphy of core S3 at Dounie. The arrow marks the core section analysed.

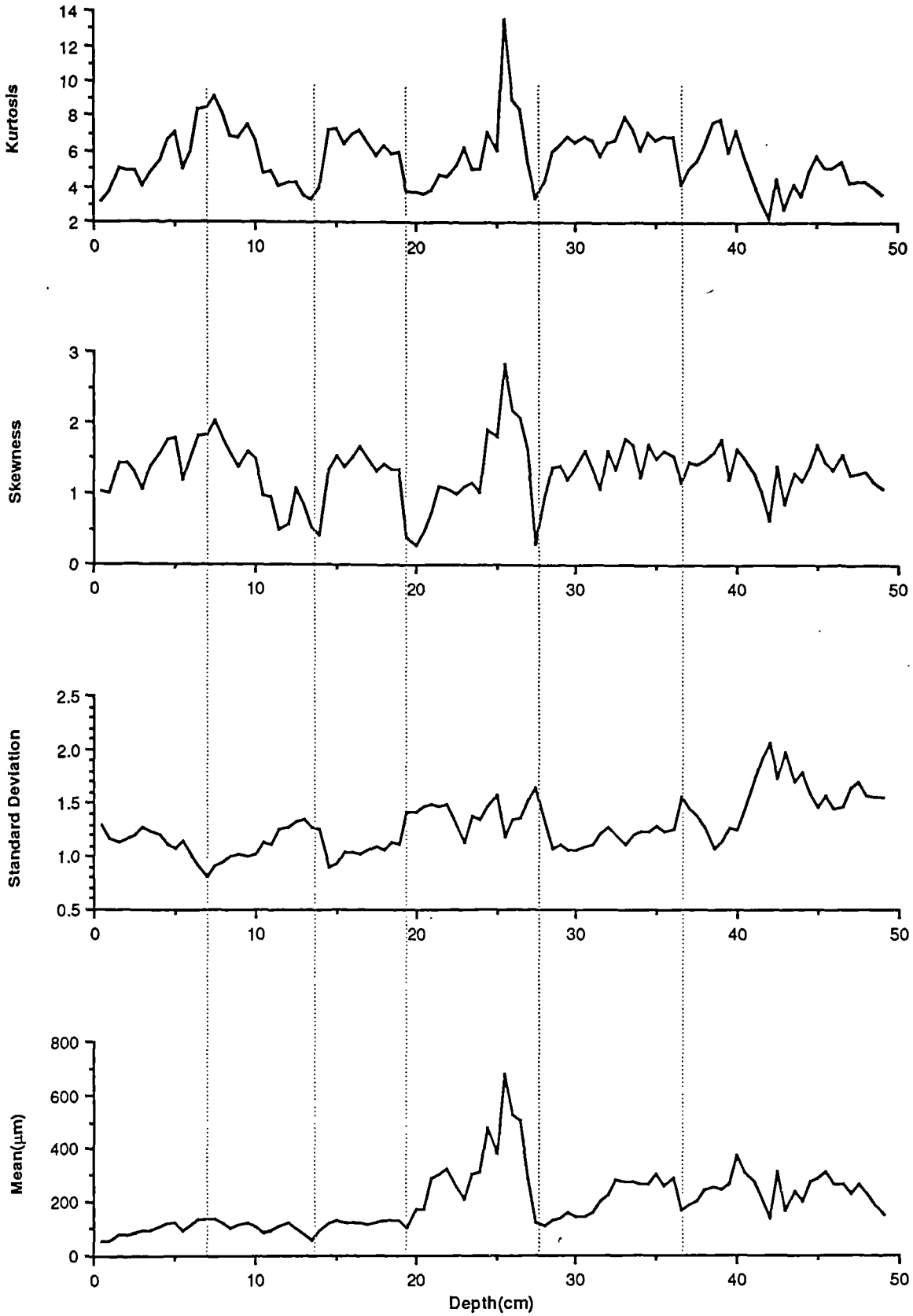

Figure 5.34. Variations in the particle size parameters within the sand layer at borehole S3, Dounie (Figure 5.33).

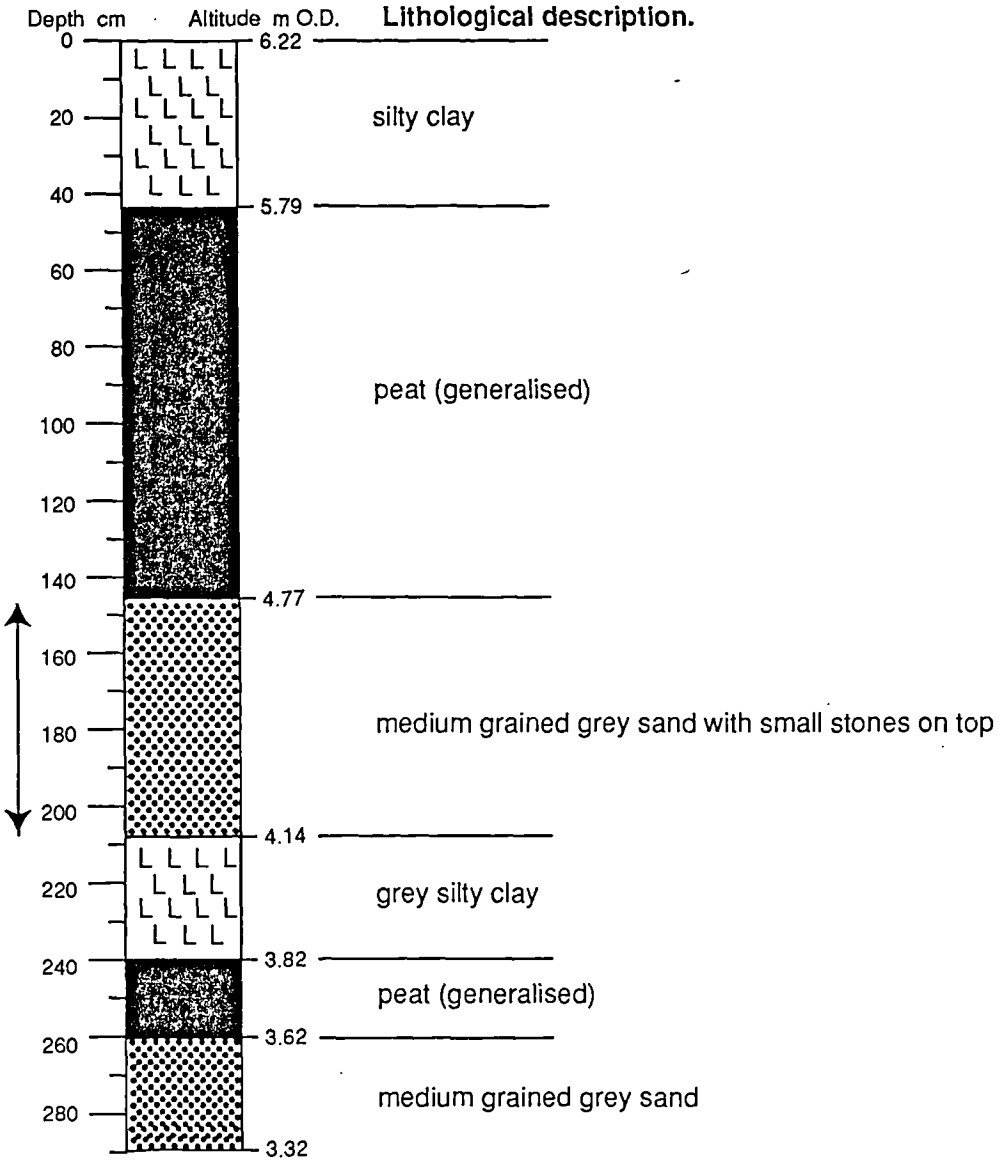

Figure 5.35. Lithostratigraphy of core S6 at Dounie. The arrows mark the core section analysed.

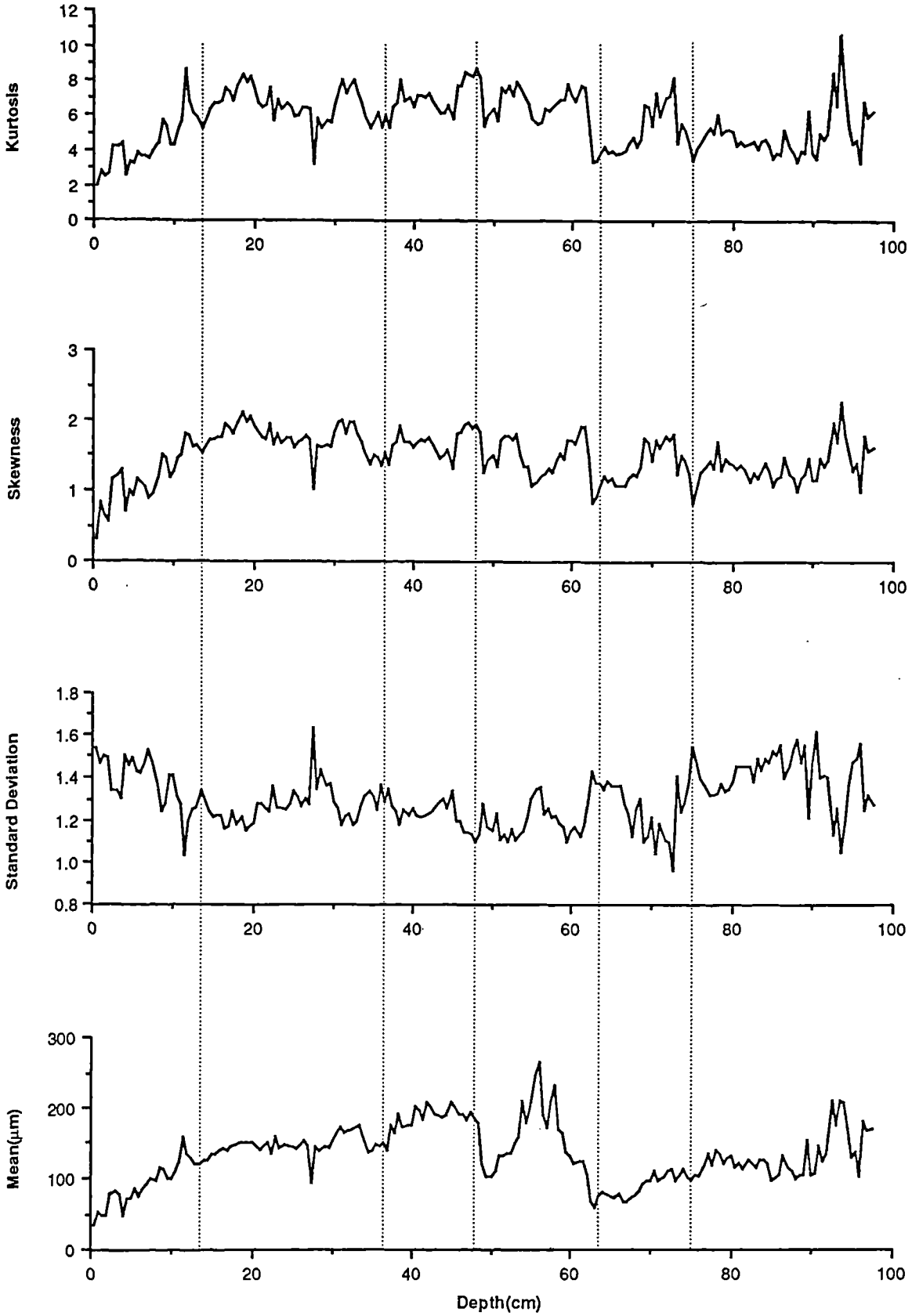

Figure 5.36. Variations in the particle size parameters within the sand layer at borehole S6, Dounie (Figure 5.35).

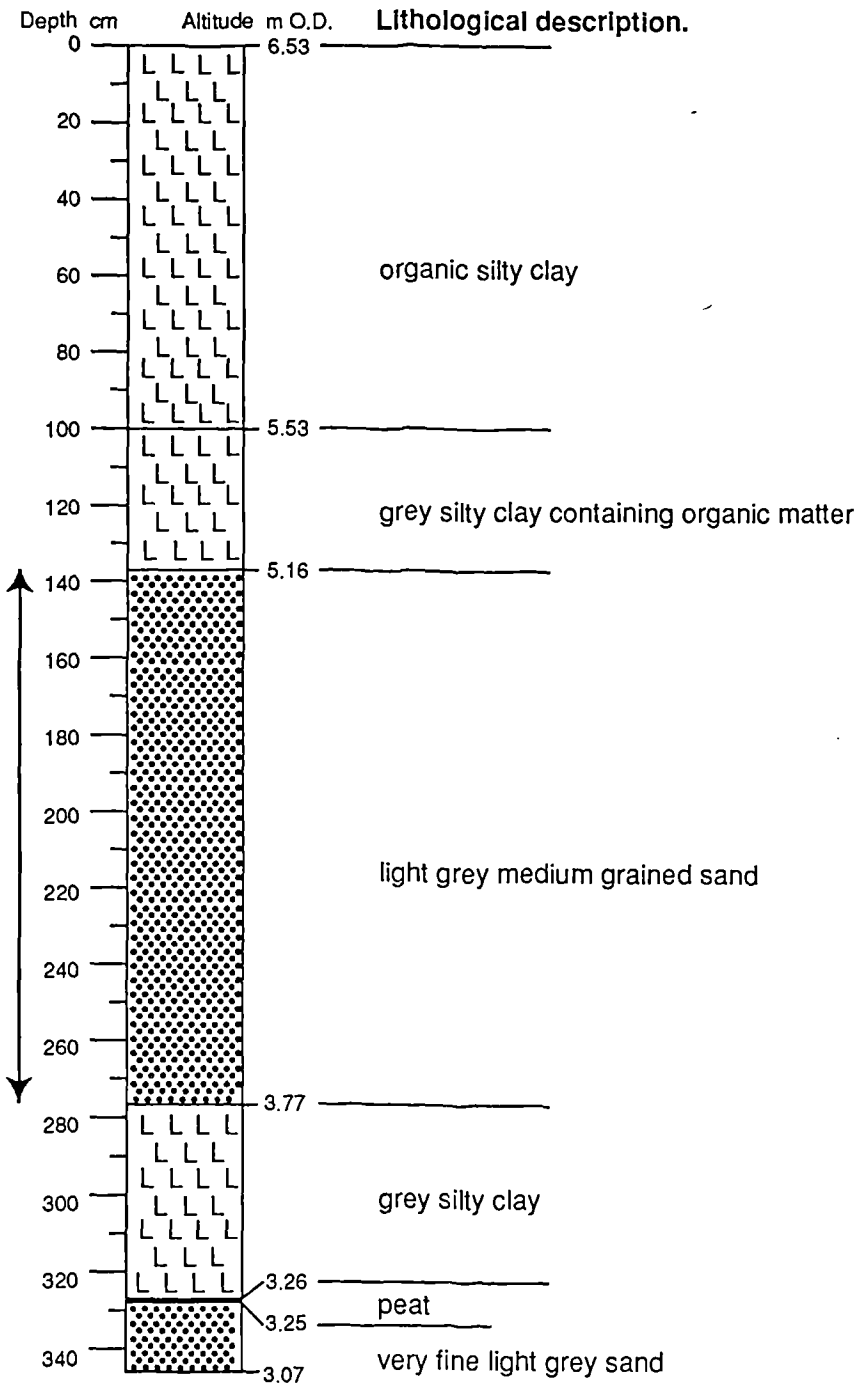

Figure 5.37. Lithostratigraphy of core S9 at Dounie. The arrows mark the core section analysed.

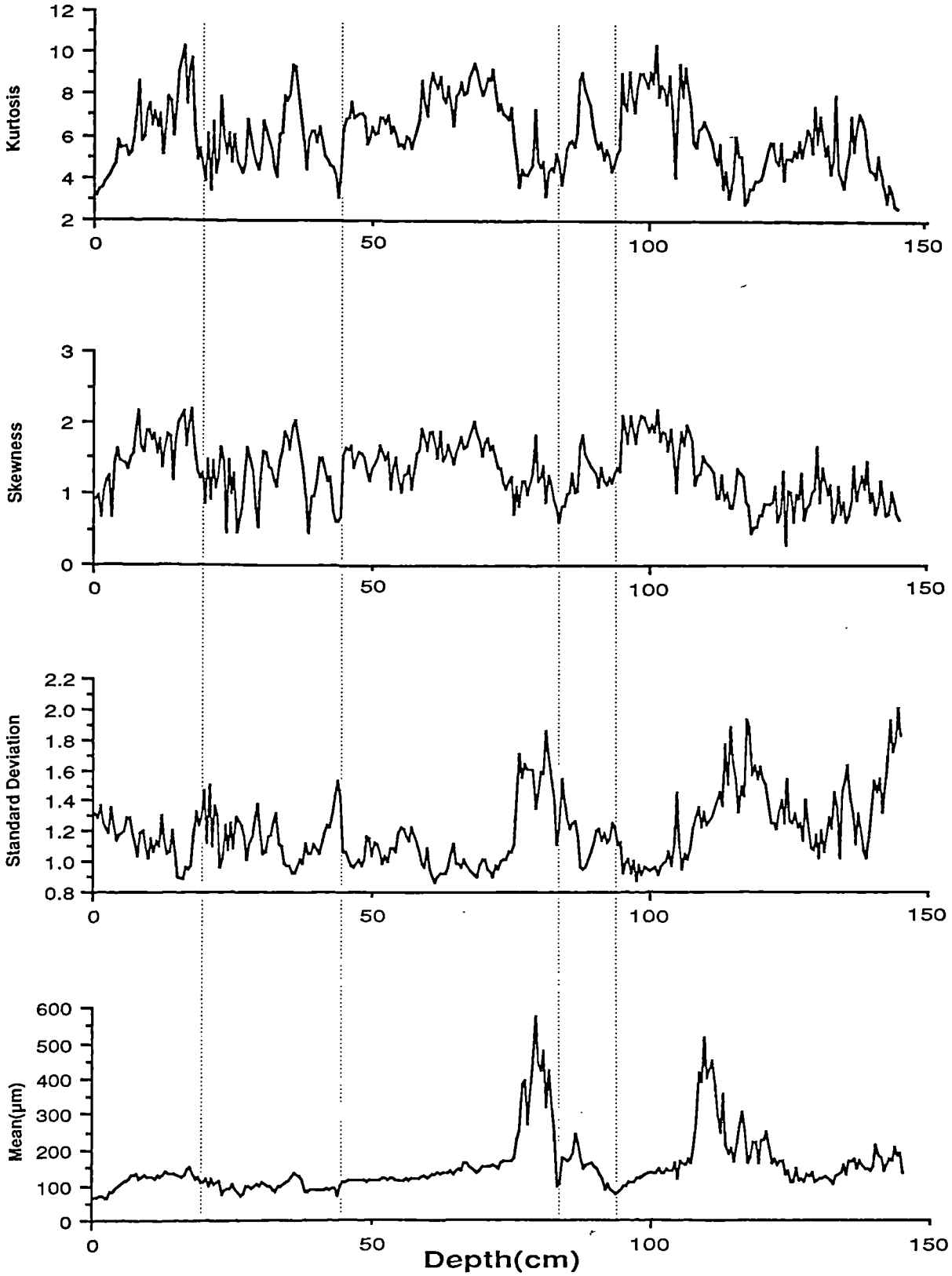

Figure 5.38. Variations in the particle size parameters within the sand layer at borehole S9, Dounie (Figure 5.37).

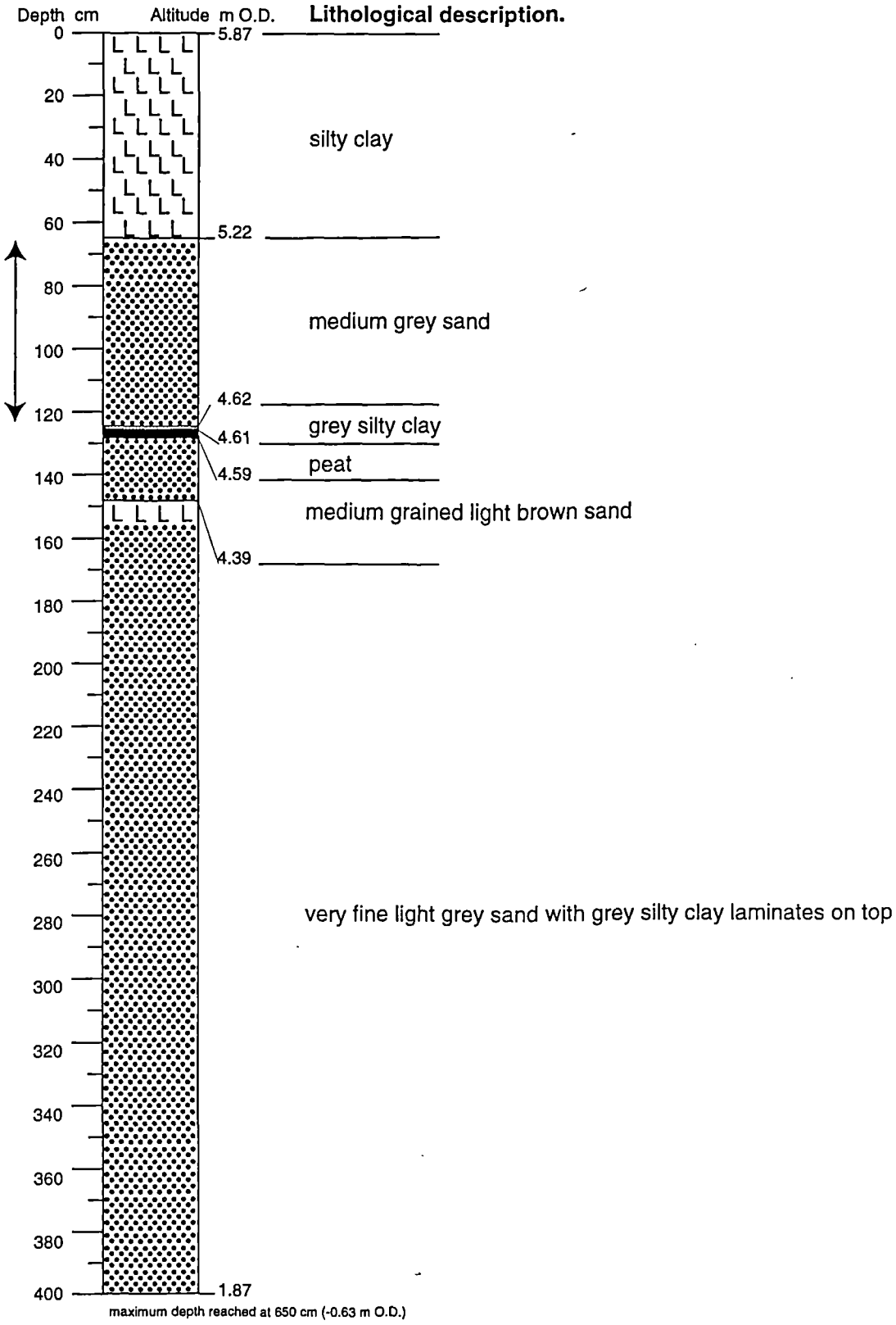

Figure 5.39. Lithostratigraphy of core S44 at Dounie. The arrows mark the core section analysed.

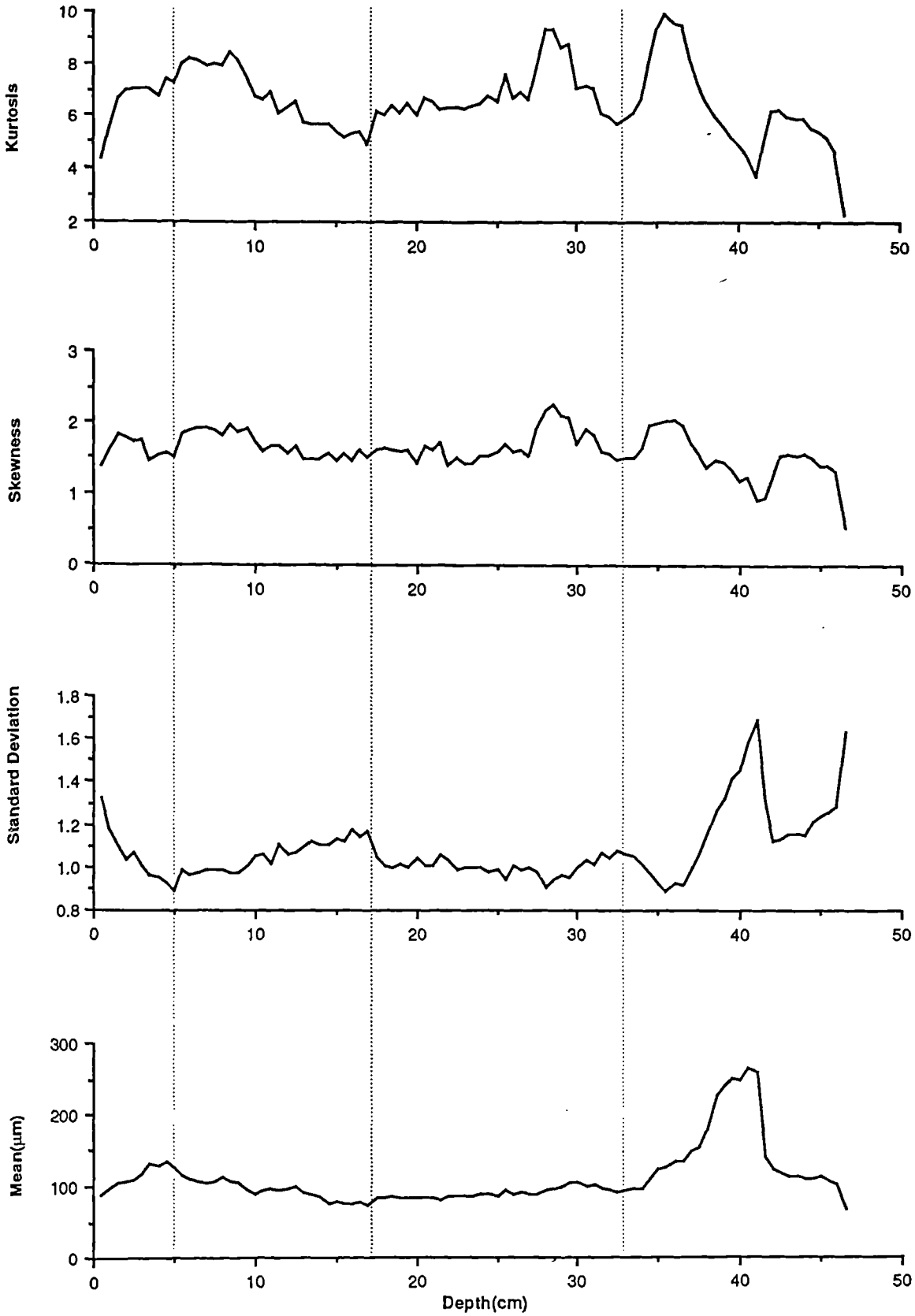

Figure 5.40. Variations in the particle size parameters within the sand layer at borehole S44, Dounie (Figure 5.39).

of such evidence and the distinctively increased abundance in sand implies that the source sediment of the sand layer was largely drawn from the area where the ridge occurs.

The variations in ions extracted from primary and secondary minerals imply a general uniformity in mineral composition of the sand throughout the core. The variations in ions bonded to organic matter suggest that there is a marked enrichment of organic detritus in the upper part of the cores and that the two distinct horizons (*circa* 7 and 18 cm deep from the top of the sand layer) probably mark the levels of larger organic detritus intraclasts. The general trend of increasing concentrations downward through the sediment, indicated by the variation in concentration of the exchangeable ions and ions bonded to carbonates, probably results from groundwater influence through leaching processes.

Particle size distributions of the sediment are clearly multimodal, confirming that the sediment differs from beach sand. Variations with depth of mineral magnetic and particle size parameters clearly illustrate two major depositional sequences in the fining-upward sediment. As the sediment supply was abundant and the sand layer is much thicker at this site, further horizons can be classified and may represent episodes of marine inundation of smaller magnitude. It was previously thought that particle size results can be used to infer the number of waves as well as correlating depth-particle size series with time-series of mathematically simulated fluctuations (Dawson, Foster, Shi, Smith and Long, 1991). However, in addition to that it is now considered that sedimentation rate could have varied during the accumulation process of the sediment and thus that a depth-particle size curve can not be directly matched with a time-amplitude curve, further detailed information obtained during this research suggests that there is great spatial variability in the number of fining-upward sequences and the Flores study reveals that complexity exists in coastal sedimentation processes of tsunami inundation (seé Chapter 4). Therefore, it is considered that it is difficult to establish the number of inundations from the results of particle size analysis, but it is possible to estimate episodes of deposition. Based on the results of

particle size and mineral magnetic analyses, two major successive and several smaller episodes of deposition are inferred there. The episodic variations in particle size distribution are considered to be one of important characteristics of tsunami sediments. It is perhaps possible in the future to attribute different episodes of deposition determined with particle size analysis to individual processes of runup and backwash of tsunami inundation when tsunami sedimentation processes are better understood.

There is a close association of the coarsest sediment levels and the distinct peaks of mineral magnetic susceptibility, SIRM and HIRM, but there are lags between the occurrances of the peaks in the magnetic parameters and mean particle size. This indicates that the variation in particle size does not correlate exactly with variations in the mineral magnetic parameters and that the variations in the magnetic parameters can not be explained solely by attributing to variations in particle size parameters. As indicated in a recent study (cf. Bjorck, Dearing and Jonsson, 1982), natural minerals of different kinds tend not to spread evenly in particle size distribution over a size scale and magnetic minerals have been found to cluster or concentrate in particular particle size fractions. The strong magnetic signals probably reflect a higher concentration of magnetic minerals, which have particular geometric dimensions and, very likely, higher specific gravities. The magnetic minerals settled out together with coarsest quartz grains and also were subject to differential settling resulting in varied assemblages of magnetic minerals within each band of enriched magnetic mineral composition.

In summary, it seems likely that the sediment of the sand layer was derived from the area where the most landward shingle ridge lies and the mudflats and laid down by a high energy marine inundation, which had at least two large episodes in addition to superimposed smaller episodes at *circa* 7,000 years BP. The marine inundation could have overflowed and partially breached the buried, the sand and shingle ridge located farthest inland, exceeded the uppermost limit reached by the Holocene relative sea level (i.e. the uppermost limit reached by the estuarine silty clay) and reached at least 2.5 m above the contemporary high water

mark, as indicated by stratigraphic evidence. The base of the sand layer marks contemporary surfaces of the peat bogs and the mudflats below, which meet at a boundary indicative of the former high water mark. The elevation of the uppermost level of the sand layer relative to this boundary provides a minimal estimation of the flood run-up (Figure 5.18).

5.1.2 Creich

5.1.2.1 Stratigraphy

At Creich, a small area of raised mudflats of *circa* 1 km^2 lies on the northern side of the Dornoch Firth, facing the mouth of the estuary, between a rocky outcrop to the south and the hillside to the north (Plate 11; Figures 5.15 and 5.41). Its surface lies mainly between 5 and 6 m O.D., and at its seaward margin, a small terrace in the raised mudflats lies at a lower altitude of between 3 and 4 m O.D.. At the landward edge of the raised mudflats, peat outcrops from beneath the estuarine sediments, whilst at the seaward edge the foreshore is backed with a small area of laminated organic deposits. The stratigraphy of this site, described in Smith *et al.* (1992), was determined by lithostratigraphic information from borehole records (Figure 5.42). This discloses a sequence of deposits which taper out landwards and abut against a rising surface of fluvioglacial deposits. To seaward the lower deposit is a grey clay, sometimes faintly laminated, with a level surface at *circa* -1.5 m O.D.. Above this a compact peat extends inland across both the clay and the surface of glaciofluvial sediments. Overlying the peat rests a grey silty clay, tapering landwards into peat which reaches the surface. The grey silty clay is overlain at its landward edge by part of a continuation of the peat beneath. Spreading through the grey silty clay and the peat accumulation lies a prominent layer of sand, which rises in altitude and decreases in thickness landwards, whilst to seaward part of the stratigraphy is truncated and laminated organic deposits rest upon a small area of gravel and mudflats. The sediments in this

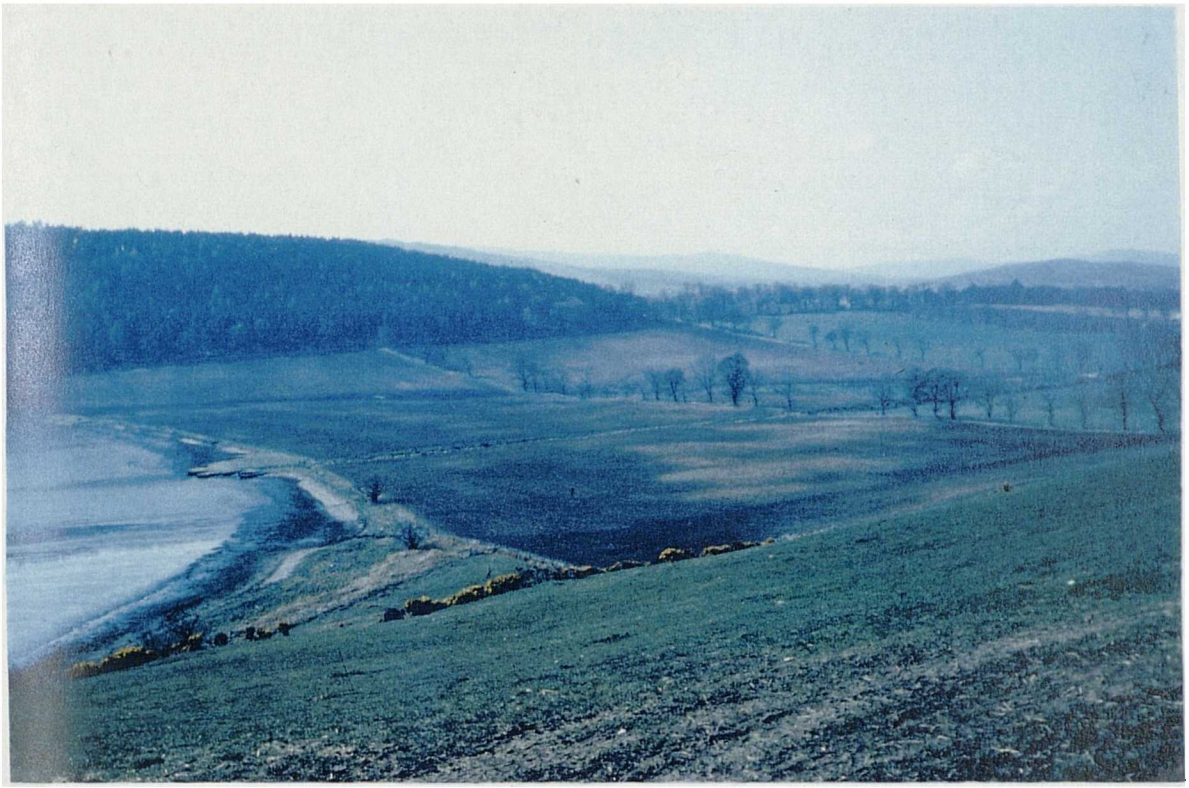

Plate 11. Site at Creich, Dornoch Firth. The surface of a small area of raised mudflats of *circa* 1 km^2 lies between 5 to 6 m O.D..

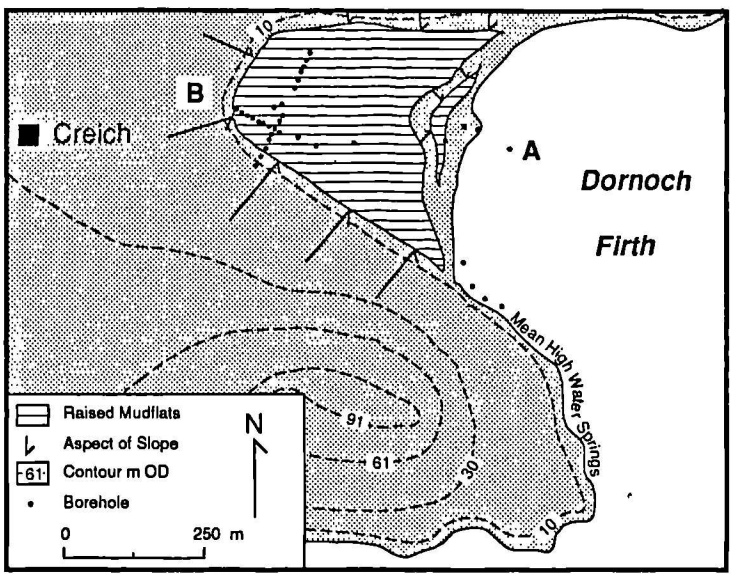

Figure 5.41. Morphology and borehole locations at the Creich site. Letters A and B mark the ends of the stratigraphical section shown in Figure 5.42.

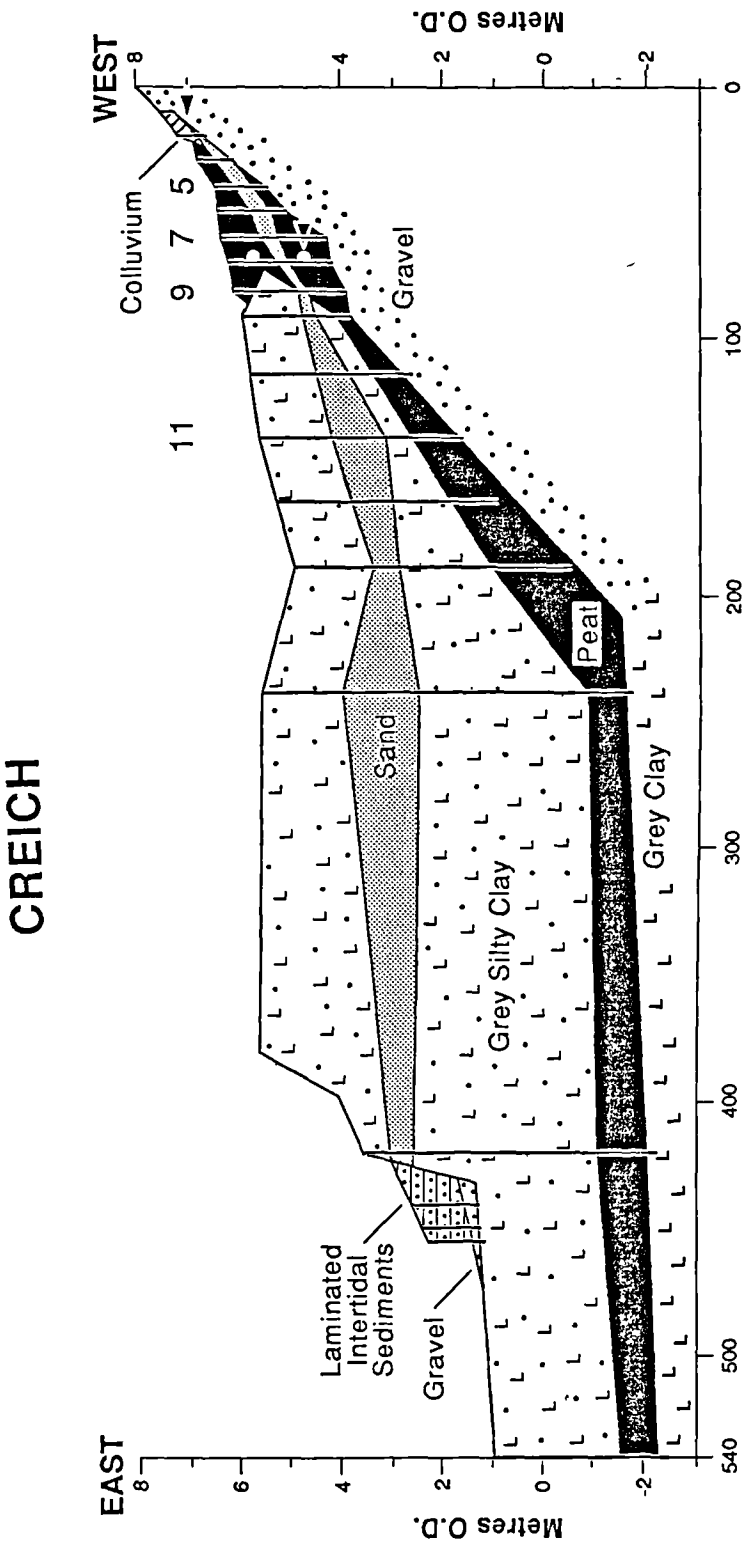

Figure 5.42. Stratigraphy at Creich.

sequence were analysed for pollen and diatoms by Smith *et al.* (1992), and are analysed for particle size and mineral magnetic properties in this study.

5.1.2.2 Radiocarbon Dates

9 ^{14}C dates were obtained from critical horizons (Smith *et al.*, 1992). Given below are the results of dating 3 cm thick samples of peat directly above and below a grey silty sand layer, considered to represent a marine flood in borehole 7.

Sample	Lab. Number	Altitude (m O.D.)	Material	Age(^{14}C Years BP)
CR4	SRR-3693	+5.34 to +5.37	Peat above sand	6950 ± 60
CR5	SRR-3694	+5.60 to +5.65	Peat below sand	6960 ± 55

5.1.2.3 Diatom Evidence

Diatom analysis (Smith *et al.*,, 1992) at cores 5, 7, 11 and 36 shows that the upper and lower organic deposits contain fossil assemblages dominated by freshwater and freshwater-brackish species, whereas the grey silt and grey sand are characterised by dominating representations of brackish-marine to marine species, notably the benthic *Paralia sulcata.* The diatoms of these minerogenic layers are very broken and corroded. This indicates a marine origin for both layers.

At this site, cores at boreholes 11, 9, 7 and 5 were obtained for detailed mineral magnetic and particle size analysis. Two cores were collected covering the upper and lower parts of the sand layer at borehole 11, due to to the difficulty of recovering the whole sequence with a single core. The gap between the two cores is not clear, but is not thought to be greater than 10 cm. The gap is denoted by dashed lines (Figure 5.46). All cores were sliced into contiguous samples at *circa* 1 cm intervals and each sample was analysed with both

techniques. The results of such analyses are illustrated in Figures 5.43, 5.46, 5.47, 5.50 and 5.51, and variations exhibited are discussed below:

5.1.2.4 Particle Size Analysis

The particle size analysis reveals that the grey sand is poorly sorted and that a variety of different subpopulations of particles in the sand, silt and clay ranges, with their modal classes occurring at *circa* 150, 50, 20 and 10 μm respectively (Figure 5.43). Generally speaking, the sand subpopulation is of a predominant percentage and varies in its proportion. The modal classes of the silt and clay subpopulations remain relatively constant throughout. The modal classes of the silt and clay subpopulations correspond to those of the grey silty clay deposits below and above the sand layer.

At borehole 11, two separate sequences can be identified within the sand layer, and are considered as two general fining-upward sequences, although an increase in mean particle size with depth is also observed at the base of the sand layer (Figure 5.46). This coarsening-upward trend is reflected by an enrichment of the component sand subpopulation, shown by decreasing values for the standard deviation and increasing values of kurtosis. However, this level represents the poorest sorting. Within the top 10 cm of the sand, the decrease in the mean is also accompanied by a decrease in sorting, as indicated by the values of kurtosis and standard deviation. Samples from the grey silty clay immediately above and below the sand layer were also analysed and the values of their particle size parameters remain relatively constant, in contrast to the variations within the sand.

At borehole 9, a single peak in mean particle size can be identified within the sand layer, immediately below which a peak in standard deviation and a trough in kurtosis occur (Figure 5.47). From the depth of 7 cm upwards, a fining-upward trend is accompanied by a decrease in sorting (increasing standard deviation and decreasing kurtosis). The carse

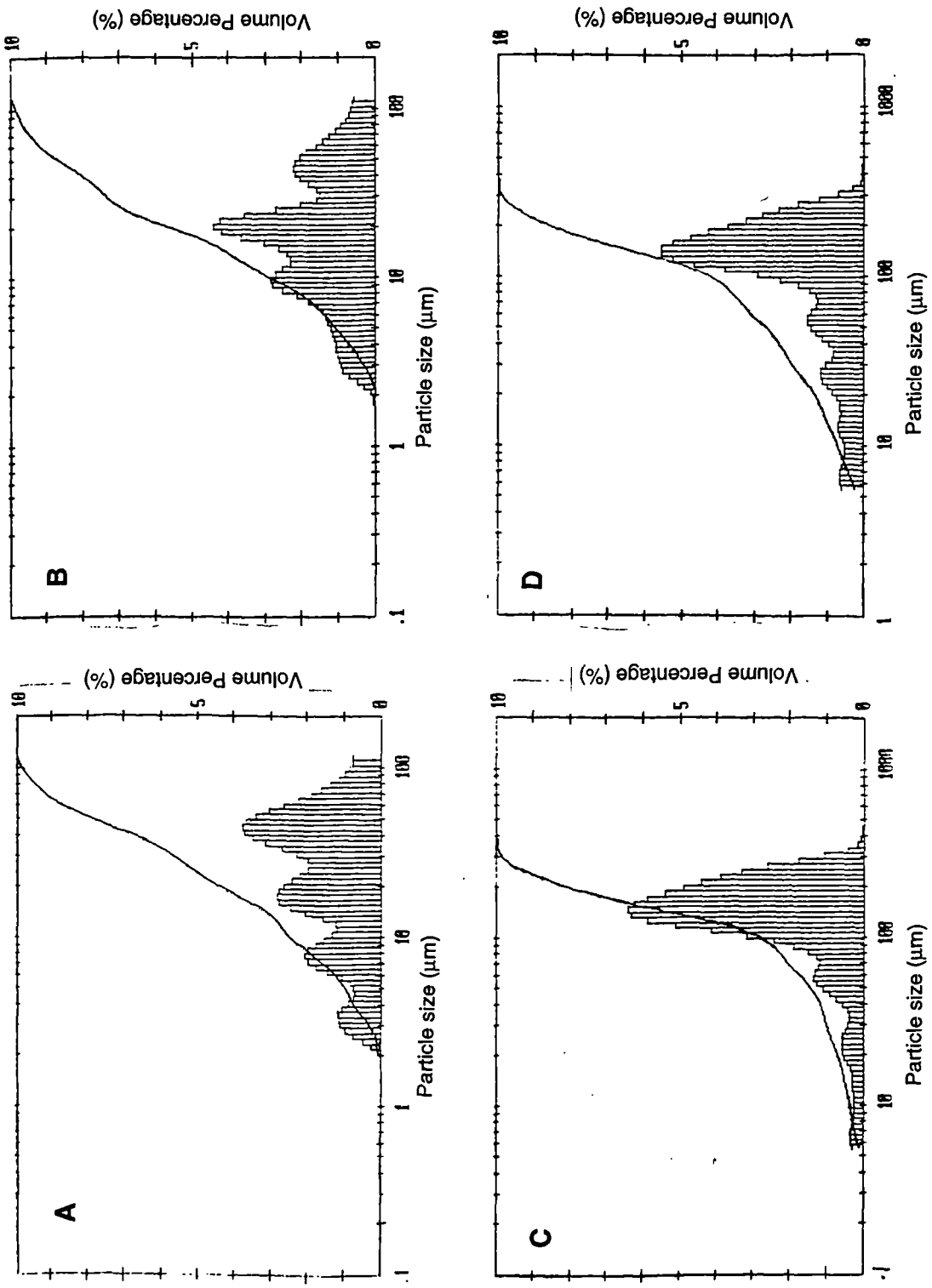

Figure 5.43. Representative particle size distributions of the deposits at Creich. A and B represent estuarine silty clay above and below the sand layer respectively; C and D are examples from the sand layer, displaying varying concentration of the sand subpopulation and finer subpopulations which correspond to the respective ones exhibited by grain size distributions of the estuarine silty clay.

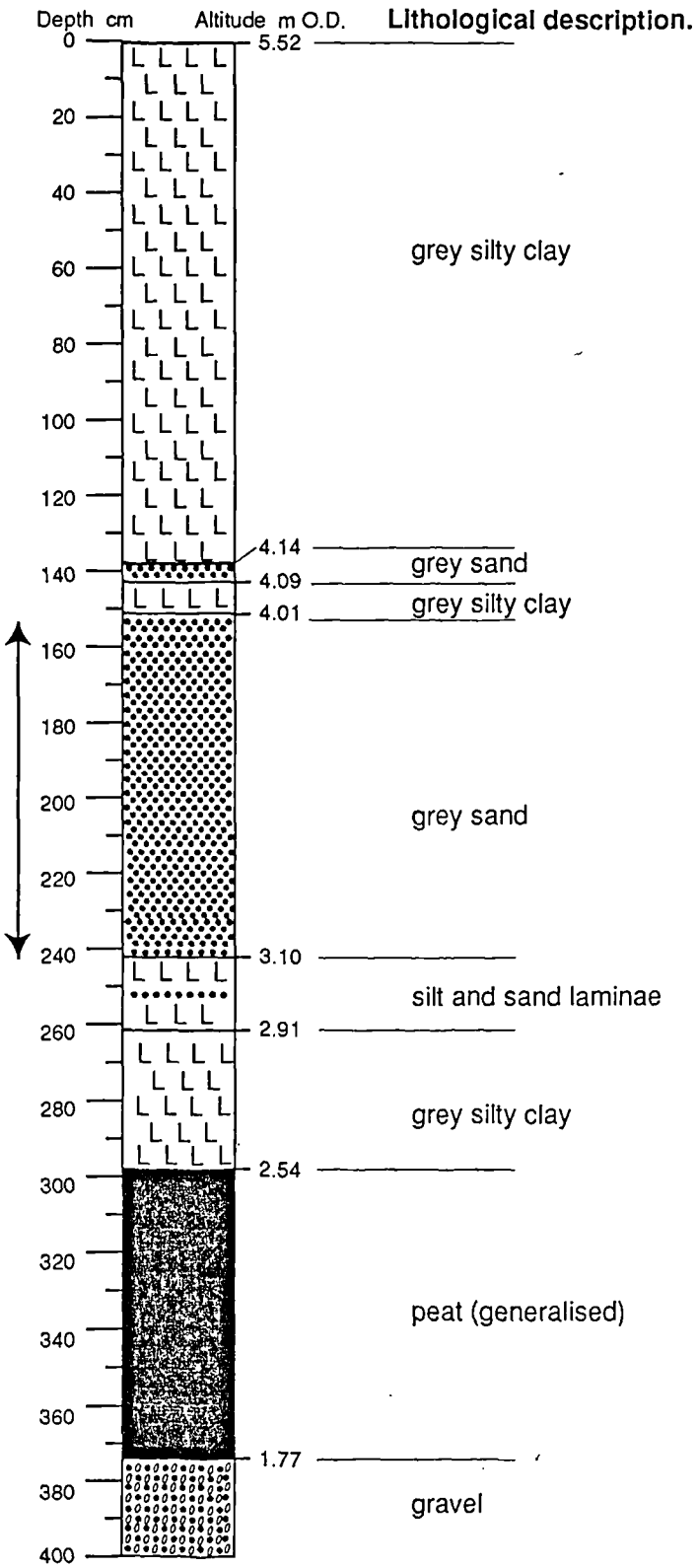

Figure 5.44. Lithostratigraphy of core 11 at Creich. The arrows mark the core section analysed.

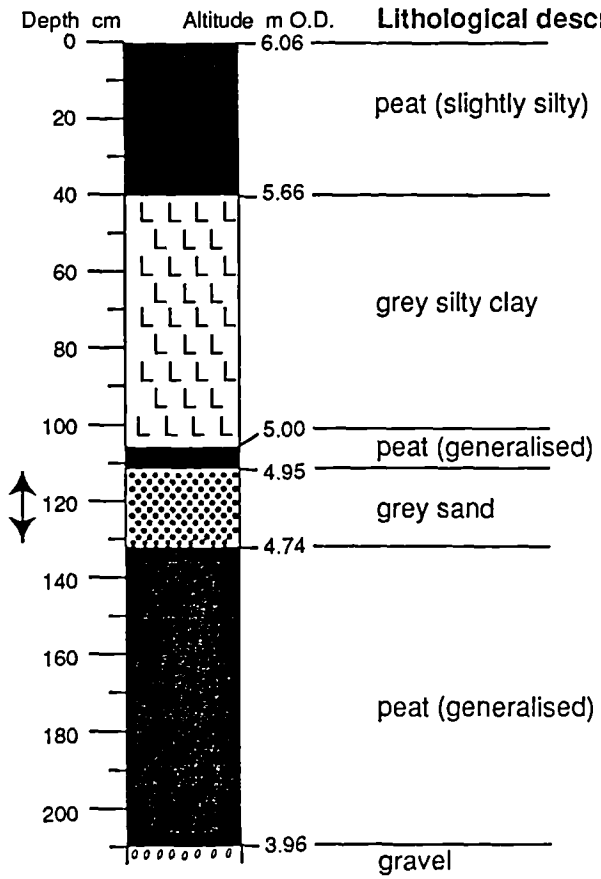

Figure 5.45. Lithostratigraphy of core 9 at Creich. The arrows mark the core section analysed.

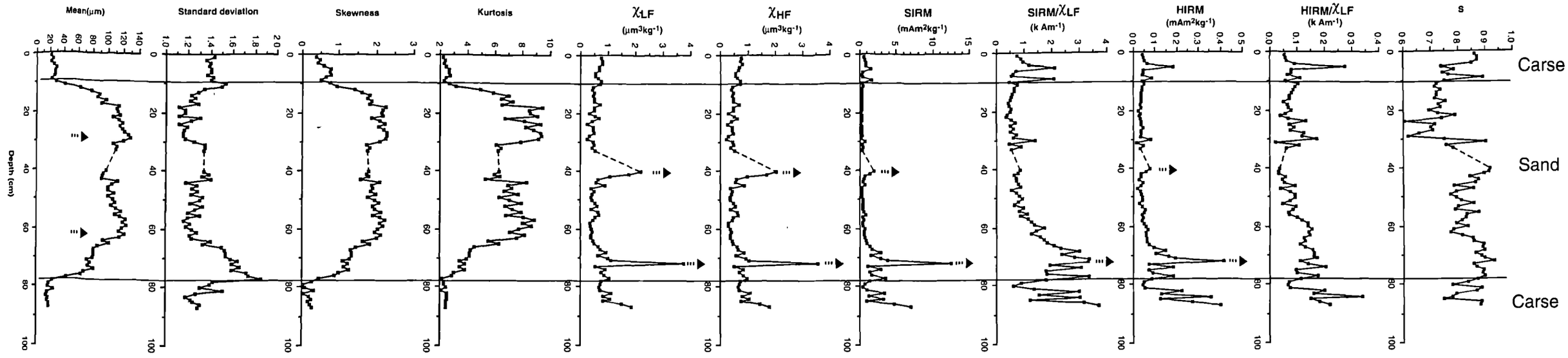

Figure 5.46. Variations in the particle size and mineral magnetic parameters at borehole 11, Creich (Figure 5.44).

⋯▶ denotes basal levels of peak-trough sequence in mean and corresponding peaks in mineral magnetic parameters.

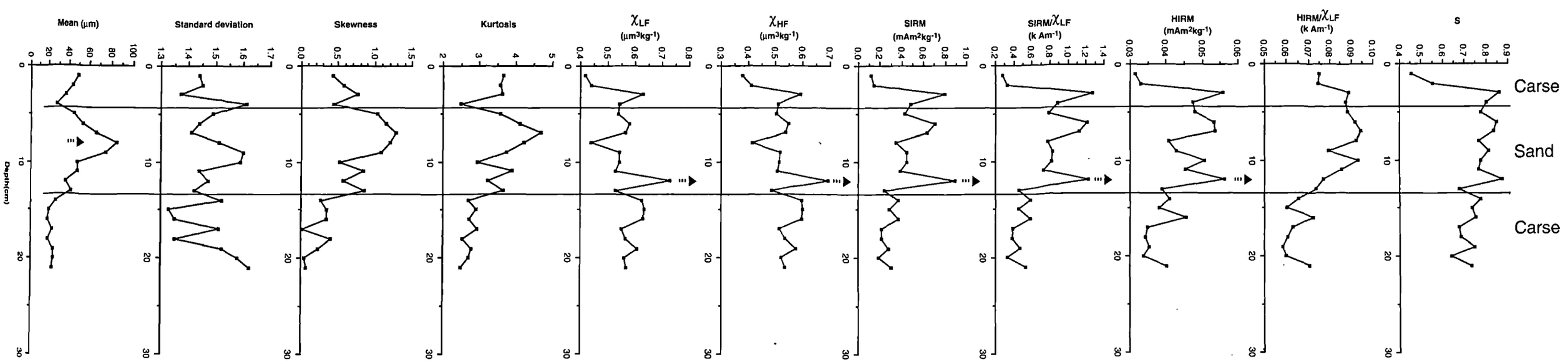

Figure 5.47. Variations in the particle size and mineral magnetic parameters at borehole 9, Creich (Figure 5.45).

⋯▶ denotes basal levels of peak-trough sequence in mean and corresponding peaks in mineral magnetic parameters.

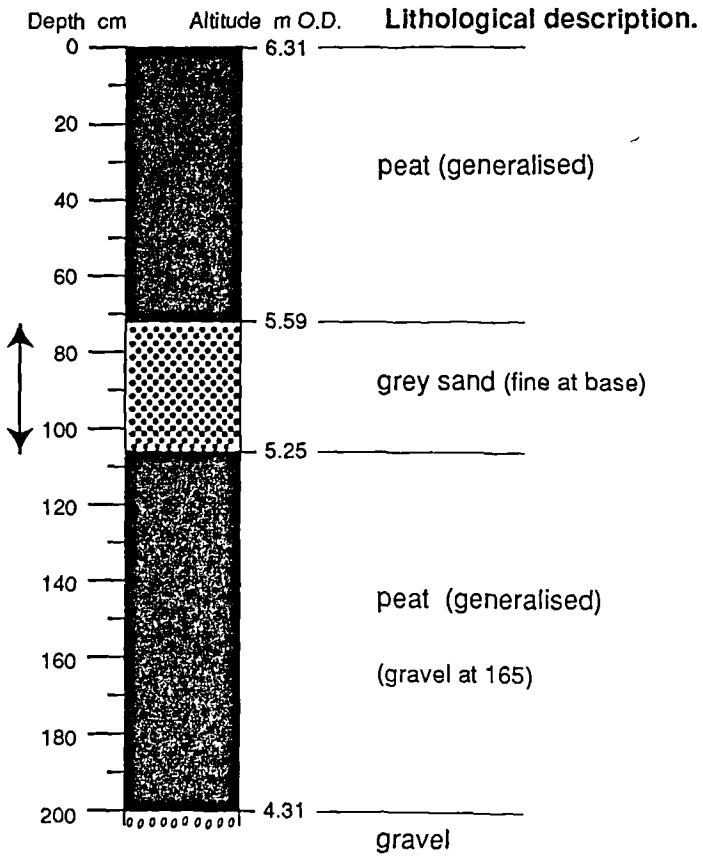

Figure 5.48. Lithostratigraphy of core 7 at Creich. The arrows mark the core section analysed.

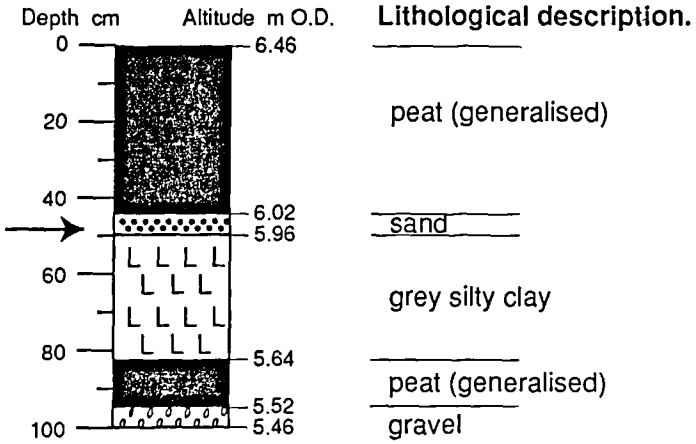

Figure 5.49. Lithostratigraphy of core 5 at Creich. The arrow marks the core section analysed.

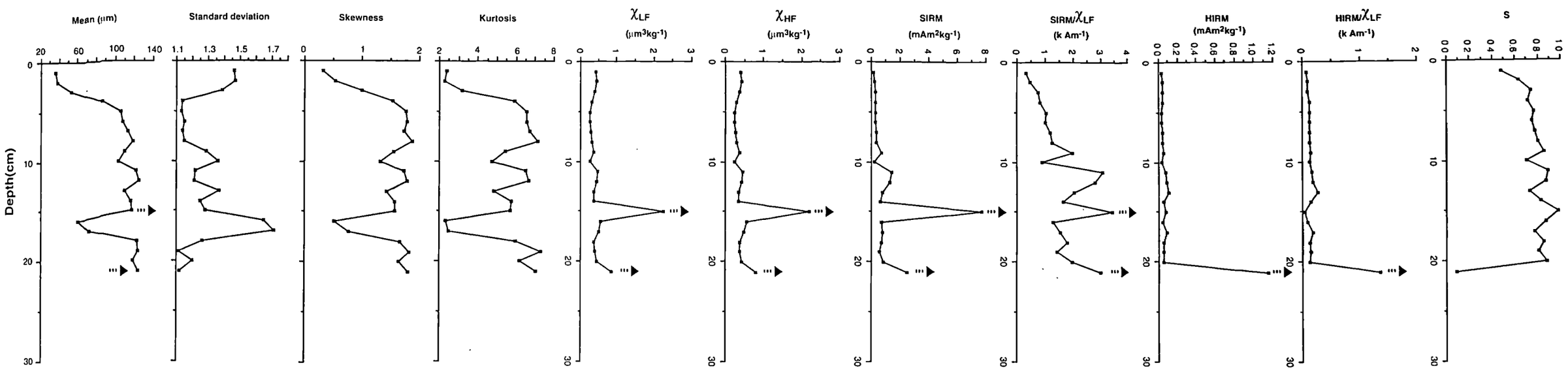

Figure 5.50. Variations in the particle size and mineral magnetic parameters within the sand layer at borehole 7, Creich (Figure 5.48).

⋯▶ denotes basal levels of peak-trough sequences in mean and corresponding peaks in mineral magnetic parameters.

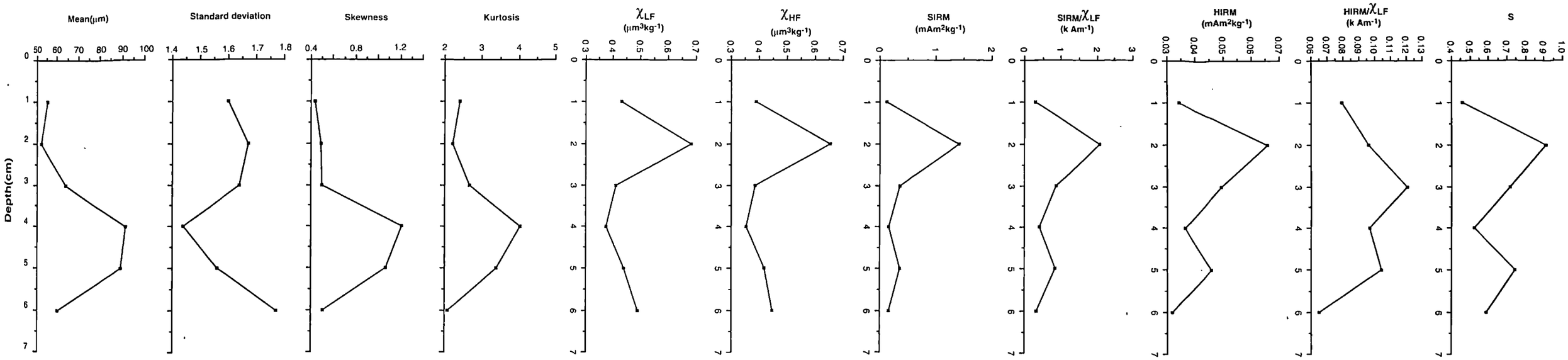

Figure 5.51. Variations in the particle size and mineral magnetic parameters within the sand layer at borehole 5, Creich (Figure 5.49).

immediately above the sand layer is generally coarser and higher in kurtosis value than the carse immediately below.

At borehole 7 (Figure 5.50), two fining upward sequences can be determined, and variations in the mean are positively related to kurtosis and vary negatively with the standard deviation: sorting is improved when the mean is high and low when the mean is low. Such relationships are also present at borehole 5, but only one peak in mean can be identified (Figure 5.51).

There is a general fining landward trend in particle size as indicated by mean particle size values at boreholes 11, 7 and 5, although mean particle size values at borehole 9 do not fit into the general trend.

5.1.2.5 Mineral Magnetic Analysis

Mineral magnetic study was undertaken of the exactly same samples as those used for the particle size analysis at respective levels. Within the sand layer, in cores 11, 9 and 7, peaks in χ_{lf}, χ_{hf} and SIRM, sometimes also in SIRM/χ_{lf}, HIRM or HIRM/χ_{lf}, occur similarly, at or *circa* 1 to 5 cm below the base of each fining upward sequence (Figures 5.43, 5.46, 5.47, 5.50 and 5.51). χ_{lf} and χ_{hf} at all boreholes vary within a relatively low and narrow value range of *circa* 0.2 to 4 $\mu m^3 kg^{-1}$. This discloses that the concentration of magnetic minerals is low in the sand layer. SIRM is roughly a measurement of the content of ferrimagnetic minerals and canted antiferromagnetic and HIRM can be understood as a measurement of antiferromagnetic content. Comparing variations in magnetic parameters and their ranges, it is considered that the magnetic mineral assemblage within the sand layer is predominantly composed of ferrimagnetic minerals, e.g. titanomagnetite (J. A. Dearing, pers. comm.). As shown in Figures 5.43, 5.46, 5.47, 5.50 and 5.51, high values of mineral magnetic parameters correspond closely to each other, and thus mark two bands of enriched

concentrations of magnetic minerals. The peaks in the magnetic parameters clearly offset the peaks in mean particle size. This marks changes in the mineral composition of the sediment. Core 5 is relatively short and does not exhibit any clear pattern (Figure 5.51). The magnetic study of the carse immediately above and below was also conducted, and values in χ_{lf}, χ_{hf}, SIRM, SIRM/, HIRM and HIRM/χ_{lf} generally rise and fall with each other. The variations are more or less haphazard and do not illustrate any particular pattern or trend.

In summary, a maximum of two fining upward sequences can be identified within the sand layer at this site, and there appears to be a general landward-fining trend in particle sizes of the sediment. Moreover, the degree of sediment sorting is highly related to the percentage of the component sand subpopulation. When the sand subpopulation is present as a high percentage, values of standard deviation and kurtosis indicate an improvement in sorting. Correlation of the particle size and mineral magnetic results shows that strong mineral magnetic signals are associated with levels of the coarsest sediment but lags exist between the peaks of particle size and mineral magnetic parameters.

5.1.2.6 Interpretation

At Creich, the lithostratigraphic and diatom assemblage evidence indicates that peat and estuarine silty clay accumulation were interrupted by deposition of a sand layer between 6960±55 and 6950±60 radiocarbon years BP (Smith, Dawson, Hickey, Firth, Brooks, Dawson and Shi, 1993), and that the sand layer rises in altitude and decreases in thickness landwards. Together with such evidence, variations in its particle size characteristic imply that the sand layer was formed during a high energy marine incursion.

The particle size analysis reveals that the sand layer is actually a mixture of size populations of particles in the sand, silt and clay range, reflected by a multimodal grain size distribution. Such a characteristic is distinctly different from that of beach sand produced by prolonged

wave action. Mineral and particle size analyses suggest that two separate fining upward sequences are present within the layer. An upward progression of particle size distribution within each fining upward sequence is reflected by a decrease in mean particle size and an associated decrease in the proportion of the sand subpopulation whilst the modal classes of the subpopulations remain relatively constant. Such a progression suggests that the source material was largely drawn from estuarine mudflats and that the sand was deposited as the result of fast settling processes, as discussed in the previous section (Chapter 4).

Similar to the site at Dounie, there is a clear association of the coarsest sediment with distinct variations of mineral magnetic parameters. The strong magnetic signals probably reflect a higher concentration of magnetic minerals, which have particular geometric dimensions and probably higher specific gravities. However, at this site the associated strong magnetic signals occur, sometimes, especially at seaward locations, below the coarsest calibre of each fining upward sequence. At such levels the sand is the least well sorted. Such a phenomenon may be explained by an initial simultaneous deposition of a high proportion of heavier mineral particles and particles in all subpopulations at relatively similar and very high flux rates, before the flux rates were differentiated due to an improved sorting process. It is believed that sediment would be very poorly sorted and represent more closely characteristics of a transported sediment in a waterbody, when the concentration of the sediment is very high. After this initial undifferentiated settling of various sized particles, the sediment concentration decreases to such a degree that the sorting process improves and starts playing an important role in forming the granulometric characteristics of the sediment. The results of particle size analysis also suggest a general fining landward trend in sediment particle size, which implies that the sand was subject to landward transportation.

In summary, it seems likely that the sand layer was transported mainly from mudflats and laid down by a high energy inundation, which had at least two large episodes of sediment deposition at *circa* 7,000 radiocarbon years BP. The marine flood could have reached at

least 2.5 m above the contemporary high water mark, as indicated by stratigraphic evidence (from the point where the highest part of the lower layer of the estuarine deposit is overlain by the sand).

5.2 Other Sites

5.2.1 Lochhouses

The site near the farm of Lochhouses, south of Dunbar, is a small area of low-lying land containing a peat moss (Figure 5.52). The depression is situated in an area of glacial deposits with stabilised sand dunes to seaward and is caused by the confluence of two dry valleys, probably formed at least partly during a periglacial climate. The adjoining coast north and south of the area is characterised by steep cliffs.

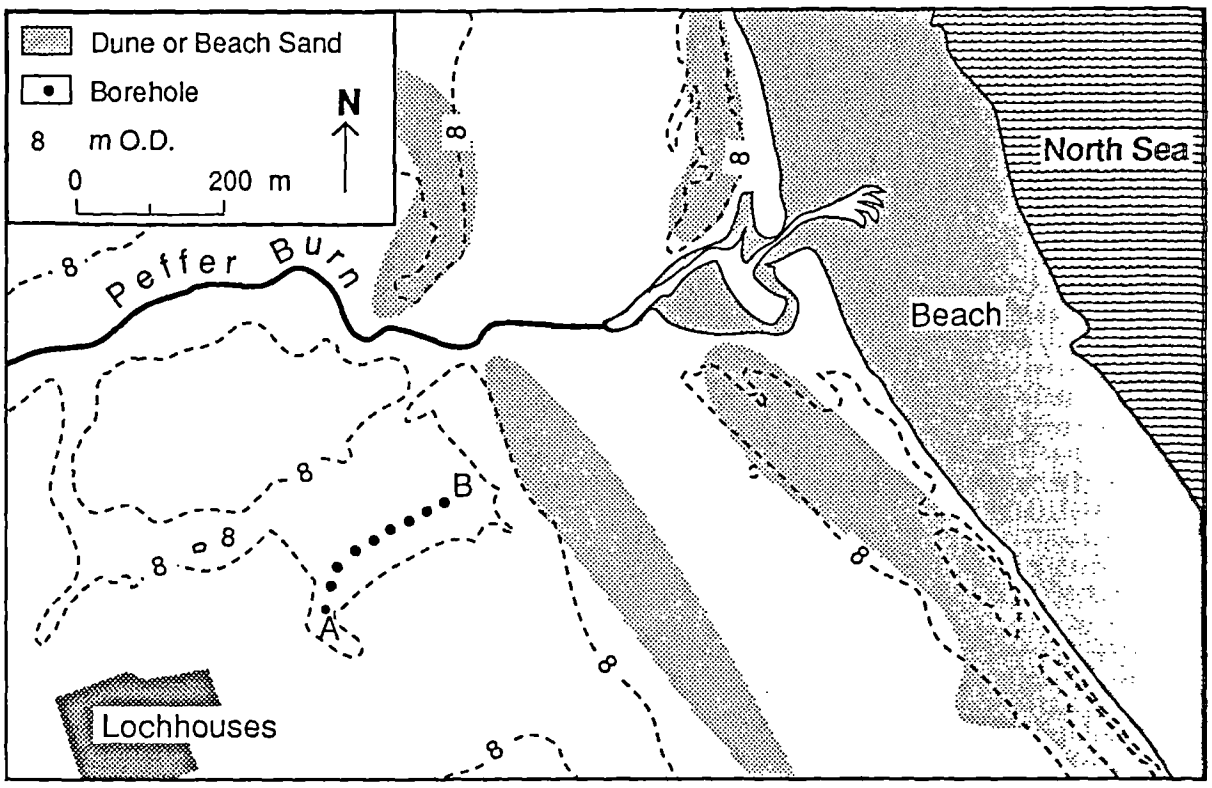

Figure 5.52. Borehole locations at the Lochhouses site. Capital letters A and B mark the ends of a traverse along which a stratigraphical cross-section is constructed as illustrated in Figure 5.53.

The previous investigations at the site revealed that the peat moss, accumulated since the middle Flandrian, is *circa* 5 m in depth at its deepest point (Newey, 1965; Robinson, 1977). Robinson (1982) carried out diatom analysis of a core from the site and identified a minerogenic layer containing marine diatoms which she dated at between 7490 ± 70 and 7450 ± 60 radiocarbon years B.P. from peat samples respectively below and above the layer.

5.2.1.1 Stratigraphy

A stratigraphical cross-section of the site has been produced from borehole records along a transect running seawards and has been generalized to focus on the minerogenic layer (Figure 5.53). Broadly speaking, upon a basal silty sand lies a layer of peat, which in turn is overlain by a layer of minerogenic deposits. The minerogenic deposits were identified from visual inspection as consisting of a lower fine sand and a upper silty clay. Upon the minerogenic layer lies peat with silt lenses, which is covered by peat with blown sand.

This study focuses on the origin of the main minerogenic layer. Four cores were obtained at boreholes AB16, AB1, AB3 and AB5 respectively, along the transect running seawards. The minerogenic layer was sliced into contiguous 1 cm-thick samples for particle size analysis. Figures 5.55, 5.57, 5.59 and 5.61 illustrate variations of particle size parameters with depth and examples of particle size distributions which represent the general clastic characteristics of each horizon at different boreholes respectively.

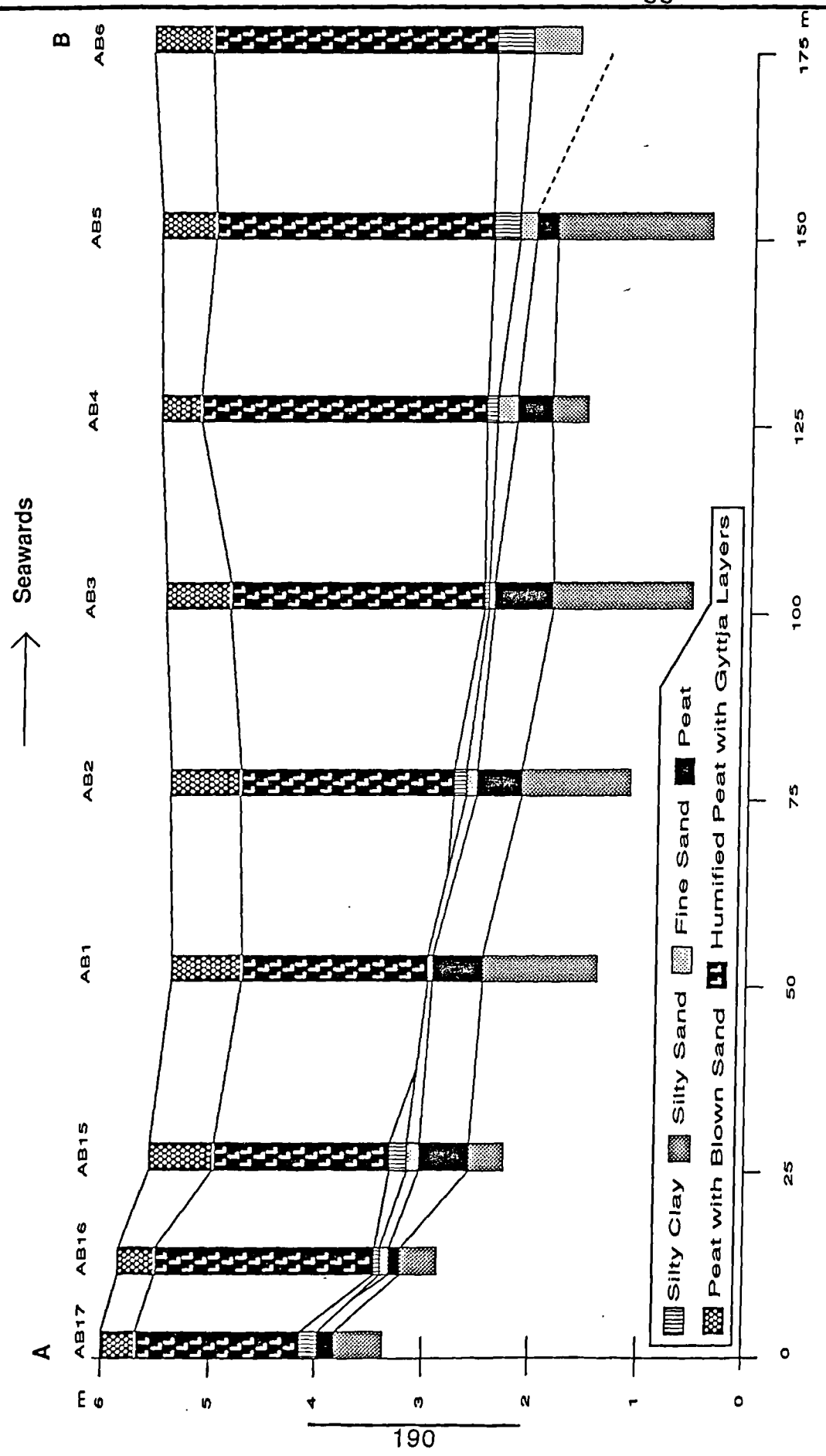

Figure 5.53. Generalized stratigraphical section at the Lochhouses site. Borehole locations are indicated in Figure 5.52.

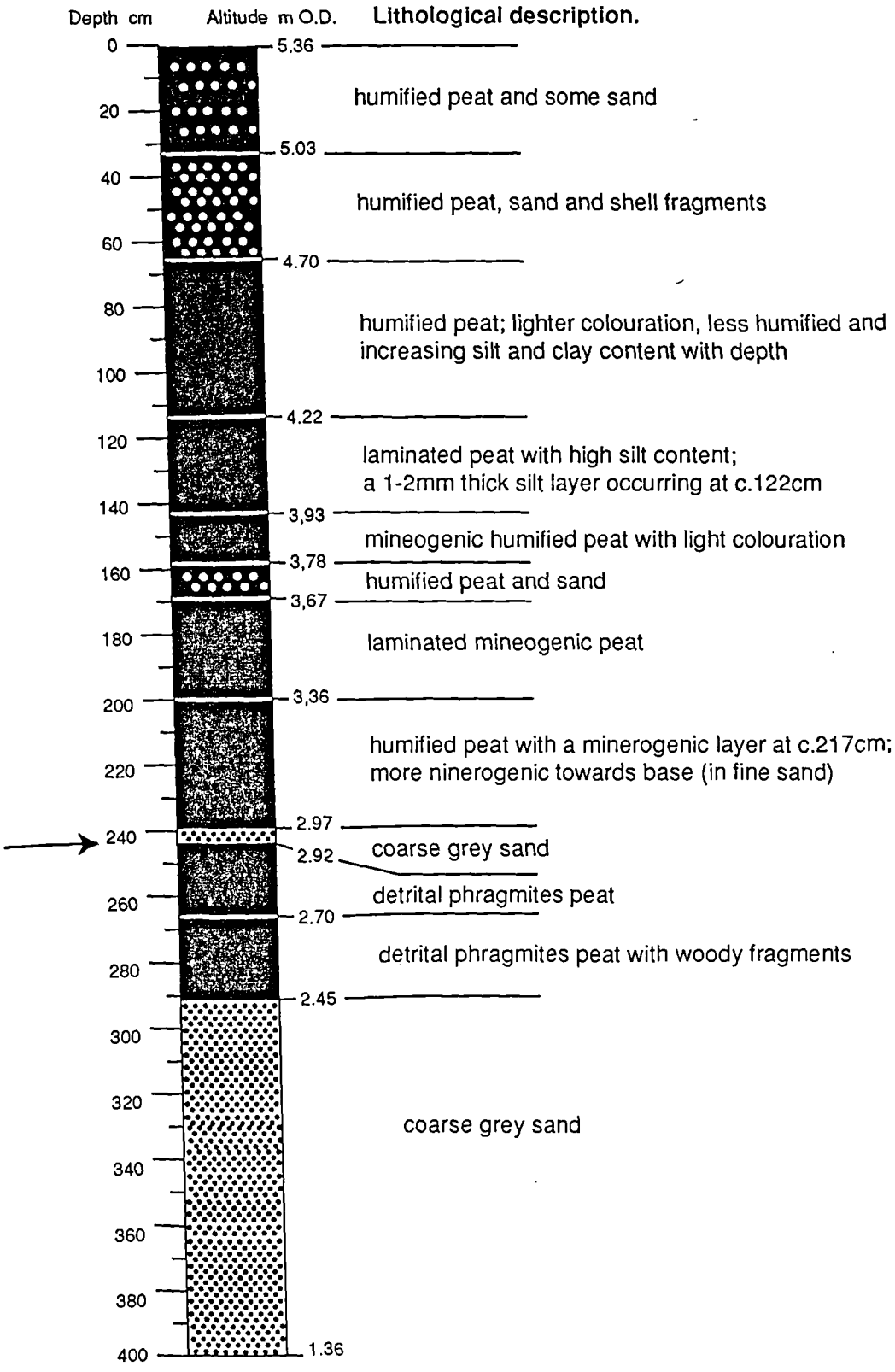

Figure 5.54. Lithostratigraphy of core AB1 at Lochhouses. The arrow marks the core section analysed.

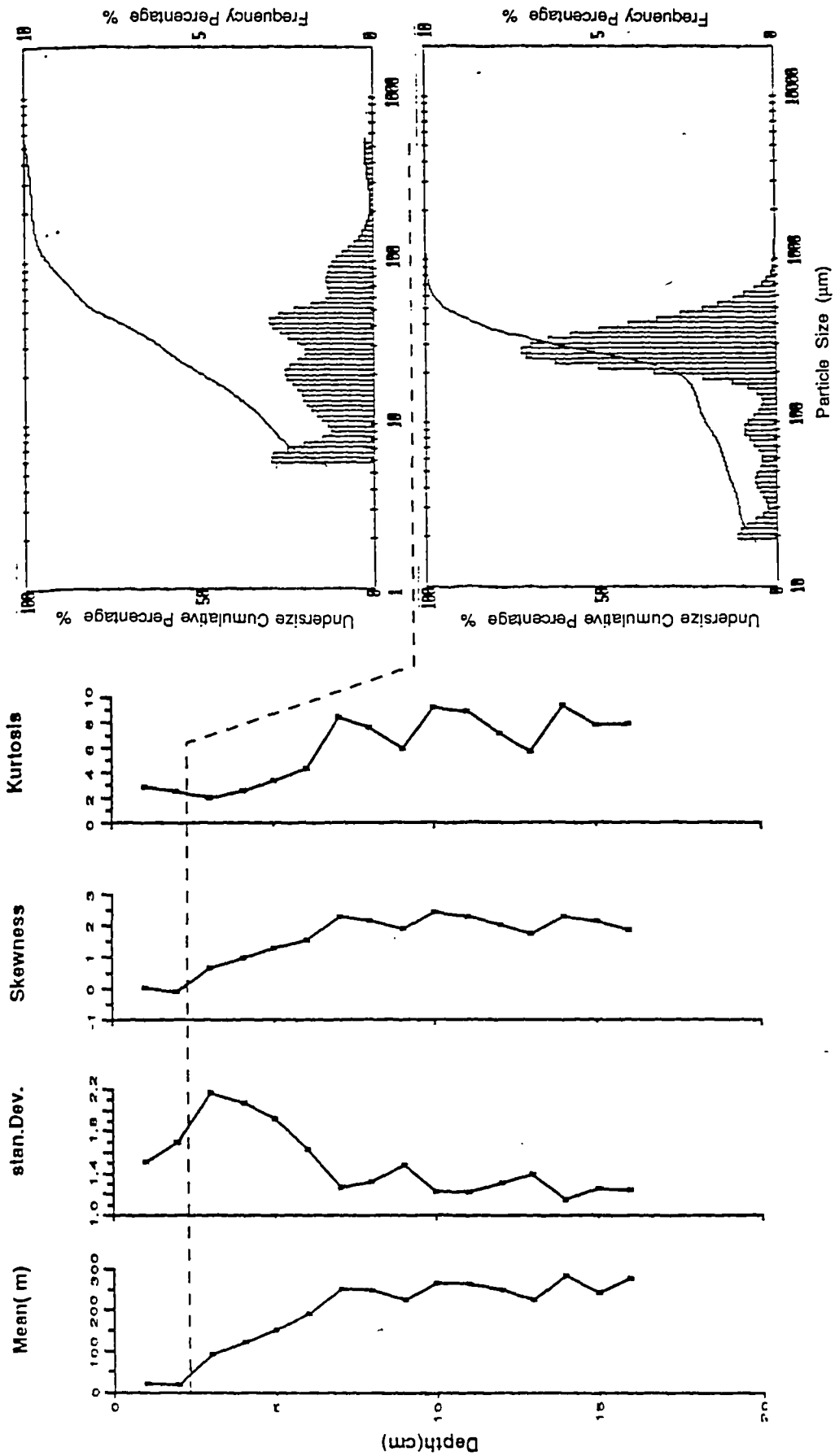

Figure 5.55. Representative particle size distributions and vertical variations in the particle size parameters at Borehole AB1, Lochhouses (Figure 5.54).

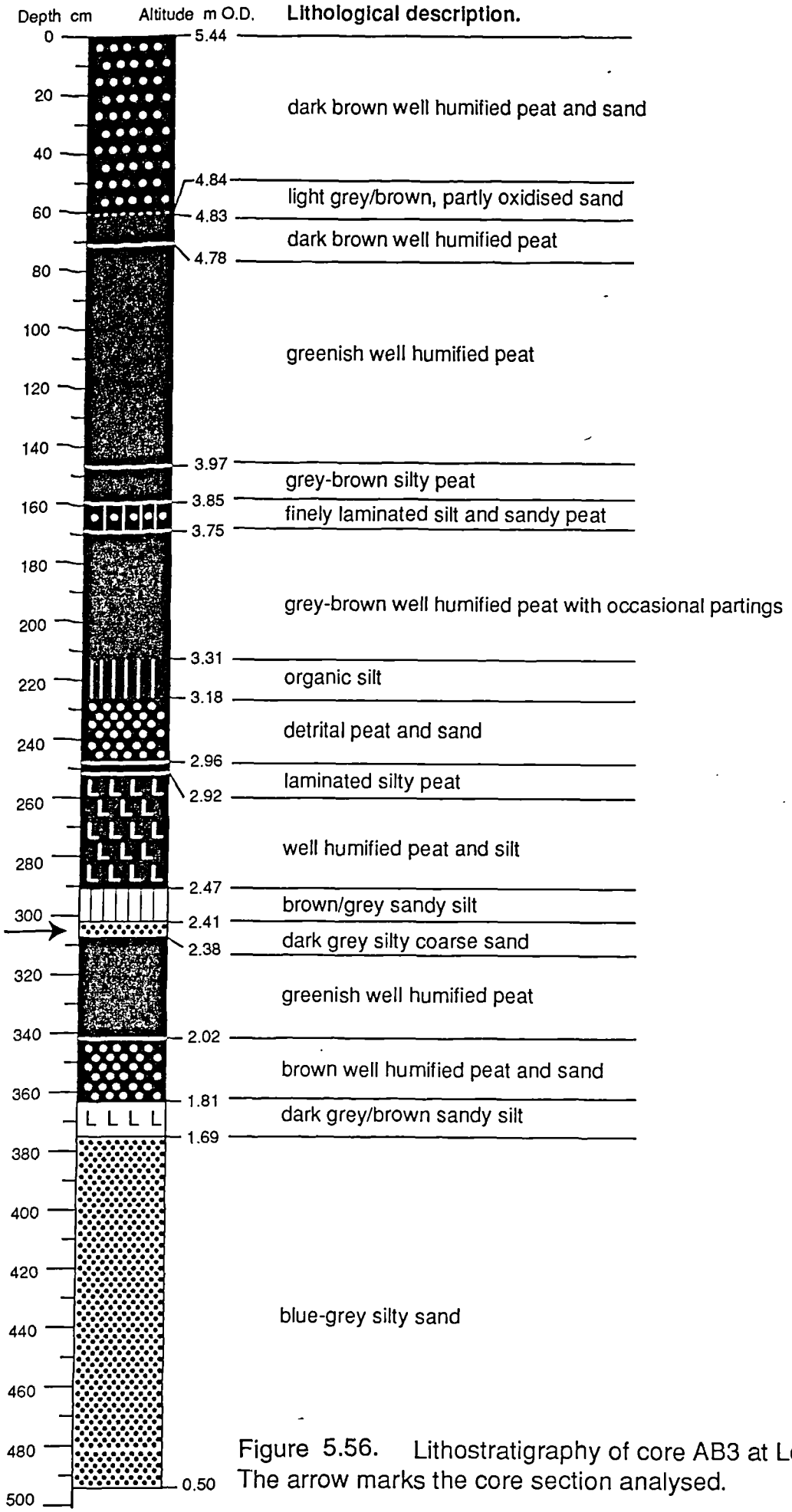

Figure 5.56. Lithostratigraphy of core AB3 at Lochhouses. The arrow marks the core section analysed.

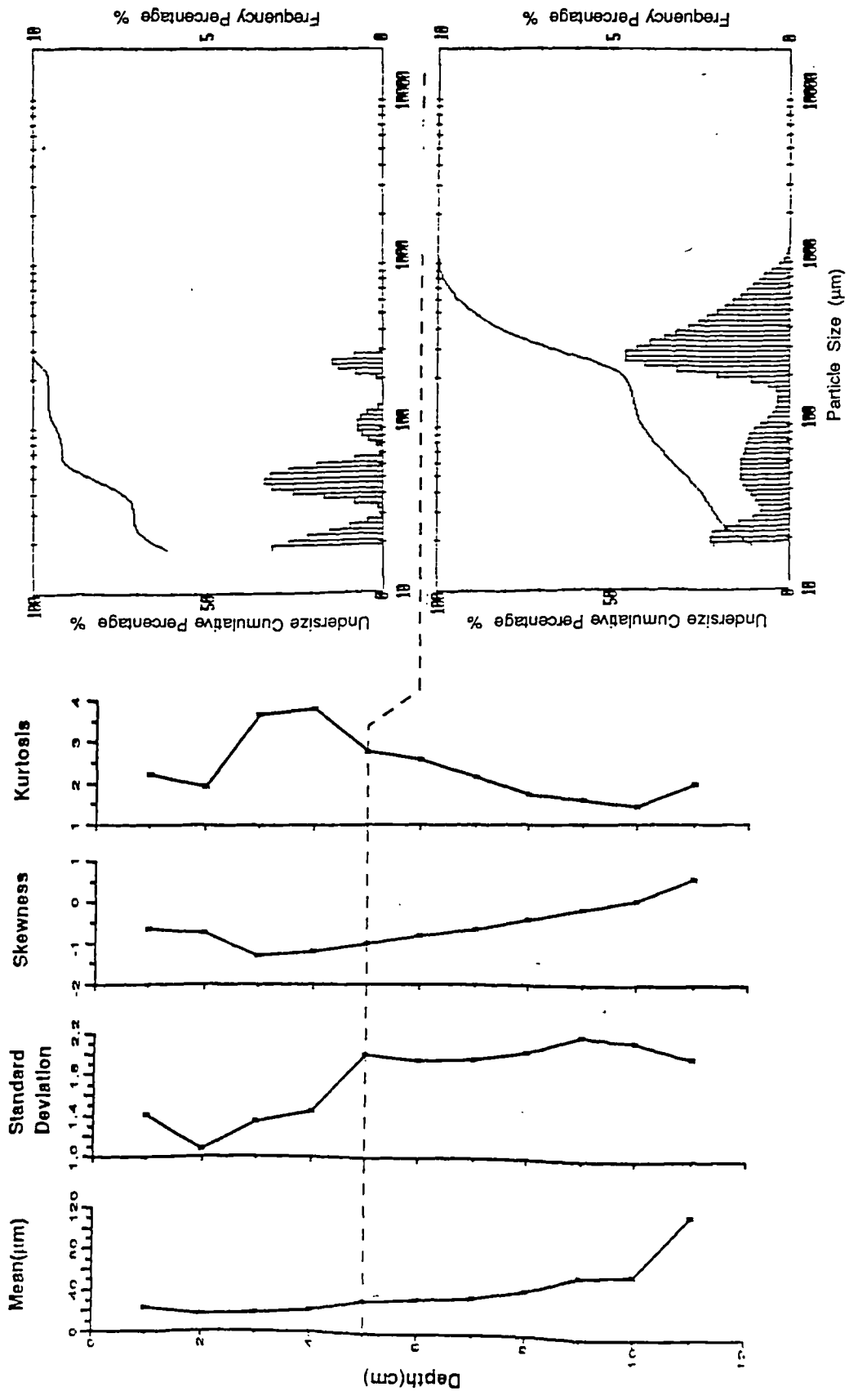

Figure 5.57. Representative particle size distributions and vertical variations in the particle size parameters at Borehole AB3, Lochhouses (Figure 5.56).

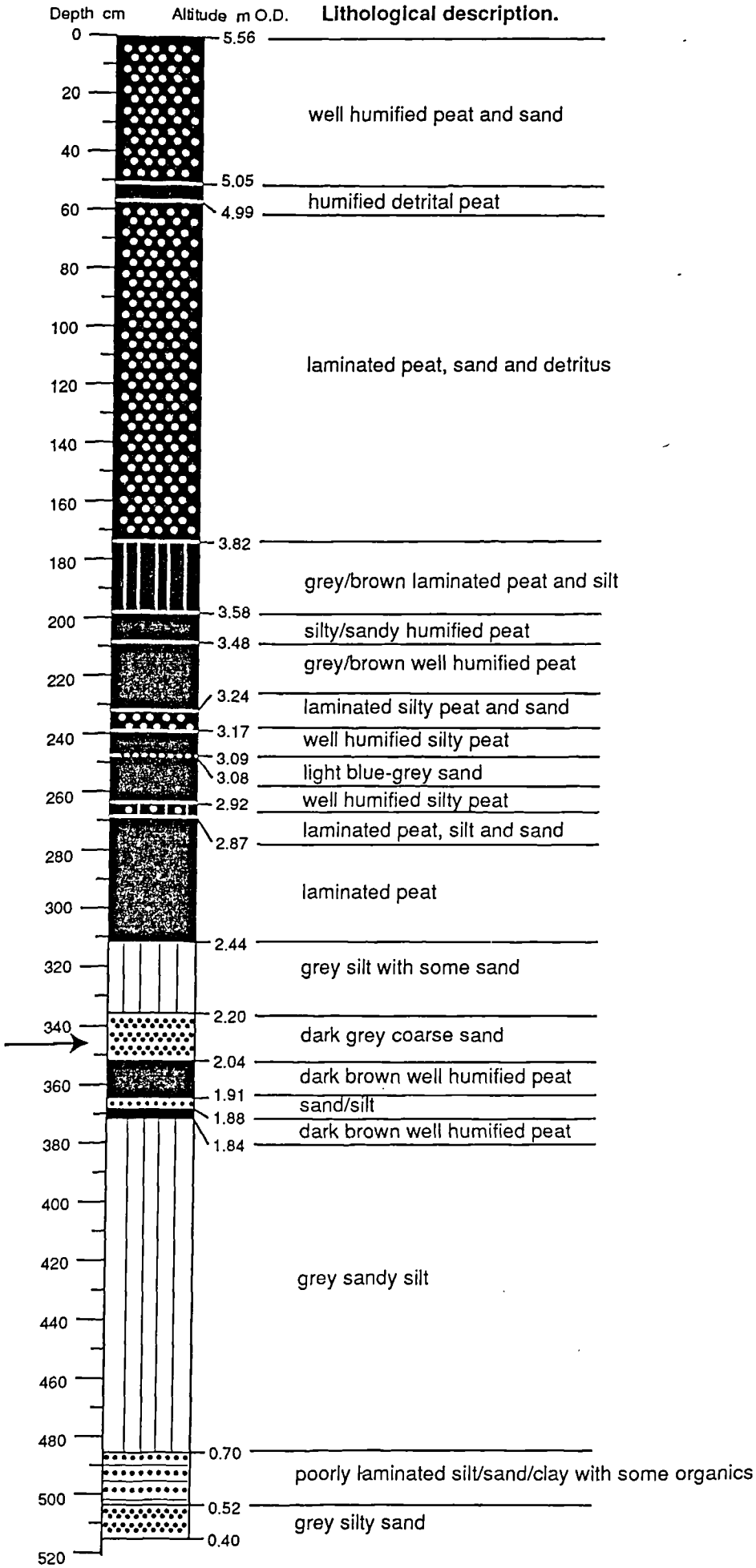

Figure 5.58. Lithostratigraphy of core AB5 at Lochhouses. The arrow marks the core section analysed.

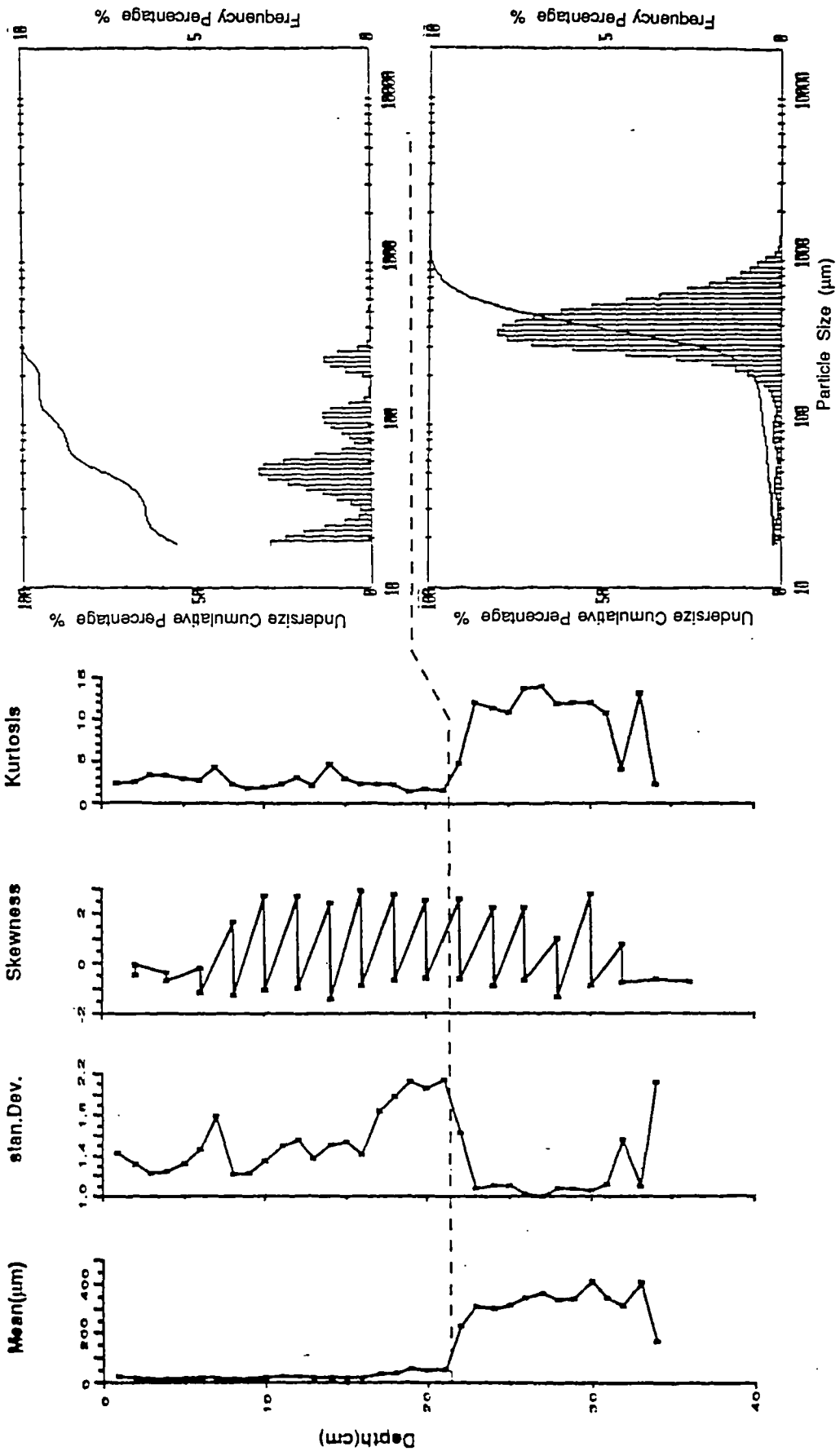

Figure 5.59. Representative particle size distributions and vertical variations in the particle size parameters at Borehole AB5, Lochhouses (Figure 5.58).

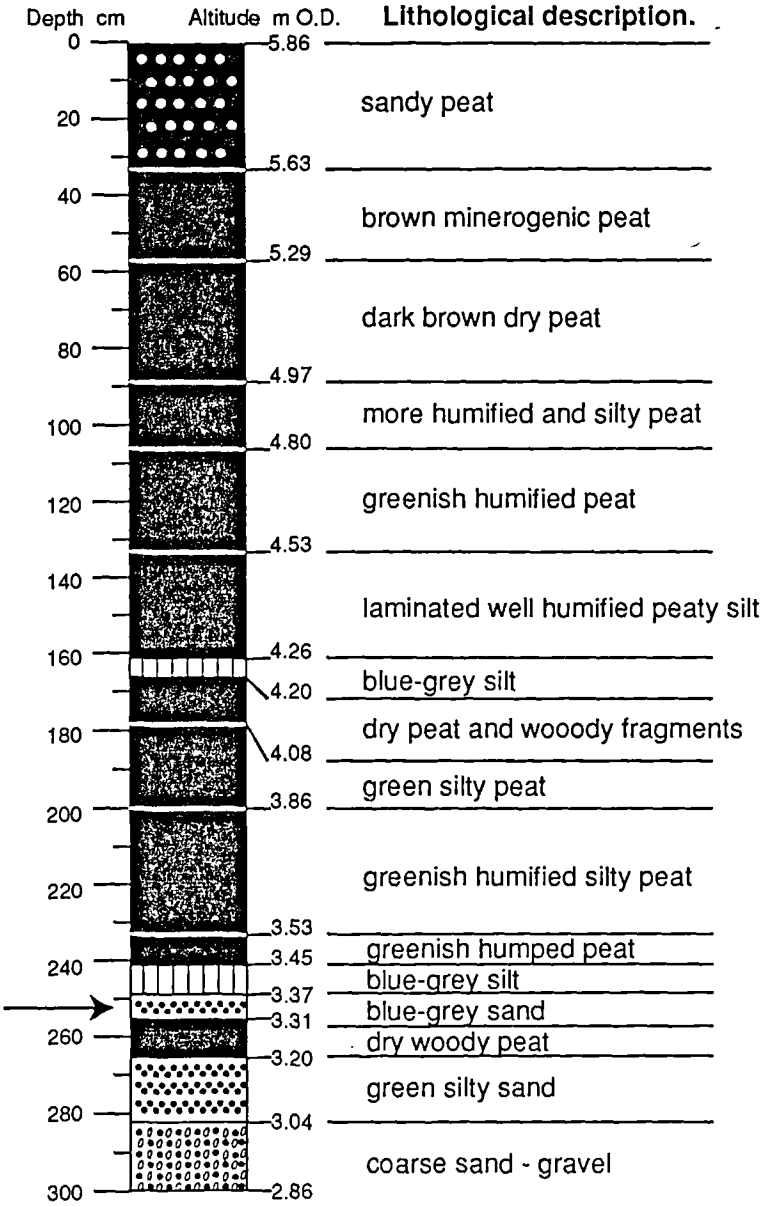

Figure 5.60. Lithostratigraphy of core AB16 at Lochhouses. The arrow marks the core section analysed.

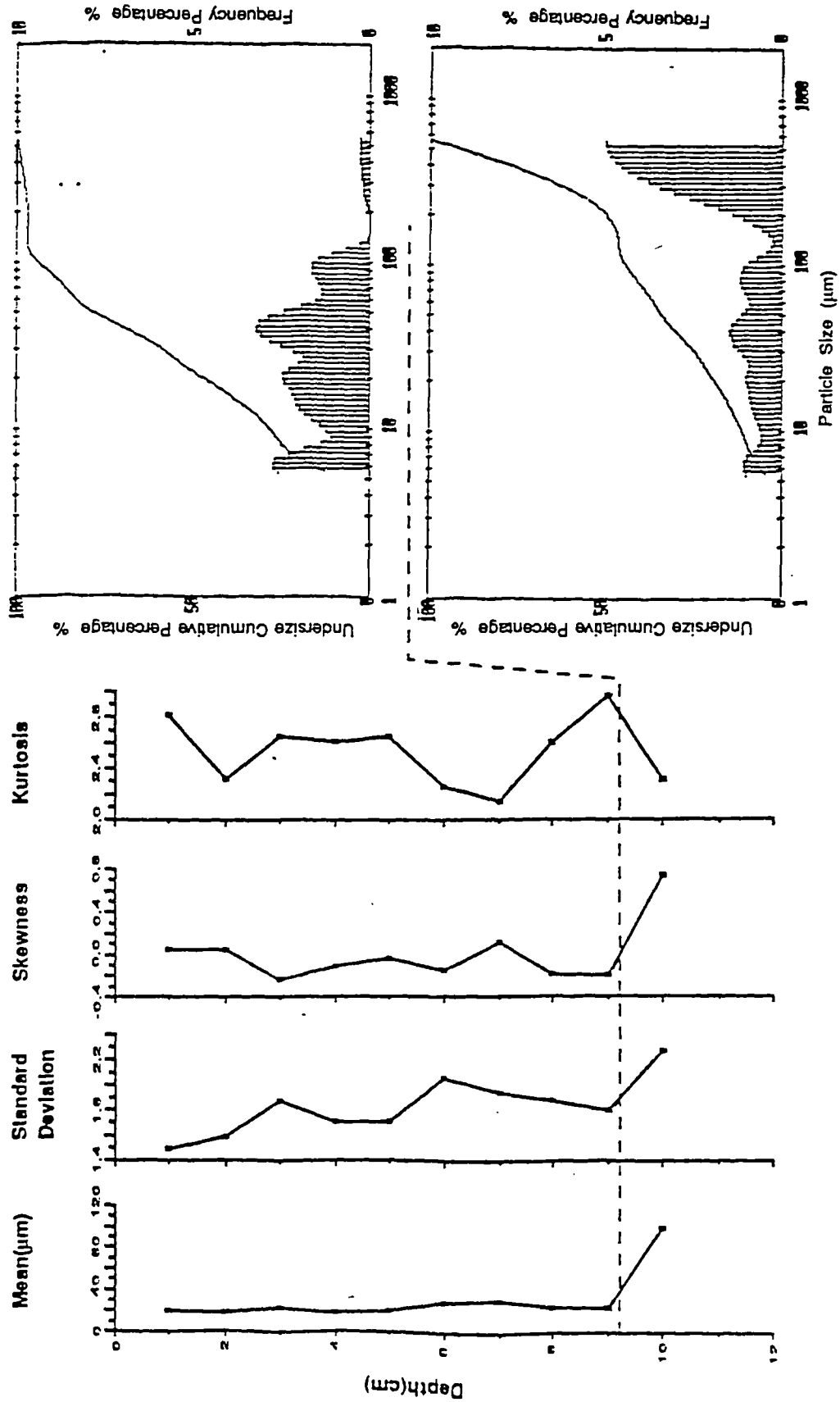

Figure 5.61. Representative particle size distributions and vertical variations in the particle size parameters at Borehole AB16, Lochhouses (Figure 5.60).

5.2.1.2 Radiocarbon Dates

Further radiocarbon dating was conducted by Smith *et al.* (1991) to date the prominent minerogenic horizons in the sequence. Given below are the dating results of 2.5 cm-thick samples of peat from below and above the relevant minerogenic layer at borehole AB4.

Sample	Lab. Number	Altitude (m O.D.)	Material	Age (^{14}C Years BP)
LH2	SRR-3912	+2.415 to +2.44	Peat above minerogenic layer	~7410*
LH1	SRR-3913	+2.015 to +2.04	Peat below minerogenic layer	7880±45

After Smith *et al.* (1991). * This approximate date is due to a laboratory error (D. D. Harkness, pers. comm.).

5.2.1.3 Diatom and Pollen Evidence

In Robinson's work (1982), 1 cm-thick samples from chosen levels were analysed, and three microfossil zones were identified (Figure 5.62). These zones do not correspond to the lithostratigraphic variations of the section. It should be however noted that in zone 2 which includes the minerogenic layer, the percentage of Oligohalobian (Freshwater and Freshwater-Brackish) diatoms is relatively low and reaches its lowest at the level of +2.44-2.45 m O.D., whilst Euhalobian, Mesohalobian-Oligohalobian and Mesohalobian species increase in proportion. Present in abundance amongst the species noted are diatoms of the benthic Euhalobian taxon *Paralia sulcata*, Euhalobian *Coscinodiscus* species, Mesohalobian *Navicula digitoradiata var. angustior tumida.*

Further preliminary diatom analysis of core AB4 in this study was kindly undertaken by Dr. B. A. Haggart. 17 samples were taken from the minerogenic layer at contiguous intervals, and the diatom assemblage revealed generally indicates a similar mixed assemblage of species from various saline regimes, from marine to freshwater. Diatoms are scarce in the lower part of the minerogenic layer, where the sediment is coarse. In the upper part, the result confirms Robinson's finding, that it contains a prominent amount of marine diatoms including *Paralia sulcata, Coscinodiscus spp., Navicula digitoradiata var. angustior.*

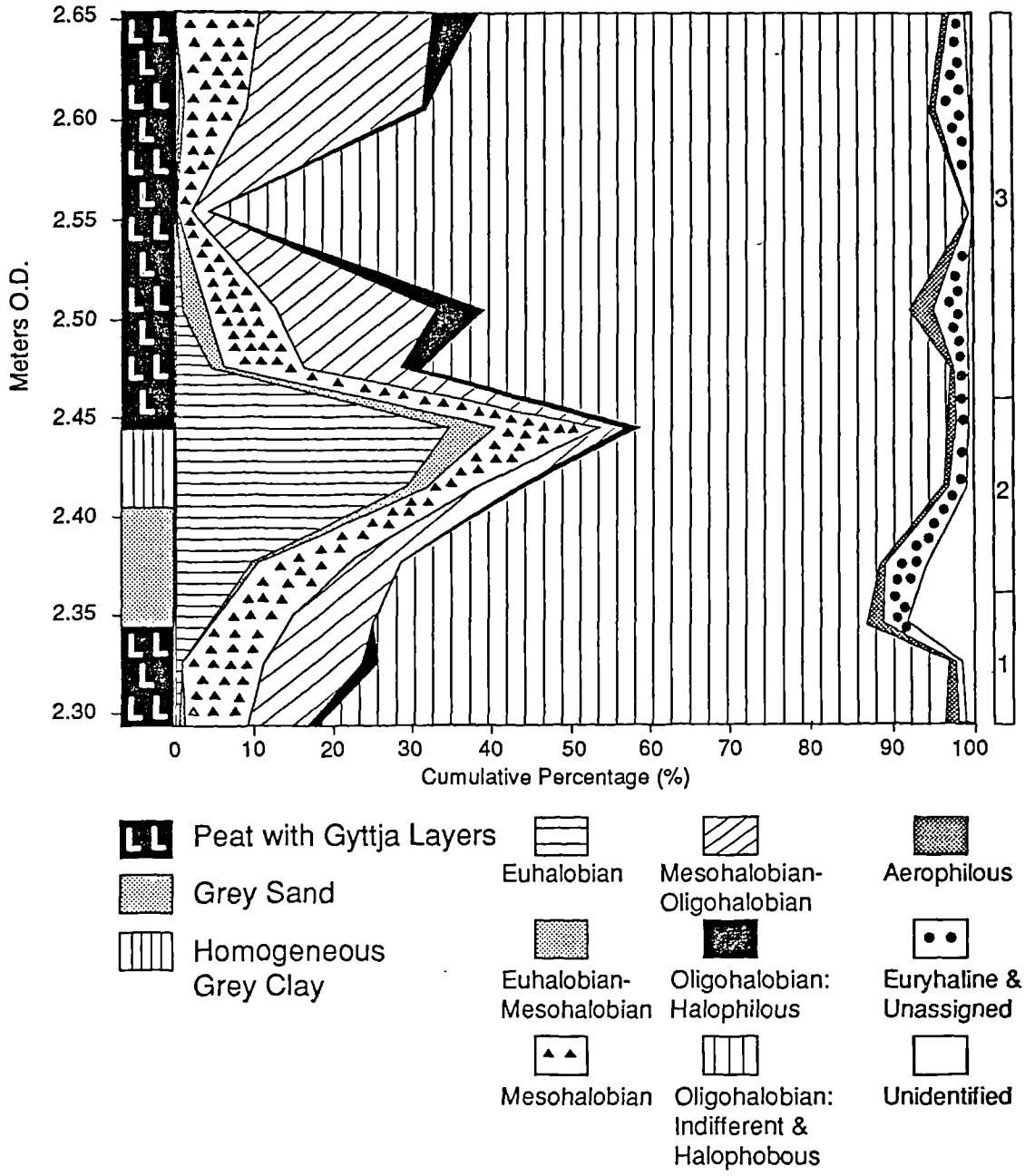

Figure 5.62. Cumulative percentage diagram of diatom assemblage at Lochhouses and generalised corresponding lithostratigraphy (modified after Robinson, 1982).

Pollen analysis (Smith *et al.*, 1990) revealed a marked enrichment in frequencies of *Chenopodiaceae* and *Plantago maritima*, during and after the deposition of the minerogenic sediment. These two pollen forms, together with relatively substantial counts of some other pollen types, are characteristic of saltmarsh plants (Smith *et al.*, 1990). This prominent difference probably implies the presence of marine influence.

5.2.1.4 Particle Size Analysis

The particle size analysis of the minerogenic layer discloses that the layer can be distinguished into two distinctively different horizons: 1) a lower horizon of fine sand and 2) an upper horizon of silt and clay (Figures 5.55, 5.57, 5.59 and 5.61). The grain size characteristics of the sand layer are predominantly of a near uni-modal size distribution of a sand subpopulation and containing subpopulations in small proportion in the size range of less than *circa* 100 μm. The sand layer at the boreholes AB16 and AB3 is too thin to display any clear upward trend in particle size. However, in boreholes AB1 and AB5, a general fining upward sequence can be identified and it is accompanied by a general decrease in proportion of the sand population whilst the modal classes of the subpopulations in the finer size range remain relatively constant. Comparison of mean particle sizes of the sand layer between these two boreholes indicates that the sand becomes finer landwards. The silt-clay layer is composed of size subpopulations mainly in the silt and clay size range, and also subpopulations in the sand range which are only present in small proportions. Peaks of subpopulations can be readily identified and their modal classes remain relatively constant on the size scale. The silt-clay layer is only 2 cm in thickness in borehole AB1. In the other three boreholes, a general fining upward sequence can be observed, but there are no clear lateral variations in particle size between them. This fining upward sequence is accompanied by a decrease in proportion of the sand subpopulation and conversely a increase in the silt and clay subpopulations.

5.2.1.5 Interpretation

The lithostratigraphic and diatom and pollen assemblage evidence indicates that peat accumulation was interrupted by deposition of a minerogenic layer, between 7880±45 and ~7410 radiocarbon years BP (Smith *et al.*, 1993), which rises in altitude landwards. It also implies that the minerogenic layer was formed under marine influence, which could have been brought about by two hypothetical possibilities: a gradually and steadily rising sea level, or a short-lived impulsive marine incursion.

The particle size analysis reveals that the minerogenic sediment is of multimodal grain size distribution. The sediment contains prominent and constant silt and clay subpopulations in addition to the largest sand subpopulation, which are consistently absent in beach sand due to prolonged wave-washing. The upward fining in mean particle size and the accompanying decrease in proportion of the sand subpopulation suggests the clastic particles settled out of a waterbody simultaneously but flux rates of different sized particles were different. The flux rates were seemingly related to the geometric dimensions of particles and the concentrations of specific size groups in the transporting waterbody. Firstly, when the current was rapidly losing its energy, coarse particles had a higher flux rate. Thereafter, while the coarse particles grew to be depleted and the concentration of fine particles became relatively high, a higher percentage of fine particles were being deposited with coarse ones together. By this time, the current probably had lost most of its energy, and thus lost its capacity of carrying sediment. It is maintained here that this type of particle settling is associated with rapid depositional processes.

The presence of a large percentage of marine diatoms, especially a dominating high proportion of two tychopelagic taxa (*Fragilaria pinnata* and *Paralia sulcata*) in the minerogenic layer, strongly suggests that a large amount of clastic material was drawn from mudflats. *Fragilaria* species are benthic on mudflats and Paralia sulcata is known as a

benthic species in neritic environments. Moreover, oceanic planktonic taxa such as the *Coscinodiscus* species and *Chaetoceros* species are never abundant at this site (Robinson, 1982). Certain brackish taxa such as *Achnanthes hauckiana*, *Navicula peregrina* and *Amphora commutata* are also present in the minerogenic layer, probably indicating that the coastal lowlands were subject to erosion by the marine inundation.

The scarcity of diatoms in the lower and coarse part of the minerogenic layer and the abundance in the upper and fine part, are perhaps related to the sedimentation process. Diatoms are of small sizes relative to minerogenic sediment, and probably few were deposited with coarse sediment at the beginning of deposition, but settled out in large numbers with silt and clay at the end.

It seems likely that the minerogenic sediment was transported mainly from mudflats and laid down by marine inundation, and that only one major episode of deposition can be inferred from the sedimentary record at this site. However, the radiocarbon dates obtained are significantly older than those for a similar layer at other sites, where dates of *circa* 7,000 years BP have generally been obtained for similar horizons. Discussion of this is given at the end of this chapter (Section 6).

5.2.2 The Montrose Area

5.2.2.1 Stratigraphy and radiocarbon dates

The Montrose basin is a large estuarine embayment at the mouth of the river South Esk. The basin is surrounded to landward by Flandrian (Holocene) and Late Devensian deposits, and almost enclosed to seaward by a broad southward-trending spit on which the town of Montrose is situated. Stratigraphical investigations in the raised Flandrian estuarine deposits have been carried out at sites at Puggieston, Maryton and Fullerton by Smith *et al.*, (1980)

and by Smith *et al.* (1985) (Figure 4.47). At these sites, a basal laminated clay of late Devensian age rests upon till or sands and gravels, whilst above the laminated clay lies peat, in turn overlain by the raised estuarine deposits. The latter taper out into the peat at the valley sides and in gullies. Spreading through both the raised estuarine deposits to seaward and peat to landward, lies a prominent sand layer up to 30 cm in thickness (Figure 4.49). ^{14}C dates from 2 cm-thick samples of peat from directly below and above the sand layer are 7140 ± 120 and 6880 ± 110 (at Fullerton) and 7120 ± 75 and 6850 ± 75 (at Puggieston) years BP respectively. At Maryton, the sand layer was radiometrically dated as having been deposited after 7340 ± 75 (Morrison *et al.*, 1980). The culmination of deposition of the raised estuarine deposits has been dated at between 7086 ± 50 and 6704 ± 55 radiocarbon years, BP (at Fullerton) (Smith *et al.*, 1980).

Sample	Lab. Number	Altitude (m O.D.)	Material	Age (^{14}C Years BP)
Fullerton	Birm-867	+5.52 to 5.50	Peat above grey micaceous silty fine sand	6880 ± 110 (1)
Fullerton	Birm-823	+5.32 to 5.30	Peat below grey micaceous silty fine sand	7140 ± 120 (1)
Puggieston	SRR-2119	+4.90 to 4.88	Peat above grey micaceous silty fine sand	6850 ± 75 (2)
Puggieston	SRR-2120	+4.73 to 4.71	Peat below grey micaceous silty fine sand	7120 ± 75 (2)

Sources: (1) Smith *et al.*, 1980; (2) Smith *et al.*, 1985.

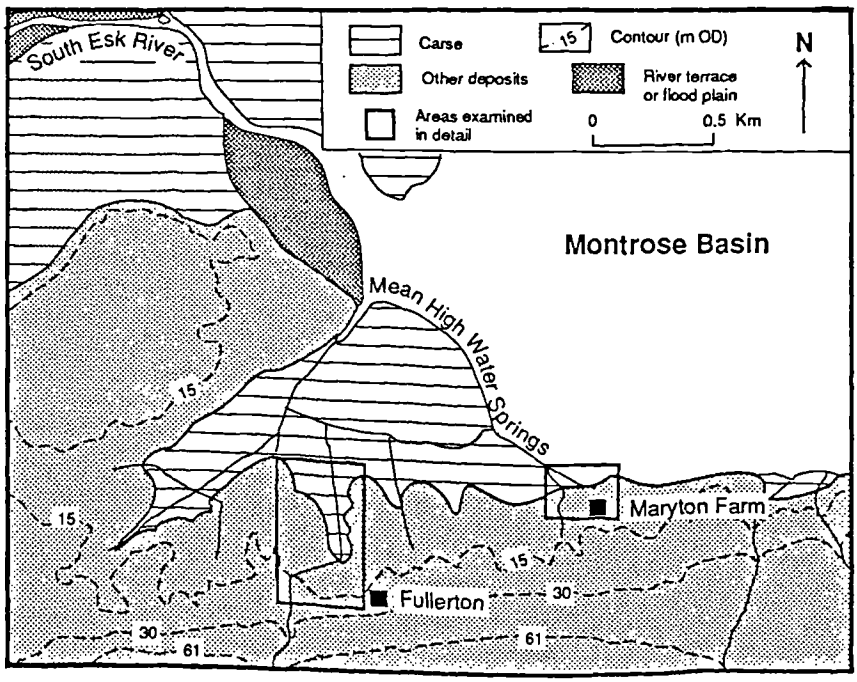

Figure 5.63. Location and morphologic map of the study area at Montrose Basin (after Smith et al, 1980)

5.2.2.2 Particle Size Analysis

In this study, further work has been undertaken on the sand layer at Maryton and Fullerton (Figure 5.63). One monolith section was taken at Maryton (Figure 5.63) and six cores using a Russian-type peat sampler along a 120 m transect running seawards at Fullerton (Figure 5.64). Cores at boreholes 2 and 3 were chosen for x-ray photography at the British Geological Survey, Edinburgh, but examination of the photos did not reveal any particular pattern and variation within the sand layer. The sand layer was sliced into contiguous samples at *circa* 1 cm intervals, for particle size analysis, apart from the two most landward cores as they are too thin to be analysed for vertical trend. The results of particle size analysis are illustrated in Figures 5.67, 5.69, 5.71, 5.73 and 5.75, in the form of an upward progression of histograms for each borehole.

At both sites, the apparently sandy sediment is composed of fine sand, silt and clay-sized particles. However, the histograms reveal interesting detail. At Fullerton, most levels in the four boreholes disclose a bimodal particle size distribution. Two distinct groups of levels in the sequences can be identified, corresponding to the lower and upper parts of the boreholes. Each group is marked by a progressively fining upward sequence. Such progressions are in two different forms: 1) the bimodal peaks occur in progressively finer size ranges as depth decreases; 2) The subpopulation in the coarse size range decreases in proportion upwards through the cores (eg. boreholes 1-3). Sometimes, the two effects take place jointly. In borehole 4 there is no apparent trend in the upper part, but mean particle size displays a fining upward sequence. At Maryton, again two fining upward sequences can be identified, corresponding to the lower and upper parts of the monolith. Here, the modal peak occurs in progressively finer size ranges upwards through each sequence (Figure 5.67).

At Fullerton, the upper sequence in boreholes 1, 2 and 3 is generally coarser than the lower, but at Maryton and at borehole 1 at Fullerton there is little difference between the two

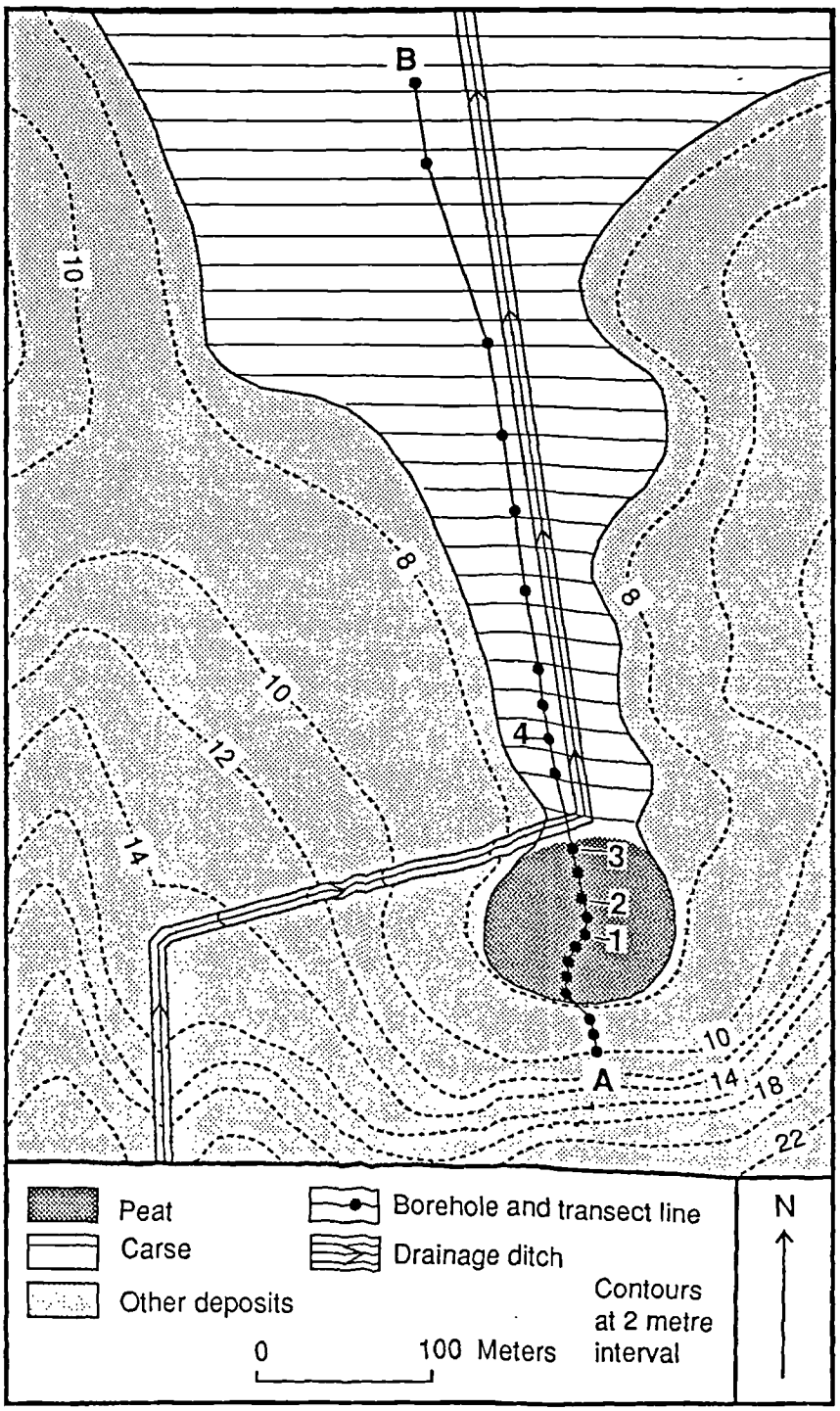

Figure 5.64. Borehole Locations at the Fullerton Gully
(Smith, D. E., Morrison, J., Jones, R. L. and Cullingford, R. A., 1980)

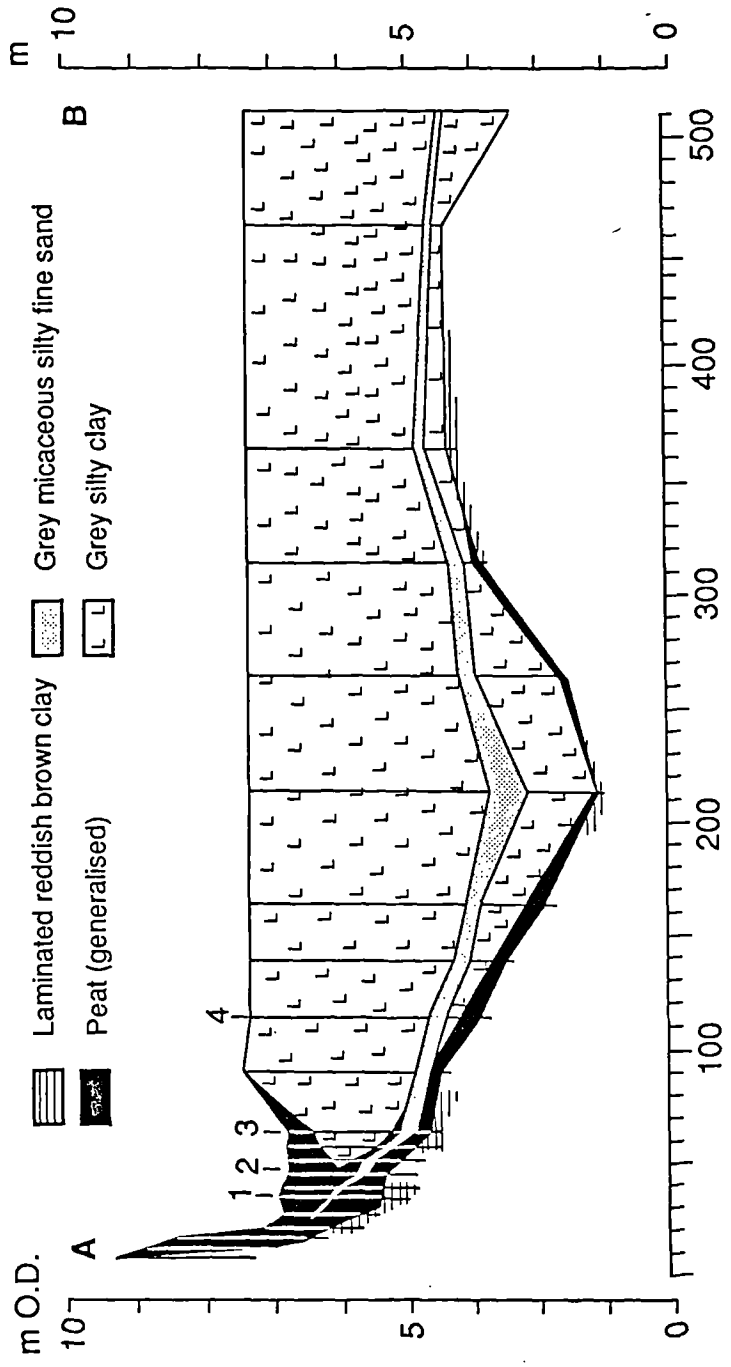

Figure 5.65. Stratigraphical section through the deposits at Fullerton.

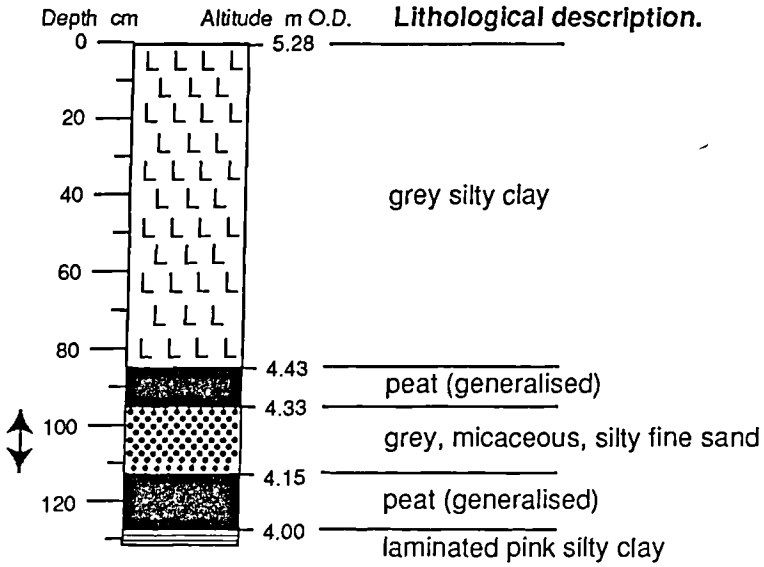

Figure 5.66. Lithostratigraphy of a monolith tin at Maryton. The arrows mark the core section analysed.

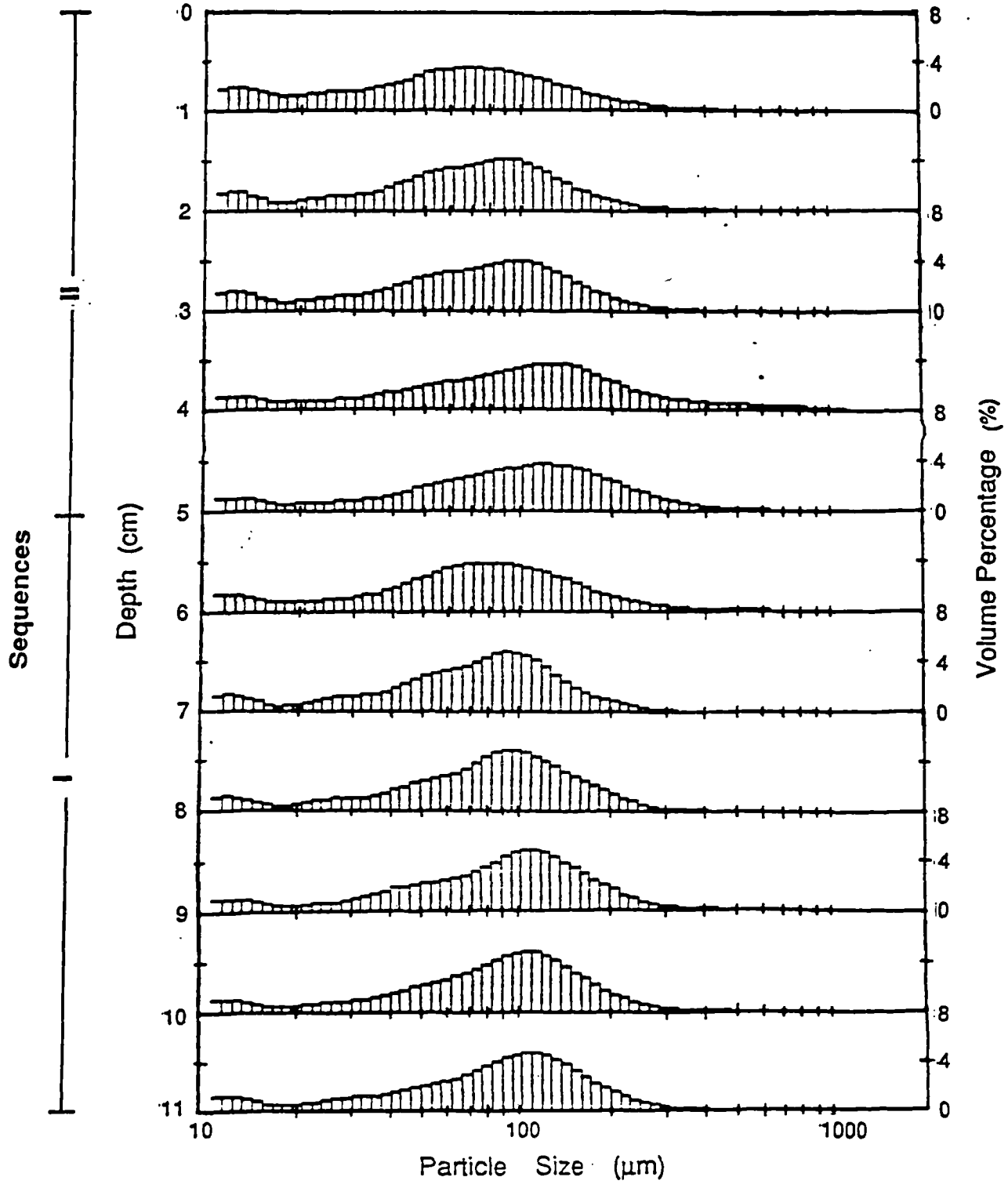

Figure 5.67. Upcore progression in the particle size histograms of the sand sediment at Maryton, Montrose Basin. Two fining-upward sequences (I and II) can be identified (Figure 5.66).

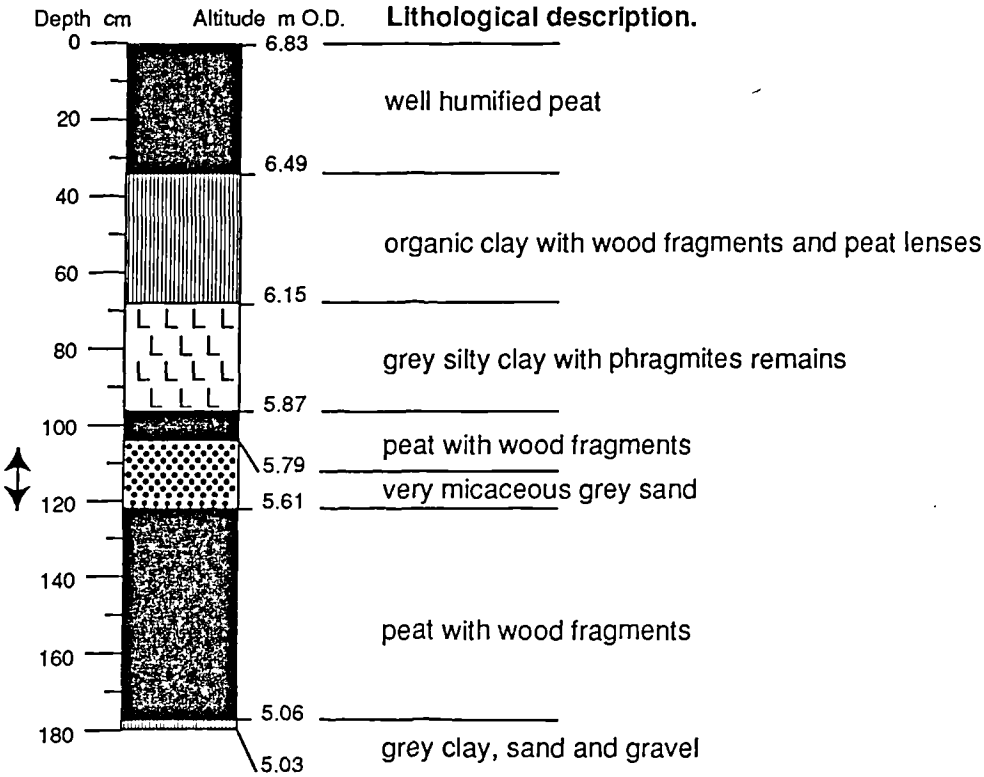

Figure 5.68. Lithostratigraphy of core 1 at Fullerton.
The arrows mark the core section analysed.

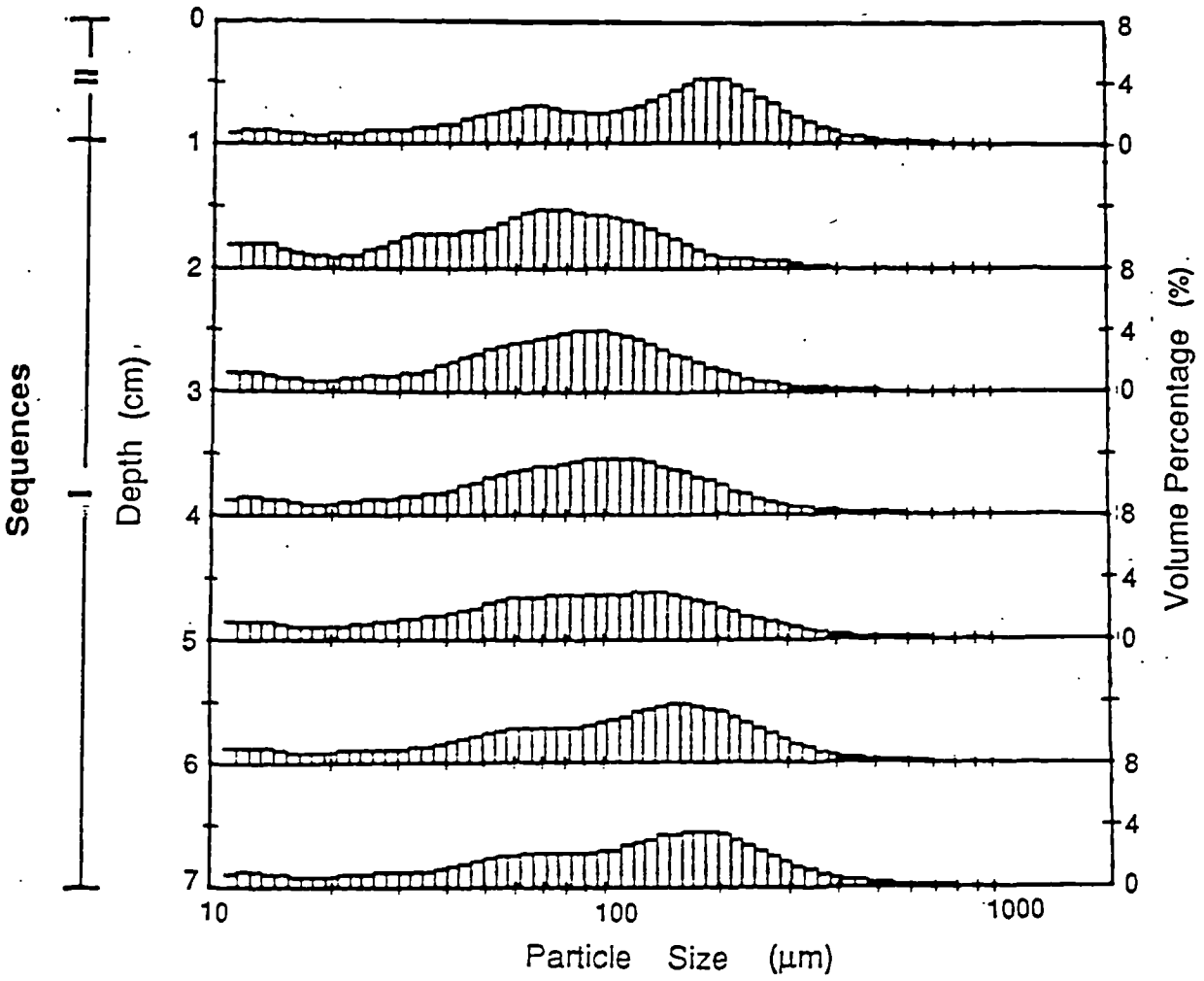

Figure 5.69. Upcore progression in the particle size histograms of the sand sediment at Borehole 1, Fullerton. One fining-upward sequence (I) can be identified and the uppermost part of the sediment marks a distinctively separate sequence (II) (Figure 5.68).

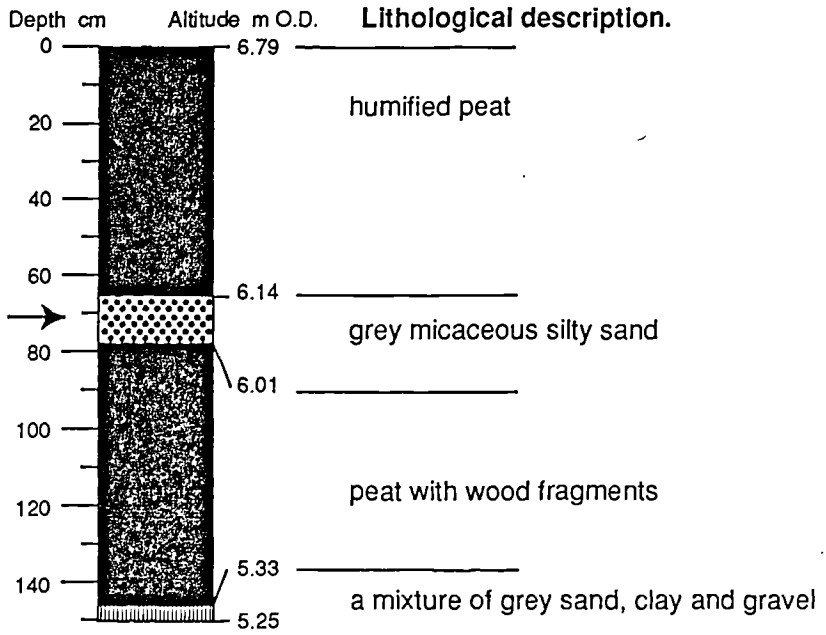

Figure 5.70. Lithostratigraphy of core 2 at Fullerton. The arrow marks the core section analysed.

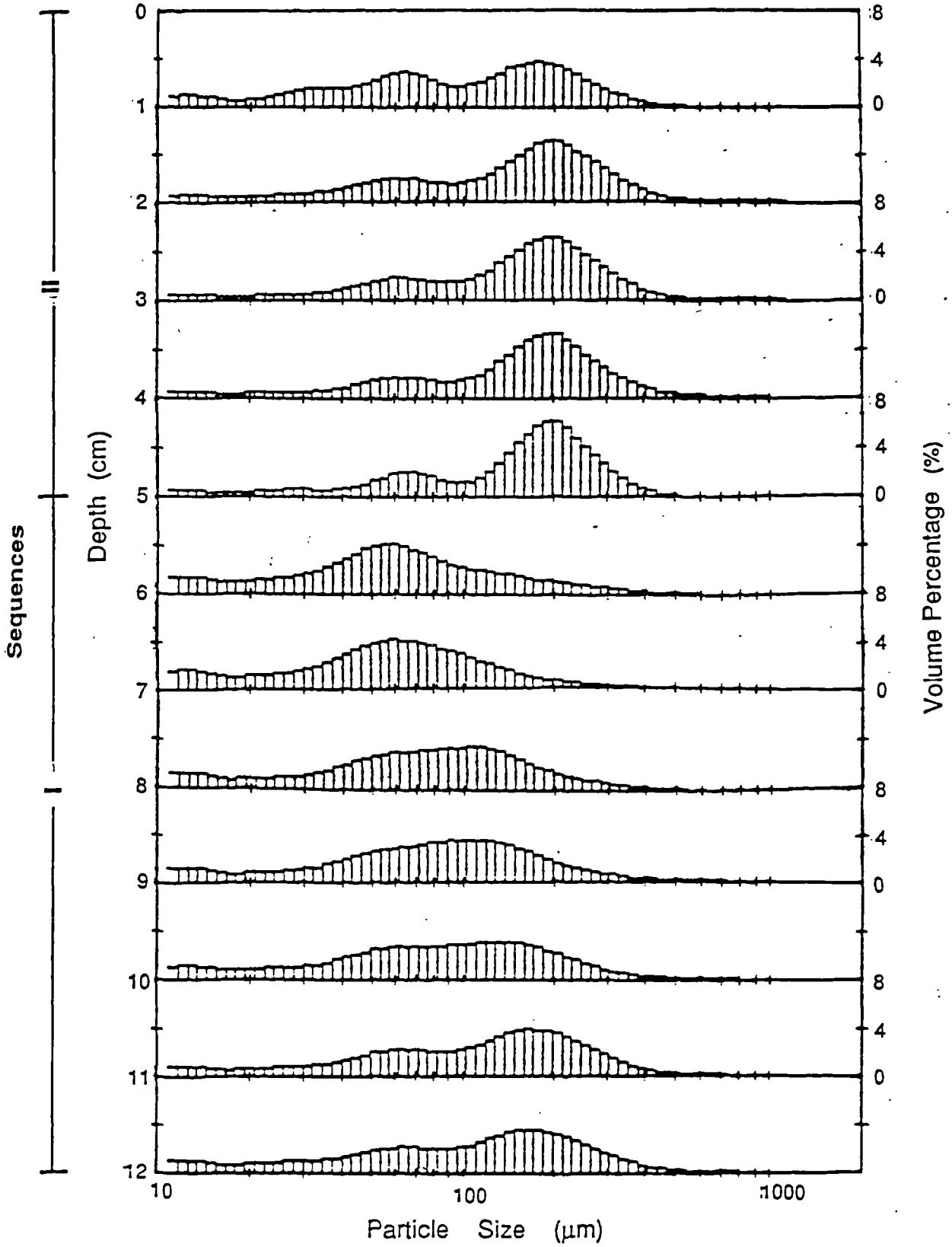

Figure 5.71. Upcore progression in the particle size histograms of the sand sediment at Borehole 2, Fullerton. Two separate sequences (I and II) can be identified. Sequence I displays distinctive fining-upward variations whilst Sequence II exhibits slight fining-upward changes (Figure 5.70).

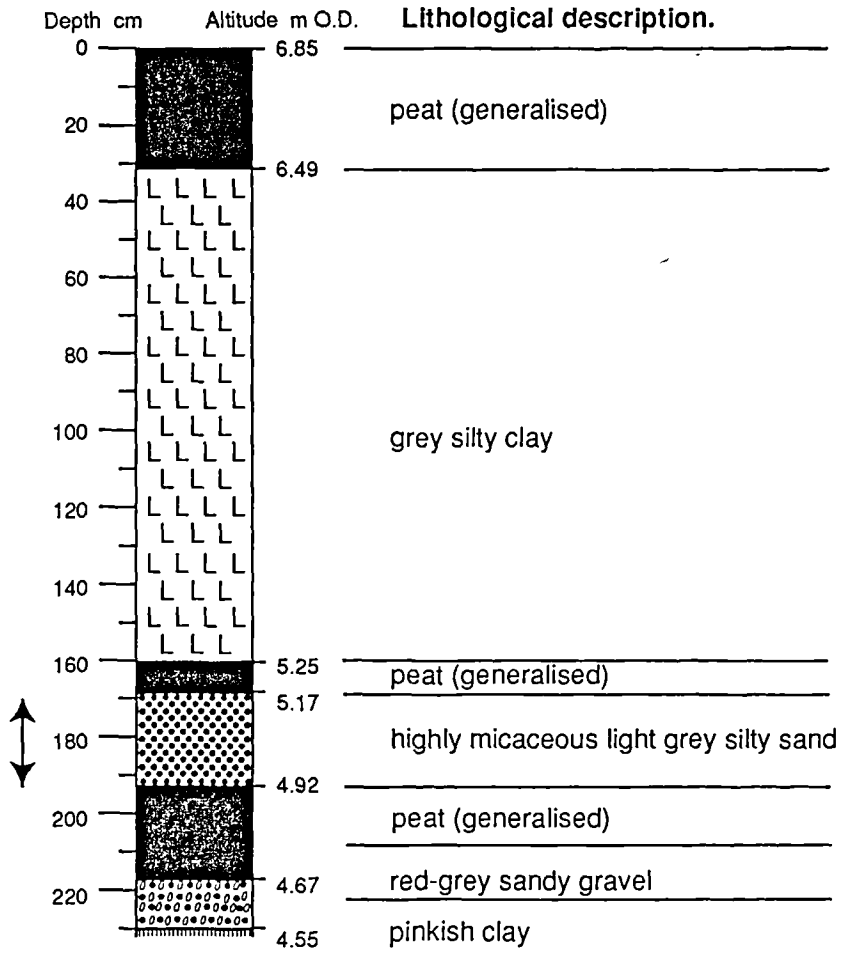

Figure 5.72. Lithostratigraphy of core 3 at Fullerton. The arrows mark the core section analysed.

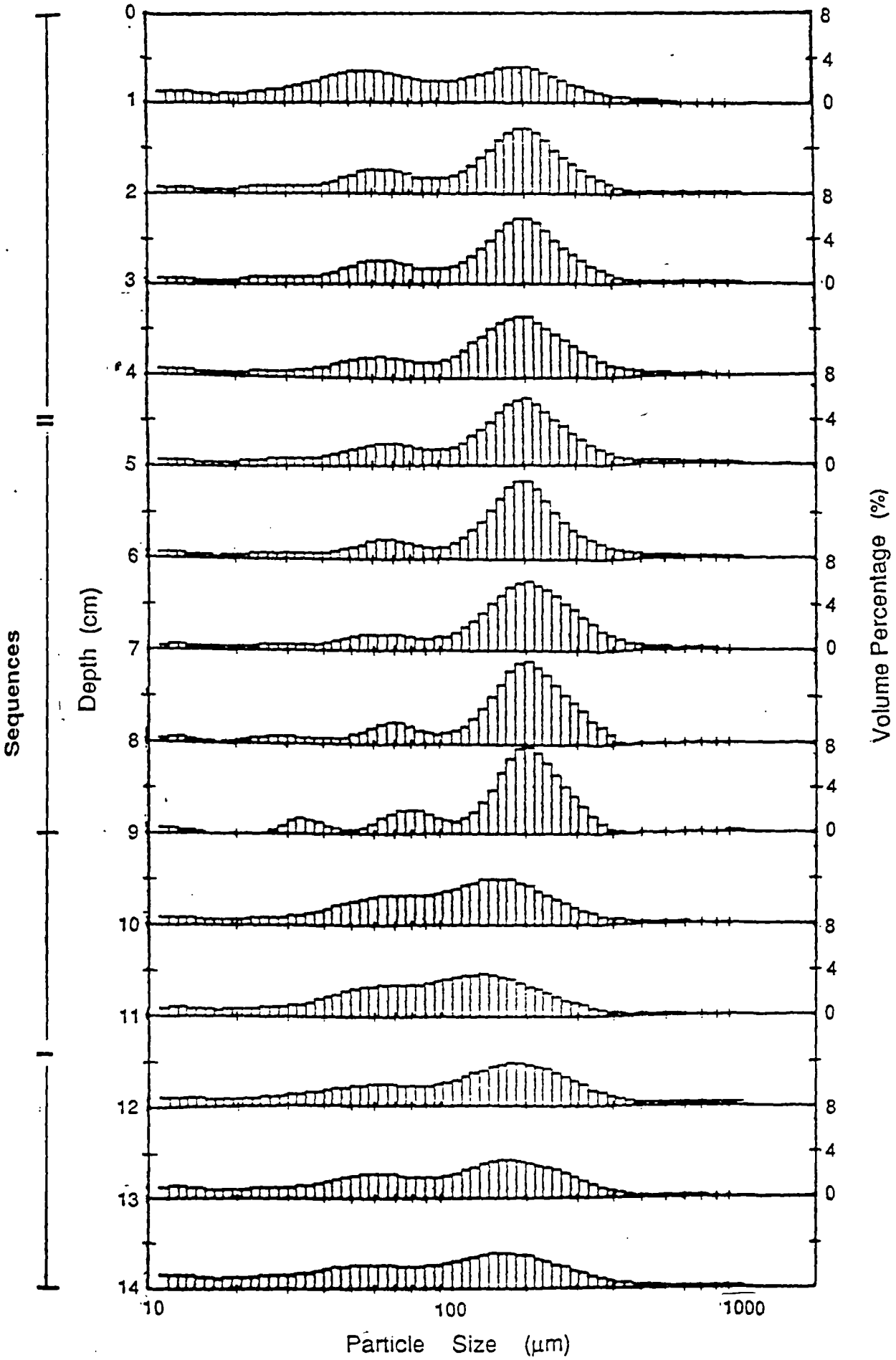

Figure 5.73. Upcore progression in the particle size histograms of the sand sediment at Borehole 3, Fullerton. Two separate sequences (I and II) can be identified. Sequence I displays distinctive fining-upward variations whilst Sequence II exhibits slight fining-upward changes (Figure 5.72).

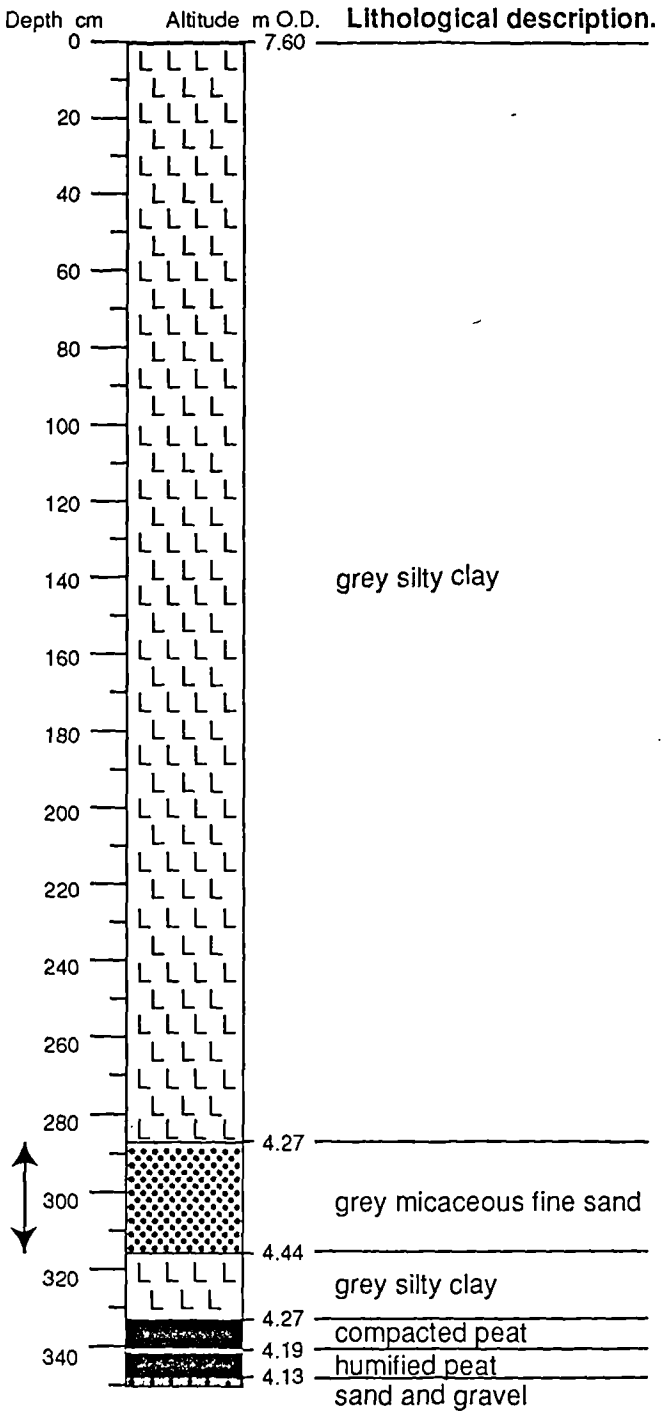

Figure 5.74. Lithostratigraphy of core 4 at Fullerton. The arrows mark the core section analysed.

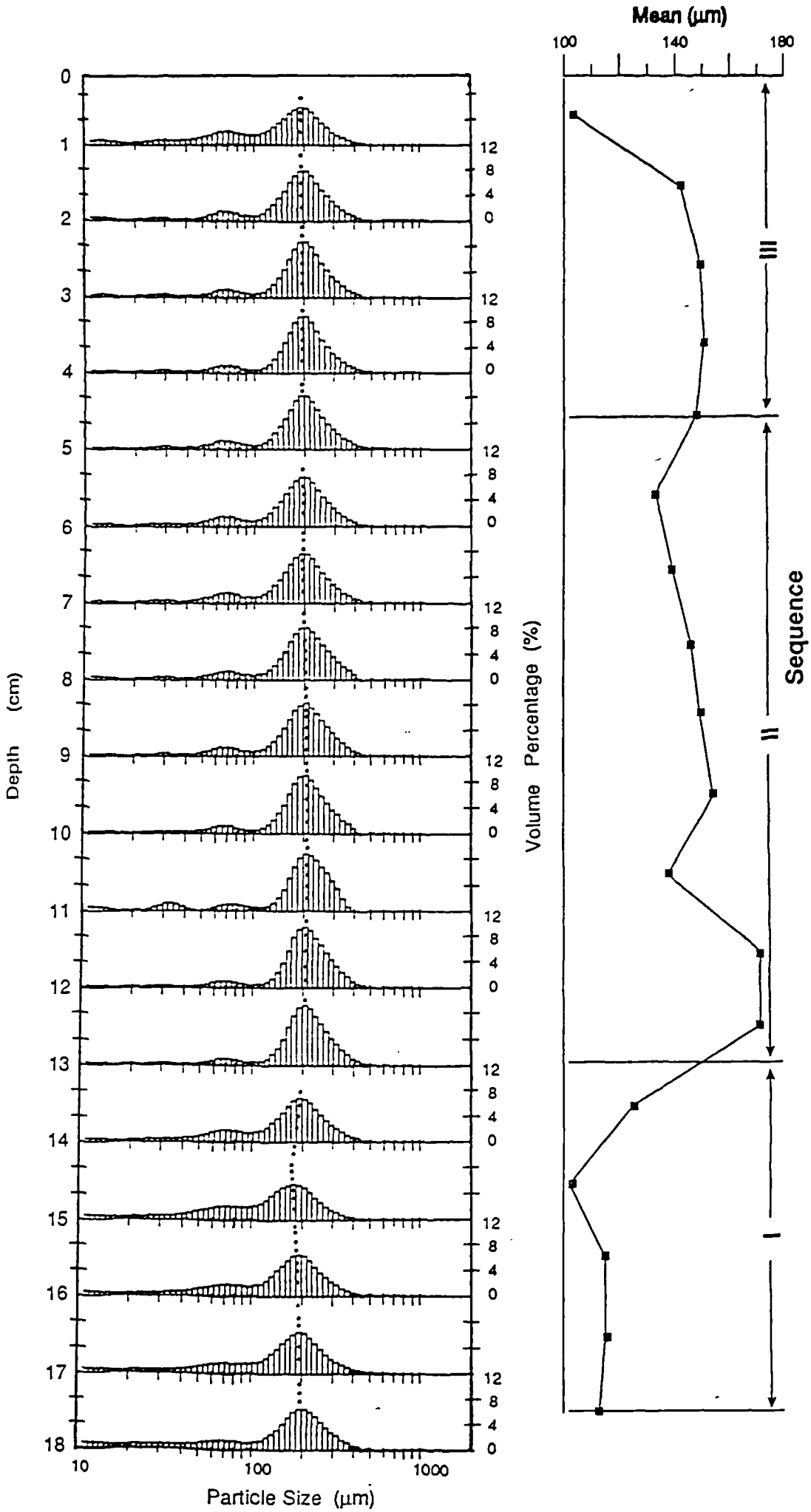

Figure 5.75. Upcore progression in the particle size histograms of the sand sediment at Borehole 4, Fullerton. Two separate sequences can be identified and the upper sequence may possibly be divided into two parts, as indicated by the variations in mean particle size. (Figure 5.74).

sequences. At Fullerton, the variations of averaged histograms indicate sediment fining landwards in both sequences (Figure 5.76).

In summary, two fining upward sequences can be identified and the sand layer can be divided into two horizons at Maryton and Fullerton. At Fullerton, general fining landward trends are also present in the both horizons, and the sediment in the upper horizon is generally coarser than in the lower.

5.2.2.3 Interpretation

At both Maryton and Fullerton, peat accumulation was interrupted by the deposition of a grey micaceous silty fine sand at *circa* 7,000 radiocarbon years BP. Clearly, the overlying and underlying silty clay deposits were laid down in an estuarine environment, as confirmed by the microfossil evidence, for the deposits contain pollen assemblages reflecting possible saltmarsh conditions (Smith *et al.*, 1980). Although the pollen evidence does not provide any clear indication as to the origin of the micaceous fine sand, its stratigraphical relationship with the adjacent layers and the general landward fining in particle size strongly suggest that it was deposited by a marine flood.

Two fining upward sequences and general landward fining trends in both divided horizons within the sand layer suggest that the layer was formed by at least two successive episodes of sediment deposition. As the sediment in the upper horizon is generally coarser than in the lower, it is very likely that the flooding process associated later episode was more powerful that the earlier one.

The characteristics of particle size distribution of the sediment and its vertical progression within are very similar to what was revealed at the previously described site at Lochhouses, and therefore suggest that its formation was associated with a fast depositional process.

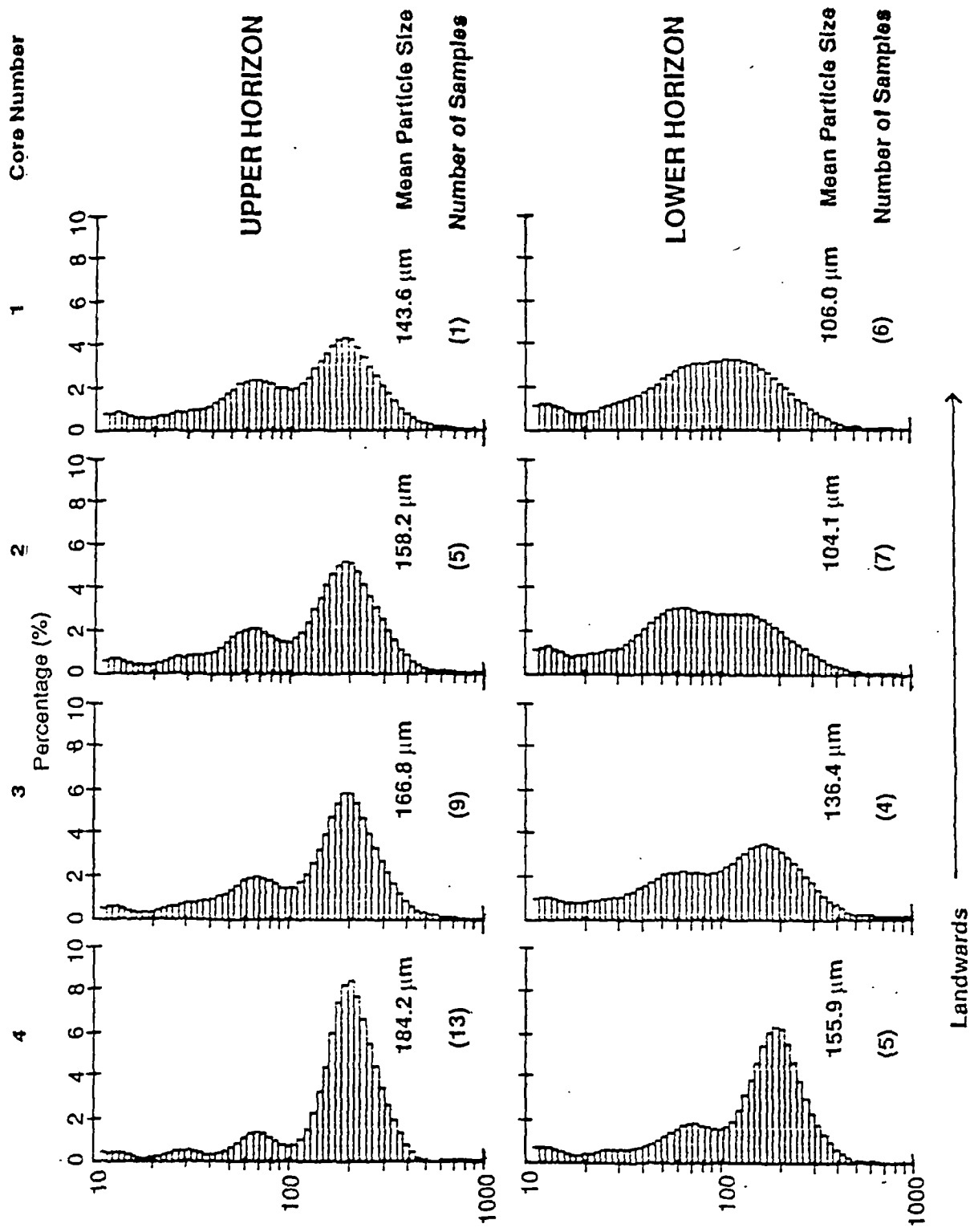

Figure 5.76. Averaged particle size histograms for divided units at boreholes 1, 2, 3 and 4, illustrating fining - landward trends at both levels.

Putting all the evidence together, it seems likely that the grey micaceous sand layer was deposited by a event of high energy marine inundation with at least two episodes of sediment deposition, which flooded up to at least 2 m above the contemporary high water mark, i.e. from the boundary between the estuarine deposit and the underlying peat accumulation.

5.2.3 Moniack

5.2.3.1 Stratigraphy and Radiocarbon Dates

Moniack is one of the two sites near the head of the Beauly Firth (Figure 5.14), previously studied by Haggart (eg.1986 and 1988). The other site is at Barnyards, which is located at the most inland end of the Beauly Firth, approximately 4 miles northwest of Moniack. At both sites, a similar layer of sand was found to be intercalated within peat and minerogenic mudflat deposits. Figure 5.77 shows the local morphology and lithostratigraphy at Moniack. The latter displays a thin layer of micaceous silty sand running through the lower part of estuarine carse and extends ascendingly farther into peat accumulation over a considerable distance. Haggart (1988) noted that the sand layer lies unconformably upon the peat beneath and is believed to have been deposited between 7430 ± 170 and 7270 ± 90 radiocarbon yrs. B.P.. Haggart interpreted its origin as marine based upon the diatom assemblages present.

5.2.3.2 Particle Size Analysis

Samples from cores at boreholes 4B and 5B were provided by Haggart and particle size analysis undertaken by the author. The result shows that the sediment is characterised by a multi-modal distribution and modal peaks of prominent subpopulations are identifiable at *circa* 30, 60 and 200 μm respectively (Figures 5.79 and 5.81). The sediment here is very poorly sorted and shows similar characteristics to that found in other sites. Within core 4B, one fining-upward sequence is certainly present within the greater part of the sediment, excluding the samples at the very top which seem to form an individual short fining-upward

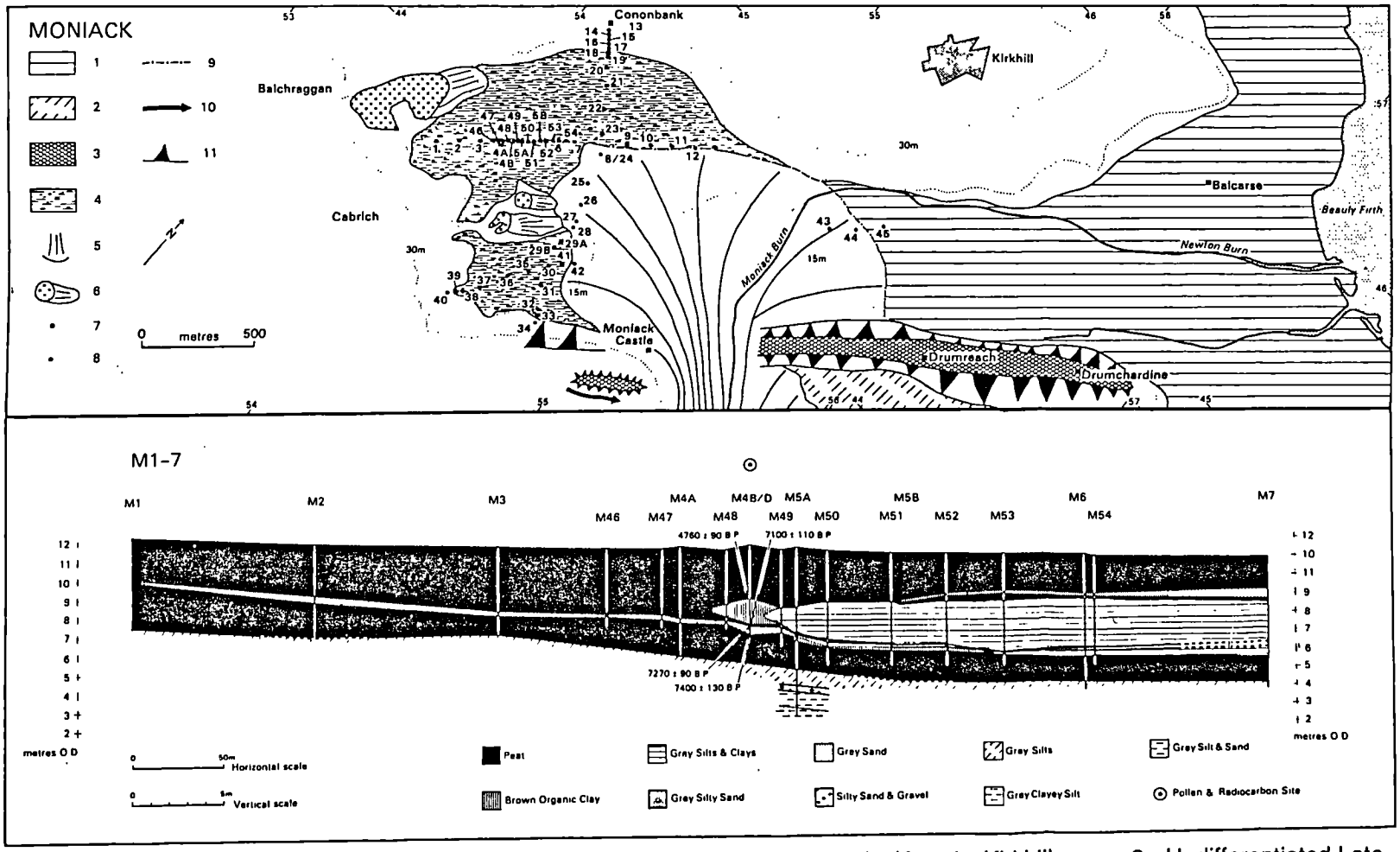

Figure 5.77. Morphology and stratigraphy of the site at Moniack (after Haggart, 1988). Key: 1= Kirkhill carse, 2= Undifferentiated Late Devensian marine deposits, 3= Ridge forms, 4= Surface peat, 5= Alluvial fans, 6= Crag and tail forms, 7= Pollen, diatom and ^{14}C sampling sites, 8= Boreholes, 9= Boundary of fan uncertain, 10= Meltwater channel, 11= Steep slope. Arrows in the lower section of the diagam indicates the positions of ^{14}C samples.

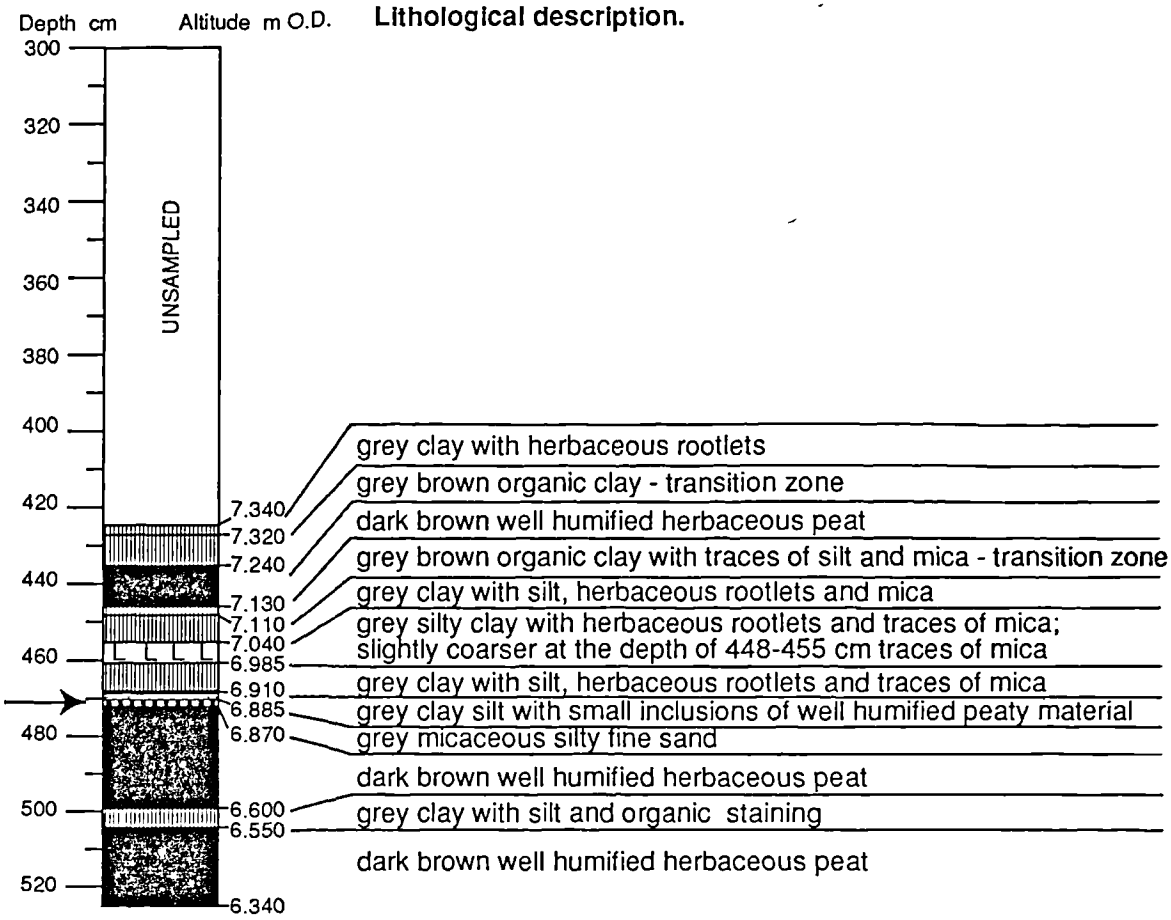

Figure 5.78. Lithostratigraphy of core 4B at Moniack.
The arrow marks the core section analysed.

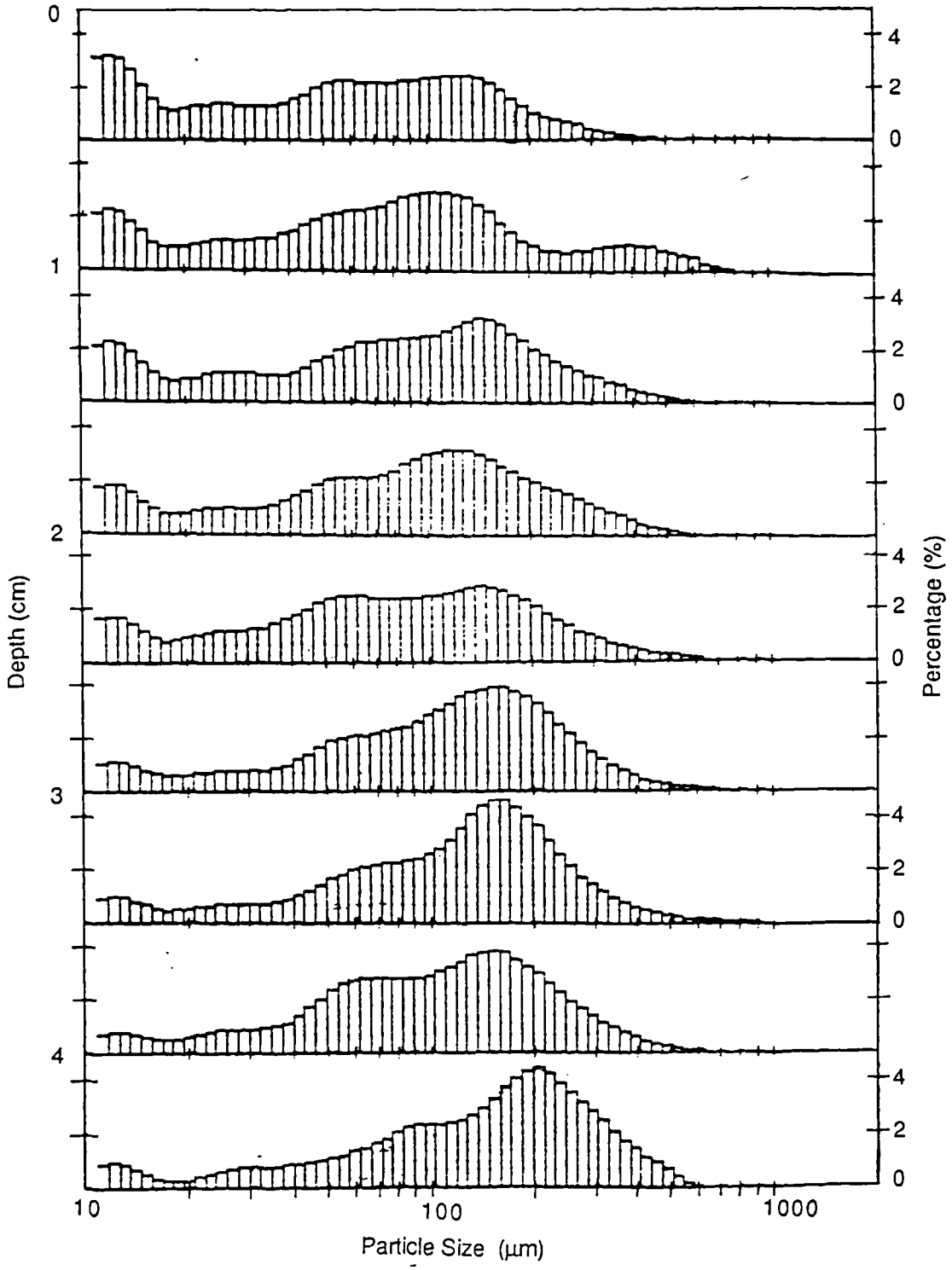

Figure 5.79. Upcore progression of particle size histograms within the sand layer at Borehole 4B, Moniack (Figure 5.78).

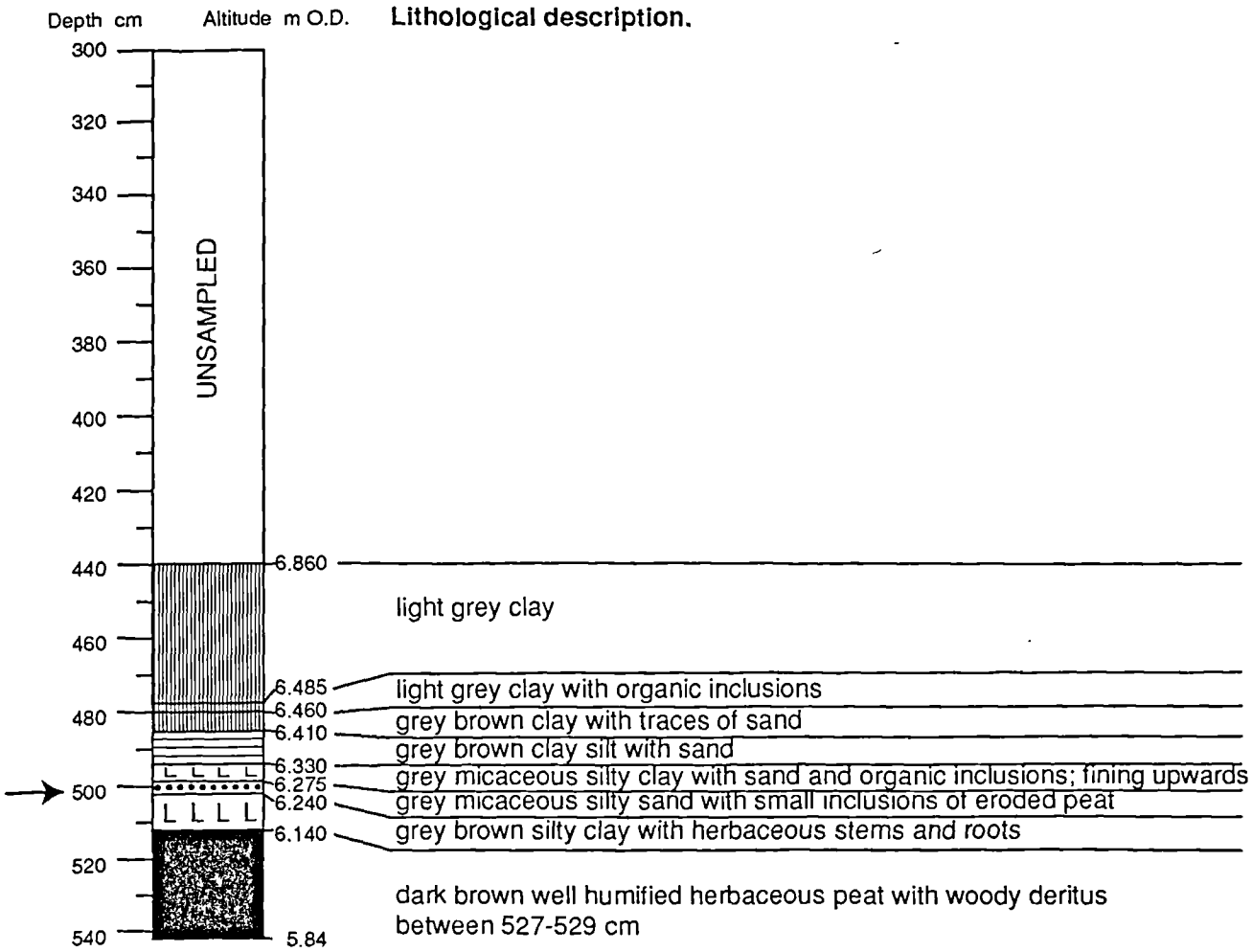

Figure 5.80. Lithostratigraphy of core 5B at Moniack.
The arrows mark the core section analysed.

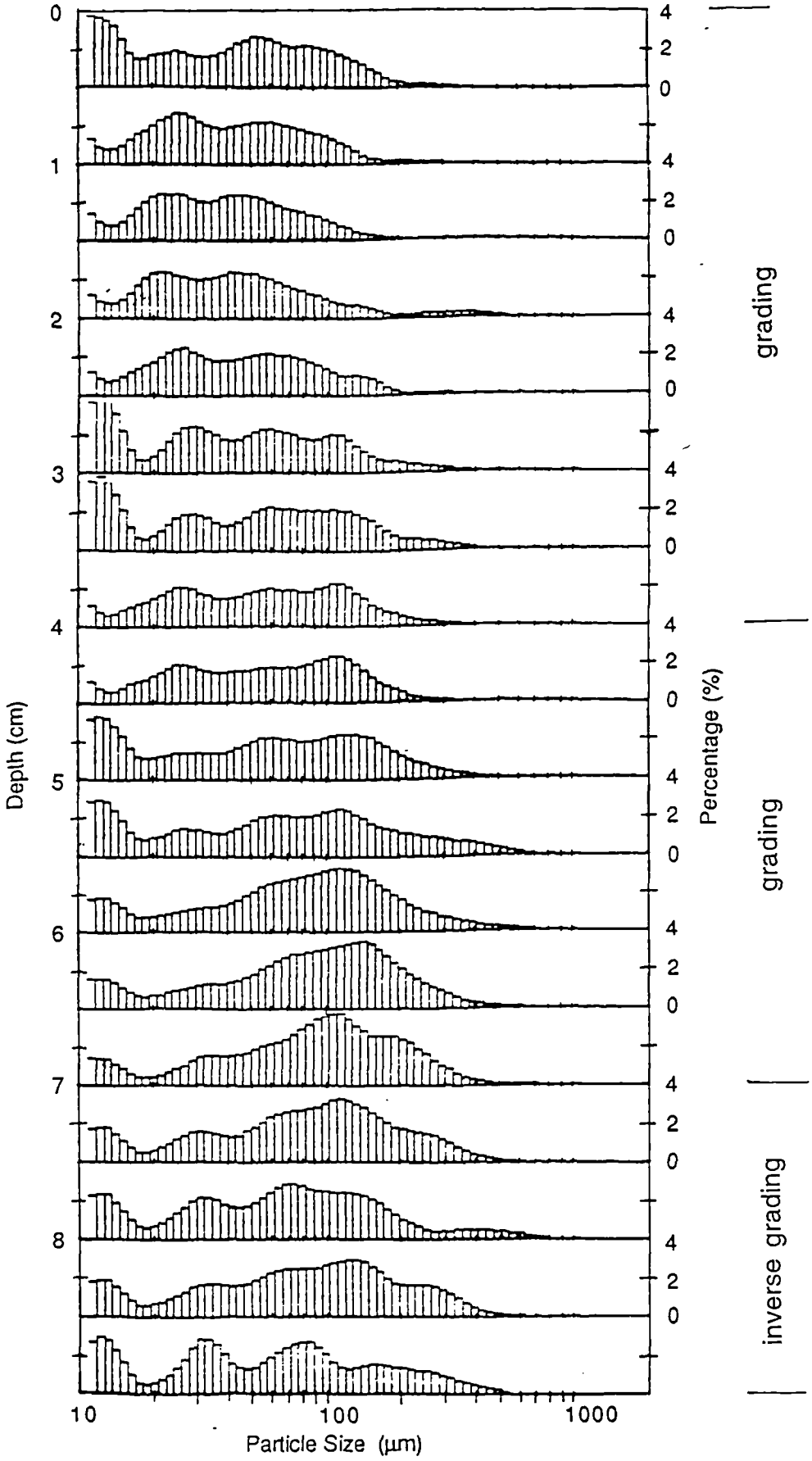

Figure 5.81. Upcore progression of particle size histograms within the sand layer at Borehole 5B, Moniack (Figure 5.80).

sequence (Figure 5.79). At borehole 5B, one general fining-upward sequence is clearly identifiable, which appears to consist of two separate progressive fining-upward sequences following an initial inverse grading of a limited thickness (Figure 5.81).

5.2.3.3 Interpretation

As studied and interpreted by Haggart (1988), the grey micaceous silty fine sand layer marks an horizon of marine intrusion dated to have occurred at sometime between *circa* 7430 and 7270 radiocarbon yrs B.P.. Particle size analysis revealed that the sediment is poorly sorted and consists of multimodal subpopulations and that there is at least one general fining-upward sequence and more possibly two. The particle size characteristics and its fining-upward sequences are believed to reflect episodic rapid deposition as the way in which the sediment was accumulated. The episodic rapid deposition is interpreted as having been induced by high-energy marine inundation, which flooded to at least 4 m above the inferred high water mark.

5.2.4 Ythan valley

Flandrian estuarine deposits in the Ythan valley have been previously studied for relative sea-level changes by Smith *et al.* (1983), and a detailed description of the general geomorphology and deposits of the area was given in their paper (Figure 5.82). The River Ythan flows generally eastwards for about 10 km through a varied landscape to reach the North Sea coast about 16 km north of Aberdeen. The lower Ythan is a relatively sheltered estuarine area, into which several tributaries flow. The deposits examined here are confined to an area in the lower valley around the present estuary.

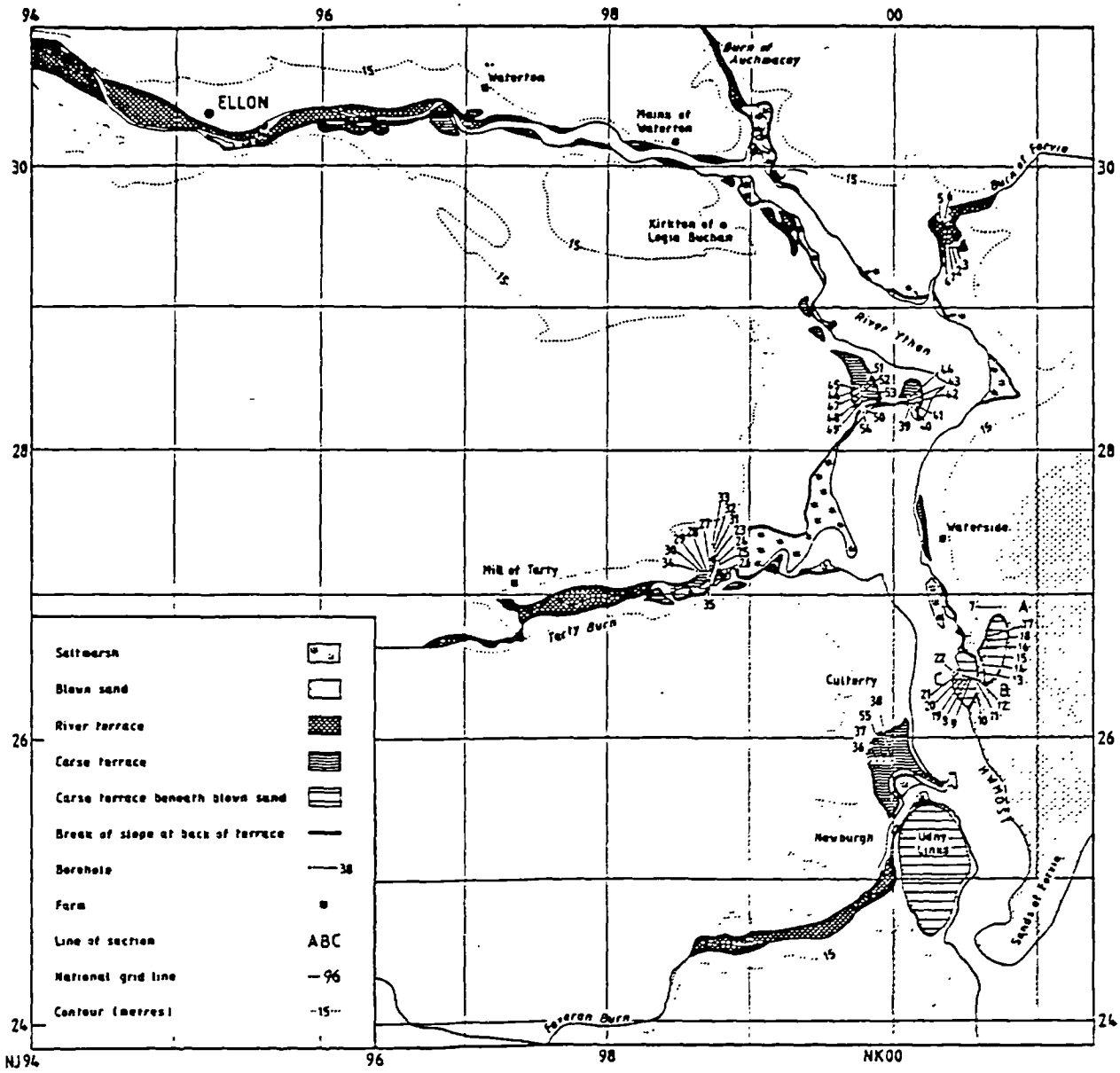

Figure 5.82. Holocene terraces in the lower Ythan Valley (after Smith *et al.*, 1983).

5.2.4.1 Stratigraphy and Radiocarbon dates

The detailed stratigraphy at Waterside in one of the tributary valleys has been described and published by Smith *et al.* (1983) (Figure 5.82). The surface deposit of an embayment at the valley side is blown sand, which is widely underlain by peat. Within the peat, grey silty clay forms a wedge, tapering landwards. Of particular importance to this study is an additional thin wedge of grey, micaceous, silty fine sand within the peat below the grey silty clay to landward, and passing into the grey silty clay to seaward. As also noted by the authors of the paper, the grey silty clay at Waterside is identical in appearance to that of the carseland areas elsewhere in the valley which occupy a similar stratigraphical position. They thus considered that the sedimentary sequence at Waterside is part of a widely occurring sequence. They obtained a composite sample of 2 cm-thick samples of *Phragmites-Carex* peat above and below the grey micaceous silty fine sand layer (Figure 5.83) for radiocarbon dating, and the date obtained was 6850±140 yrs B.P.. They also published the results of pollen analysis of the sediment throughout the sequence and noted that the inferred age of the sand layer from the pollen assemblage is in the early to middle Flandrian.

5.2.4.2 Stratigraphy, Radiocarbon Dating and Particle Size Analysis at Tarty Burn, Ythan Valley

As elsewhere in the area, a similar stratigraphical sequence was examined in the tributary valley of the Tarty Burn (Figures 5.82, 5.84 and 5.85). Although thinner than the site at Waterside (see above), a layer of grey micaceous silty fine sand is evidently present in the sequence (Figure 5.85). It spreads through estuarine grey silty clay accumulations, extends into and rises in altitude through terrestrial peat deposits. Radiocarbon assay has been undertaken of 2 cm thick peat deposits above and below the sand layer at Borehole TB/63

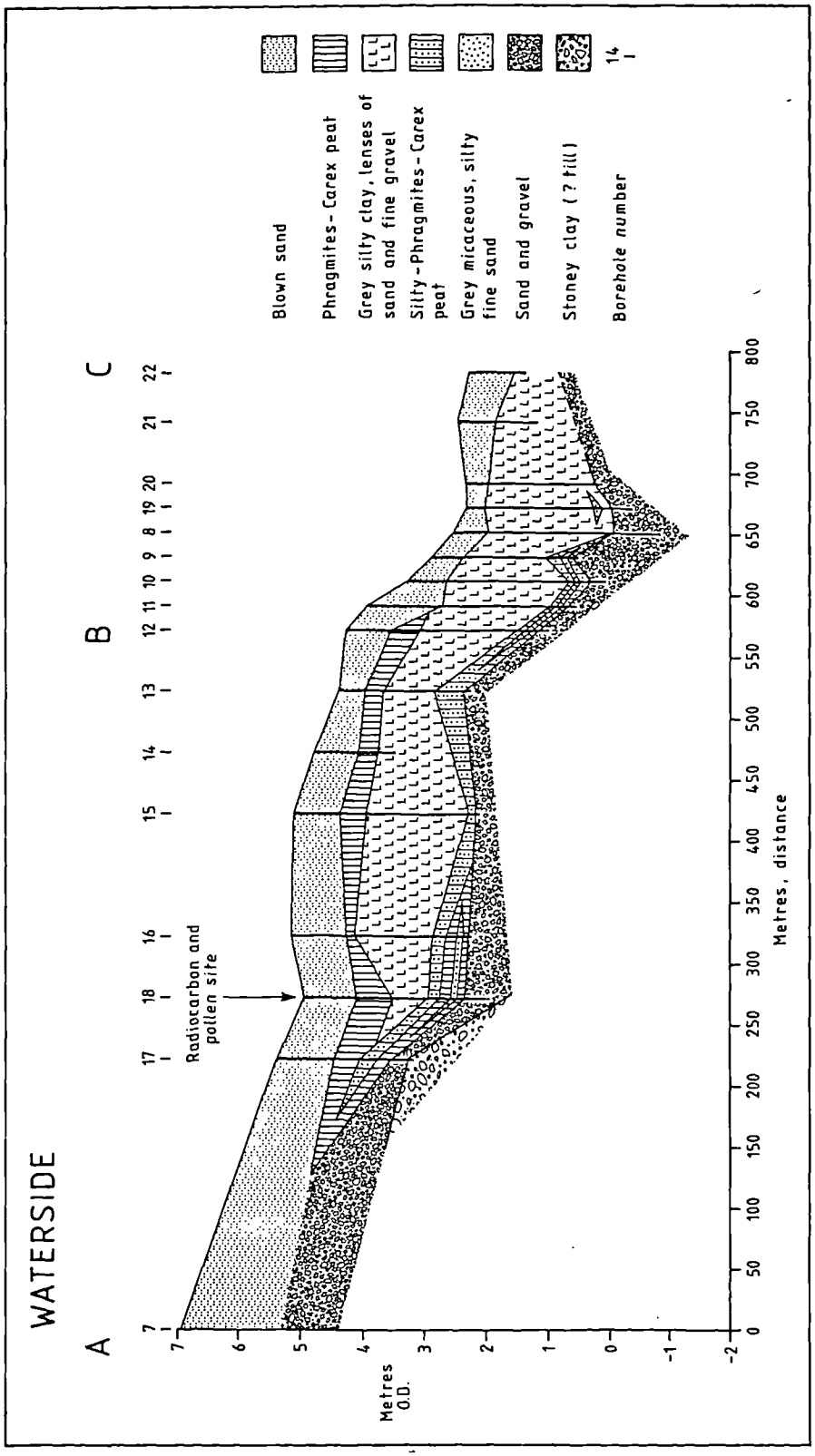

Figure 5.83. Stratigraphy at Waterside (after Smith *et al.*, 1983). The borehole locations are indicated in Figure 5.82.

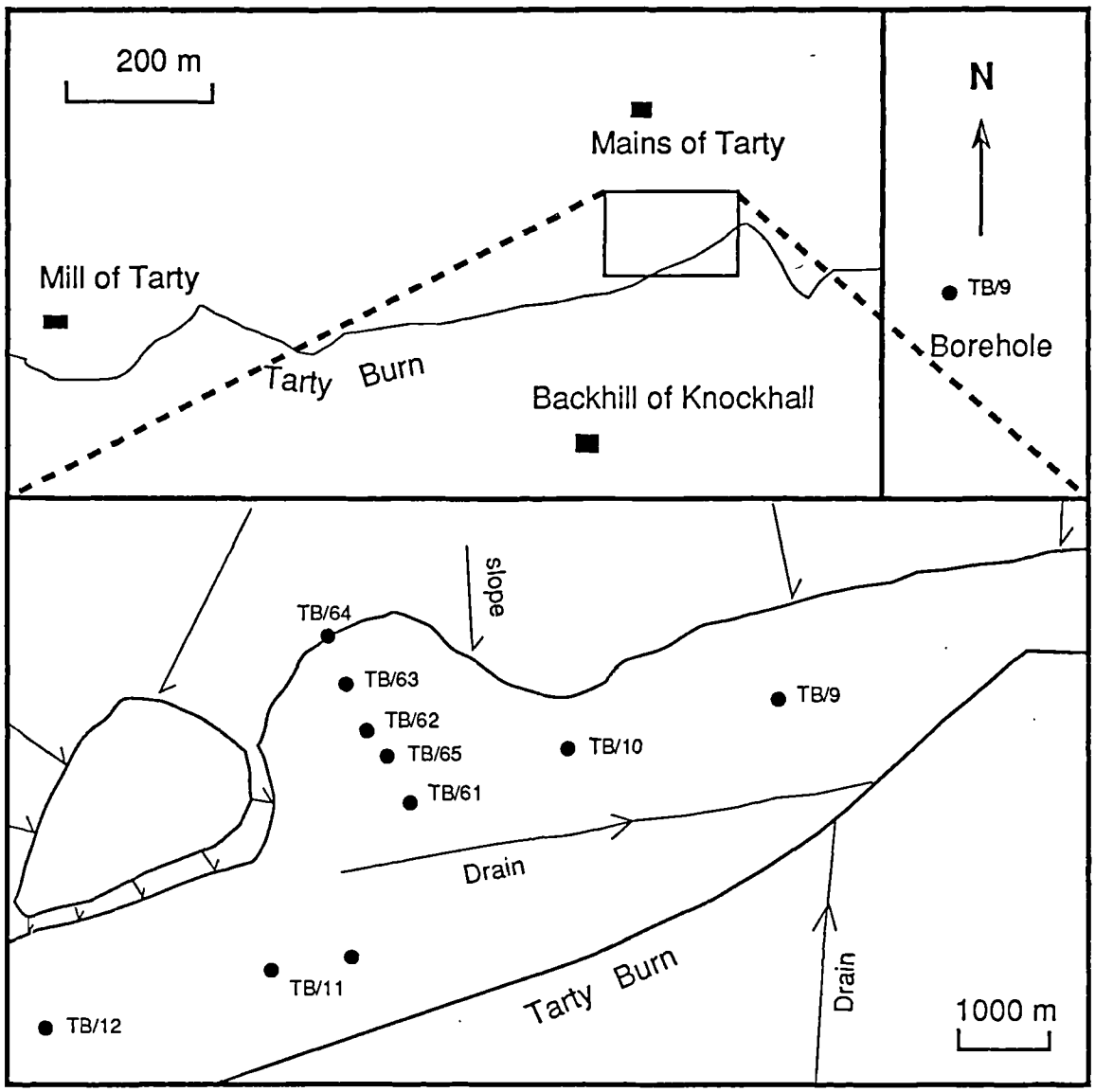

Figure 5.84. Borehole locations at the Tarty Burn site. The site location is marked in Figure 5.82.

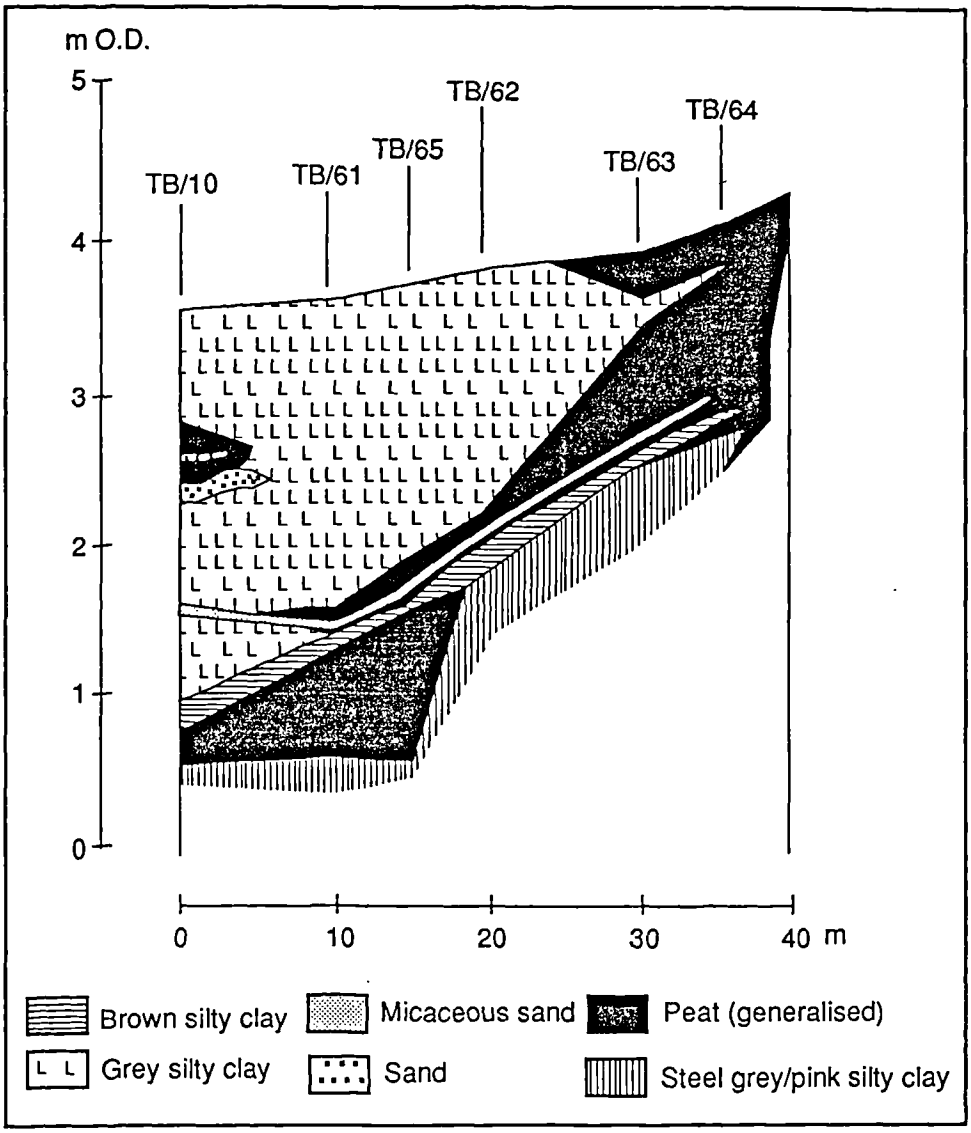

Figure 5.85. Stratigraphical section through the coastal deposits at the Tarty Burn site. Radiocarbon dates were obtained directly above and below the sand layer and a sediment core was analysed for particle size at Borehole TB/63. The site and borehole locations are marked in Figures 5.82 and 5.84.

and dates obtained are 7131±45 (SRR-4717) and 7400±45 (SRR-4718) respectively (Smith *et al.*, 1993) (Figure 5.85).

Borehole	Lab. Number	Material	Age (^{14}C Years BP)
TB/63	SRR-4713	Peat above grey micaceous silty fine sand	7131 ± 45
TB/63	SRR-4718	Peat below grey micaceous silty fine sand	7400 ± 45

Particle size analysis has been undertaken on the sand layer at borehole TB/63 in the present study. The sand layer is *circa* 3 cm thick here and 7 contiguous samples were obtained at intervals of *circa* 0.4 cm for the analysis. Particle size distributions of the sediment contained in the sand layer are characteristically multi-modal and the individual modal peaks of distinctive subpopulations occur at *circa* 7, 25 and 600 μm (Figure 5.87). The vertical variations in histograms are generally not pronounced and the positions of each modal peak remain relatively constant on the size scale. However, a general fining upward trend is present, as indicated by variations in mean particle size, and the trend is associated with a general decrease in the proportion of the coarsest subpopulation.

5.2.4.3 Interpretation

As studied and interpreted by Smith *et al.* (1983), the grey micaceous silty fining sand layer marks a horizon of marine intrusion dated as having occurred at *circa* 7,000 radiocarbon yrs B.P.. Particle size analysis revealed that the sediment is poorly sorted and consists of multimodal subpopulations and that there is one general fining-upward sequence, which corresponds to a general decrease in the proportion of the coarsest subpopulation. The particle size characteristics and its fining-upward sequence are believed to reflect an episode of rapid sediment deposition. The rapid deposition is interpreted as having been induced by a high-energy marine inundation, which ran up to at least 1.5 m at Tarty Burn and 4.5 m at Waterside above the inferred high water mark.

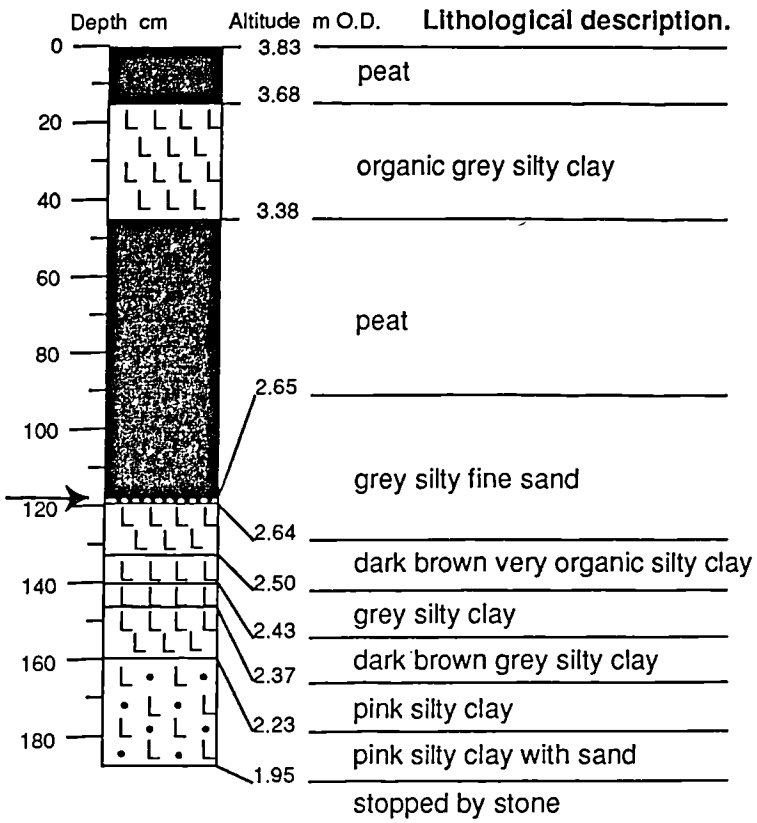

Figure 5.86. Lithostratigraphy of core 63 at Tarty Burn. The arrow marks the core section analysed.

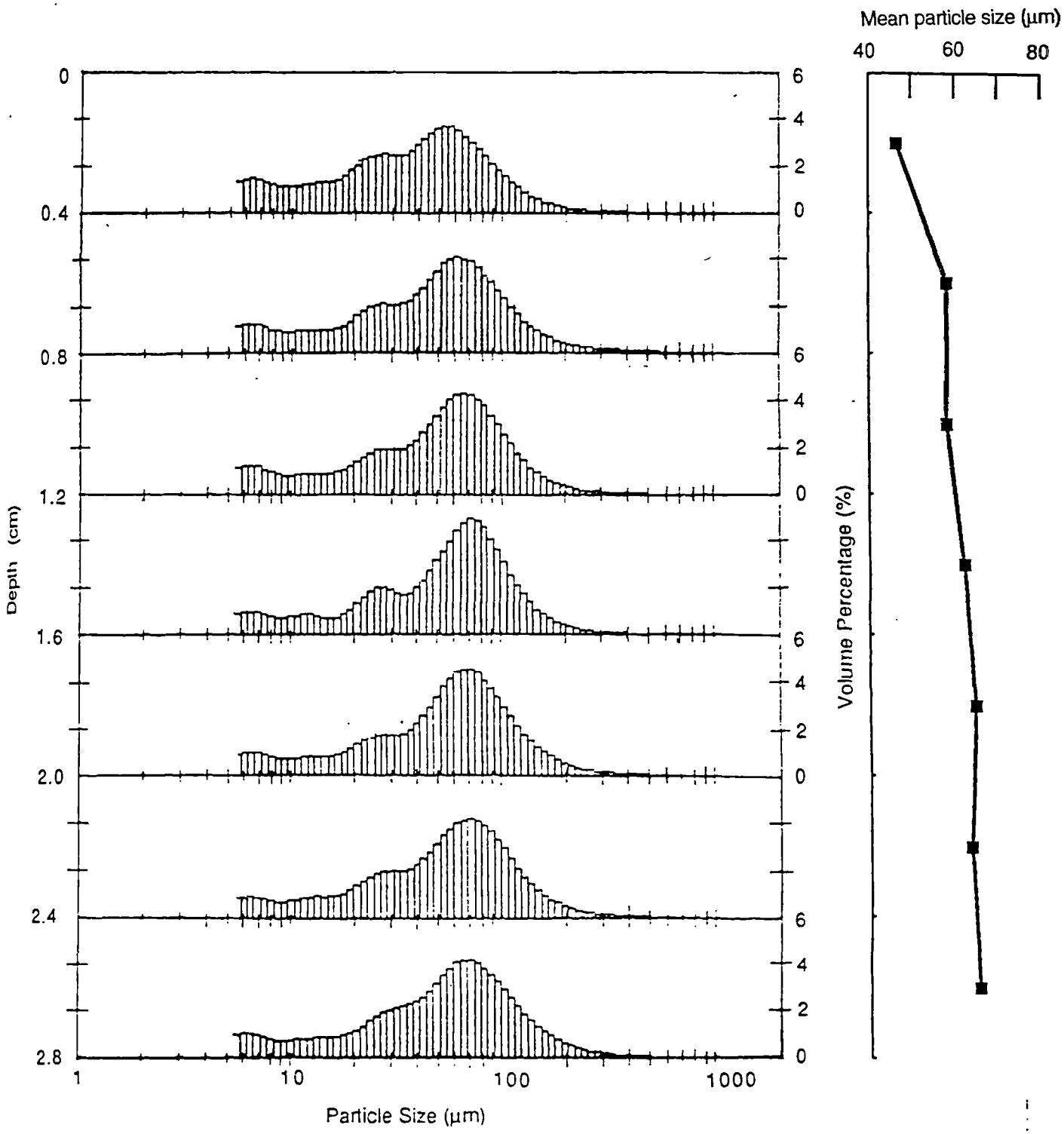

Figure 5.87. Upcore progression of particle size histograms within the sand layer at Borehole TB63, Tarty Burn. One fining-upward sequence is identified (Figure 5.86).

6. INTERPRETATION AND DISCUSSION

6.1 Stratigraphy, Microfossil Evidence, Marine Flooding and Age of the Sand Layer

The stratigraphy at all the sites studied is evidently comparable, exhibiting a thin sand layer intercalated into both estuarine silty clay (carse) and peat. The estuarine silty clay extends as a wedge into the peat deposits, as a result of marine transgression and subsequent regression associated with the Main Postglacial Transgression. As maintained by previous authors (see respective sections), the widespread sand layer at all the sites is of marine origin, based on the lithostratigraphical and microfossil, especially diatom, evidence. Furthermore, the stratigraphical position of the sand layer shows that it is unusually extensive upon the former terrestrial deposit (the underlying peat) and reaches well above the inferred former high water mark at each individual site, reflecting the severity of the marine flood.

Radiocarbon dates obtained from peat samples directly above and directly below the widespread sand layer from various sites are compiled in Table 5.3. It is conventionally accepted that the paired values of earlier and later radiocarbon dates suggest the likely time-span during which a sediment layer is deposited and that considerations are necessarily taken into account in interpretation since no absolute certainties or certain clearly-set rules exist due to various analytical and environmental factors. On the assumption that the radiocarbon dates obtained with peat samples do not deviate much from their actual ages, statistically the youngest of the earlier dates and the oldest of the later dates would best define the time span during which the sand layer was deposited. However, such an assumption may not always be correct. Since at some locations the peat underlying the sand layer shows evidence of surficial erosion, the basal dates at these sites are likely to be too old. Here, the later dates may be closer to the actual age of the event. Drawing upon the consensus of the dates listed in Figure 5.88, it is thought to be the most likely case that the marine flooding had occurred at *circa* 7,000 radiocarbon yrs B.P.. However, from the sites at Moniack and Lochhouses, the dates obtained with peat samples above the marine flooding layer deviate considerably

from the general consensus by *circa* 200 to 400 radiocarbon years. However, it should be noted that only at Lochhouses both dates fall outside the range of the remainder by 2δ.

Table 5.3 Radiocarbon dates for the *circa* 7,000 B.P. coastal flood (modified after Smith, Turbayne, Dawson and Hickey, 1991 and Smith *et al.*, 1993).

Location	Laboratory Number	Horizon	^{14}C Age, B.P.	Calibrated date (in parentheses) and range in calendar years, B.P.**
Smithy House, Golspie	SRR-3791 SRR-3792	above the layer below the layer	6580 ± 55 6980 ± 65	7518 (7397) 7389 7889 (7755) 7677
Creich, Dornoch Firth	SRR-3693 SRR-3694	above the layer below the layer	6950 ± 60 6960 ± 55	7798 (7713) 7659 7871 (7721) 7669
Dounie, Dornoch Firth	SRR-3789 SRR-3790	above the layer below the layer	5190 ± 65 7120 ± 45	5989 (5930) 5905 7933 (7912) 7839
Tarty Burn, Ythan Valley	SRR-4717 SRR-4718	above the layer below the layer	7131 ± 45 7400 ± 45	7939 (7917) 7845 8176 (8136) 8124
Waterside, Ythan Valley	SRR-1565	composite date	6850 ± 140	7768 (7634) 7537
Puggieston, Montrose	SRR-211 SRR-2120	above the layer below the layer	6850 ± 75 7120 ± 75	7687 (7634) 7565 7949 (7912) 7824
Fullerton Montrose	Birm-867 Birm-823	above the layer below the layer	6880 ± 110 7140 ± 120	7768 (7653) 7560 8059 (7921) 7804
Silver Moss St Andrews	SRR-1333 SRR-1334	above the layer below the layer	7050 ± 100 7555 ± 110	7927 (7889, 7860, 7829) 7714 8410 (8335) 8174
Easter Ofference Forth Valley	SRR-1603	below the layer	6870 ± 50	7683 (7647) 7615
Castle Street, Inverness	GU-1377	below the layer	7080 ± 85	7934 (7899, 7852, 7843) 7775
Moniack, Beauly Firth	Birm-1126 Birm-1127	above the layer below the layer	7270 ± 90* 7430 ± 170	8128 (8061, 8043, 8001) 7940 8369 (8167) 7997
Lochhouses Dunbar	SRR-1431 SRR-1430	above the layer below the layer	7490 ± 70* 7450 ± 60	8339 (8309, 8262, 8257, 8224, 8210) 8162 8319 (8176) 8134
Lochhouses Dunbar	SRR-3912 SRR-3913	above the layer below the layer	7410~* 7880 ± 45	8167 (8139) 8134 8707 (8578) 8551

* indicates the dates obtained from above the sand layer which are considerably older than 7,000 radiocarbon yrs B.P.. ** The calendar year figures are calculated using a radicarbon age calibration program, called CALIB (version 3.0), which is based on correlated data sets of radiocarbon age and dendrochronology (Stuviver and Reimer, 1993). The program offers various options and calibration methods. The adopted method here performs simple curve interceptions with a linear interpolation of the datapoints of bidecadal treering datasets (Linick, Long, Damon and Ferguson, 1986; Stuiver *et al.*, 1993; Pearson, Becker and Qua, 1993). The calculated age ranges (front and rear figures) are given at 1 σ (68.3%) probability level, and calibrated ages are listed between them in parentheses. These calendar dates indicate probable true ages rather than mere radiometric estimations and are for reference only.

The relationship between the sand layer of the Second Storegga Slide tsunami and the Main Postglacial Transgression in eastern Scotland is particularly interesting. It will be recalled that deposits of the Main Postglacial Transgression are a major feature of the Holocene shoreline sequence in eastern Scotland (See pages 124-131, above). As shown in the stratigraphical sequences described earlier, the sand layer occurs within the Main Postglacial Shoreline deposits to seaward, and tapers landward below the highest deposits of the Main

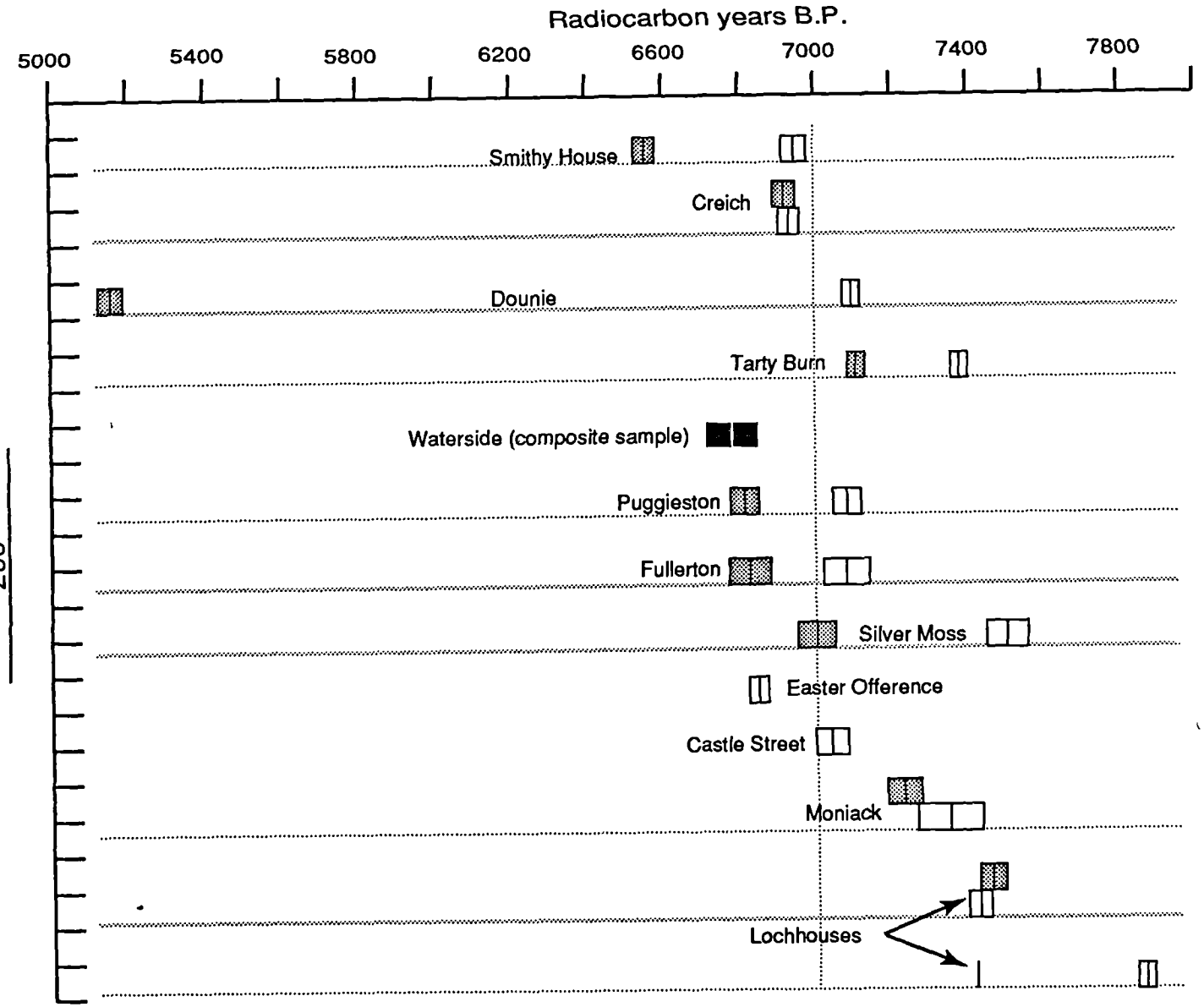

Figure 5.88. Distribution of uncalibrated radiocarbon dates for the *circa* 7,000 yrs B.P. coastal flood. The data are from Table 5.3 and the location of sites indicated in Figure 5.1.

Postglacial Shoreline. The sand layer is therefore silghtly older than the culmination of the Main Postglacial Transgression. The maximum altitude of the Main Postglacial Transgression deposits and their associated shoreline have been described in a number of studies (e.g. Cullingford *et al.*, 1991) and have been shown to be differentially isostatically uplifted as shown in Figures 5.9 and 5.10, above. The age for the culmination has been obtained from a number of locations (e.g. Smith *et al.*, 1982 and Cullingford *et al.*, 1991). These show that the culmination took place earlier towards the centre of uplift, perhaps as much as 6,800 radiocarbon years B.P., and much later towards the edge of the isostatically uplifted area, for example at Fraserburgh an age range of 6,095±75 to 5,700±90 radiocarbon years B.P. has been obtained. The ages for the sand layer, as listed above, contrast with the ages for the culmination of the Main Postglacial Transgression in that, whilst they are older, they show no trend spatially. This reinforces the view that whilst the culmination of the Main Postglacial Transgression was a diachronous event, the deposition of the sand layer occurred at a similar time at all locations. Indeed, the sand layer stands out in the deposits of Holocene shorelines in eastern Scotland, not only as a distinctive depositional horizon but also as a layer probably accumulated very rapidly and over a short time span. As such, it represents a distinct marker horizon.

6.2 Sediment characteristics, compositional changes and depositional processes

Particle size analysis undertaken during this research reveals that the sedimentary characteristics of the sand layer in eastern Scotland bears no resemblance to those of dune or beach sand and that the sediment contains various subpopulations as indicated by the multimodality of the particle size distributions. Such subpopulations include those in the silt and clay range, which are frequently transported out of beach and dune sediments during their accumulation. Previous studies have found that dune sand is very well sorted and very close to log-normal distribution and that beach sand is often well-sorted, distinctively unimodal and often slightly negatively-skewed (Friedmand, 1961; Visher, 1969 and Friedman, 1979). Furthermore, the sediment from the widespread sand layer is frequently found to contain a significant amount of mica, which possesses a distinctively smaller specific gravity and disc-like shape in contrast to other types of constituent particles, such as quartz grains, and has a different settling velocity. Summing up the multimodality and distinctive heterogeneity of the particle composition of the sediment indicates that it was subject to very limited sorting during its accumulation in contrast to sediments subjected to a constant sorting action. The sediment might have been laid down rapidly due to a suddenly reduced current velocity rather than undergoing sorting processes to a high degree.

Apart from a general fining-landward trend, the upcore variations in particle size illustrate episodic fluctuations, predominantly reflected by multiple sets of fining-upward sequences, as well as by a general fining-upward trend. The changes in the composition of the sediment are revealed not only by the composition of particle size, but also by the mineral magnetic properties of the sediment at two sites (Dounie and Creich), as indicated by the relevant parameters. Although these parameters do not provide information upon the specific mineral composition of the sediment, it is nevertheless likely that their variations are due to changes in magnetic mineral concentration and they thus provide important information on the patterns and trends present in the changes in magnetic mineral concentration within the sediment. In addition, it is found that there is a close association of the coarsest sediment

levels and the distinct peaks of mineral magnetic parameters such as susceptibility, SIRM and HIRM. Since the sediment is mainly composed of quartz grains, the strong magnetic signals at particular horizons reflect higher concentrations of magnetic minerals, which have particular geometric dimensions and higher specific gravities. It is interpreted that the heavier magnetic minerals settled out together with coarsest quartz grains and also were subject to differential settling resulting in varied assemblages of magnetic minerals within each band of enriched magnetic mineral concentration.

Summing up the characteristics of the sediment and patterns of changes in magnetic mineral concentration, the depositional processes can be inferred as follows. It is highly likely that, at all sites, the sediment was formed as a result of several episodes of accumulation. The accumulation process is highly likely to have taken place in the form of rapid deposition, which resulted in simultaneous deposition of transported particles of all sizes at different rates, as indicated by progressions of particle size composition within the sediment. Such characteristics of the accumulation process are likely to have been associated with episodic marine flooding. From a comparison of depositional processes associated with storm surges and tsunamis, the episodic marine flooding is interpreted here as having been the result of a large palaeo-tsunami, which has been interpreted by Dawson *et al.* (1988) as having been generated by the Second Storegga Slide on the continental slope west of Norway at *circa* 7,000 yrs B.P.. The number of fining-upward sequences is, however, variable from site to site. At present, as indicated by the study of the Flores tsunami (Chapter 4), there are uncertainties in determining the number of marine inundations from particle size analysis, because of the complexity of the depositional processes involved. At most sites along the coast of eastern Scotland, two successive major episodes of rapid sediment deposition can be inferred unequivocally from particle size analysis. Further inference will depend upon future development in the understanding of the application of particle size analysis and hydrodynamics associated with tsunami inundation. The difficulty

of relating sediment sublayers divided with particle size and mineral magnetic analysis to individual processes of runup and backwash remains to be solved.

6.3 Possible source sediments

The character of the sediments comprising the widespread tsunami sandlayer are very similar from site to site except at Dounie. At all the sites except Dounie, the sediments are characteristically grey micaceous silty fine sand, which was probably derived largely from the former estuarine mudflats, i.e. from the accumulating carse. Theoretically, broken tsunami waves translate into turbulent horizontal passages of water which are characterised by erosive power and ability to carry a large amount of sediment. Such power and ability have been observed to have caused great morphological impact on coasts in previous studies and in the current study of the recent Flores tsunami (see Chapter 4). However, at Dounie, the tsunami sediment is largely of grey medium to coarse sand and is distinctly thicker and more extensive. Here, morphological and stratigraphical investigations disclosed a buried sand and shingle ridge lying to seaward of the embayment, which is covered by estuarine silty clay. The sand layer, inferred to have been deposited by the Storegga tsunami, spreads over the landward side of the ridge and reached a distinctively higher level farther inland while on the seaward side of the ridge no similar sand layer has been found. Therefore, it is believed that the buried sand and shingle ridge was breached and was at least in part the source of the sediment: a process analogous to the 1960 Chilean tsunami and the 1983 Japan Sea tsunami cited in Chapter 3.

6.4 Magnitude of the inundation

Because the characteristics of resultant sediment were controlled largely by both tsunami hydrodynamics and the source sediment, complications exist in inferring the magnitude of flooding energy from particle size evidence, as has been shown in the study of the Flores tsunami sediment. At present, it is maintained that the extent of the sediment spreading upon the land provides important information on the magnitude of inundation. The uppermost elevation of the sand layer is considered to provide the minimum estimation of

the tsunami flood level. The estimation of palaeo-tsunami runup heights can be made in relation to inferred contemporary high water marks, which are the transitions between underlying peat and mudflat deposits (Dawson *et al.*, 1988). However, at the present time, it is not possible to calculate with any precision the changes in tidal level that took place during the southward propagation of the tsunami across the North Sea. Therefore, it is not possible to determine whether the tsunami struck individual section of the coastline during high water or low water.

The values of the runup heights provide important information on the magnitude of the tsunami inundation for the reconstruction of the tsunami event and provide a general guide to the validity of numerical models, which can help in determining the dynamic processes of tsunami generation, propagation and inundation. Geological investigations and numerical modelling combined may contribute to the accumulation of information on the vulnerability and history of the coastline of the North Sea.

6.5 Conclusion

From the results of the investigations described above, it can be concluded that

1. The high resolution particle size analysis employed here is a useful method for studying the particle size profiles of sediments and the detail which it provides enables the processes involved in the accumulation of those sediments to be interpreted;

2. In the case of the layer of grey micaceous silty fine sand in eastern Scotland, the method, supported by further stratigraphical work and by mineral magnetic analysis, enables the tsunami hypothesis of Dawson *et al.* (1988) be verified and provides detail on the manner of deposition of the sediments.

7. IMPLICATIONS

7.1 Storegga tsunami deposits as a stratigraphical marker

As has been observed above, a great deal of effort has been made to correlate former shoreline fragments along the coastline of Scotland. As pointed out by several authors (eg. Cullingford and Smith, 1980), there are inherent problems in the correlation of shorelines, including the comparability of various types of shoreline fragments formed in different energy environments, together with the possible effect of shoreline diachroneity. In particular, the diachroneity of the Main Postglacial Shoreline may be detectable with radiocarbon assay (Smith *et al.*, 1983; Cullingford, *et al.*, 1991). This implies that the changes from transgressive to regressive phases of relative sea level fluctuation do not match chronologically over sufficiently wide areas. In addition to such problems, dating has been a fundamental problem in studies of relative sea level change, with both a lack of appropriate dating material and in some cases problems of accuracy, as in the case of regressive contacts at Waterside (Smith *et al.*, 1983) and Creich (Smith *et al.*, 1992).

As described in previous sections, the short-lived inundation of the Second Storegga tsunami laid down a widespread sand layer at a number of sites along the coast of eastern Scotland. This implies that similar sediments were deposited synchronously and preserved in coastal sedimentary sequences over a long tract of coastline in eastern Scotland, and perhaps over an even wider area. Thus, the identification of the tsunami deposit provides an important and precise stratigraphical marker in part of the North Sea and East Atlantic region. The stratigraphical marker also allows correlation of shorelines in affected areas surrounding the North Sea and thus allows studies of the relative displacement of their altitudes since the tsunami event. The differences in altitude may reflect regional variations in crustal movement.

7.2 Patterns of isostatic uplift since *circa* 7,000 yrs B.P.

Along the coast of eastern Scotland, the synchronous formation of the sand layer has led to the burial of the contemporaneous shorelines, as disclosed at a number of sites over a wide area. The transition between underlying terrestrial deposit (peat) and estuarine carse clay has been inferred to be the former high water mark (Dawson, *et al.*, 1988). The inferred shoreline elevations and corresponding coordinates are compiled (Table 5.4) and studied using trend surface analysis. Figure 5.89 shows the isobases of a quadratic trend surface inferred from the elevations of the high water mark points. The isobases define a dome-shaped surface with its apex located in the vicinity of Rannoch Moor and seems likely to reflect the pattern of isostatic uplift in Scotland since *circa* 7,000 radiocarbon yrs. B.P..

Table 5.4 Inferred high water mark data associated with the *circa* 7,000 B.P. tsunami

Location	National Grid Codes	Coordinates		Elevation (m O.D.)
		x	y	z
Golspie	NH	28114	89908	4.12
Dounie	NH	27060	88640	5.01
Philorth	NK	40135	86404	-0.19
Ythan	NK	40056	82640	0.68
Easter Offerance	NS	25790	69630	10.36
Barnyards	NH	25254	84645	6.00
Moniack	NH	25050	85960	6.00
Munlochy	NH	26040	85030	6.10
Puggieston	NO	36984	76008	4.04
Creich	NH	26488	88878	4.72
Silver Moss	NO	34546	72345	4.39
Dryleas	NO	36678	76008	4.71
Fullerton	NO	36778	75658	4.71
Lochhouses	NT	36158	68214	2.04

The coordinates are derived from National Grid References and their origin refers to the False Origin of the National Grid.

In contrast to the data for the Main Postglacial Shoreline, the shoreline data associated with the synchronous deposition by the tsunami do not include errors of diachroneity, and thus may provide more accurate information on patterns of isostatic uplift. The comparison between the isobases of these two shorelines indicates a change of the centre of isostatic uplift between the tsunami event of *circa* 7,000 and the diachronous Main Postglacial Shoreline of 6,800 to 6,000 radiocarbon yrs B.P. (Figure 5.90). The quadratic trend

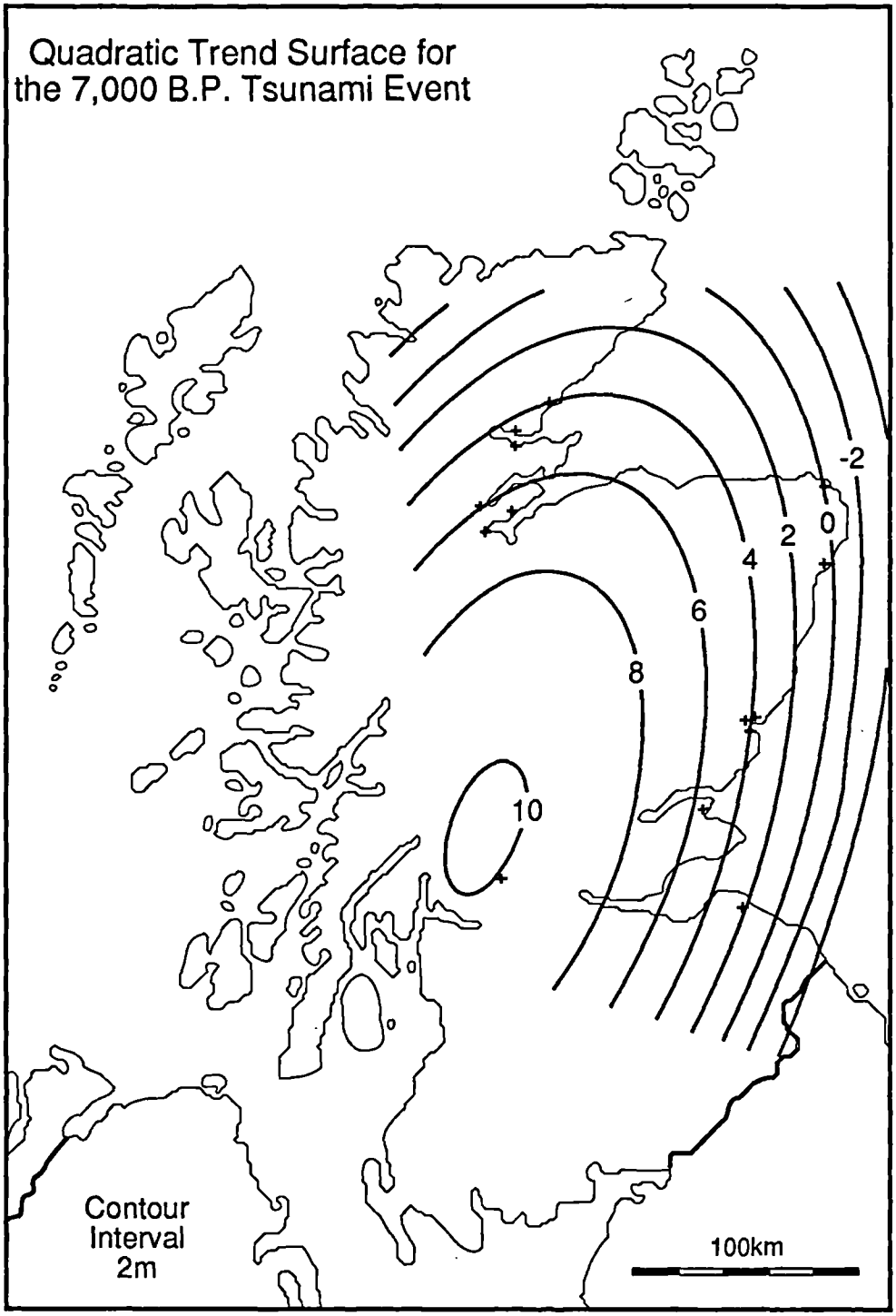

Figure 5.89. The isobases of the quadratic trend surface calculated from the inferred high water mark data.

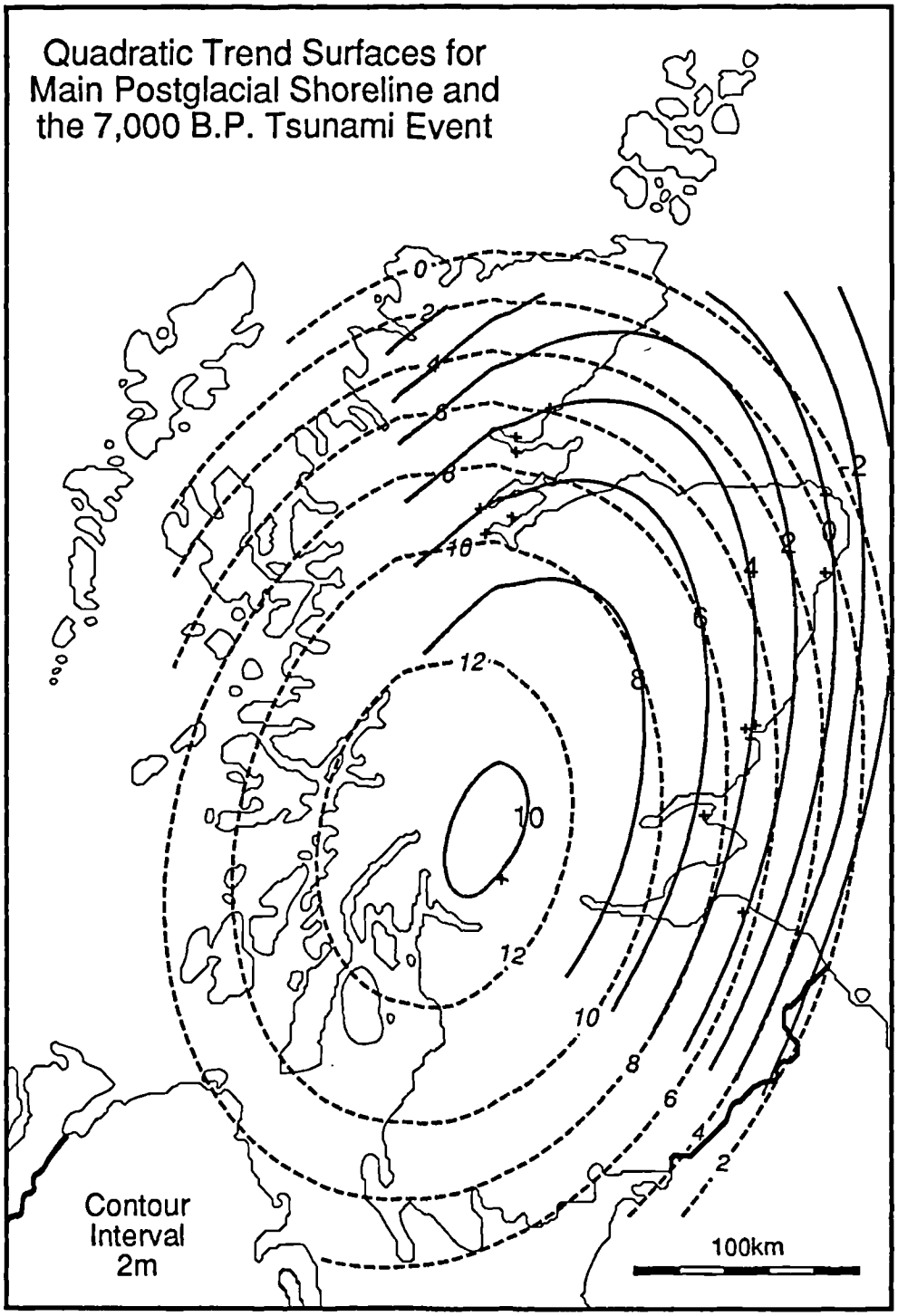

Figure 5.90. Comparison between the quadratic trend surfaces for the Main Postglacial Shoreline and the 7,000 B.P. tsunami event.

surface isobases for the Main Postglacial Shoreline are taken from Firth, Smith and Cullingford (1993). The quadratic surface of the Main Postglacial Shoreline is generally higher than that of the high water mark associated with the tsunami event. This is because relative sea level continued to rise after the tsunami had occurred, reaching its maximum at the culmination of the Main Postglacial Transgression.

However, both elliptical domes are only broad generalisations of the uplift patterns and the general patterns of the uplift isobases for the Main Postglacial Shoreline (6,800 - 6,000 yrs. B.P., Cullingford *et al.*, 1991) and the 7,000 B.P. tsunami event appear to differ from each other markedly. The dome defined by the latter appears to be more elongated than that of the former, in addition to a suggested westward shift in the centre of uplift from *circa* 7,000 to *circa* 6,500 yrs B.P. (Figure 5.90). It is important to point out that the reconstruction of the uplift patterns for the Main Postglacial Shoreline was based upon altitude measurements on quite different shore features. All the shoreline altitudes from eastern Scotland are derived from raised estuarine mudflats whereas the shorelines from western Scotland are made up of terraces from a number of marine environments including gravel terraces and rock platforms. These shorelines represented by marine terraces and rock platforms are poorly dated and are correlated with the Main Postglacial Shoreline on the premise that the latter forms the highest Holocene marine feature in the area (Firth *et al.*, 1993). In addition, it has been suggested that the Main Postglacial Shoreline may become progressively younger with increasing distance from the centre of isostatic uplift (Smith *et al.*, 1983; Cullingford *et al.*, 1991). Moreover, these altitude measurements were made in detail in some areas whereas in other areas the evidence for the shoreline is either fragmentary or absent. Consequently, the spatial distribution of the data points is rather clustered and trend surface analysis only presents a generalised statistical model of the shoreline uplift by taking all the data into account as a whole. In addition, in western Scotland where there is a general lack of data, an observation made recently by Shennan *et al.* (1994) indicates that the Main Postglacial Shoreline may have lower altitudes than estimates made from the isobases.

A limited number (15) of data points for the tsunami event, together with the clustered nature of their spatial distribution, pose a question of accuracy. In particular, a number of closely-spaced points present different values of shoreline elevation, so that the inferred contemporaneous high water marks at Dounie (5.01 m O.D.) and Creich (4.72 m O.D.) differ by 0.29 m, whilst that at Fullerton (4.71 m O.D.) differs from that at Puggieston (4.04 m O.D.) by 0.65 m. At first sight, these differences might appear to indicate that differential erosion by the tsunami might have occurred over the contemporaneous coastal areas, and that this might in turn explain the different patterns of the isobases for the 7,000 B.P. tsunami event and the Main Postglacial Shoreline. At present, this explanation should be considered speculative owing to the limited (15) number of available data points for the 7,000 B.P. tsunami shoreline. The fact that predicted elevation values calculated by trend surface analysis deviate significantly from the measured values at individual locations suggests that the isobases for the tsunami shoreline only provide a preliminary and general model until more data are available.

In addition to all the factors mentioned above, local variations such as possible shoreline dislocations, variations in altitude due to varied exposure and lithology and possible isostatic readjustment of the landmasses in part as individual blocks (e.g. Sissons, 1972; Firth *et al.*, 1993) may also reduce the accuracy and reliabilty of the isobase maps. For instance, Sissons (1972) and Firth *et al.* (1993) observed that dislocation of the Main Postglacial Shoreline may have occurred. By implication, it is possible also that the tsunami shoreline, which occurred before the Main Postglacial Shoreline, may also have been subject to neotectonic disturbances. Therefore, the isobase maps, especially for the tsunami shoreline, only provide generalised models of isostatic uplift and need to be refined and tested when more data become available.

Chapter 6
General Conclusion

The following text presents a summary of the findings made and existing problems identified during this research, presents a general conclusion of the research and and outlines areas of further research.

1. Methodology

It has been demonstrated in this research that laser particle size, geochemical and mineral magnetic analyses are suitable methods for high-resolution sedimentological investigation to provide detailed information on the depositional processes involved in the accumulation of the sediments studied. The methods used require only small quantities of sediment (10 to 20 gm) and thus enable samples to be taken at fine, often sub-centimetre, intervals. This is held to be of great practical value to obtaining detailed variations in the physical properties of sediment of limited thickness and to analysing the same samples simultaneously with different methods. Since the sediments studied in this research often do not possess distinctively visible textural or compositional variations and structure, the most obvious advantage of high-resolution analytical results is to enable internal variations to be detected,

revealed and defined by instrumental means. The most important advantage of analysing the same samples is to ensure that analytical results obtained with different techniques may be compared with confidence, without any uncertainties arising from relating possibly mismatched different depth-series.

Mineral magnetic analysis has been found to be useful in determining variations in the concentration of magnetic minerals, although it does not provide detailed information on the mineralogical composition of a sample on its own. In this research, it has been found that the variations in magnetic parameters such as susceptibility fluctuate distinctively in the form of pulses, marking bands of high concentrations of magnetic minerals. The main advantages of these are to allow the division of sediment into sublayers to be achieved and to provide further information on depositional processes when compared with other analytical results. In contrast, although it could be a useful technique, geochemical analysis as applied was found to provide only limited information and in this case proved to be a very tedious practice.

The Malvern laser granulometer (2600) used in this research proved to be rapid, of wide particle size coverage (1.9 μm to 1,880 μm) and the measurements obtained are of high reproducibility in contrast to other techniques including dry sieving, sedimentation (Sedigraph) and microscopy (Optomax). In particular, since the Malvern granulometer has both a high reproducibility and requires only a small quantity of sample (several grammes), it permits granulometric variations within the sediments studied to be determined at a far finer resolution and with more confidence than had previously been possible. It has been demonstrated in this research that detailed information obtained on contiguous samples enables changes in particle size composition to be revealed within thin samples of sediment so that a large amount of granulometric information becomes available and can be used for the reconstruction or interpretation of depositional processes with confidence, perhaps for

the first time.

However, there are distinctive differences between the results obtained with the Malvern and the results produced with other analytical techniques. This means that a large amount of information on particle size distributions of sediments obtained with other techniques, especially previously established analogues, can not be directly used for comparison with results from the Malvern results with confidence. Further studies are required in this area.

2. Tsunami sedimentation (coastal sedimentation processes of modern tsunami)

The study of the 1992 Flores tsunami undertaken during this research represents a detailed study of modern coastal sedimentation processes associated with tsunami inundation and presents detailed geomorphological accounts of the coastal impacts caused by the inundation of this large tsunami together with detailed investigation into the tsunami sediments with high-resolution particle size analysis. Conclusions and implications of coastal tsunami sedimentation processes can be drawn as follows:

The tsunami caused dramatic geomorphological effects up to a general level of approximately 3 m and a maximum level of 26 m above the contemporaneous sea level along the northern coast of the island of Flores and along the coasts of adjacent smaller islands, including large-scale erosion and deposition of coastal deposits including sand and coral boulders, morphological alteration of coastline, and stripping of the vegetation cover.

The Flores study shows clearly that tsunami flooding is associated with both seaward and landward sediment movement and the deposition of sediment at levels considerably higher than the modern coastal zone. The observation made of the sediment deposition as a result of tsunami inundation indicates that tsunami sediments upon coastal lowlands may often form widespread sediment sheets but that the maximum flood levels generally exceed the

maximum landward limits of the sediments. Moreover, the Flores study shows that tsunami backwashes can be powerful enough to carry seawards and re-deposit a large amount of terrestrial material and cause intensive erosion of coastal lands.

Although the Flores tsunami sediment was visually observed not to display distinctive structure or grading, its characteristics as defined by particle size analysis exhibits multiple sets of grading (fining-upward) sequences and a general trend of landward-fining, as a result of spatial changes in particle size composition. Particle size analysis also reveals that the particle size composition of the sediment varies from well sorted to poorly sorted and is controlled by both the characteristics of the source sediment (local coastal sediments) and sedimentation processes associated with tsunami inundation.

The sedimentation processes are theoretically inferred here to include modification of eroded/transported source sediment as a combined result of the seaward transportation of fine fractions of the sediment and sorting processes associated with landward transportation and sediment accretion. The net accretion of sediment in general is believed to be a complex product of accumulation and erosion. The final (post-tsunami) sediment accumulation is believed to reflect episodic rapid deposition of sediment in which transported particles of different subpopulations are released simultaneously but settle out at different rates. However, it is difficult, at present, to attribute subunits of the sediment accumulation defined by particle size analysis to individual processes of tsunami runup and backwash. A conceptual model of coastal sedimentation processes associated with tsunami inundation has been established, as detailed Chapter 4.

It is also concluded here that the results of particle size analysis do not necessarily facilitate the estimation of energy magnitudes of tsunami inundation currents due to the controlling factor of the characteristics of the source sediment. The current energy can be severely

underestimated from particle size parameters.

3. The Storegga tsunami (investigation into palaeo-tsunamis)

The stratigraphical and sedimentological investigation into a widespread sand layer at various sites along the eastern coast of Scotland reveals that the layer represents a low-frequency, high-energy marine event, is intercalated between estuarine silty clay and terrestrial peat accumulations of Holocene age and extends up to levels above local highest elevations reached by sea levels associated with the Main Postglacial Shoreline. The marine origin of the sand layer is determined by stratigraphical evidence and published microfossil evidence (pollen and diatom). The anatomy of the seemingly structureless sand layer has been defined by particle size analysis at all sites studied, and with mineral magnetic analysis at two sites (Dounie and Creich, in the Dornoch Firth) and contains multiple sets of fining-upward sequences and often a general fining-landward trend. The particle size characteristics of the sediments are represented by multimodal distributions or of a prominent sand population amalgamated with a distinctive proportion of finer-grained populations, frequently together with a large amount of mica (of low specific density), distinctively different from the characteristics of the sediments deposited through wave and wind actions, e.g. processes associated with beach and dune formation. It is interpreted that the sediments were accumulated through episodic rapid depositional processes associated with turbulent marine flooding. At two sites (Dounie and Creich), mineral magnetic analysis marks out bands of enriched concentrations of magnetic minerals, which are found in general to correspond to but offset the coarsest calibres of the sediment. Thus, it is interpreted that sorting of the sediment during deposition occurred not only according to particle size but to the specific densities of the grains since magnetic mineral grains are heavier than non-magnetic grains (such as quartz) comprising the largest proportion of the sediment. At all sites except one (Dounie), it is believed that the source sediment for the layer was largely drawn from former estuarine mudflats while at Dounie it was derived largely from a buried sand and shingle ridge, thought to have been overwhelmed and

breached by the flooding event.

With modern analogues, established in this dissertation, of both tsunami and storm surge sedimentary characteristics and sedimentation processes as the key, competing hypotheses of the likely causes of the marine flooding by either a tsunami event or storm surge during the Holocene have been tested during this research. It is concluded here that the low-frequency and high-energy marine flooding event represents a major tsunami, which was initially proposed by Dawson *et al.* (1988) to have been generated by the Second Storegga submarine landslide off the western coast of Norway. The slide was dated between *circa* 8,000 and 6,000 radiocarbon yrs B.P. (Jensen *et al.*, 1987). The dating of the event suggests that it took place at *circa* 7,000 B.P., prior to the culmination of the Main Postglacial Transgression, which is determined from available radiocarbon dates obtained with peat samples associated with the layer.

Sediment runup heights at various sites have been estimated from stratigraphical evidence, based on the difference in altitude between the uppermost limits of the tsunami deposit and the contemporaneous high water mark. The determination of the high water mark follows the definition proposed by Dawson *et al.* (1988), that is the boundary between terrestrial and marine or estuarine deposits underlying the tsunami layer, i.e. underlying peat and estuarine silty clay in this case. The runup heights of continuous sediments associated with the Storegga tsunami are generally about 2 metres along the eastern coast of Scotland. As indicated in the Flores study, tsunami flood levels are generally much higher than the levels reached by associated deposition of sediment and sedimentary sheets may be continuous as well as discontinuous. Consequently, it is considered that the tsunami runup values (flood levels) may have been much higher and could be underestimated from the stratigraphical evidence of the sediments. It is speculated here that flooding evidence could be recovered from areas farther inland from the landward limits of the continuous sediments through the

use of microbiological approaches, such as diatom analysis.

It is also concluded here that depth-particle size series can not be used to correlate with time-amplitude series of mathematically simulated sea surface fluctuations since accumulation rates could have been quite variable during the formation of the sediments. Furthermore, tsunami sedimentation processes have been found to be very complex as revealed in the study of the Flores tsunami. It was previously thought that five tsunami waves could be inferred from the results of particle size analysis (Dawson *et al.*, 1991). However, further particle size analysis and the study of the Flores tsunami sediments reveals that there is great spatial variability in the number of fining-upward sequences. At present, difficulty exists in the inference of sedimentary contributions by individual processes of tsunami runup and backwash.

4. Comparison of the Flores and Second Storegga Slide tsunamis

The Flores and Second Storegga Slide tsunamis clearly differ in their mechanisms of generation. The former was due to submarine faulting associated with a major earthquake and the latter is attributed to the consequences of a large scale submarine slide. This difference in generation mechanism gives rise to differences in the characteristics of consequent tsunami wave forms, such as wave periods and wavelengths. For both tsunamis, no instrumentally measured data are availabe for a definitive comparative study of the hydrodynamic characteristics and only estimates derived from numerical modelling are available (Imamura, 1994 and Harbitz, 1991, 1992), whilst turbulent flooding processes were described by eyewitnesses of the Flores tsunami.

For the Flores tsunami, Imamura (unpublished report, 1993) estimated the likely mechanisms of faulting and associated crustal deformation and in turn numerically simulated the subsequent tsunami waves based on the information on the magnitude of the

Flores earthquake and aftershock locations. The results indicated predicted tsunami runup values in the magnitude of several metres and a wave period of between 10 to 20 minutes, although the wave parameters vary markedly between coastal areas. It is generally understood that the characteristics of tsunami waves are partly controlled by the local bathymetry and coastal configuration, but in modelling to date this has not been taken into account.

Studying the Storegga tsunami, Harbitz (1991) noted that the characteristics of tsunami waves for relatively slow bed motion such as for submarine slides, are strongly dependent on the time-displacement history of the movement, i.e. velocity. Harbitz referred to the empirical results of flood runup as defined from geological evidence and thereby estimated the most probable velocity of the slide motion and in turn simulated the likely tsunami wave forms propogating across the open seas. From the simulated wave forms, the period of the primary waves at points off the eastern coast of Scotland were estimated as 2.83 and 2.57 hours. It is important to note here that the coastal hydrodynamics and wave characteristics of the Second Storegga tsunami runup processes were not reconstructed by numerical simulation. At present, tsunami runup processes have not been sufficiently well simulated with any numerical models to assist in the reconstruction of geomorphic and sedimentary processes, even when better empirical information is available as in the case of Flores tsunami (e.g. Imamura, 1994) due to non-linearity, and have been avoided by most of modellers. The difficulty arises largely from uncertainties of local topographical effects including resonance, interference, focusing or trapping of wave energy. As a result, any discussion on the nature of inundation associated with the Second Storegga tsunami remains speculative. Assuming the period of the Second Storegga tsunami to be about 2.5 hours and runup values to be in the order of several metres, the tsunami inundation might have taken place at a relatively gentle rate. Due to this, it might not have caused great geomorphologic impact on the open coasts of eastern Scotland although it might have flooded up to such a

level. However, the sea surface fluctuations due to the Storegga tsunami in the outer estuarine areas could have produced bores or resonance waves, which propagated inland, broke suddenly and caused significant geomorphic changes. If this were true, the erosion, transportation and deposition of the sediments studied could have been due to the breaking of the tsunami bores or resonance waves due to local bathymetric conditions within estuarines. However, since the characteristics of the tsunami remain almost unknown in these aspects and detailed runup processes can not be reconstructed and such speculation is probably unwarranted at present.

In the case of the Flores tsunami, the sediment has been found to generally lack particles finer than sand. By contrast, the Storegga tsunami sediment generally consists of a considerable portion of fine particles (silt and clay) in addition to a predominent sand fraction. This difference in composition is believed to reflect the type and availability of sediments at the time of inundation in the coastal areas concerned. In Flores, there was a general lack of loose sediment on the coral reefs and only a limited amount of sand size sediment present in the beaches. Here, the tsunami sediment in Flores appears to have been derived largely from coastal sandy soil, which contains only a small amount of silt and clay and is not cohesive in nature. Because of this lack of cohesion, the silt and clay was easily dispersed in tsunami currents and removed by backwash. However, in Scotland, the sites investigated lie largely in estuarine areas, where the sediment contains abundant estuarine silt and clay accumulations with only sporadic sand bodies in areas. The sediments were largely cohesive and during the short period of tsunami inundation, the sediments could not have been dispersed sufficiently and sorted apart in the transporting tsunami currents, and may have been deposited simultaneously or partly left behind by backwashes. The different characteristics of the tsunami sediments in Scotland and Flores are thus considered as reflecting the nature of sediment supply.

Although the source of sediments imposes control over the characteristics of the sediments deposited by tsunamis, the spatial variations in particle size composition within the sediments in Flores and Scotland share similar patterns and trends of variation, reflecting consequences caused by sedimentary processes. The spatial patterns and trends of particle size variation are considered to be related to the ways in which sediments were deposited. This is considered important with respect to the identification of sediment layers deposited by tsunamis and the interpretation of coastal sedimentary sequences. The evidence of recent tsunamis such as the Flores tsunami bears important implications for the interpretation of the evidence for ancient tsunamis, as in the case of the deposits found in Scotland. For instance, as indicated by the Flores evidence, tsunami flooding in Scotland could have reached levels well above the upper sediment limit. This implies that stratigraphically determined runup values only provide minimal estimates of flood heights. Since the actual flood level above the sea surface level contemporaneous to the tsunami is virtually unknown, the runup values adopted for numerical models by Harbitz (1991) and by Henry and Murty (1992) may well be substantially underestimated. This implies that the velocity of the Second Storegga Slide may have been considerably underestimated in numerical models. Until more detailed geomorphological and stratigraphical evidence of this tsunami becomes available, numerical models will remain at best very general reconstructions of the events investigated.

5. Future research

As indicated above and in the text of this dissertation, further studies are required to improve our understanding of tsunami sedimentation processes and our ability to identify palaeotsunami deposits. Recent tsunamis provide evidence for such studies. Following the 1992 Flores tsunami, several large tsunamis have recently occurred including the 1993 tsunami in Hokkaido, Japan, the 1993 tsunami in Java, Indonesia and the 4th October 1994 tsunami in the southern Kurile islands. Some cores of the sediments deposited by the 1993 Hokkaido tsunami and the 1993 Java tsunami are presently under investigation. It is hoped

that further sedimentological information on modern tsunami sedimentary characteristics and sedimentation processes can be obtained to help confirm or improve the models established during this research.

As indicated in the study of the palaeo-tsunami sediments preserved in the sedimentary sequences along the eastern coast of Scotland, better dating of the event is required. It is considered here that the radiocarbon dating method can not offer dates of high accuracy with good confidence, and that the tsunami could have just lasted for a few hours or even less. Thermoluminescence dating is generally regarded as an alternative dating method and is generally thought to provide supplementary dating. However, it is uncertain whether the Storegga tsunami occurred during daytime or at night and thus it is considered the thermoluminenscence dating method is unsuitable here since sediment is required to be exposed to sunlight for radioactive signals to be zeroed. It is envisaged here that dendrochronological dating may provide a more accurate age for the event since there are established dendrochronological timetables and it may provide dates accurate to an annual base. It is thought that the tsunami could have caused widespread destructive effects upon coastal vegetation and sites may exist where trees were felled during the tsunami. The study of felled trees may provide the opportunity for improved dating when matched to the well-established dendrochronology of the Holocene.

Although mineral magnetic analysis has provided important information on the changes in the concentration of magnetic minerals within the Storegga tsunami sediments, it is thought that detailed mineralogical studies with more direct methods in the future may provide further information to disclose mineralogical changes as a result of sedimentation and to allow the characteristics of the tsunami sediments to be defined in such a context.

In parallel with the possible further studies of tsunami sedimentation processes, methodologies can also be further developed and refined. For instance, comparison of the results obtained with Malvern laser granulometer and other methods may provide conversion schemes or guidances for utilizing data and sediment characterisations made with other methods.

6. Final remarks

The results contained in this Ph.D. dissertation are intended to contribute to an understanding of tsunami sedimentary characteristics and sedimentation processes. Although it is by no means comprehensive, it attempts to provide detailed information in this subject for the first time and it is hoped that such information can contribute to knowledge in geomorphology and sedimentology and provide a stepping stone for future study.

References

Adams, J., 1990. Paleoseismicity of the Cascadia Subduction Zone: Evidence From Turbidites off the Oregon-Washington Margin. Tectonics, 9, pp.569-583.

Aigner, Thomas and Reineck, Hans-Erich, 1982. Proximality Trends in Modern Storm Sands from the Heligoland Bight (North Sea) and their Implications for Basin Analysis. Senchkenbergiana Maritima, PT14, pp.183-215.

Allen, J. R. L., 1985. Principles of Physical Sedimentology. Chapman & Hall.

Allen, T., 1990. Particle Size Measurement, Chapman and Hall.

Analytical Instruments Ltd.. Optomax Image Analyzer Manual. Shire Hill Industrial Estate, Saffron Walden, Essex, CB11 3AQ.

Andrade, C., 1992. Tsunami Generated Forms in the Algarve Barrier Islands, In: A. G. Dawson (Editor), European Geophysical Society 1992 Tsunami Meeting. Science of Tsunami Hazards, 10, pp.21-34.

Atwater and Yamaguchi, 1991. Sudden, probably coseismic submergence of Holocene trees and grass in coastal Washington State. Geology, Vol. 19, pp.706-709.

Atwater, B. A., 1987. Evidence for Great Holocene Earthquakes Along the Outer Coast of Washington State. Science, 236, pp.942-944.

Atwater, B. A., 1992. Geologic Evidence for Earthquakes During the Past 2,000 Years Along the Copalis River, Southern Coastal Washington. Journal of Geophysical Research, 97, B2, pp.1901-1919.

Atwater, B. F. and Yamaguchi, D. K., 1991. Sudden, probably coseismic submergence of Holocene trees and grass in coastal Washington State. Geology, 19, pp.706-709.

Atwater, B. F., 1986. Evidence for Great Holocene Earthquakes along the Outer Coast of Washington State. Science, 236, 942-944.

Bernhardt, C., 1988. Preparation of suspension for particle size analysis. methodical recommendations, liquids and dispersing agents: Advances in Colloid and Interface Science, 29 (1988) 79-139. Elsevier Science Publishers B.V..

Bjorck, S., Dearing, J. A. and Jonsson, 1982. Magnetic susceptibility of Late Weichselian deposits in southeastern Sweden. Boreas, Vol. 11, pp.99-111.

Bondevik, S. and Svendsen, J. I., 1993. Paleotsunamis in the Norwegian Sea and the North Sea. Interim report of GITEC project undertaken for the European Community Commission, unpublished. University of Bergen, Allegatn 41, N-5007 Bergen, Norway.

Bondevik, S., Gusiakov, V., Kurbatov, A., Melekestsev, I., Minoura, K. and Svendsen, J., 1994. Investigation of Geological Traces of Paleotsunamis in Kuril-Kamchatka Region. Report on the 1993 summer field works on the east coast of Kamchatka. Novoshibirsk.

Bourgeois, J., 1993. Tsunami Deposits From 1992 Nicaragua Event: Implications for Interpretation of Palaeotsunami Deposits. EOS Abstracts, O32C-7, 350, American Geophysical Union 1993 Fall Meeting, San Franscisco.

Bourrouilh-Le Jan, F. G. and Talandier, 1985. Sedimentation et Fracturation de Hautes Energie en Milieu Recifal: Tsunamis, Ouragans et Cyclones et Leurs Effets sur la Sedimentologie et la Geomorphologie d'un Atoll: Motu et hoa, a Rangiroa, Tuamotu, Pacifique SE. Marine Geology, 67, pp.263-333.

Brenchley, Patrick J., Newall, Geoffrey and Stanistreet, Ian G., 1979. A Storm Surge Origin for Sandstone beds in an Epicontinental Platform Sequence, Ordovician, Norway. Sedimentary Geology, 22, pp.185-217.

Bryant, E. A., Young, R. W. and Price, D. M., 1994. Tsunamis as a major control on coastal evolution, Southeastern Australia (unpublished manuscript).

Bugge T., 1983. Submarine slides on the Nowegian continental margin, with special emphasis on the Storegga area. Continental Shelf Inst. Publ., 110, 152pp.

Bugge T., Befring S., Belderson R. H., Eidvin T. Jansen E., Kenyon N., Holtedahl H. and Sejrup H. P., 1987. A giant three-stage submarine slide off Norway. Geo-Marine Letters 7:191-198.

Bugge T., Belderson R. H. and Kenyon N. H., 1988. The Storegga Slide. Phil. Trans. R. Soc. Lond. A 325, 357-388.

Clague, J. J. and Bobrowsky, P. T., 1994. Evidence for a Large Earthquake and Tsunami 100-400 Years Ago on Western Vancouver Island, British Columbia. Quaternary Research, 41, pp.176-184.

Clague, J. J., Bobrowsky, P. T. and Hamilton, T. S., 1994. A Sand Sheet Deposited by the 1964 Alaska Tsunami at Port Alberni, British Columbia. Estuarine, Coastal and Shelf Science, 38, pp.413-421.

Clarke, S. H., Jr. and Carver, G. A., 1992. Late Holocene Tectonics and Paleoseismicity, Southern Cascadia Subduction Zone. Science, 255, pp.188-192.

Coles, J., 1971. The early settlement of Scotland: excavations at Morton, Fife. Proc. Prehist. Soc., 37, 2, 284-366.

Cullingford R. A., Caseldine C. J. and Gotts P. E., 1989. Evidence of early Flandrian tidal surges in Lower Strathearn, Scotland. Journal of Quaternary Science, 4(1), 51-60.

Cullingford R. A., Smith D. E. and Firth C. R., 1991. The Altitude and Age of the Main Postglacial Shoreline in Eastern Scotland. Quaternary International, Vol. 9, pp.39-52.

Cullingford, R. A., Caseldine, C. J. and Gotts, P. E., 1980. Early Flandrian sea level changes in lower Strathearn. Nature 184, pp.159-61.

Darienzo, M. E. and Peterson, C. D., 1990. Episodic Tectonic Subsidence of Late Holocene Salt Marshes, Northern Oregon Central Cascadia Margin. Tectonics, 9, pp.1-22.

Darienzo, M. E., Peterson, C. D. and Clough, C., 1994. Stratigraphical evidence for great subduction-zone earthquakes at four estuaries in northern Oregon, U.S.A.. Journal of Coastal Research, 10 (4), pp.850-876.

Dawson A. G., Long D. and Smith D. E., 1988. The Storegga Slides: evidence from eastern Scotland for a possible tsunami. Marine Geology, 88, 271-276.

Dawson, A. G., 1980. Shore erosion by frost: an example from the Scottish Lateglacial. In J. M. Gray and J. J. Lowe (eds.), Studies in Lateglacial Environment of NW Europe, Pergamon Press, pp.45-53.

Dawson, A. G., 1984. Quaternary sea-level changes in western Scotland. Quaternary Science Reviews, Vol. 3, pp.345-368.

Dawson, A. G., Foster, I. D. L., Shi, S., Smith, D. E. and Long, D., 1991. The identification of tsunami deposits in coastal sediment sequences. Science of Tsunami Hazards, 9, 1, 73-82.

Dawson, A. G., Long, D., Smith, D. E., Shi, S. and Foster, I. D. L., 1993. Tsunamis in the Norwegian Sea and North Sea caused by the Storegga submarine landslides. In S. Tinti (ed.), Tsunamis in the world, Kluwer Academic Publishers, Netherlands, pp.31-42.

Dawson, A. G., Shuto, N. and Takahashi, T., 1995. Tsunami sedimentation associated with the Java earthquake of 1994. Tsunami Symposium, XXI IUGG General Assembly, Boulder, Colorado, Paper OA12A-07.

Dawson, A. G., Smith, D. E. and Long D., 1990. Evidence for a Tsunami from a Mesolithic Site in Inverness, Scotland. Journal of Archaeological Science 1990, 17, 509-512.

de Meijer R. J., Lesscher H. M. E., Schuiling R. D. and Elburg M. E., 1990. Estimate of the heavy mineral content in sand and its provenance by radiometric methods. Nucl. Geophys. Vol. 4, No.4., pp.455-460.

de Meijer R. J., Put L. W., Schuiling R. D., de Reus J. H. and Wiersma J., 1988. Provenance of coastal sediments using natural radioactivity of heavy mineral sands. Radiation Protection Dosimetry, Vol. 24, No. 1/4, pp.55-58.

Dearing, J., 1994. Environmental magnetic susceptibility - using the Bartington MS2 system. Chi Publishing, Kenilworth, U.K..

Firth C. R. and Haggart B. A., 1989. Loch Lomond Stadial and Flandrian shorelines in the inner Moray Forth area, Scotland. Journal of Quaternary Science, 4, 37-50.

Firth C. R., Smith D. E. and Cullingford R. A., 1993. Late Devensian and Holocene Glacio-isostatic Uplift Patterns in Scotland. Quaternary Proceedings No.3, Quaternary Research Association, Cambridge, pp. 1-14.

Foster, I. D. L., Albon, A. J., Bardell, K. M., Fletcher, J. L., Jardine, T. C., Mothers, R. J., Pritchard, M. A. and S. E. Turner, 1991. High energy coastal sedimentary deposits: an evaluation of depositional processes in southwest England. Earth Surface Processes and Landforms, 16, pp.341-356.

Foster, I. D. L., Albon, A. J., Bardell, K. M., Fletcher, J. L., Jardine, T. C., Mothers, R. J., Pritchard, M. A. and Turner, S. E., 1991. High Energy Coastal Sedimentary Deposits: An Evaluation of Depositional Processes in Southwest England. Earth Surface Processes and Landforms, 16, pp.341-356.

Friedman, G. M., 1961. Distinction between dune, beach and river sands from textural characteristics. J. Sedim. Petrol., 31, 514-529.

Friedman, G. M., 1962a. Comparison of moment measurements for sieving and thin-section data in sedimentary petrological studies. Jour. Sed. Pet. 32, 15-25.

Friedman, G. M., 1962b. On sorting, sorting coefficients, and the lognormality of the grain-size distribution of sandstones. J. Geol. 70, 737-756.

Friedman, G. M., 1979. Differences in size distributions of populations of particles among sands of various origins. Sedimentology, 26, 3-32.

Gadow, S. and Reineck, H.-E., 1969. Ablandiger Santransport bei Sturmfluten. Senckenbergiana marit., 1, pp.63-78.

Gilbert, G. K., 1897. Recent earth movement in the Great Lakes region. U. S. Geol. Survey, 18th Ann. Rep. part ii, p.601.

Gray J. M., 1974. The Main Rock Platform of the Firth of Lorn, Western Scotland. Transactions of the Institute of British Geographers, 61, 81-99.

Gray J. M., 1978. Low-level shore platforms in the south-west Scottish Highlands: altitude, age and correlation. Transactions of the Institute of British Geographers, New Series, 3, 151-164.

Gusiakov, S., 1993. Filename "flo-history-9". In: Tsunami Data Repository. Internet address: tsunami@noaapmel.gov (electronic publication).

Haggart B. A., 1982. Flandrian sea-level changes in the Moray Firth area. Unpublished PhD thesis, University of Durham.

Haggart B. A., 1986. Relative sea-level change in the Beauly Firth Scotland. Boreas, 15, 191-207.

Haggart B. A., 1988. The stratigraphy, depositional environment and dating of a possible tidal surge deposit in the Beauly Firth area, north-east Scotland. Palaeogeography, Palaeoclimatology, Palaeoecology, 66, 215-30.

Haggart, B. A., 1987. Relative se-level changes in the Moray Firth area, Scotland. In: M. J. Tooley and I. Shennan (Editors), Sea Level Changes. Blackwell. Oxford. pp.67-108.

Haggart, B. A., 1989. Variations in the pattern and rate of isostatic uplift indicated by a comparison of Holocene sea-level curves from Scotland. Journal of Quaternary Science, 4, 67-76.

Hansom, J. D. and Briggs, D. J., 1991. Sea-level change in Vestfirdir, northwest Iceland. In J. K. Maizels and C. Caseldine (eds.) Environmental Change in Iceland: Past, Present and Future, Kluwer Academic Publishers, Dordrecht, pp.79-91.

Harbitz, C. B., 1991. Model simulations of tsunami generated by the Storegga Slides. Institute of Mathematics, University of Oslo, Series No.5, 30pp.

Harbitz, C. B., 1992. Model simulations of tsunamis generated by the Storegga Slides. Marine Geology, Vol.105, pp.1-21.

Hatch, T. and Choate, S. P., 1929. Stratigraphical description of the size properties of non-

uniform particular substances. J. Franklin Inst., 207, 369-387.

Heaps, N. S. 1967. Storm surges. In Oceanography and Marine Biology, H. Barnes (ed.), Vol. 5, 11-47. London: Allen & Unwin.

Heaps, N. S. 1983. Storm surges, 1967-82. Geophys. J. R. Astron. Soc. 74, 331-76.

Heath, R. A., 1979. Significance of storm surges on the New Zealand coast. N. Z. J. Geol. Geophys., 22, pp.259-266.

Henry, R-F. and Murty, T. S., 1992. Model studies of the effects of the Storegga Slide Tsunami. Science of Tsunami Hazards, Vol.10, No.1, pp.51-62.

Hutcheson, A., 1886. Notice of the discovery of a stratum containing worked flints at Broughty Ferry, Proc. Soc. Antiquities, Scotland, 20, 166-169.

Imamura, F., 1994. Study on some problems of the 1992 Indonesian Flores island tsunami. In: "Proceedings of the Conference of 9th Asian and Pacific Division of the International Association for Hydraulic Research, Singapore", August 24-26.

Jaggar, T. A., 1946. The great tidal wave of 1946. Natural History, PT.55, pp.263-268.

Jamieson, T. F., 1865. On the history of the last geological changes in Scotland. Quarterly Journal of the Geological Society of London, 21, 161-203.

Jansen, E., Befring, S., Bugge, T., Eidvin, T., Holtedahl, H. and Sejrup, H. P., 1987. Large submarine slides on the Norwegian continental margin: Sediment transport and timing. Marine Geology, 78. pp.77-107.

Jardine, W. G., 1982. Sea-level changes in Scotland during the last 18,000 years. Proceedings of the Geologists' Association, 93, 25-41.

Kane, W. T. and Hubert, J. F., 1963. Fortran program for calculation of grain-size textural parameters on the IBM 1620 computer. Sedimentology 2, pp.87-90.

Kawana, T. and Nakata, T., 1994. Timing of Late Holocene Tsunamis Originated Around the Southern Ryukyu Islands, Japan, Deduced From Coralline Tsunami Deposits. Journal of Geography, 103 (4), pp.352-376 (in Japanese).

Krumbein, W. C., 1936. Application of logarithmic moments to size frequency distribution of sediments. Jour. Sed. Pet. 6, 35-45.

Lacaille, A. D., 1954. The Stone Age in Scotland. Wellcome Historical Medical Museum, Oxford, 345pp.

Lambeck K., 1993a. Glacial rebound of the British Isles - I. Preliminary model results. Geophys. J. Int., 115, 941-959.

Lambeck K., 1993b. Glacial rebound of the British Isles - II. A high-resolution, high precision model. Geophys. J. Int., 115, 196-990.

Lemke, R. W., 1967. Effects of the earthquake of March 27, 1964, at Seward, Alaska - U. S. Geological Survey Professional Paper 542-E. The Alaska Earthquake, March 27, 1964: Effects on Communities.

Linick, T. W., Long, A., Damon, P. E. and Ferguson, C. W., 1986. Radiocarbon, 28, 943-953.

Long D., Dawson A. G. and Smith D. E., 1989. Tsunami risk in northwestern Europe: a Holocene example. Terra Nova, 1, 532-537.

Long D., Smith D. E. and Dawson A. G., 1989. A Holocene tsunami deposit in eastern Scotland. Journal of Quaternary Science, 4 (1), pp.61-66.

Malcolm, C. W., 1981. More skewed against than skewing. In: S. -D. Nio, R. T. E. Shuttenhelm and Tj. C. E. Van Weering (eds), "Holocene Marine Sedimentation in the North Sea Basin". Special publication Number 5 of the International Association of Sedimentologists. Blackwell Scientific Publications.

Malvern Instruments, 1989. Series 2600 - User Manual. Spring Lane South, Malvern, Worcs. WR14 1AQ, U.K..

McBride, E. F., 1971. Mathematical treatment of size distribution data. In Carver: Procedures in Sedimentary Petrology. Wiley. New York.

McCave, I. N., Bryant, R. J., Cook, H. F., and Coughanowr, C.A., 1986. Evaluation of a

Laser-diffraction-size Analyse for Use With Natural Sediments: Journal of Sedimentary Petrology, v. 56, p.561-564.

McCave, I. N., Manighetti, B. and Robinson, S. G., 1995. Sortable Silt and Fine Sediment Size/Composition Slicing: Parameters for Palaeocurrent Speed and Palaeoceanography. Paleoceanography (in press).

McInelly, G. W. and Kelsey, H. M., 1990. Late Quaternary Tectonic Deformation in the Cape Arago-Bandon Region of Coastal Oregon as Deduced From Wave-Cut Platforms. Journal of Geophysical Research 95, No. B5, pp.6699-6713.

Miller, B. V., Lines, R. W., 1988. Recent advances in particle size measurements: A critical review: CRC Critical Reviews in Analytical Chemistry, Vol. 20, Issue 2, 1988.

Miller, D. J., 1960. Giant waves at Lituya Bay, Alaska -U. S. Geological Survey Professional Paper 354-C.

Minoura K. and Nakaya S., 1991. Traces of tsunami preserved in inter-tidal lacustrine and marsh deposits: some examples from Northeast Japan. Journal of Geology, Vol. 99, pp.265-287.

Minoura, K. and Nakata, T., 1994. Discovery of an Ancient Tsunami Deposit in Coastal Sequences of Southwest Japan: Verification of a Large Historic Tsunami. The Island Arc, 3, pp.66-72.

Minoura, K. and Nakaya, S., 1991. Traces of Tsunami Preserved in Inter-tidal Lacustrine and Marsh Deposits: Some Examples From Northern Japan. Journal of Geology, 99, pp.265-287.

Minoura, K., Nakaya, S. and Uchida, M., 1994. Tsunami Deposits in a lacustrine Sequence of the Sandriku Coast, Northern Japan. Sedimentary Geology, 89, pp.25-31.

Moore, G. W. and Moore, J. G., 1988. Large-scale Bedforms in Boulder Gravel Produced by Giant Waves in Hawaii. In: H. E. Clifton (Editor), Sedimentologic Consequences of Convulsive Geologic Events. Geol. Soc. Am. Spec. Pap., 229, pp.101-110.

Moore, G. W. and Moore, J. G., 1988. Large-scale bedforms in boulder gravel produced by giant waves in Hawaii. In: H. E. Clifton (Editor), Sedimentologic Consequences of

Convulsive Geologic Events. Geol. Soc. Am. Spec. Pap., 229, 101-110.

Moore, J. G. and Moore, G. W., 1984. Deposit From a Giant Wave on the Island of Lanai, Hawaii. Science, 226, pp.1312-1315.

Moore, J. G. and Moore, G. W., 1984. Deposit from a giant wave on the island of Lanai, Hawaii. Science, 226, pp.1312-1315.

Moore, J. G., Clague, D. A., Holcom, R. T., Lipman, P. W., Normark, W. R. and Torresan, M. E., 1989. Prodigious Submarine Landslides on the Hawaiian Ridge. Journal of Geophysical Research, 94, pp.17465-17484.

Moore, J. G., Normark, W. R. and Gutmacher, C. E., 1992. Major Landslides on the Submarine Flanks of the Manua Loa Volcano, Hawaii. Landslide News, pp.13-16.

Morrison, J., Smith, D. E., Cullingford, R. A. and Jones, R. L., 1981. The culmination of the Main Postglacial Transgression in the Firth of Tay area, Scotland. Proceedings of the Geologists' Association, 92, 197-209.

Myles, D., 1985. The Great Waves. Robert Hale. London.

Nelson, A. R. and Atwater, G. F., 1993. Radiocarbon Dating of Earthquake-Killed Plants Along the Cascadia Subduction Zone. EOS (Transactions of the American Geophysical Union) 74, no. 43, October 26, 1993/supplement, 199-200.

Nelson, A. R., 1992. Contrasting Styles of Late Holocene Relative Sea-Level Changes Revealed by Tidal-Marsh Stratigraphy, South-Central Oregon Coast, Cascadia Subduction Zone. In: C. P. Fletcher and J. F. Wehmiller (Editors), Quaternary Coasts of the United States - Marine and Lacustrine Systems. SEPM-IGCP Special Publication no. 48, pp.287-301.

Nelson, A. R., Ota, Y., Stafford, T. W., Jr., Umitsu, M., Kashima, K. and Matsushima, Y., 1992. High-Precision Accelerator-Mass-Spectrometer Radiocarbon Dating of Buried Tidal-Marsh Soils - An Approach to Estimating the Frequency and Coastal Extent of Subduction Zone Earthquakes in Oregon and Washington. Proceedings of the U.S. Nuclear Regulatory Commission, Nineteenth Water Reactor Safety Information Meeting, Vol. 3, NUREG/CP-0119, pp.261-276.

Newey, W. W., 1965. Post-glacial vegetational and climatic changes in part of south-east Scotland as indicated by the pollen-analysis and stratigraphy of some of its peat and lacustrine deposits. Unpublished Ph.D. thesis, University of Edinburgh.

Paskoff, R., 1991. Likely Occurrence of a Mega-tsunami Near Coqimbo, Chile. Revista Geologica de Chile, 18, pp.87-91.

Pearson, G. W., Becker, B. and Qua, F., 1993. Radiocarbon, 35, 93-104.

Pirazzoli, P. A., Montaggioni, L. F., Salvat, B. and Faure, G., 1988. Late Holocene Sea Level Indicators From Twelve Atolls in the Central and Eastern Tuamotos (Pacific Ocean). Coral Reefs, 7, pp.57-68.

Reineck, H.-E. and Singh, I. B., 1971. Der Golf von Gaeta (Thyrrhenisches Meer). III. Die Geguge von Vorstrand- und Schelfsedimenten. Senchenbergiana marit., 3, pp.185-201.

Reinhardt, M. A. and Bourgeois, J., 1989. Tsunami favored over storm or seiche for sand deposit overlying buried Holocene peat, Willapa Bay, Washington. EOS, October 24, pp.1331.

Robinson, M, 1993. Microfossil analyses and radiocarbon dating of depositional sequences related to Holocene sea-level change in the Forth valley, Scotland. Transactions of the Royal Society of Edinburgh: Earth Sciences. 84, 1-60.

Robinson, M., 1977. Glacial limits, sea-level changes and vegetational developments in part of Wester Ross. Unpublished Ph.D. thesis, University of Edinburgh.

Robinson, M., 1982: Diatom Analysis of Early Flandrian Lagoon Sediments from East Lothian, Scotland. Journal of Biogeography, 9, pp.207-221.

Roy, P. S., 1967. The recent sedimentology of Scolt Head Island, Norfolk. Ph.D. Thesis, Department of Geology, Imperial College of Science and Technology.

Sato, H., Shimamoto, T., Tsutsumi, A. and Kawamoto, E., 1995. Onshore tsunami deposits caused by the 1983 Japan Sea and 1993 Southwest Hokkaido Earthquakes. A special issue of Pure and Applied Geophysics - Tsunamis: 1992-3 (in press).

Shennan, I., Innes, J. B. and Zong, Y., 1994. Kentra Moss. In: I. Shennan (ed.), Field

Guide: IGCP Project 367 Late Quaternary Coastal Records of Rapid Change. Environmental Research Centre, Department of Geography, University of Durham, Durham DH1 2LE, U.K.. ISSN: 1356 0557. pp.15-18.

Shennan, I., Innes, J. B., Long, A. J. and Zong, Y., 1993. Late Devensian and Holocene relative sea-level changes at Rumach, near Arisaig, northwest Scotland. Norsk Geologisk Tidsskrift, 73, 161-174.

Singer, J. K., Anderson, J. B., 1988. An Assessment of Analytical Techniques For the Size Analysis of Fine-grained Sediments: Journal of Sedimentary Petrology, Vol. 58, No.3, May,1988, p.534-543.

Sissons, J. B., 1967. Glacial stages and radiocarbon dates in Scotland. Scott. J. Geol., 3, 375-381.

Sissons, J. B., 1976. Scotland (The Geomorphology of the British Isles), K. M. Clayton (ed)). Penguin.

Sissons, J. B., 1983. Quaternary. In: Geology of Scotland (Ed. G. Y. Craig). Scottish Academic Press. pp.399-424.

Sissons, J. B., 1983. Shorelines and Isostasy in Scotland. Shorelines and Isostasy (Eds. D. E. Smith and A. G. Dawson). Academic Press. London. pp.209-225.

Sissons, J. B. and Brooks, C. L., 1971. Dating of early postglacial land and sea-level changes in the Western Forth Valley. Nature Physical Science, 234, 124-7.

Sissons, J. B. and Smith D. E., 1965. Peat bogs in a post-glacial sea and a buried raised beach in the western Forth valley. Nature phys. Sci. Scott. J. Geol., 1, pp.247-255.

Sissons, J. B., 1966. Relative sea-level changes between 10,300 and 8300 BP in part of the Carse of Stirling. Transactions of the Institute of British Geographers, 39, 19-29.

Sissons, J. B., 1974. Late-glacial marine erosion in Scotland. Boreas, No.3, pp.41-48.

Sissons, J. B., 1974. The Quaternary in Scotland: a review. Scott. J. Geol., 10. pp.311-337.

Sissons, J. B., Smith, D. E. and Cullingford, R. A., 1966. Late-glacial and post-glacial

shorelines in south-east Scotland. Transactions of the Institute of British Geographers, 39, 9-18.

Smith, D. E. and Cullingford, R. A., 1985. Flandrian relative sea-level changes in the Montrose Basin area. Scott. Geogr. Mag., 101. pp.91-105.

Smith, D. E. and Dawson, A. G., 1990. Tsunami waves in the North Sea. New Scientist 4 August 1990 46-49.

Smith, D. E., Cullingford, R. A. and Brooks, C. L., 1983. Flandrian relative sea level change in the Ythan valley, north east Scotland. Earth Surface Processes and Landforms, 8, 423-438.

Smith, D. E., Cullingford, R. A. and Haggart, B. B., 1985. A major coastal flood during the Holocene in eastern Scotland. Eiszeitalter und Gegenwart, 35, 109-118.

Smith, D. E., Morrison, J., Jones, R. L. and Cullingford, R. A., 1980. Dating the Main Postglacial Shoreline in the Montrose area, Scotland. In Cullingford R. A., Davidson D. A. and Lewin J. (eds). Timescales in Geomorphology. Wiley, Chichester, 225-245.

Smith, D. E., Sissons, J. B. and Cullingford, R. A., 1969. Isobases for the Main Perth Raised Shoreline in south-east Scotland as determined by trend-surface analysis. Transactions of the Institute of British Geographers, 46, 45-52.

Smith, D. E., Turbayne, S. C., Dawson, A. G. and Hickey, K. R., 1991. The temporal and spatial variability of major floods around European coasts. Unpublished final report of work undertaken by Coventry Polytechnic for the Commission of the European Communities under Contract EV4C 0047 UK(H).

Smith, D. E., Cullingford, R. A. and Seymour, W. P., 1982. Flandrian Relative Sea-level Changes in the Philorth Valley, North-east Scotland. Transactions of the Institute of British Geographers, NS 7, 321-336.

Smith, D. E., Dawson, A. G., Hickey K. R., Firth, C. R., Brooks, C. L., Dawson, S. and Shi, S., 1993. Final report on work undertaken by Coventry University. In: Climate Change, Sea Level Rise and Associated Impacts In Europe. Final report of Contract EPOC-CT90-0015. Commission of the European Communities, Brussels.

Smith, D. E., Firth, C. R., Turbayne, S. C. and Brooks, C. L. 1992. Holocence relative sea-level changes and shoreline displacement in the Dornoch Firth area, Scotland. Proceedings of the Geologists' Association 103, 237-257.

Stearns, H. T., 1940. Geology and Ground-water Resources of the Islands of Lanai and Kahoolawe, Hawaii. Hawaii Div. Hydrography Bull., 6, 177pp.

Steers, J. A., 1953, The east coast floods: January 31 - February 1 1953. The Geographical Journal, Vol. 119, 1953, part 3.

Steers, J. A., Stoddart, D. R., Bayliss-Smith, T. P., Spencer, T. and Durbidge, P. M., 1979. The storm surge of 11 January 1978 on the east coast of England. The Geographical Journal, Vol. 145, part 1.

Stuiver, M. and Pearson, G. W., 1993. Radiocarbon, 35, 1-23.

Sutherland, D. G. and Gordon, J. E., 1993. The Quaternary in Scotland. In: (J. E. Gordon and D. G. Sutherland, eds.) Quaternary of Scotland, Chapman & Hall, London. pp.11-48.

Sutherland, D. G., 1984. The Quaternary Deposits and Landforms of Scotland and the Neighbouring Shelves: A Review. Quaternary Science Reviews, Vol. 3, pp.157-254.

Svendsen, J. I. and Mangerud, J., 1990. Sea-level changes and pollen stratigraphy on the outer coast of Sunmore, western Norway. Norsk Geologisk Tidsskrift, 70, pp.111-134.

Teissier, R., 1969. Les Cyclones en Polynesie Francaise. Bull. Soc. Etudes Oceaniennes, 14, pp.20-21.

Tessier, A., Campbell P. G. C. Campbell, and Bisson M., 1979. Sequential extraction procedure for the speciation of particulate trace metals. Analytical Chemistry, Vol. 51, No.7, 844-851.

Thompson, R. and Oldfield, F., 1986. Environmental magnetism. Allen & Unwin.

Van Bijl, W., 1993. Tsunami-Golven in Het Noordseegebied. Unpublished M.Sc. thesis. Faculteit der Civiele Techniek, Vakgroep Waterbouwkunde, Sectie Vloeistofmechanica, Netherland.

Van Orstrand, C. E., 1925. Note on the representation of distribution of grains in sands. Committee on Sedimentation: Research in Sedimentation in 1924. Natl. Res. Council, 63-67.

Visher, G. S., 1969. Grain size distributions and depositional processes. Journal of Sedimentary Petrology, Vol. 39, No. 3, p. 1074-1106.

Wanogho, 1985. The forensic analysis of soils with particular reference to particle size distribution analysis. Ph.D. thesis. University of Strathclyde.

Wiegel, R. L., 1964. Oceanographical Engineering. Prentice-Hall, Inc. / Englewood Cliffs, N. J..

Wordsworth, J., Bradley, R., Dickson, C., Harman, M., Mate, I. and Harden, G., 1985. The excavation of a Mesolithic horizon at 13-24 Castle Street, Inverness, Proc. Soc. Antiquities, Scotland, 115, 89-103, fiche 1: A3-B14.

Wright, C. and Mella, A., 1963. Modifications to the soil pattern of South-Central Chile resulting from seismic and associated phenomenona during the period May to August 1960. Bulletin of the Seismological Society of America. Vol. 53, No. 6, pp.1367.

Yeh, H., Imamura, F., Synolakis, C., Tsuji, Y., Liu, P. and Shi, S. 1993. The Flores Island Tsunamis. EOS, Transactions, American Geophysical Union. Vol. 74, No. 33, pp.371-373.

Young, R. W. and Bryant, E. A., 1992. Catastrophic Wave Erosion on the Southeastern Coast of Australia: Impact of the Lanai Tsunamis ca. 105ka? Geology, 20, pp.199-202.

Appendices

Table 1. Results of Sand A and Sand B obtained with dry sieving

Sand A (Scilly Isles, Sand dune)									Sand B (Sand dune, Dornoch Firth)			
High Limit	Lower Limit	High Limit	Lower Limit	Band Mean	Weight (gram)	Percentage in Size Band		Undersize Cumulative Percentage	Weight (gram)	Percentage in Size Band		Undersize Cumulative Percentage
Ø		µm		di	Vi	Xi	di*Xi		Vi	Xi	di*Xi	
-0.75	-0.50	1700	1400	1542.72	0.0000	0.00	0.00	100.00	0.00	0.00	0.00	100.00
-0.50	-0.25	1400	1180	1285.30	0.0000	0.00	0.00	100.00	0.00	0.00	0.00	100.00
-0.25	0.00	1180	1000	1086.28	0.0549	0.01	11.27	99.99	0.00	0.00	0.00	100.00
0.00	0.25	1000	850	921.95	0.0142	0.00	2.47	99.99	0.00	0.00	0.00	100.00
0.25	0.50	850	710	776.85	0.0538	0.01	7.90	99.98	0.00	0.00	0.00	100.00
0.50	0.75	710	600	652.69	0.0872	0.02	10.76	99.96	0.00	0.00	0.00	100.00
0.75	1.00	600	500	547.72	0.0342	0.01	3.54	99.95	0.22	0.05	29.27	99.95
1.00	1.25	500	425	460.98	1.1034	0.21	96.15	99.75	0.62	0.15	70.10	99.79
1.25	1.50	425	355	388.43	6.7437	1.27	495.17	98.47	2.29	0.56	217.59	99.23
1.50	1.75	355	300	326.34	19.9078	3.76	1228.13	94.71	7.83	1.92	624.96	97.32
1.75	2.00	300	250	273.86	66.1358	12.50	3423.85	82.20	29.45	7.20	1972.77	90.12
2.00	2.25	250	212	230.22	154.7840	29.26	6736.15	52.94	68.10	16.66	3835.01	73.46
2.25	2.50	212	180	195.35	166.1110	31.40	6134.10	21.54	165.96	40.59	7929.88	32.86
2.50	2.75	180	150	164.32	52.9342	10.01	1644.24	11.54	96.31	23.56	3870.98	9.31
2.75	3.00	150	125	136.93	55.2879	10.45	1431.13	1.09	35.76	8.75	1197.79	0.56
3.00	3.25	125	106	115.11	4.9054	0.93	106.74	0.16	1.66	0.41	46.70	0.15
3.25	3.50	106	90	97.67	0.5071	0.10	9.36	0.06	0.39	0.09	9.25	0.06
3.50	3.75	90	75	82.16	0.1132	0.02	1.76	0.04	0.18	0.04	3.59	0.01
3.75	4.00	75	63	68.74	0.0497	0.01	0.65	0.03	0.06	0.01	0.96	0.00
4.00	4.25	63	53	57.78	0.0753	0.01	0.82	0.02	0.00	0.00	0.00	0.00
4.25	4.50	53	45	48.84	0.0652	0.01	0.60	0.01	0.00	0.00	0.00	0.00
4.50	-	45	0	0.00	0.0276	0.01	0.00	0.00	0.00	0.00	0.00	0.00
Total =				529		100	21344.81		408.83	100	19808.84	
Mean = 213.45 µm									Mean = 198.09 µm			
Weight pre-sieving 529.41grams; Loss of Weight after Sieving 0.41 grams									Weight pre-sieving 409.09 grams; Loss of Weight after Sieving 0 26 grams			

Table 2. Results of Sand A and Sand B obtained with Optomax

Sand A - Sand Dune Sand From the Scilly Isles.

Number of slide			1		2		3		4		5		6	
Higher Limit µm	Lower Limit µm	Band Mean	%	C	%	C	%	C	%	C	%	C	%	C
1000	850	921.95	0.00	100.00	0.00	100.00	0.00	100.00	0.00	100.00	0.00	100.00	0.00	100.00
850	710	776.85	0.00	100.00	0.00	100.00	0.00	100.00	0.00	100.00	0.00	100.00	0.00	100.00
710	600	652.69	0.00	100.00	0.00	100.00	0.00	100.00	0.00	100.00	0.00	100.00	0.00	100.00
600	500	547.72	0.00	100.00	0.00	100.00	0.00	100.00	0.00	100.00	0.00	100.00	0.00	100.00
500	425	460.98	0.00	100.00	2.63	97.37	1.87	98.13	6.18	93.82	6.72	93.28	0.00	100.00
425	355	388.43	8.72	91.28	7.02	90.35	7.98	90.15	7.09	86.73	4.14	89.14	5.64	94.36
355	300	326.34	15.63	75.65	24.18	66.17	19.45	70.70	18.05	68.68	13.03	76.11	13.03	81.33
300	250	273.86	27.18	48.47	24.20	41.97	26.65	44.05	28.76	39.92	27.00	49.11	26.64	54.69
250	212	230.22	29.48	18.99	20.55	21.42	23.53	20.52	22.56	17.36	25.69	23.42	24.39	30.30
212	180	195.35	15.34	3.65	14.62	6.80	14.64	5.88	11.75	5.61	15.46	7.96	18.91	11.39
180	125	150.00	3.51	0.14	6.56	0.24	5.34	0.54	5.22	0.39	7.75	0.21	10.77	0.62
125	106	115.11	0.04	0.10	0.07	0.17	0.14	0.40	0.06	0.33	0.03	0.18	0.18	0.44
106	90	97.67	0.00	0.10	0.02	0.15	0.10	0.30	0.12	0.21	0.05	0.13	0.03	0.41
90	75	82.16	0.03	0.07	0.03	0.12	0.12	0.18	0.05	0.16	0.03	0.10	0.11	0.30
75	63	68.74	0.01	0.06	0.04	0.08	0.07	0.11	0.07	0.09	0.04	0.06	0.09	0.21
63	53	57.78	0.03	0.03	0.03	0.05	0.04	0.07	0.04	0.05	0.02	0.04	0.06	0.15
53	45	48.84	0.02	0.01	0.02	0.03	0.03	0.04	0.02	0.03	0.03	0.01	0.06	0.09
45	38	41.35	0.01	0.00	0.03	0.00	0.03	0.01	0.02	0.01	0.03	0	0.07	0.02
Mean	(µm)		262.52		270.48		267.34		276.76		264.61		247.16	

% = Percentage of Volume in Size Band C = Undersize cumulative percentage of volume

Sand B - Sand Dune Sand From Dornoch Firth

Number of slide			1		2		3		4	
Higher Limit µm	Lower Limit µm	Band Mean	%	C	%	C	%	C	%	C
1000	850	921.95	0.00	100.00	0.00	100.00	0.00	100.00	0.00	100.00
850	710	776.85	0.00	100.00	0.00	100.00	0.00	100.00	0.00	100.00
710	600	652.69	0.00	100.00	0.00	100.00	0.00	100.00	0.00	100.00
600	500	547.72	0.00	100.00	0.00	100.00	0.00	100.00	0.00	100.00
500	425	460.98	1.75	98.25	0.00	100.00	2.34	97.66	0.00	100.00
425	355	388.43	6.03	92.22	2.53	97.47	3.74	93.92	6.01	93.99
355	300	326.34	11.00	81.22	15.46	82.01	14.29	79.63	9.97	84.02
300	250	273.86	26.38	54.84	28.97	53.04	35.04	44.59	29.86	54.16
250	212	230.22	32.66	22.18	35.41	17.63	35.02	9.57	36.83	17.33
212	180	195.35	19.48	2.70	15.86	1.77	8.90	0.67	15.89	1.44
180	125	150.00	2.66	0.04	1.73	0.04	0.62	0.05	1.38	0.06
125	106	115.11	0.00	0.04	0.00	0.04	0.00	0.05	0.02	0.04
106	90	97.67	0.00	0.04	0.02	0.02	0.00	0.05	0.00	0.04
90	75	82.16	0.01	0.03	0.00	0.02	0.02	0.03	0.01	0.03
75	63	68.74	0.01	0.02	0.00	0.02	0.00	0.03	0.01	0.02
63	53	57.78	0.01	0.01	0.00	0.02	0.02	0.01	0.00	0.02
53	45	48.84	0.00	0.01	0.01	0.01	0.02	0.00	0.01	0.01
45	38	41.35	0.01	0.00	0.00	0.01	0.00	0.00	0.01	0.00
Mean	(µm)		256.89		254.76		266.86		255.60	

% = Percentage of Volume in Size Band C = Undersize cumulative percentage of volume

Appendix B Publications arising from this work

Paper 1- A. G. Dawson, I. D. L. Foster, S. Shi, D. E. Smith and D. Long, 1991: The Identification of Tsunami Deposits in Coastal Sediment Sequences. Science of Tsunami Hazards, Volume 9, No 1, pp773-82 (published).

THE IDENTIFICATION OF TSUNAMI DEPOSITS IN COASTAL SEDIMENT SEQUENCES

A.G.DAWSON[1], I.D.L.FOSTER[1], S.SHI[1], D.E.SMITH[1] and D.LONG[2]

(1) Department of Geography, Coventry Polytechnic, Coventry, U.K., CV1 5FB.

(2) Marine Geology Research Programme, British Geological Survey, West Mains Road, Edinburgh, EH9 3LA.

ABSTRACT

The study of tsunamis has mostly been undertaken by physical oceanographers, geophysicists, seismologists, mathematicians and historians. Increasingly, however, geologists and geomorphologists also have an interest because many tsunamis deposit sediment. The study of sediments deposited by tsunamis is enormously important since it may enable scientists to identify past tsunamis that took place in pre-history, thus greatly extending our knowledge of the frequency and magnitude of past events. The study of sediments deposited by tsunamis in the past is also important since valuable information can be provided on former wave run-up. This information is much more precise than eye-witness accounts of tsunami run-up and is invaluable in the development of accurate numerical models of tsunamis. Despite the enormous potential of geological techniques in tsunami research, a major problem to be overcome, is the need to differentiate between coastal flood sediments deposited by tsunamis from those attributable to storm surges. In this paper, preliminary geological evidence from northern Scotland and the Scilly Isles, SW England is used to develop a model of tsunami coastal sedimentation.

Content removed due to third-party copyright

Content removed due to third-party copyright

Content removed due to third-party copyright

Content removed due to third-party copyright

Content removed due to third-party copyright

Content removed due to third-party copyright

Content removed due to third-party copyright

Content removed due to third-party copyright

Content removed due to third-party copyright

Paper 2- A. G. Dawson, D. Long, D. E. Smith, S. Shi and I. D. L. Foster, 1992: Tsunamis in the Norwegian Sea and North Sea caused by the Storegga Submarine Landslides. In S. Tinti (ed.) "Proceedings of the Symposium on Tsunamis", International Union of Geodesy and Geophysics, Vienna, Austria, August 1991 (published).

TSUNAMIS IN THE NORWEGIAN SEA AND NORTH SEA CAUSED BY THE STOREGGA SUBMARINE LANDSLIDES.

A.G. Dawson*, D Long**, D.E.Smith*, S. Shi* and I.D.L. Foster*.

* Department of Geography, Coventry Polytechnic, Coventry, U.K. CV1 5FB.
**Marine Geology Research Programme,British Geological Survey,
West Mains Rd., Edinburgh, U.K. EH9 3LA.

INTRODUCTION

The Storegga submarine landslide complex in the Norwegian Sea is one of the largest areas of slope failure in the world. The three submarine slides that occur in this area were first described by Bugge (1983) and detailed accounts of the features have been subsequently provided in several papers (Bugge et al. 1987; Jansen et al. 1987; Bugge et al. 1988). Later, Dawson et al. (1988) proposed that the Second Storegga submarine landslide that took place *circa* 7,000 years ago generated a large tsunami that led to extensive coastal flooding of coastlines bordering the Norwegian Sea and North Sea. These authors showed that evidence for such flooding was evident in eastern Scotland where many Holocene coastal sediment sequences contained a layer of sediment thought to have been deposited by the tsunami. Detailed field evidence for this tsunami was provided in a subsequent paper (Long et al. 1989) while additional accounts described the potential risk to the northwest Europe coastlines posed by such landslide-generated tsunamis (Long et al. 1990; Smith and Dawson 1990). More recently, Svendsen and Mangerud (1990) and Hansom and Briggs (1991) have respectively described evidence from sites in western Norway and northwestern Iceland for a possible major tsunami flood inundation at *circa* 7,000 yrs B.P.

These studies have been paralled by the development of numerical models of the *circa* 7,000 yrs B.P. tsunami generated by the Second Storegga Slide (Harbitz (1991 and in press) and Murty And Falconer (unpublished)). These research investigations have been particularly valuable since they have enabled comparisons to be made between the 'theoretical' model predictions and the 'empirical' field information on tsunami run-up. In addition, studies have been undertaken on the physical characteristics of the coastal sediments considered to have been deposited by the Storegga tsunami (Dawson et al. 1991; Shi et al. 1991). Although these studies are in their infancy, they are of great importance since very little is known on the physical characteristics of tsunami deposits. The few studies that have been undertaken on tsunami deposits in other areas of the world have shown that the processes of sediment deposition are extremely complex (Darienzo and Peterson 1990; Foster et al. 1991; Minoura and Nakaya 1991).

This paper is intended to provide an up-to-date account on research on the tsunamis generated by the Storegga submarine landslides. Most information, however, is concerned with the tsunami generated by the Second Storegga landslide. It is almost certain that large tsunamis were generated by the First and Third Storegga slides. However, there is at present no field evidence for the occurence of these tsunamis. However, a numerical model for the tsunami generated by the First Storegga Slide has been developed by Harbitz (1991 and in press) and shows clearly that the magnitude of this tsunami was similar to that generated by the Second Storegga Slide. This paper also provides information on research that is currently being undertaken on sediments deposited by tsunamis. This is a relatively new area of research and is of great importance to the identification of ancient tsunamis in the geological record.

1. Ages of the First, Second and Third Storegga Slides

Three separate submarine landslide are known to have taken place in the Storegga area (Bugge 1983; Bugge et al. 1988)(Figure 1). The oldest of these (known as the First Storegga Slide) was the largest and involved a movement of approximately 3880 km^3 of sediment. The age of this slide is not known with any accuracy although estimates of its age based on oxygen isotope stratigraphy suggest values between

Content removed due to third-party copyright

Content removed due to third-party copyright

Content removed due to third-party copyright

Content removed due to third-party copyright

Content removed due to third-party copyright

Content removed due to third-party copyright

Paper 3- A. G. Dawson, S. Shi, D. E. Smith and D. Long, 1993: Geological Investigations of Tsunami Generation and Long-term Tsunami Frequency. Natural Disasters: Protecting Vulnerable Communities, P. A. Merriman and C. W. A. Browitt (Eds.), Thomas Telford, London, pp.140-146 (published).

11. Geological investigations of tsunami generation and long-term tsunami frequency

A. G. DAWSON, S. SHI and D. E. SMITH, Coventry University, and D. LONG, British Geological Survey

INTRODUCTION

The word tsunami is derived from the Japanese word meaning harbour wave. Tsunamis are large ocean waves with very long wavelengths and very high velocities. They are frequently described as tidal waves but this view is incorrect since they have nothing to do with tides. Most tsunamis are generated by fault displacement on the seabed caused by earthquakes. However, many tsunamis are generated by submarine landslides and are therefore unrelated to seismic activity. In ocean floor areas where sediment or rock has been displaced, water rushes in from the surrounding sea to restore the water level. When this happens, there is a rapid lowering of sea level at the coast, usually below the level of the lowest tides. Thereafter, large kinematic waves travel outwards as a tsunami from the area located above the zone of seabed displacement. The velocity of the waves is mostly a function of the depth of the water over the area of seafloor at which the displacment or landslide has taken place. Areas of very deep water generate the fastest waves that may often exceed 480km/hr. The height of the waves in the open ocean is usually quite small (often no more than 1-2 m). so that sailors on ships often do not notice the passage of a tsunami. At the coast, the flood levels (runup) associated with a tsunami is partly a function of the dimensions of the propagated waves but it is also greatly influenced by the topography and bathymetry of the coastal zone where frequently the effects of wave resonance may result in the amplification of the advancing waves.

Tsunamis occur relatively infrequently and are most common in the Pacific region. For example, over 40 tsunamis have struck the Hawaiian islands since 1819 with five of these having caused severe damage and loss of life. Recently, during 1992, two exceptionally large tsunamis have attracted considerable media attention as a result of the considerable loss of life and widespread destruction that they caused. On 2nd September 1992, an offshore earthquake of magnitude 5.3 occurred west of the Pacific coastline of Nicaragua. The earthquake magnitude was remarkably low in proportion to the size of tsunami that was generated. Indeed, in some areas devastated by the tsunami, the earthquake was not even felt (Ref.1). However, the tsunami caused immense destruction along most of the Pacific coastline of Nicaragua and neighbouring Costa Rica. More recently, on 12th December 1992, a large tsunami followed an earthquake that occurred north of the island of Flores in Indonesia and led to the loss of life of approximately 2,000 people. In eastern Flores, several villages were completely destroyed by waves associated with runup levels up to a maximum height of 26m.

The relative infrequency of tsunamis and the complex processes of tsunami generation make it extremely difficult to predict the likely recurrence

interval of tsunamis for any given coastal region. The greatest problem in estimating recurrence frequency is the limited timescale over which tsunamis have been documented. Usually this time interval corresponds to the length of time for which there is historical and archaeological evidence. Thus, whereas the list of known tsunamis in Hawaii extends no farther back than 270 years, our knowledge of historically documented tsunamis in the Aegean Sea region extends as far back as circa 1600 BC to the well-known Thera eruption on Santorini that is alleged to have led to the destruction of the Minioan civilisation.

Content removed due to third-party copyright

Content removed due to third-party copyright

Content removed due to third-party copyright

Content removed due to third-party copyright

Content removed due to third-party copyright

Paper 4- H. Yeh, F. Imamura, C. Synolakis, Y. Tsuji, P. Liu and S. Shi. 1993: The Flores Island Tsunamis. EOS, Transactions, American Geophysical Union, Vol.74, No.33, pp.369-373 (published).

Eos, Transactions, American Geophysical Union, Vol. 74, No. 33, August 17, 1993, Pages 369, 371–373

The Flores Island Tsunamis

Harry Yeh, Fumihiko Imamura, Costas Synolakis, Yoshinobu Tsuji, Philip Liu, and Shaozhong Shi

On December 12, 1992, at 5.30 A.M. GMT, an earthquake of magnitude Ms 7.5 struck the eastern region of Flores Island, Indonesia (Figure 1), a volcanic island located just at the transition between the Sunda and Banda Island arc systems. The local newspaper reported that 25-m high tsunamis struck the town of Maumere, causing substantial casualties and property damage. On December 16, television reports broadcast in Japan via satellite reported that 1000 people had been killed in Maumere and two-thirds of the population of Babi Island had been swept away by the tsunamis.

The current toll of the Flores earthquake is 2080 deaths and 2144 injuries, approximately 50% of which are attributed to the tsunamis. A tsunami survey plan was initiated within 3 days of the earthquake, and a cooperative international survey team was formed with four scientists from Indonesia, nine from Japan, three from the United States, one from the United Kingdom, and one from Korea.

Background

Flores Island is one of several large islands in the East Nusa Tenggara region of Indonesia, approximately 1800 km east of Jakarta (Figure 2a). The Indonesian region is located at the intersection of three lithosphere plates: the Indian-Australia plate, the Pacific plate, and the Asian continental plate. The Asian continental plate is fragmented into several deformed subplates. The Indian Ocean lithosphere subducts beneath the fragmented Asian continental subplates along the Sunda Trench and forms an arc system. Beyond the Sunda trench, the Banda sector continues eastward to where the oceanic arc collides with Australia. Detailed tectonic setting of this area was given by *Hamilton* [1988], for example.

The epicenters of the December 12 mainshock and the area of aftershocks were determined by the U.S. Geological Survey (see Figure 2b). The location of the epicenter is at 8.482°S, 121.930°E, approximately 50 km northwest of Maumere. The hypocenter was estimated to be 15 km deep. The fault parameters, based on seismic surface and body waves, were obtained from the Harvard University centroid moment tensor (CMT) solution (M121292y), strike direction 61°, dip angle 32°, slip angle 64°, and seismic moment 6.4×10^{27} dynes-cm. The earthquake area is considered to be in a backarc region of the eastern Sunda arc or western Banda arc, a segment containing many active volcanos. We conjecture that this is a backarc-thrust earthquake with tectonic setting (G. Plafker, personal communication, 1993), such a backarc thrust must be located between the existing Flores thrust and the minor thrust near the eastern peninsula of Flores Island (Figure 2b). The mechanism of this earthquake resembles the 1983 Nihonkai Chubu earthquake in the Sea of Japan, which also caused significant tsunami damage, and more recently, the 1991 Costa Rica earthquake, which also generated tsunamis [*Plafker and Ward*, 1992]. (The earthquake that struck Okushiri Island, Japan, on July 12, 1993, can be considered to be a back-arc earthquake.)

To make an initial estimate of the tsunami generation, a fault plane was determined based on the distribution of after shocks directly related to the mainshock, those aftershock locations are shown in Figure 2b. The estimated fault plane is located in an area approximately 100 km long and 50 km wide. Using these parameters and assuming the value of rigidity = 4.0×10^{11} dynes/cm^2, the computed dislocation was found to be 3.2 m, and the maximum vertical displacement of the sea bottom was computed to be 1.3 m, which directly translates to the sea-surface magnitude of the initial tsunami formation. With this initial condition, a preliminary prediction of tsunami propagation and run-up was computed by the numerical simulation model [*Shuto et al.*, 1990]. The predicted tsunami run-up heights along the coast of Flores Island are shown in Figure 3a. The model indicates that the hardest hit area would be an approximately 100-km-long coastline east of Maumere with a maximum predicted height of 14 m at the north shore of the Hading Bay. Surveying efforts were focused on this area.

Tsunami Survey

Seventeen days after the earthquake, the team began its survey on Flores Island, gathering data from December 29 through January 5. The survey consisted of measurements of maximum tsunami run-up heights and distances, average run-up heights and areas of inundation, flow patterns of run-up and run-down, eyewitness accounts, and observations of subsidence, uplift, and landslides.

Fig. 1. Tsunami attack site in Riangkroko, looking toward inland. See Figure 3 for location. (Photo courtesy of H. Yeh.)

Address all correspondence to Harry Yeh, Dept. of Civil Engineering, FX-10, University of Washington, Seattle, WA 98195. Fumihiko Imamura, Tohoku University, Japan; Costas Synolakis, University of Southern California, Los Angeles; Yoshinobu Tsuji, University of Tokyo, Japan; Philip Liu, Cornell University, Ithaca, N.Y.; and Shaozhong Shi, Coventry University, United Kingdom

0096/3941/7433/93/369/$01.00.

Content removed due to third-party copyright

Content removed due to third-party copyright

Paper 5- S. Shi, A. G. Dawson and D. E. Smith, 1995: Geomorphological Impact of the Flores Tsunami of the 12th December 1992. In: Y. Tsuchiya and N. Shuto (Editors), Tsunamis: Progress in Prediction, Disaster Prevention and Warning, Series of Advances in Natural and Technological Hazards Research. Kluwer Academic Publishers, Dordrecht, pp.187-185 (published).
Also published as S. Shi, A. G.Dawson, and D. E. Smith, 1993: Geomorphological Impact of the Flores Tsunami of 12th December 1992. TSUNAMIS '93, Proceedings of the IUGG/IOC International Tsunami Symposium, Wakayama, Japan, Auguest 23-27, 1993, pp.689-696 (published).

GEOMORPHOLOGICAL IMPACT OF THE FLORES TSUNAMI OF 12TH DECEMBER, 1992

Shaozhong Shi, Alastair G. Dawson and David E. Smith
Division of Geography
School of Natural and Environmental Sciences
Coventry University
Coventry CV1 5FB
United Kingdom

ABSTRACT

This paper presents a description of geomorphological change associated with the Flores tsunami of 12th December 1992. Evidence for severe coastal erosion during the tsunami is indicated by extensive eroded coral boulder complexes, considerable lowering of coastal land surfaces and the formation of ephemeral clifflines. Detailed measurement has shown that locally at least 43m of sediment per metre of coastline was removed during the tsunami. Many areas of coastline were characterised by the deposition of extensive and continuous sediment sheets locally up to 1m in thickness. Farther inland, the sediment cover becomes discontinuous and generally extends as far as the limit of tsunami runup. Other features observed include earthquake-induced coastal landslides and liquefaction phenomena and transported man-made structures by the tsunami.

1. INTRODUCTION

The island of Flores is located approximately 1800 km east of Jakarta in eastern Indonesia. The island lies at the intersection of several tectonic plates and at the transition between the Sunda and Banda island arcs. The region is thus tectonically active and is characterised by a rugged interior consisting of dormant and active volcanoes. The coastal region, by contrast is characterised by relatively flat coastal lowlands that are locally incised as a result of fluvial activity. In the nearshore zone coral reefs are frequently well developed and form a narrow belt fringing the coast. As a result, the coastal zone is

Content removed due to third-party copyright

Content removed due to third-party copyright

Content removed due to third-party copyright

Paper 6 S. Shi, A. G. Dawson and D. E. Smith, 1994: Coastal Sedimentation Associated with the December 1992 Tsunami in Flores, Indonesia. A topical issue of Pure and Applied Geophysics. Also In: K. Satake and F. Imamura (Editors), Tsunamis: 1992-3, Brikhauser Verlag, 17p. (accepted).

Coastal Sedimentation associated with the December 12th 1992 Tsunami in Flores, Indonesia

Shaozhong Shi, Alastair G. Dawson and David E. Smith

Division of Geography, School of Natural and Environmental Sciences,

Coventry University, CV1 5FB, UK

Abstract

This paper presents the result of the first detailed investigation of sediments deposited by a modern tsunami, the 1992 tsunami in Flores, Indonesia. Eye-witness accounts indicate that large volumes of sediment were deposited upon coastal lowlands over wide areas as a result of the tsunami inundation. Highly distinctive vertical and lateral variations in particle size composition are characteristic features of the tsunami deposits and these are intimately related to sedimentary processes associated with flood inundation. The geomorphological and sedimentary evidence is used here to establish a preliminary model of tsunami sedimentation. This information is believed to be of great value in understanding sedimentary processes associated with tsunami flooding and in the interpretation of palaeo-tsunami deposits.

1. Introduction

On 12th December, 1992, 1:30 pm (05:30 GMT), a major back-arc thrust earthquake of magnitude Ms 7.5 took place offshore approximately 50km north of Maumere, the capital of Flores Island (Figure 1). Several minutes later a large tsunami struck the

Content removed due to third-party copyright

Content removed due to third-party copyright

Content removed due to third-party copyright

Content removed due to third-party copyright

Content removed due to third-party copyright

Content removed due to third-party copyright

Content removed due to third-party copyright

Content removed due to third-party copyright

Content removed due to third-party copyright

Content removed due to third-party copyright

Content removed due to third-party copyright

Content removed due to third-party copyright